Distinct Nuclear-Cytoskeletal LINCages Position the Nucleus for Homeostasis, Polarization and Migration

Ruijun Zhu

Submitted in partial fulfillment of the
requirements for the degree of
Doctor of Philosophy
under the Executive Committee
of the Graduate School of Arts and Sciences

COLUMBIA UNIVERSITY

2017

ABSTRACT

Distinct Nuclear-Cytoskeletal LINCages Position the Nucleus for Homeostasis, Polarization and Migration

Ruijun Zhu

Nuclear positioning occurs in different cellular contexts: from dividing yeast to more specialized cells like neuronal glial progenitor and skeletal muscle cells. Interestingly, abnormal nuclear positioning is associated with diseases such as muscular dystrophy where nuclei occupy a central rather than peripheral location. Moreover, rearward nuclear positioning is typical of migratory cells. Active nuclear movement in most cases involves coupling of cytoskeletal components with the nucleus by a group of transmembrane proteins in the nuclear envelope called the LINC (**li**nker of **n**ucleoskeleton and **c**ytoskeleton) complex. It is composed of the inner nuclear membrane SUN (**S**ad1p, **UN**C-84) proteins associated with nuclear lamins and the outer nuclear membrane KASH (**K**larsicht, **A**NC-1, **S**yne **H**omology) proteins, which interact with the cytoskeleton.

In my thesis, the murine fibroblast cell line NIH3T3 was used as a model system to study nuclear positioning in states of active movement and static homeostatic positioning. Nuclear positioning and centrosome reorientation are hallmarks of cell polarity in migrating fibroblasts. The Gundersen lab has established that the nucleus moves rearward to orient the centrosome in serum starved fibroblast monolayers stimulated by the serum-derived factor lysophosphatidic acid (LPA) [1]. LPA stimulates the GTPase Cdc42, which in turn activates the Cdc42 effector MRCK to phosphorylate myosin II and activate actin retrograde flow to move the nucleus to the

rear. A second Cdc42 effector, Par6 functions with Par3 and dynein to maintain the centrosome in the cell centroid [2]. The nucleus is moved rearward by the attachment of retrograde dorsal actin cables to the nucleus through transmembrane actin-associated nuclear (TAN) lines [3]. TAN lines are composed linear arrays of the LINC complex proteins nesprin-2G (N2G) and SUN2 and dorsal actin cables. Disrupting TAN lines components blocks nuclear movement and efficient cell migration. Interestingly, TAN lines are analogous to other membrane adhesions, such as focal adhesions, in that they are transmembrane structures linked to the actin cytoskeleton and transmit force. Given the large number of proteins composing structures such as focal adhesions, we predicted there would be additional components in TAN lines necessary for their formation and function. Thus, I set out to identify and study cytoplasmic factors required for TAN line formation and/or function during active nuclear positioning in fibroblast.

A collaborator detected N2G as a hit in a yeast two-hybrid screen for FHOD1 interactors. FHOD1 is an actin regulator and belongs to the formin family. Like other formin family members, it has an FH2 actin binding domain, an FH1 domain and DID and DAD domains that interact to autoinhibit FHOD1. Unlike other formins, FHOD1 is not activated by GTPase binding and contains a second actin binding domain (ABS domain), giving it actin bundling activity. We show that spectrin repeats (SRs) 10-13 of N2G and the N-terminus of FHOD1 interacts with each other directly by biochemical assays with purified proteins. SiRNA against FHOD1 and overexpression of either FHOD1 or N2G interacting domains prevented LPA-stimulated nuclear movement in wounded monolayers of NIH3T3 fibroblasts, suggesting that the interaction between FHOD1 and N2G is required for nuclear movement and centrosome reorientation. FHOD1 was required for TAN line formation, but was dispensable for the formation of dorsal actin cables and retrograde actin flow. By re-expressing an artificial construct containing the

N2G-binding domain of FHOD1 and the actin-binding domain of α–actinin in FHOD1 depleted cells, we show that the FHOD1 ABS domain provides N2G with an additional contact to actin filaments required for nuclear movement. This study thus identifies FHOD1 as a new TAN line component and suggests that the interaction of FHOD1 with N2G may reinforce TAN lines so that they can resist the force necessary to move the nucleus.

The above study identifies a new component in a pathway that actively moves the nucleus. We have far less knowledge about the mechanism that maintains the nucleus in position when it is not moving. For example, it is unknown whether the static nuclear positioning is an active process or simply an inactivation of mechanisms that actively move nuclei. To answer this question, I developed a novel method to artificially displace the nucleus in adherent cells by centrifugation and used this system to identify active mechanisms of homeostatic nuclear positioning.

By subjecting wounded monolayers of starved NIH3T3 fibroblast on coverslips to centrifugal force perpendicular to the wound, I find that nuclei are displaced towards the direction of centrifugal force, so that on one wound edge, the nuclei are in the cell rear while on the other, in the cell front. After returning centrifuged cells to the incubator, I used fixed and live cell recordings to show that the displaced nuclei actively re-center within one hour, although nuclei moving rearward did so faster than those moving forward. Treating centrifuged cells with cytoskeletal drugs, revealed an actin/myosin II-dependent rearward recentration and a microtubule (MT)/dynein-dependent forward recentration. I knocked down LINC complex components to test their involvement in these movements. N2G was required for both rearward and forward movement while SUN1 and SUN2 were required for forward and rearward movement, respectively. Overexpression of different N2G constructs in N2G-depleted cells

showed that different regions of N2G were necessary for each direction of movement: N-terminal constructs rescued rearward nuclear recentration whereas C-terminal constructs rescued forward recentration. Based on the minimal N2G construct that rescued forward (MT dependent) nuclear recentration, I identified a dynein and dynactin site in the C terminus of N2G. To test whether the homeostatic nuclear positioning mechanisms were active in uncentrifuged cells, I depleted cells of nesprin-2 and then re-expressed nesprin-2 constructs capable of interacting with actin, MTs or both cytoskeletal elements. Nuclei in nesprin-2-depleted cells were no longer maintained at the cell centroid and only re-expression of a construct that contained sites for interaction with both actin and MTs rescued this defect. Thus, both actin- and MT- interaction domains of N2G are required for homeostatic nuclear positioning.

To test whether the actin and MT activities of N2G were important for cell migration, I depleted NIH3T3 fibroblasts of nesprin-2 and re-expressed N2G constructs capable of interaction with actin, MTs or both and tested these cells in single and collective cell migration assays. I found that only the MT-dependent activity of N2G is required for the directionality of single cell migration while both N- and C- terminal (actin- and MT- dependent) N2G are required for the velocity of collective cell migration. These results show that different cytoskeletal linkages are used in different modes of cell migration.

My thesis studies identify the first cytoplasmic factor required for TAN lines structure, establish a novel method to artificially displace the nucleus in adherent cells, and reveal different mechanisms of LINC complex coupling cytoskeletons during active and homeostatic nuclear positioning, as well as specific cytoskeleton-dependent contributions of nuclear envelope protein N2G during cell migration

TABLE OF CONTENTS

LIST OF FIGURES

LIST OF CHARTS

ACKNOWLEDGEMENTS

This work would have been possible without all the mentorships that I have received from members in Dr. Gregg Gundersen's lab in Columbia. First and foremost, I own all my gratitude to Gregg, whose guidance, mentorship and support have been invaluable assets for my training as a scientist. As a mentor, Gregg really helped me to learn to formulate good questions and experiments; he provided opportunities for me to attend conferences and to practice for mentoring students myself. Most importantly, Gregg has taught me how to deliver one's work, both through speaking and writing. His creativity and overall enthusiasm for biology has provided constant inspiration for me during my training. Besides, it has been my distinct privilege to be able to work with the many talented post-docs, graduate students and technicians who contributed to the interactive and diverse lab environment provided by Gregg.

Specially, I would like to thank Dr. Wakam Chang for his general mentorship in lab and interactive discussions after seminars. I am indebted Dr. Susumu Antoku for many interactive discussions, which had often paved the way for new findings against technical hurdles. I will also recognize Dr. Nagendran Ramalingam, who leads me to run marathon, for keeping me fit while working long hours. In addition, I will thank numerous other current and former lab members-- Dr. Keeley Mui, Safiya Cesar, Ahbishek Sinha, Alba Moreno, Dr. Guilherme Nader and Sara Nik for your support and guidance.

I must thank Dr. Francesca Bartolini for her guidance being a female scientist and her lab members, Xiaoyi "Lily" Qu and Dr. Maria Elena Pero for their support and contribution to a friendly research environment. I must recognize Dr. Julie Canman for her generous mentoring on

genetics and GTPases, as well as on how to be an awesome cat owner. I would like to express my gratitude to my other committee members- Drs. Fred Chang, Howard Worman and Richard Vallee- for your advice, support and guidance throughout my graduate training. I would also like to thank Dr. Megan King for serving as my external committee member. Moreover, I am indebted to Dr. Mimi Shirasu-Hiza for calming me down with her generous guidance during my post-doc searching and her advice on fly genetics after I landed my post-doc position. I must also recognize Ms. Zaia Sivo for her constant support and advice. I would also like to thank Dr. Ron Liem for his guidance and insight.

Outside Columbia, I would like to thank Dr. Geri Kreitzer for her generous advice and guidance since my graduate school interview. As for our collaborators, I own my special thanks to Dr. Oliver Fackler for initiating the collaboration on FHOD1 and his constant support. I would like to thank Dr. Tanmay Lele for his biophysical expertise during collaboration. In addition, I would like to thank Dr. Dan Conway for bringing us the nesprin-2 FRET sensor during collaboration.

Apart from academia, I would like to thank my parents Jiaren and Xiaofeng for providing me a free and equal environment since I was born. I would like to thank Tigger for her fluffy paws.

Lastly, I owe it to Dr. Chenshu Liu, my beloved husband, who has been a constant source of inspiration for me in both science and life, for his loving support, insightful opinion and sense of humor throughout the process.

PREFACE

For all cellular life on this planet, one of the most important phenomena is the ability to break the symmetry and achieve cell polarity. Cell migration is a representitve and fascinating example of cell polarity. Migrating cells must establish a protrusive cell front and a trailing cell rear. Cell migration is essential for embryonic development, immunal response, wound healing and cancer metastasis. Many types of cell migration have been visualized and studied for over 60 years since the first application of time-lapse recording by phase-contract microscopy [4]. Interestingly, nuclear movement in migrating cells has not been characterized well until very recently. This is partially because people have focused on nuclear movements associated with cell division and because the nucleus has been considered merely as a "bag" that carries the chromosomes [5-7]. Even though the first image of a migrating fibroblast, showed that the nucleus was rearward in the cells [8], the notion of nuclear positioning as a hallmark of cell polarity is fairly new. More recently, additional attention has been placed on the nucleus as its function as a mechansensitive element has become clearer [9].

Nuclear positioning is observed in different cellular processes from dividing cells to developing tissues from single cell organisms like yeast to multi-cellular organisms like human [10, 11]. Abnormal nuclear positioning has been observed in muscular dystrophy patients and is postulated to contribute to other diseases such as lissencephaly and cardiomyopathy [12]. Specific nuclear postision is achieved by either passive nuclear movement or active nuclear movement depending on direct ATP consumption. And active nuclear movement involves the participation of the cytoskeleton, a major player in cell motility. The cytoskeletons directly moves the nucleus by generating force that is frequently transmitted to the nucleus through a set

of protein in the nuclear envelope, called the linker of nucleoskeleton and cytoskeleton (LINC) complex [13]. The LINC complex is composed of two families of conserved proteins: outer nuclear membrane KASH proteins and inner nuclear membrane SUN proteins [14, 15]. By the time I started this thesis project, the LINC complex was known to mediate nuclear movements in different species from yeast, worm and fly to mammalian systems. The question I found most intriguing was why the nucleus is positioned.

In this thesis, I first discuss the physical solution to this question by answering how the machinery moves the nucleus in polarizing NIH3T3 fibroblasts in more detail. In this study, I identified the first cytoplasmic factor participating in the nuclear-cytoskeletal structure that moves the nucleus [16, 17]. Second, I introduce a method, first developed for this project, that uses physical force to artificially disrupt nuclear positioning in adherent cells. This novel method could potentially be used to study the question of why the nucleus is positioned. However as another showcase for the serenpidity of scientific research, in the second project, I will focus on my discovery of homeostatic nuclear positioning mechanisms, which includes the finding that a single KASH protein engages both actin filaments and MTs. Then, I will describe how I have used this information about the KASH protein to dissect different requirements for nuclear engagement with actin and MTs during both single and collective cell migration. I will discuss further the broader significance and future applications in the last chapter of this thesis.

Chapter One: Introduction

Cell Polarity and Cell Migration

Imagine there is no cell polarity, there will be no asymmetric cell division and no directional cell migration. Then a multi-cellular organism becomes a colony of millions and millions of identical cells. Cell polarity enables cells to perform specialized activity. It is a process where some form of symmetry is broken and asymmetry is established. By breaking more symmetry, more structures will be formed, which enables the possibility of more functions. Among many processes, cell migration is one of the most classic examples for cell polarity.

Cell migration is a fundamental process observed in living organisms and this process plays a key role in embryonic development, immune response as well as tissue repair and regeneration. During embryogenesis, cell migation is important for the formation of tissues and organs. Abnormal cell migration is observed *in vitro* after expressing neurological mutants associated with brain malformation in cells [18]. During the immune response and body surveillance, leukocytes exhibit different types of cell migration. In order for a leukocyte to meet an antigen-bearing dentritic cells in the lymph node to produce antibodies, it translocates in the circulatory system to reach the lymph node and then transmigrates through the endothelium to get inside the lymph node. Then, with the help of intricate extracellular matrix in the lymph node, it migrates towards dentritic cell to allow for the antigen presenting process [19]. During skin regeneration and repair, different cells including basal cells, epidermal stem cells and fibroblasts are activated to migrate during wound healing [20]. Though accurate (in terms of speed and direction) and ample (in terms of frequency) cell migration is important for the development and maintanence of multicellular organisms, excessive cell migration may also be a problem. When cancer metastasis happens, it creates more difficulties to treat the disease. Thus

understanding the fundemental mechanism of cell migration may offer new clinical treatments towards diseases and abnormalities.

When Abercrombie made time lapse movies of cultured chick fibroblasts with phase-contrast microscopy in the 1950s, he first described the cell-motility cycle [4]. This laid the foundation for current cell migration research. In his later cinemagraphs of cell migration, he described the anterior region of a fibroblast as a "flattened sheet of cytoplasm" and called it the leading lamella, or lamellapodia. And there was "ruffled membrane" at or near the front of the cell. The trailing portion of the migrating chick fibroblast separated from the substratum and retracted [21]. It is obvious to us these two regions within the cell have different morphologies, in other word, they are asymmetric. Thus a migrating fibroblast is also polarized along a front-back axis. The nuclear centrosomal axis aligns with the front-back axis and the orientation of the nuclear centrosomal axis relative to the morphological axis is postulated as a hallmark of polarity in many migrating cells [22]. Apart from this, there are polarized distributions of molecules between the front and back of migrating cells as well, including the actin cytoskeleton, myosin II, members of the Rho family of GTPases, focal adhesions, cell junctions [23-27], many of which are involved with force transmission during cell migration. Importantly, disrupting those proteins affects cell migration behavior.

Only until recently, people have stressed that the nucleus is positioned specifically in migrating cells [11]. Intriguingly, the nucleus is at the rear of many types of migrating cells. This polarized position of the nucleus becomes a new form of cell polarity.

Nuclear Positioning

The nucleus is the largest organelle in most of the cells and contains genetic information encoded in the chromosomes, which needs to be separated equally during cell mitosis. Thus it is not surprising that the first focus on nuclear positioning was in mitosis. In fungi, including both budding yeast *Saccharomyces cerevisiae* [28] and fission yeast *Schizosaccharomyces pombe* [29] closed mitosis occurs. As opposed to "open" mitosis, closed mitosis is a process where the nuclear envelope does not break down during prophase. The intact nucleus can be moved by mitotic motors [30] and different nuclear positioning is observed in both asymmetric division and symmetric division. For example, in budding yeast division, the nucleus is positioned in the bud neck such that it can be separated into each daughter cell. In fission yeast division, the nucleus is actively moved to the middle of the cell, ensuring symmetric division. Interestingly, people have observed that by actively changing nuclear position in fission yeast, the position of the cell division plane including the contractile ring assembly was affected [31]. Another interesting example is the process following fertilization where male and female pronuclei move toward each other, which is important for zygote formation [32]. For example in the worm *Caenorhabditis elegans*, the posterior positioned sperm-derived pronucleus together with its associated centrosome move away from cell cortex towards the cell center while the anterior positioned oocyte-derived pronucleus migrate towards the sperm pronucleus [33].

Yet recently, more cases of nuclear positioning have been found in interphase cells including migratory fibroblasts, neuronal progenitor cells and other cell types. Nuclei are actively positioned rearward in almost all migrating cells (2D and 3D migration of fibroblasts, endothelial cells and astrocytes, neuronal migration in vitro and in brain slices; and macrophage

migration). Disruption of rearward nuclear positioning reduces cell migration kinetically [3, 16, 34, 35]. The mechanisms of nuclear positioning have been studied most intensively in migratory cells, which will be further discussed in the next section.

In the developing neocortex, the nucleus shuttles between the apical and basal side of neural epithelium during the cell cycle of neural progenitor cells. This process, called interkinetic nuclear migration, is mediated by both kinesin and dynein in radial glial progenitor cells [36, 37]. Pathologically, the human orthologues of LIS1/ PAFAH1B1, encoding cytoplasmic dynein pathway component LIS1, is found mutated in human lissencephaly or smooth brain, a condition where the convolutions are absent in the cerebral cortex [38]. Interestingly, in rat brain slices where LIS1 is disrupted by in utero eletroportion of RNAi against the gene, both interkinetic nuclear migration oscillations between layers in radial glial progenitor cells and the cell divisions at the apical side were abolished [39].

Moreover, specific nuclear positioning is observed in mammalian tissue. For example, in the cross section of kidney cortex, the nucleus in the proximal convoluted tubule is located basally while the nucleus in the distal tubule is located in the center [11]. In the cross section of skeletal muscle, the nuclei are positioned at the periphery of the muscle fiber. However in skeletal muscle from muscular dystrophy patients, nuclei are found in the center of the muscle fiber. This defect is also recapitulated in muscular dystrophy mouse model by noninvasive imaging [40]. Another example of mispositioned nuclei in a pathological condition is in the hearing system. The nuclei in the outer hair cells are mispositioned to an apical location from their usual basal localization in mutant mice with a hearing behavior defect where nuclear

envelope proteins SUN1 or SYNE4/nesprin 4, which will be further discussed in the next sections, are disrupted [41].

SUN Proteins

The SUN domain, short for **S**ad1p, **UN**C-84 (spindle architecture disrupted 1/uncoordinated 84) domain, is a ~200 C-terminal amino acids motif [42]. As a conserved domain, it not only displays homology among SUN-domain protein family proteins of one species, but also across different species from yeast to mammalian systems. SUN proteins are integrated into the inner nuclear membrane (INM). The SUN domain interacts with the KASH peptide in perinuclear space (PNS) based on cell biology, biochemistry [14, 15] and structural biology [43-45] evidence. The N-terminal domain of SUN proteins in the nucleoplasm varies in length within the protein family and across species. The nucleoplasmic domain can interact with components of the nuclear lamina, chromosomes, or other inner nuclear membrane proteins [46]. The single-pass transmembrane (TM) domain in mammlian SUN proteins classifies them as type II transmembrane protein [47].

Mammalian SUN2 domain forms a trimer with the KASH peptide

Crystallographic evidence provides insight into both the structure of the SUN domain residing in between the nuclear membranes and the interaction of the SUN domain with the KASH peptide [43, 44]. Most importantly, the SUN domain of human SUN2 assembles into a trimer and this oligomerization is important for creating a pocket to bind to KASH domain. The formation of this trimer depends not on the SUN domain, but on the trimeric coiled-coil that precedes it. There are several residues in the C-terminal KASH peptide of both human nesprin-1 and nesprin-2 crucial for the contact between SUN and KASH and they are quite conserved

between human nesprin-1-4. Amazingly, adding the smallest amino acid to the very C-terminus of the KASH peptide abolishs the binding to the SUN domain, consistent with the hypothesis that accurate positioning of the KASH peptide into its binding pocket on the SUN protein is required for KASH-SUN interaction. So what forms this binding pocket? From the crystal structure, there are serveral hydrophobic residues at positions -7 to -10 from the C-terminus that bind to a region ~25 residues from the N terminus of the SUN domain. This region of the SUN domain has been termed the "KASH-lid" (Figure 1.2), because it seems to undergo a conformation change upon binding the KASH peptide [43, 48]. Therefore, one KASH peptide tightly fits into the binding groove formed by two SUN protomers. While there are over 20 residues within the SUN domain forming noncovalent interactions with the KASH peptide, the crystal structure shows a cysteine in the KASH-lid that forms a disulfide covalent bond with a cysteine at the position -23 of the KASH peptide. Both cysteines are evolutionarily conversed in SUN and KASH proteins in mammals. Disruption of this disulfide bond by mutating the cysteine -23 to serine on either nesprin-1 or nesprin-2 abolishes high molecular weight complex between KASH and SUN2 and also significantly inhibits high molecular weight complexes between KASH and SUN1. However, there are still residue SUN1:GFP-nesprin oligomer and monomer left (Sosa, et al, Figure S3A [43]). This suggests that 1) the cysteine enhances the binding between SUN and KASH; 2) SUN1 and SUN2 are different in terms of KASH binding ability *in vivo*. This notion will be discussed further later.

The relationship between trimer formation and SUN2-KASH interaction remains unclear. $SUN2_{522–717}$, which lacks the coiled-coil, remains as a monomer in solution. Interestingly, purified $SUN2_{521–717}$ binds to immobilized KASH2 only after extending the N-terminal SUN2

sequences or attaching an unrelated coiled-coil to its N-terminus. Because the unrelated coiled-coil is responsible for trimeric version of another protein, it implies that oligomerization of SUN2 is required for SUN2-KASH binding. Therefore, without the full length SUN structure, how oligomization of SUN protein affects SUN-KASH binding, especially binding pocket formation and other higher order structure, requires further investigation. The oligomeric structure of SUN1 has not been determined. From biochemical cross-linking experiments, SUN1 appears to form dimers and tetramers [49].

SUN protein localization and anchorage

Proper SUN protein localization is required for the formation of a functioning LINC complex. Previous studies have shown that membrane proteins that localize to the INM are retained there by a "selective retention process" that involves interaction with the nuclear lamina, heterochromatin or other INM proteins [50, 51]. SUN protein localization to the INM requires several transport signals and pathways. There is a classical nuclear localization signals (cNLS) residing at the N-terminal nucleoplasmic region of SUN2. This cNLS element, via interating with importin α/importin β heterodimer, helps targeting SUN2 to the INM. A second element contributing to SUN2 localization is a four arginine (4R) motif close to the cNLS. When this 4R motif is mutated, SUN2 accumulates in the Golgi complex and its interaction with the coatomer complex I (COPI) is lost, suggesting that a Golgi retrieval signal is important for retaining SUN2 in the ER and allowing its transfer to the INM. Additionally, elements within the SUN domain promote SUN2 localization to INM [52]. Studies on SUN1 localization to the INM have not been conducted.

A parallel study of the *C. elegans* SUN-domain protein UNC-84 shows that there are additional INM-targeting sequences in the SUN protein. While two cNLS motifs are important, SUN-nuclear envelope localization signal (SUN-NELS) and inner nuclear membrane sorting motif (INM-SM) also contribute to UNC-84 localization to the NE. Only mutating all four elements abolishes UNC-84 INM localization completely, suggesting there is funcational redundancy among these elements [53]. Apart from this, mislocalization of yeast SUN protein Mps3 variant could be rescued by overexpressing histone variant H2A.Z, suggesting that nucleoplasmic elements can also contribute to SUN protein localization to the INM [54].

SUN proteins in plants, fungi, ecdysozoan

Homologues of SUN domain proteins have been found in several plants, such as maize and *Arabidopsis*. There are five SUN proteins identified in maize (ZmSun1-5). ZmSun1-2 are orthologues of mammalian SUN1 and SUN2 while the other three are not closely related. ZmSun3-5 possess three (instead of one) transmembrane domains and a SUN domain in the middle (instead of in the C-terminus) [55]. Similar to testes-specific isoforms of SUN in mammalian cells, ZmSun5 is mainly found in pollen. These SUN-domain proteins localize to the NE [56] and regulate nuclear shape in different plant tissues, including root hair cells, leaf epidermal and trichome in *Arabiposis* [57, 58].

In fungi, Mps3 and Sad1 are identified as SUN-domain proteins in budding yeast and fission yeast, respectively. Both have been shown to localize to the spindle pole body (SPB) and are important for SPB function. Specifically, Mps3 is known to play a role in SPB duplication

[54], whereas Sad1 is important for SPB assembly [59]. Interestingly, both Mps3 and Sad1 may exhibit different functions when forming complexes with different ONM proteins [60-63].

As one of the eponym of this class of proteins, UNC-84 was the first SUN protein identified in the worm. The phenotypes of *unc*-84 mutants include: uncoordinated locomotion, disruption of vulval formation and egg laying defects [64, 65]. UNC-84 is the somatic version of SUN proteins in the worm and affects nuclear migration of many cell types during embryonic development [42]. Matefin/SUN-1 is another SUN domain protein identified in the worm [66]. SUN-1 is expressed in the NE in all early embryonic cells and germ cells and it colocalizes as well as interacts with LMN-1, the nuclear lamin protein in worms [66]. SUN-1, together with the KASH protein ZYG-12, is required for homologous recombination in meiosis [67, 68].

There are two SUN-domain proteins identified in the fruit fly: Klaroid (Koi) and SPAG4 (sperm-associated antigen 4). Koi forms a complex with the KASH protein Klar and both of them are required for the eye development. Koi localizes to the perinuclear region in third instar larval eye discs determined by antibody recognizing N-terminal Koi and it is unclear whether Koi decorated NE in oocyte [69]. Similar to mammalian SUN isoforms functioning in testes, Spag4 mRNA is only found in testes and *spag4* mutant males are sterile in *Drosophila* [70].

SUN proteins in mammals

The complexity of SUN-domain proteins increases in mammals. Also, mammalian SUN-domain proteins and their isoforms participate in different yet specialized cellular contexts. There are five genes containing SUN-domain proteins identified in mammlian systems. Among

them, SUN3-5 are found in testes. SUN3 is expressed at the posterior of the developing sperm head after mouse meiosis [71]. SUN4/SPAG4 is expressed highly in rat spermatids (as well as small instestine) and interestingly, in humans, SUN4 is expressed in pancreas, stomach, lymph node, pituitaruy gland and small instestine, besides testes [72]. Several isoforms of SUN5 are cloned from testicular tissue and are not detected in other mouse tissues analyzed [73]. In the developing sperm, two SUN5 proteins are observed in the NE, more concentrated beneath the acrosome, at the apical side of the nucleus. Interestingly, these SUN5 isoforms, when expressed ectopically in fibroblasts, were observed in ER, suggesting a sperm-specific regulation of SUN5 nuclear localization [74].

Mammlian SUN1 and SUN2 are expressed in many tissues and form functional LINC complexes with several KASH domain proteins and function in many cellular contexts [46, 75]. Because I have used NIH3T3 mouse fibroblasts as a model system, I will focus on mouse SUN1-2. Both of them are composed of a N-terminal nucleoplasm domain, an adjacent transmembrane (TM) domain, several predicted coiled-coil domains and a C-terminal SUN domain that binds to the KASH peptide [43, 44]. Although these two proteins are considered to be paralogues and only SUN1/SUN2 double knockout in mouse leads to neonatal lethality, there is evidence suggesting that these proteins are not entirely functionally equivalent. First, overexpressing either GFP-SUN1 or GFP-SUN2 together with RFP-lamin A and using Förster resonance energy transfer (FRET) acceptor photobleaching shows that there is higher FRET between lamin A and SUN1 than between Lamin A and SUN2. This suggests lamin A is more closely associated with SUN1 than SUN2 [76]. Notably, the nucleoplasmic domain of SUN1 is larger than SUN2 (Figure 1.2). Second, by overexpressing KASH proteins and then running SDS gels under both

reduced and oxidized environment followed by western blotting for SUN1 and SUN2, there are more DTT-sensitive SUN1 bands than SUN2 bands, suggesting that SUN1 forms disulfide complexes with KASH proteins more readily than SUN2 [43]. Indeed, when comparing the sequences of SUN1 and SUN2, there are more conserved cysteines in SUN1 in both the nuclear lumen and nucleoplasm than in SUN2 (Figure 1.3). Also, SUN1 has more predicted coiled-coil domains in the nuclear lumen than SUN2 (Figure 1.2) and these may contribute to oligomerization as well (not necessarily through disulfide bond), which requires thorough structural and biochemical investigation. Interestingly, a GFP-tagged nesprin-2 truncation construct is more mobile after cells are treated with RNAi against SUN2 but not SUN1; however the affinities measured by Biacore experiment between the nesprin-2 KASH domain and the luminal domains of SUN1 or SUN2 are quite similar [76].

In mouse models, even though SUN1 and SUN2 appear to function redundantly; phenotypes in individual SUN1 or SUN2 knockout mice are actually quite different. In two SUN1 mouse models targeting different exons, both mice are reported to be sterile and have under-developed gametes in meiosis and hearing loss is observed as well [41, 77, 78]. Notably, both male and female SUN1-/- mice are infertile [79]. Knockout mice targeting to exons 11-16 of SUN2, showed no overt phenotype initially [80], but displayed progressive hair loss with alopecia together and abnormal hair follicle morphology during the first round of hair growth [81]. Interestingly, these phenotypes were not observed in the SUN1 knockout mouse.

KASH Proteins

KASH domain, short for **K**larsicht, **A**NC-1, **S**yne **H**omology domain, is a motif consisted of ~30 C-terminal amino acids [82]. Similar to the SUN domain, it not only displays high homology among different KASH domain proteins within one species, but across kingdoms with several conserved amino acids. Additionaly, there is a conserved proline/leucine-rich hydrophobic transmembrane domain (about 20 amino acids) residing at N-terminal end of the KASH domain, with only ~7 residues in between the KASH peptide and the tranesmembrane domain [43]. KASH proteins are on the outer nuclear membrane (ONM). KASH proteins, like other tail-anchored proteins, are targets of post-translational tail insertion into ER membranes via the GET pathway [83, 84].

KASH protein localization

There are numerous observations indicating that KASH proteins localize to the ONM in a SUN-dependent fashion. In worms, UNC-84 SUN domain is required for KASH protein UNC-83 localization to the NE *in vivo* [85]. In mammals, RNA knockdown or gene ablation of SUN proteins reduced the accumulation of KASH proteins in the ONM [15, 86, 87]. Moreover, in cells overexpressing the KASH domain of the KASH proteins, endogenous KASH proteins are observed in the ER, rather than the ONM. This suggests that excess KASH peptide saturates endogeneous SUN binding pockets and allows them to return to the ER [82, 88].

By forming a functional LINC complex, KASH and SUN proteins are able to link the nucleus to cytoskeletal elements. Over the years, different LINC complexes have been reported.

One SUN domain protein is able to intereact with different KASH domain proteins while one KASH domain proteins is able to interact with different SUN domain proteins. As the different KASH proteins can interact with the each of three major cytoskeletal elements, this allows for a high level of combinatorial interactions between the nucleus and the cytoskeleton, raising the possibility of different functions, which will be discussed later. Additionally, nesprin-3 binding to nesprin-1 and nesprin-2 calponin homology domains [89] and SUN1 binding to SUN2 [90] biochemically suggests the potential of forming hetero-oligomers within KASH and SUN proteins, which further increases the combinatorial possibilities.

Are different functions linked to different forms of the LINC complex? Interestingly, a study into the macro-structure of fluorescence labeled lamin A/C by three-dimensional structured illumination microscopy suggests that lamin A/C proteins underneath the INM forms a distinct fiber meshwork in fibroblasts while this structure is disrupted in cells depleted of lamin A/C or lamin B1. Nuclei lacking lamin A/C has slightly bigger meshwork faces with some shape changes [91]. Because mammlian lamin proteins are important for SUN proteins localization, which in turn affect KASH proteins, we can infer from the result that SUN/KASH proteins also form a macro-strucutre on the NE.

KASH proteins in plants, fungi, ecdysozoan

In *Arabidopsis*, a plant-specific WPP (tryptophan-proline-proline motif)-interacting proteins have been identified as the KASH-domain proteins. These WPP-interacting proteins recruit a Ran GTPase activating protein to the NE [92] and interact with SUN-domain proteins to regulate nuclear shape in plant tissues [58]. In *S.cerevisiae*, two ONM proteins Mps2 and Csm4

lack a conserved KASH peptide but do have KASH-like functions where they can form a LINC complex with the sole SUN protein Mps3. It has been reported that Mps3/Mps2 LINC complex is critical for the SPB to duplicate and insert into the NE [92] whereas the Mps3/Csm4 LINC complex is important for chromosome movement and homologous recombination in meiosis [60, 93-95]. In *S.pombe*, two KASH-domain proteins have been identified. Sad1/Kms1 LINC complexes are essential for the formation and progression of the chromosomal bouquet during meiosis [96]. Sad1/Kms2 LINC complex is important for nuclear positioning by linking the nucleus to MTs [97]. Similar to Mps2, Kms2 is important for remodeling the SPB [98].

In *C. elegans*, several KASH domain proteins have been identified and they have different abilities to interact with the cytoskeleton. ANC-1 links the nucleus to the actin cytoskeleton and contributes to nuclear anchorage [82]. Another KASH domain protein ZYG-12 is localized to the NE by forming a dimer with a KASH-less splice variant that localizes to the centrosome, which has been implicated maintaining the centrosome near the nucleus [99]. SUN1/ZYG-12 forms a functional LINC complex important for meiotic chromosome pairing. This complex functions as a connection between chromosomal pairing centers and cytoplasmic MT network, including dynein, such that forces generated by dynein and MTs can be transmitted to chromosomes [67]. UNC-83 is a third KASH domain protein in worms and it has been reported to interact with both dynein and kinesin. UNC-83 recruits kinesin-1 through kinesin-1 light chain KLC-2 to the NE [100] and recruits dynein to the NE through both the NudE homolog NUD-2 and the BicaudalD homolog BICD-1 as well as the egalitarian homologue EGAL-1[101]. Both kinesin and dynein are required for bidirectional nuclear migration in worm hyp7 (hypodermal syncytium) cells [100].

In *Drosophila*, two KASH-domain proteins have been identified. MSP-300 plays a role in muscle development and also promotes nuclear anchorage in an actin-dependent manner in developing oocytes [102-105]. It also contributes to the proper localization of mitochondria and ER in muscle cells [106]. Another KASH-domain protein Klarsicht (Klar) is also found to be important for proper nuclear distribution in muscle fibers. Besides, genetic interaction between N-terminal Klar and dynein is identified in cells of the developing eye and this linkage is required for nuclear migration [107, 108].

KASH proteins in mammals

Most KASH proteins in mammals are referred to as nesprins (**n**uclear **e**nvelope **sp**rectrin **r**epeat). There are four nesprins (nesprin-1 though -4) in mammals and several other KASH proteins. These KASH proteins allow mammalian cells to interact with all three cytoskeletal elements (i.e. MTs, intermediate filaments and actin microfilaments).

Nesprin-1/nesprin-2 or Syne-1/Syne-2 were the first KASH-domain proteins identified in mammals and are widely expressed [109, 110]. There are several isoforms of both nesprin-1/nesprin-2 arising from splicing and alternative start sites. The full-length or giant isoforms are ~1 mDa and ~ 800 kDa, respectively [111]. Both giant forms contain paired CH (calponin homology) domains and can interact with actin filaments [112, 113]. While there is no giant nesprin-1 isoform in NIH3T3 fibroblasts [3], nesprin-2G forms a linkage between SUN-2 and dorsal actin cables to form TAN lines to move the nucleus to the cell rear during LPA stimulated cell polarization [3]. Both nesprins have been identified to interact with kinesin-1 via direct binding to KLC1/2 through their LEWD motif near the C-terminus [114]. Both nesprins also

associate with dynein/dynactin by co-immunoprecipitation assays from mouse brain extracts [115]. These MTs motor interactions are important for nuclear migration in photoreceptors in the retina, neuronal migration in the cerebral cortex, interkinetic nuclear migration during retinal photoreceptor formation and nuclear spacing in syncitial myotubes [114-116].

Nesprin-1/nesprin-2 variants are involved in the pathogenesis of Emery–Dreifuss muscular dystrophy patients [117]. SYNE1 (nesprin-1) mutants also cause progressive cerebellar ataxia [118, 119]. Defective neuronal migration is observed in the cerebral cortex in nesprin-2 knockout mice and double knockout of nesprin-1 and nesprin-2 gives rise to a more severe phenotype of neuronal migration [115]. Consistently, besides neuronal defects, mouse knockouts of nesprin-1 present disrupted nuclei organization in muscle fibers and decreased capacity for exercise [120, 121]. Similarly, mice ablated for both nesprin-1 and nesprin-2 in the myocardium exhibit early onset cardiomyopathy with nuclear morphology alterations [122].

Nesprin-3 is expressed in many cells and tissues. It localizes to the ONM and recruits plectin to the NE when expressed ectoptically. Through its interaction with plectin, which binds intermediate filaments [123], nesprin-3α mediates interactions of the nucleus with intermediate filaments. The other splice form, nesprin-3β, lacks plectin binding. Less keratin is associated with the NE when nesprin-3 loss-of-function mutant variant is expressed in zebrafish basal epidermal cells [124]. In human aortic endothelial cells, nesprin-3 abandantly expressed and localizes to the nuclear envelope. It is required for flow-induced polarization and migration in the endothelial cells [125]. Nesprin-3 has also been implicated in an unusual form of 3D migration, termed lobopodial migration, where the nucleus acts as a piston to pressurize the

leading lamella [126]. However, nesprin-3 null mice are viable and fertile and no overt phenotype is observed [86].

Nesprin-4 is expressed mainly in hair cells of the cochlea and in secretory epithelial cells including mammry tissue, salivary glands and exocrine pancreas [41, 87]. It localizes to the ONM and forms a complex with both kinesin-1 heavy chain Kif5B and light chain KLC1 [87]; later evidence indicates that nesprin-4 contains the KLC binding LEWD motif [114]. The distance bewteen the nucleus and centrosome increases when nesprin-4 is ectopically overexpressed, suggesting that the nucleus behaves as a kinesin cargo and moves away from the centrosome. Similar to nesprin-3 null mice, nesprin-4 null mice are also viable and fertile with no overt defects observed in secretory epithelia [41]. However, sensory cells are lost in the cochlea with concomitant loss of hearing in nesprin-4 null mice. The normal basally positioned nuclei in outer hair cells are disrupted in nesprin-4 null mice where they position instead toward the cell apex [41].

LRMP (lymphoid-restriced membrane protein)/Jaw1 was identified in lymphocytes and is localized on the cytosolic site of the ER membrane [127]. The C-terminus of LRMP is homologous to the KASH domain and its zebrafish paralogue *futile cycle* is implicated in pronuclear fusion [128]. Besides the N-terminal domain of *futile cycle* is homologous to the N-terminal domain of vertebrate KASH5 [78]. KASH5 contains a bona fide KASH domain and is mainly expressed in developing spermatocytes where it forms a functional LINC complex with SUN1. This LINC complex connects the end of telomeres to dynein to contribute to synaptic chromosome movements during meiosis [78, 129]. In KASH5 disrupted mice, developing sperm do not progress beyond the spermatocyte stage and arrested in prophase I of meiosis [78].

KASH5 null mice are viable, but sterile in both males and females, suggesting that it plays a role in both germ cells.

Anchorage of LINC complexes

In order to move and position the nucleus, the LINC complex needs to be anchored properly in the NE such that it can transmit force to the nucleus. While it is still unknown what anchors the LINC complex in different cellular contexts, lamins and chromatin may be important for this process. Lamins contribute to the nucleoplasmic achorage of the LINC complex. The C-terminus of lamin A binds to SUN proteins [14, 15]. Both SUN1 and SUN2 are more diffusive in cells depleted with A-type lamin [76]. Disruption of lamin in either mouse fibroblast [35] or worm hyp7 cells leads to abnormal nuclear movement [130]. However, in mammlian cells lacking A-type lamins, SUN1 is still localized to the INM properly and SUN2 is minimally localized to the ER in a small population of cells [14, 15, 131], suggesting there are other proteins affecting the anchorage of SUN proteins.

Chromatin-related proteins have been suggested to anchor the LINC complex in meiotic cells. In worms, specific pairing center proteins connect chromosomes and LINC complexes composed of SUN1/Matefin and ZYG-12, which in turn binds dynein [67]. In mice, the meiosis-specific protein CCDC79/TERB1 binds to telomeres, via telomere DNA and the telomeric protein TRF1, and recruits cohesin to hold the sister telomeres together [132, 133]. This structure may anchor the LINC complex because TERB1 is found to interact with SUN1, which forms a functional LINC complex with KASH5. This telomere-associated anchoring of the LINC complex also engages with dynein, as well as dynactin to mediate meiotic chromosome

movement [129]. Further, SUN2 is observed to localize in telomeric sites tethered at the NE, but may be dispensable for meiosis [134].

Mechanisms for Nuclear Positioning in Migratory Systems

Two processes contribute to a specific nuclear positioning: nuclear movement/migration and nuclear anchorage. Although there are cases where both seem to contribute, the relationship between the two processes is unclear. *C. elegans* mutant alleles of the anchorage defective 1 (*anc*-1) gene were discovered in which nuclei, as well as mitochondria, in the syncytial cytoplasm of hypoderm cells float freely [135]. ANC-1 was later identified as a KASH protein containing a conserved KASH domain, residing on the ONM and binding to actin filaments through CH domains [82]. Subsequently, SUN proteins were identified as proteins in the INM that form a complex with KASH proteins. This complex was named LINC complex [14, 15]. Since this initial description, much has been learned about the LINC complex and the current state of the field is described in the next two sections

Over the past decade, the LINC complex has been found to participate in many contexts of active nuclear movement. In the Gundersen lab, we have identified the molecular pathway contributing to rearward nuclear positioning in wound edge, serum-starved fibroblasts and myoblasts [1, 136]. This movement occurs independently of cell migration and polarizes the cell for migration. In this system, lysophosphatidic acid (LPA), a component of serum, triggers actin-dependent rearward nuclear movement while separately activating a dynein and MT-dependent process that maintains the centrosome in the cell centroid. Nuclear movement is driven by actin-myosin II retrograde flow and regulated by the Cdc42 GTPase through its effector MRCK, which phosphorylates and activates myosin II ([1] and Figure 1.1). This retrograde flow moves the nucleus through the attachment of dorsal actin cables to the nuclear membrane through KASH protein nesprin-2G and SUN protein SUN2. These proteins assemble into linear structures aligned with the actin cable and have been named as TAN lines [3]. Depletion of

nesprin-2G from cells abolishes TAN line formation and nuclear movement; whereas depletion of SUN2 allows nesprin-2G TAN line formation but these do not anchor to the nucleus, preventing its movement [3, 35]. Fibroblasts lacking lamin A/C or emerin or expressing Emery–Dreifuss muscular dystrophy (EDMD) variants of lamin A/C or emerin also exhibit defective nuclear movement with the same TAN line slipping phenotype [35, 136].

The LPA-stimulated rearward movement of the nucleus in wounded fibroblast monolayers explains how centrosome orientation is established at the onset of cell migration. However, it provides little information about how nuclear position is maintained during cell migration. In fact, relatively little is known about nuclear positioning during migration of traditional cells used to study migration such as fibroblasts and endothelial cells. The role of actin and myosin in positioning nuclei in migrating fibroblasts has not extensively been studied. Actomyosin tension from lamellipodial protrusion has been suggested to pull the nucleus forward in migrating fibroblast [137]. And myosin II contraction in the cell rear has been implicated in forward movement of the cell body forward during migration [138]. Dynein and its aforementioned regulator LIS1 have been implicated in fibroblast migration, even after centrosome reorientation and it may be that dynein is needed to pull the nucleus toward the centrosome, which leads the nucleus and tracks the cell centroid in 2D crawling fibroblasts and endothelial cells. In fibroblasts where dynein or its regulator dynactin are disrupted, the nucleus is located even further toward the rear [139]. A similar model is more established in migrating neurons. Neurons use a “two-stroke” mechanism for migration in which the centrosome first moves out into the advancing leading process, followed by the forward movement of the nucleus (and cell body) toward the centrosome [140, 141]. Dynein and LIS1 have been implicated in the forward movement of both the centrosome and the nucleus during neuronal cell migration [142].

Myosin-dependent contraction behind the nucleus may also contribute to the movement of the nucleus in migrating neurons [143]. Myosin-II inhibitor blebbistatin blocks nuclear movement in live brain slices [144]. Nesprin-2 and SUN1/2 have been implicated in neuronal migration in mouse knockout studies. Here the nucleus fails to move toward the centrosome, which seems to move forward normally [115]. As nesprin-2 was found to interact with dynein and kinesin 1, it maybe that the binding of these motors to the nucleus contributes to its movement in this system. In other systems, MTs have also been proposed to contribute to nuclear movement in at least three ways: 1) pushing forces generated by polymerization of antiparallel MT bundles in fission yeast [145] and pushing forces generated by growing MTs in fly oocyte [146]; 2) pulling forces through MT motor proteins or MT depolymerization in budding yeast [147]; 3) tracks for the nucleus to travel using MT motor proteins in secretory epithelial cells through nesprin-4 and kinesin 1 interaction [87].

Non-LINC dependent pathways to move the nucleus have also been found in several studies. During nuclear movement in radial glial progenitor cells, dynein can be recruited to the nucleus in two subsequent G2-specific pathways independent of LINC complexes [148]. To be specific, the nucleus first recruits dynein through nucleoporin protein RanBP2 interacting with BicD2, which in turn recruits dynein/dynactin components to the nucleus [149]; then another nucleoporin protein Nup133 recruits CENP-F, activating NudE/NudEL dependent dynein recruitment onto the nucleus [150]. Interestingly, artificially targeting dynein to the nucleus in cells silenced with aforementioned factors, defects in both nuclear migration and cell-cycle progression are rescued [148]. However, it is still unknown whether the LINC complex plays a role in other nuclear movements during neuronal migration. Besides, actomyosin and intermediate filaments dependent nuclear movement can also be LINC independent -- in

astrocyte nuclear movement, cytoplasmic intermediate filaments are required for nuclear positioning in an actin-dependent fashion while overexpressing dominant negative KASH construct does not affect the usual nuclear off-center positioning [34].

Other Functions of LINC Complexes

While LINC complexes can engage with the cytoskeleton to regulate nuclear positioning in the cytoplasm, they also affect cellular motility events happening in the nucleoplasm. As I discussed earlier about the anchorage of the LINC complexes, studies from meiotic cells suggest that LINC complexes can transmit force generated from dynein/MTs to chromosomes.

However it is unclear how the LINC complex in meiotic cells is able to transmit force to chromosomes, rather than to the nuclear lamina. Although the amount and direction of the force on either chromatin- or lamina- dependent LINC complex is unknown, there are at least two possibilities consistent with current studies in the field. One is that LINC complex components are post-translationally regulated. In *C. elegans*, checkpoint kinase CHK-2 phosphorylations of Ser/Thr in the nucleoplasmic region of SUN-1 have been observed in meiosis and are important for meiotic chromosome movements [151]. These phosphorylation could contribute to the more mobile LINC complex observed at the onset of the worm meiosis [152]. The other possibility is the modification of the lamina itself. Meiotic-specific A-type lamin, lamin C2, localizes to the LINC complex-mediated telomere tethering site [153]. Compared to somatic lamin C, lamin C2 lacking the N-terminal head and part of the middle alpha-helical rod domain shows higher diffusional mobility [154].

Recently, the LINC complex has been shown to be important for DNA damage repair. In the absence of SUN1/2, the mobility and nonhomologous end-joining of dysfunctional telomeres after double strand breaks are both inhibited. Similarly, nesprin-4 also contributes positively to nonhomologous end-joining of dysfunctional telomeres. A SUN1/SUN2/Nesprin-4/MTs pathway via nuclear 53BP1 (p53 binding protein) has been identified for double strand break

mobility during DNA repair [155]. In addition, silencing SUN1 inhibits mRNA export in mammalian cells and SUN1 is suggested to involve in the recruitment of the nuclear RNA export factor 1 (NXF1)-containing mRNP particles onto the nuclear envelope [156].

Physical Ways to Manipulate the Nucleus

To date, almost all studies of the mechanism of nuclear positioning and its possible role have relied on molecular perturbations such as knockdown or mutation of molecular components. Because it is difficult to prove that the disrupted molecules *only* function in nuclear movement, it has remained hard to know whether nuclear positioning per se has a direct role in cellular behavior. One approach to address this issue would be to physically displace the nucleus by force. Centrifugation has been used, to enucleate anchorage-dependent cells [157] and to displace displace organelles, including the nucleus in non-adherent cells [31, 158]. I developed a centrifugation approach to displace nuclei as part of my thesis (Chapter 3).

There are other ways to exert force on the nucleus within cells including microneedle pulling or pushing the nucleus [159] and using air bubbles to apply a hydrodynamic drag to cells under shear flow [160]. However, these techniques either are limited to local displacements in single cells (microneedle) or involve applying less controllable force to the cell.

Nonetheless, these techniques do support the idea that the nucleus is under force in most cells. In cells where the nucleus has been manipulated by microneedles, displacement and deformation of the nucleus is observed [159]. In shear flow, endothelial nuclei are slightly moved due to a hydrodynamic drag caused by an air bubble preceding planar cell polarity establishment [160]. In my thesis, I contributed to a study using a FRET sensor based on mini-nesprin-2G and a tension element composed of a 40 amino acid elastic domains first used in the vinculin tension sensor [161]. The FRET index of this construct is higher when the sensor loses connection to actin cytoskeleton, i.e. not under actin-dependent force and lower when the construct is under force by the actin cytoskeleton. This tension sensor was used to show that

nuclei in NIH3T3 fibroblasts were under constant tension (low FRET) because when actin or myosin were inhibited tension was reduced (high FRET) [162]. Thus, a number of approaches suggest that the nucleus is under constant tension.

That force can alter nuclear biology was shown by an elegant study by Guilluy and Burridge [163]. They applied force on isolated nuclei with magnetic beads coated with nesprin-1 antibody. They showed that nuclei get stiffer under cyclic force and that this activates Src kinase, tyrosine phosphorylation and Rho GTPase within the isolated nuclei [163]. This argues that the nucleus (and the LINC complex) can respond to force by activating signaling molecules within the nucleus. Hence, the nucleus acts as a *bona fide* mechanochemical transducer.

Figures

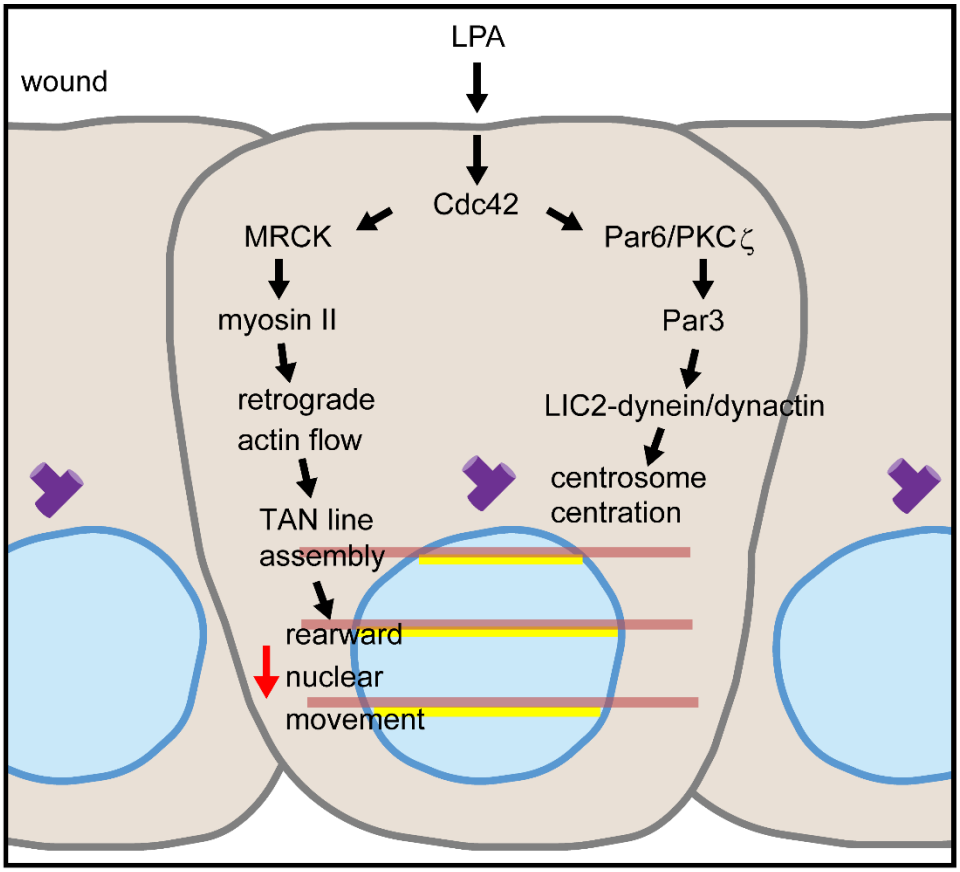

Figure 1.1* Two Cdc42-regulated pathways lead to centrosome/MTOC reorientation.

* This figure is reproduced from a manuscript by Zhu, Liu and Gundersen. *Seminars in Cell and Developmental Biology*, in submission (2017)

LPA activates Cdc42 GTPase to regulate separate actin- and MT-dependent pathways that result in centrosome/MTOC reorientation. Purple "T" is the centrosome. Based on work in [1, 2, 164].

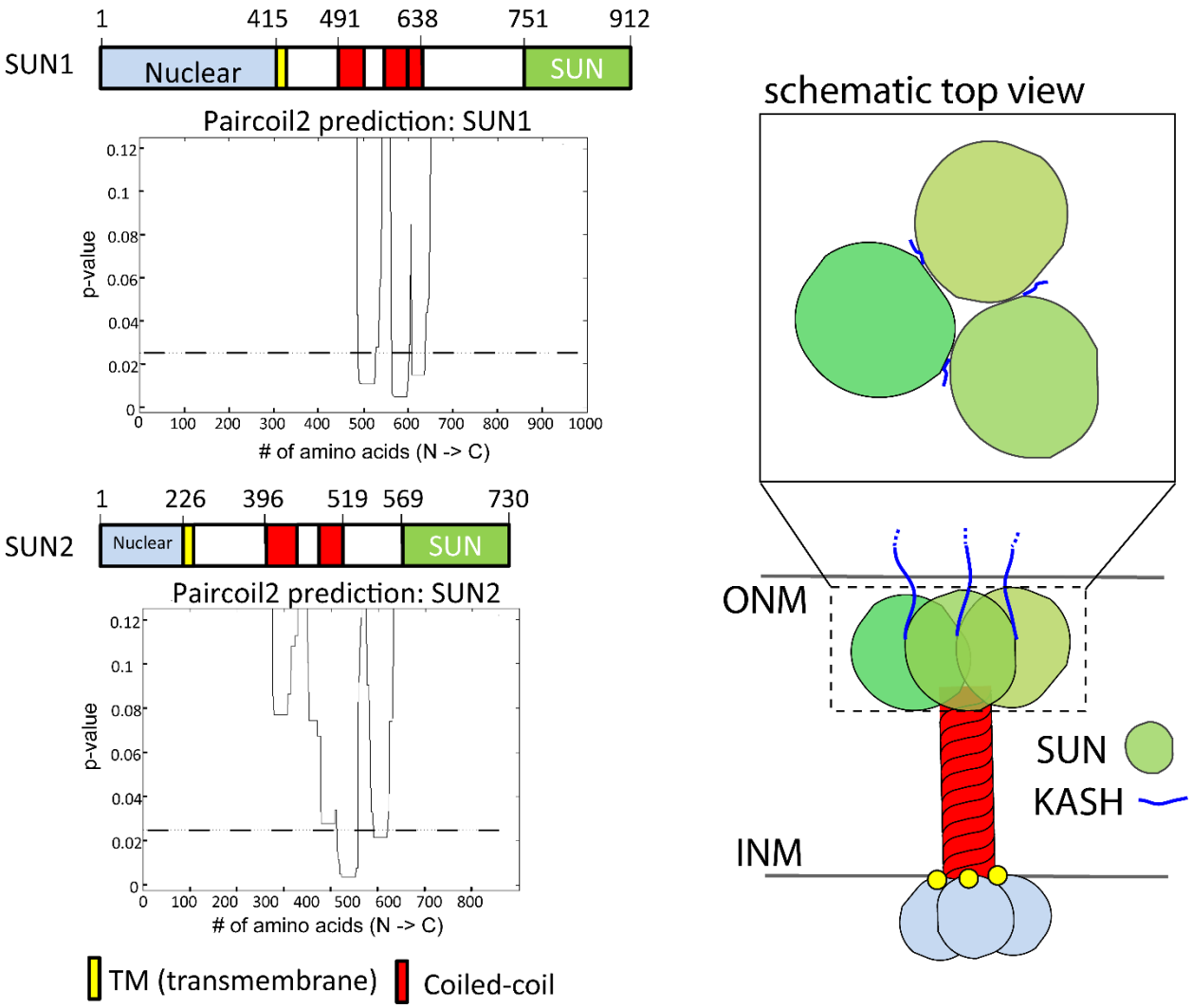

Figure 1.2 Schematic representation of mouse SUN1/2 with their predicted coiled-coil domains and schematic structure of SUN/KASH interaction

Left: Domain structure and predicted coiled-coil regions of mouse SUN1 and SUN2, generated by Paircoil algorithm[165] (http://cb.csail.mit.edu/cb/paircoil2/). Peaks that exceed the threshold (dotted line, p-value: 0.025) are predicted to be coiled-coil domains. Right: Schematic structure of SUN2/KASH interaction. The KASH-lid is in the SUN domain and forms covalent bond with KASH peptide.

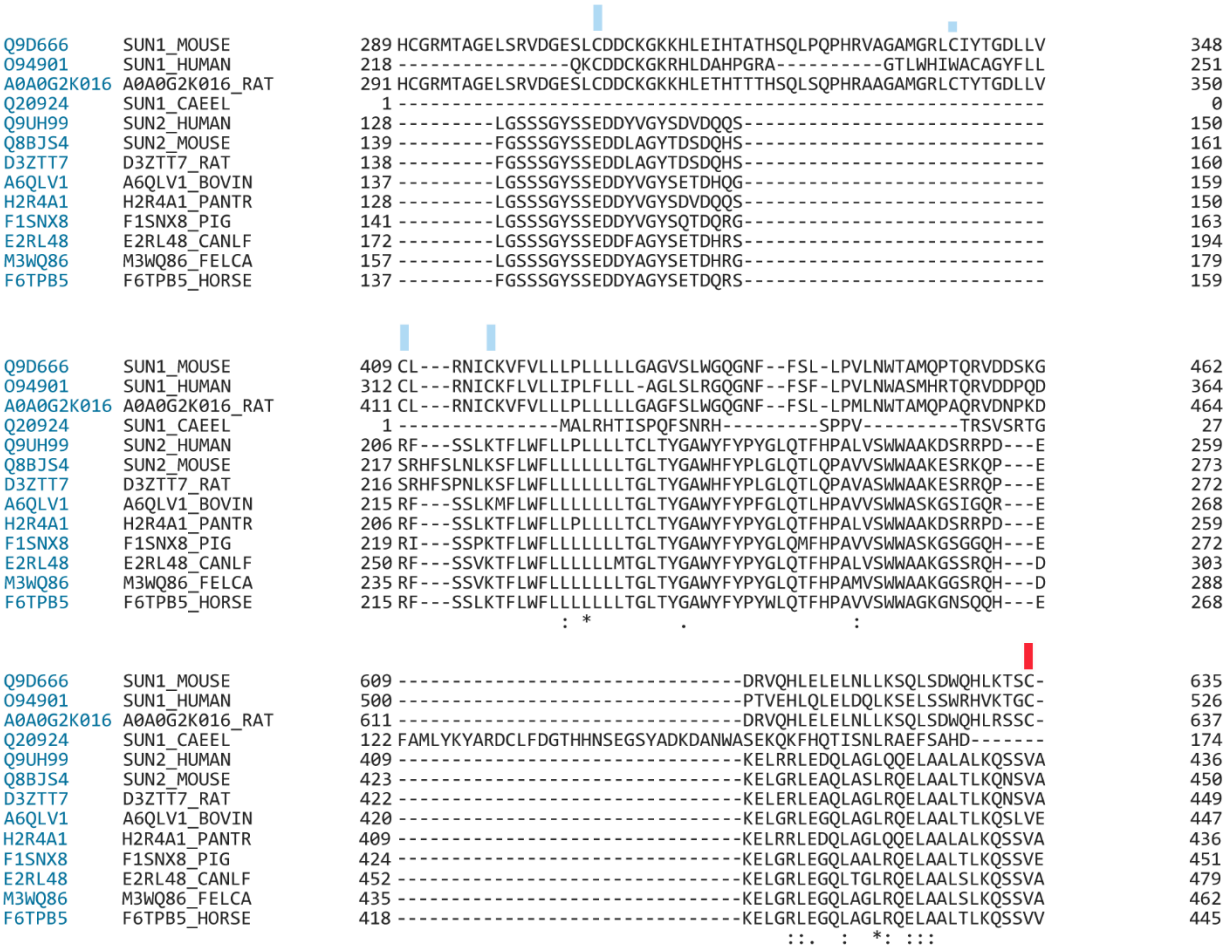

Figure 1.3 Sequences comparison for the N-terminal domains of SUN1 and SUN2

Shown are the alignments of SUN 1 and SUN2 from online Uniprot alignment program. Putative conserved cysteine residues specific to SUN1 are marked with rectangles. Blue rectangles represent sequences in the nucleoplasm and red rectangles in the nuclear lumen. The blue square represents a murine specific cysteine. Q9D666: *Mus musculus* SUN1; O94901: *Homo sapiens* SUN1; A0A0G2K016: *Rattus norvegicus* SUN1; Q20924: *Caenorhabditis elegans* SUN1; Q9UH99: *Homo sapiens* SUN2; Q8BJS4: *Mus musculus* SUN2; D3ZTT7: Rattus norvegicus SUN2; A6QLV1: *Bos Taurus* SUN2; H2R4A1: *Pan troglodytes* SUN2; F1SNX8: *Sus scrofa* SUN2; E2RL48: *Canis lupus familiaris* SUN2; M3WQ86: *Felis catus* SUN2; F6TPB5: *Equus caballus* SUN2.

Chapter Two: FHOD1 Interaction with Nesprin-2G Mediates TAN Line Formation and Nuclear Movement

This chapter is reproduced from:

FHOD1 interaction with nesprin-2G mediates TAN line formation and nuclear movement
Stefan Kutscheidt*, **Ruijun Zhu***, Susumu Antoku*, G.W. Gant Luxton, Igor Stagljar, Oliver T. Fackler and Gregg G. Gundersen. * These authors contributed equally to this work
Nature Cell Biology, 16(7):708-15. (2014)

In this project, I contributed data for Figure 2b-2h, Figure 3, Figure 4b-4c, Figure 5, Supplement Figure 4 and Supplement Figure 6.

Abstract

Active positioning of the nucleus is an integral part of division, migration, and differentiation of mammalian cells [11]. Fibroblasts polarizing for migration orient their centrosomes by nuclear movement via an actin-dependent mechanism [1]. This nuclear movement depends on nesprin-2 giant (N2G), a large, actin-binding outer nuclear membrane component of transmembrane actin-associated (TAN) lines that couple nuclei to moving actin cables [3]. Here, we identify the diaphanous formin FHOD1 as an interaction partner of N2G. Silencing FHOD1 expression or expression of fragments containing binding sites of N2G or FHOD1 disrupted nuclear movement and centrosome orientation in polarizing fibroblasts. Unexpectedly, silencing of FHOD1 expression did not affect the formation of dorsal actin cables required for nuclear positioning or their rearward flow. Rather, N2G-FHOD1 interaction provided a second connection to actin cables essential for TAN line formation and thus nuclear movement. These results reveal a unique function for a formin in coupling an organelle to actin filaments for translocation and suggest that TAN lines require multi-point attachments to actin cables to resist the large forces necessary to move the nucleus.

Introduction

Diaphanous related formins (DRFs) constitute a family of Rho GTPase regulated proteins that regulate the actin and microtubule cytoskeletons, thereby affecting multiple and diverse cellular processes [166, 167]. Most DRFs stimulate the nucleation and/or elongation of linear actin filaments required for building structures such as filopodia, lamellipodia and contractile rings. Despite similar domain organization and high sequence homology to other formins, the DRF FHOD1 does not display detectable actin nucleation or elongation activity but rather bundles them [168]. This bundling activity of FHOD1 requires a novel actin binding region in the N-terminal regulatory region as well as dimerization mediated by the FH2 domain [168]. Consistent with the biochemistry, expression of a constitutive active FHOD1 (FHOD1 ΔC) variant lacking the C-terminal autoinhibitory domain in cells induces the formation of thick actin cables that are decorated by the formin, another property that distinguishes FHOD1 from other DRFs [169]. While recent reports imply that FHOD1 is hijacked during infection by various pathogens [170, 171] and contributes to adhesion maturation [172], cellular functions of endogenous FHOD1 remain largely unexplored.

Results

Since our previous results indicated that (i) the structure and protein interactions of the FHOD1 N-terminus are distinct from other DRFs [173] and (ii) this domain is essential for actin cable formation by FHOD1 ΔC [169, 174], we sought to identify binding partners of the N-terminal domain to generate clues towards the physiological role of FHOD1. A yeast two-hybrid screen using residues 1-339 of human FHOD1 as bait identified residues encompassing 1340-1678 of human N2G as an interaction partner (Fig. 2.1a). Consistent with this interaction, GST-N2G 1340-1678 but not GST alone pulled down HA-tagged FHOD1 1-339 from HEK293T cell lysates (Fig. 2.1b). Specific binding to GST-N2G 1340-1678 was also observed with HA-FHOD1 WT and with HA-FHOD1 ΔC (residues 1-1109). Importantly, HA-FHOD1 WT also immunoprecipitated with full length endogenous N2G (Fig. 2.1c).

To further map the FHOD1 binding site in N2G, a series of fragments spanning the entire length of mouse N2G was tested by yeast two-hybrid for interaction with FHOD1 1-339. This mapping revealed that fragment H (residues 1130-1724), which encompasses the region identified in the original yeast two-hybrid screen, was the only region of N2G that interacted with FHOD1 1-339 (Fig. 2.1d). Fragments containing the C-terminus of FHOD1 (either 340-1169 or 570-1164) did not interact with the H fragment or the adjacent I or J fragments, the latter of which contains the N2G actin-binding calponin homology (CH) domains (Supplementary Fig. 2.S1a-c). A N2G construct containing the H fragment efficiently coimmunoprecipitated with HA-FHOD1 WT when coexpressed in 293T cells (Supplementary Fig. 2.1d).

These results identify a previously unrecognized association of FHOD1 with N2G mediated by the N-terminus of FHOD1 and a site in N2G spanning residues 1340-1678. This region of N2G spans three predicted spectrin repeats (SRs 10-12) and part of a fourth (SR13). Interestingly, SRs 11-13 were previously identified in a phylogenetic comparison as the second most evolutionary conserved set of spectrin repeats in N2G [175, 176]. Direct sequence alignment of these repeats reveals a higher degree of sequence conservation (28-54%) than the ~20% conservation that is generally observed between unrelated SRs (ref: [175, 176] Fig. 2.1e, Supplementary Fig. 2.1e). Consistent with a specialized function of the FHOD1 interacting region in N2G, the region is not conserved in nesprin-1G [175, 176]. To identify specific N2G SRs involved in interaction with the N-terminus of FHOD1, we used GST-tagged fragments of N2G containing single, double and triple SRs spanning SRs 10-13 to pull down HA-FHOD1 1-339 expressed in HEK293T cells. This analysis showed that fragments of N2G containing SRs 11-12 associated with FHOD1 1-339, while individual SRs did not associate (Fig. 2.1e). This identifies SRs 11-12 of N2G as the interaction site for FHOD1.

N2G is a ~800 kDa outer nuclear envelope protein essential for nuclear movement and thus centrosome orientation in migrating fibroblasts [3]. In contrast to many nuclear movements that are dependent on microtubules, N2G mediates actin-dependent nuclear movement in starved fibroblasts stimulated by lysophosphatidic acid (LPA) or serum. We tested whether FHOD1 is involved in N2G functions in LPA-stimulated nuclear movement/centrosome orientation by reducing its expression in NIH3T3 fibroblasts with four different siRNAs (Supplementary Fig. 2.2). Expectedly~ 60% of control cells treated with control siRNA (to GAPDH) displayed centrosome orientation towards the wound edge (Fig. 2.2a,b). In contrast, reduction of FHOD1

expression by each of the four siRNAs reduced centrosome orientation to about 35%, the level observed in unstimulated cells [177]. LPA-stimulated centrosome orientation results from active actin-dependent rearward movement of the nucleus while microtubules maintain the centrosome at the cell centroid [1]. Analysis of nuclear and centrosome positions revealed that FHOD1 depletion blocked rearward nuclear positioning without affecting the position of the centrosome (Fig. 2.2c). Centrosome orientation and nuclear movement in FHOD1 depleted cells were rescued by re-expression of full length FHOD1 WT or constitutively active FHOD1 ΔC, but not by FHOD1 340-1164 lacking the N2G interacting region (Fig. 2.2d-f). Consistent with the critical role of nuclear positioning for fibroblast wound closure, the migration of NIH3T3 cells into wounds was significantly reduced upon FHOD1 depletion (Fig. 2.2g,h). These results indicate that FHOD1 is required for actin-dependent nuclear movement and suggest that the interaction with N2G is important for this function.

To test directly whether FHOD1-N2G interaction was required for centrosome orientation and nuclear movement, we expressed the interacting regions of FHOD1 or N2G in starved NIH3T3 fibroblasts before stimulating them with LPA. Importantly, expression of the N2G H fragment containing SRs 11-12 that interact with FHOD1 potently disrupted LPA-stimulated centrosome orientation and rearward nuclear positioning in wound edge NIH3T3 fibroblasts (Fig. 2.2i-k). Similarly, FHOD1 1-339, which localizes to the nucleus as well as the cytoplasm [173] and interacts with N2G, also acted as a dominant negative of these processes (Fig. 2.2i-k). We conclude that the interaction of FHOD1 with N2G is essential for centrosome orientation and rearward nuclear movement.

In NIH3T3 fibroblasts, actin-dependent nuclear movement is mediated by the assembly of N2G containing TAN lines that couple the nucleus to dorsal actin cables [3]. As reported earlier [3], LPA-stimulated NIH3T3 fibroblasts treated with scrambled siRNA rapidly developed dorsal actin cables over the nucleus (Fig. 2.3a,c). Despite efficient prevention of centrosome orientation and nuclear movement (Fig. 2.2b,c), silencing of FHOD1 expression had no appreciable effect on LPA-induced dorsal actin cables as measured either by their numbers over the nucleus or the total intensity of nuclear or cytoplasmic phalloidin fluorescence (Fig. 2.3b-e). A similar lack of effect on dorsal actin cables was observed with FHOD1-silenced NIH3T3 fibroblasts stimulated with serum, even though FHOD1 silencing blocked serum-stimulated centrosome orientation (Supplementary Fig. 2.3). Importantly, LPA-stimulated retrograde actin cable flow, which is required for nuclear movement [1, 3], was unaffected by depletion of FHOD1 (Fig. 2.3f,g). FHOD1 is thus not essential for dorsal actin cable formation or retrograde flow during nuclear movement.

Nuclear movement in NIH3T3 fibroblasts also depends on the assembly of N2G along dorsal actin cables to form TAN lines that couple the nucleus to moving actin cables. To test for a potential role of FHOD1 in TAN line formation, we first investigated whether FHOD1 localized to these structures. Because antibodies for localizing FHOD1 under conditions that preserve TAN lines are unavailable, we localized expressed RFP-FHOD1 constructs. Simultaneous visualization of N2G TAN lines by expression of GFP-mini-N2G (GFP-mN2G) or anti-N2G antibody and RFP-FHOD1 WT or ΔC revealed that FHOD1 was associated with dorsal actin cables and colocalized with TAN lines (Fig. 2.4a; Supplementary Figure S4a). Importantly, in cells lacking FHOD1 expression, TAN line formation was strongly suppressed as assessed by

either expressing GFP-mN2G or staining endogenous N2G, even though dorsal actin cables were evident over the nucleus (Fig. 2.4b,c and Supplementary Fig. 2.4b,c). These results indicate that FHOD1 is a component of TAN lines and is required for their formation.

FHOD1 has two actin interacting domains: one in its FH2 domain that appears to bind actin barbed ends and one in its N-terminus (residues 340-569), termed N-terminal actin binding site (ABS), that is required for FHOD1 to decorate actin cables; both sites are required for FHOD1's actin bundling activity [168, 178]. Above, we showed that FHOD1 1-339 containing the N2G binding site but lacking the N-terminal ABS inhibited nuclear positioning required for centrosome orientation (Fig. 2.2g-i). To test the requirement of the N-terminal ABS for FHOD1 function in nuclear positioning, we expressed FHOD1 1-569, which contains the N2G interacting site and the N-terminal ABS (Fig. 2.5a), in FHOD1-depleted cells. FHOD1 1-569 completely rescued centrosome orientation and partially rescued rearward nuclear positioning (Fig. 2.5b-d). These results were surprising because they suggested that the formin's FH2 domain was not absolutely required for rearward nuclear movement. To test this further, we prepared a chimeric construct (NCH, Fig. 2.5a) composed of the N2G interacting site in FHOD1 (1-339) and the well-characterized, actin-binding CH domains of α-actinin. Strikingly, NCH rescued centrosome orientation completely and rearward nuclear positioning partially when expressed in FHOD1-depleted cells (Fig. 2.5b-d). No rescue of these parameters was observed in FHOD1 silenced cells when the CH domains of α-actinin were expressed alone (Fig. 2.5a-d). Critically, both FHOD1 1-569 and the NCH chimera colocalized with dorsal actin cables above the nucleus (Fig. 2.5e). Coupled with our earlier results that the N2G binding fragment of FHOD1 (1-339) alone acted as a dominant negative (Fig. 2.2i-k), these results establish that the N-terminal N2G

interacting site and ABS is the minimal domain of FHOD1 required for centrosome orientation and rearward nuclear positioning.

It was surprising that the FH2 domain, which defines formins, was apparently not required for centrosome orientation and nuclear positioning. Yet, both FHOD1 1-569 and the chimera NCH, did not fully rescue nuclear positioning. To test if the FH2 domain might contribute to this function, we conducted rescue experiments in FHOD1-depleted cells with a full length FHOD1 construct containing a point mutant (FHOD1 I705A, Fig. 2.5a) in a conserved residue in the FH2 domain that governs actin activity by DRFs [179]. In constitutively active FHOD1 ΔC, the I705A mutation prevented the normal stimulation of actin cable assembly of the WT protein (Supplementary Fig. 2.5; also see ref 7). FHOD1 I705A rescued centrosome orientation but only partially restored rearward nuclear positioning (Fig. 2.5b-d), suggesting that for full rearward nuclear positioning, both the N-terminal ABS and the FH2 domain are required.

Discussion

The previous model for TAN lines [3, 180] hypothesized that the nucleus and the overlying dorsal actin cables are solely connected by the CH domains of N2G. Our current data support a new model in which the soluble, cytoplasmic protein FHOD1 plays an essential role in linking the outer nuclear membrane protein N2G to actin cables (Fig. 2.5f). This model posits that FHOD1 acts to enhance the interaction between N2G and the actin cable by providing N2G with a second physical link to actin. One end of FHOD1 (residues 1-339) establishes a connection to N2G by binding to SR11-12 that are unique to N2G; the other end of FHOD1's N terminus (residues 340-569) interacts with the actin cable through its N-terminal ABS (residues ~400-530, ref: [168, 178]). We propose that the N-temrinal ABS is critical for forming TAN lines as constructs lacking this site did not rescue FHOD1 depletion and a FHOD1 construct containing only the N2G binding site was dominant negative for nuclear movement. Additionally, a FHOD1 construct that contained both the N2G interaction site and the N-terminal ABS fully rescued centrosome orientation and largely rescued nuclear movement, as did a chimeric construct containing FHOD1's N2G-interacting domain and the actin binding CH domains from α-actinin.

Our model has new implications for how N2G connects to dorsal actin cables during nuclear movement. We previously showed that the actin binding ability of N2G's CH domains was essential for formation of TAN lines [3]. Our current data stress that the actin binding capability of FHOD1 is also necessary for N2G to form TAN lines and move the nucleus. This implies that a multivalent connection between the nesprin and the actin cable may be required to resist the force generated by moving such a large organelle as the nucleus. Such a role for

FHOD1 may be analogous to that played by the multiple actin binding proteins that mediate connections between membrane integrin receptors in focal adhesions and actin filaments in stress fibers. In addition, the association of FHOD1 with N2G puts its N-terminal ABS in proximity to that of N2G and this would be expected to increase the avidity of N2G interaction with actin filaments and enhance the capture actin cables as they move over the surface of the nuclear envelope. Finally, connecting N2G to actin cables via FHOD1 may provide the possibility of regulation as interactions of the FHOD1 N-terminus with its C-terminal autoinhibitory domain or activating GTPases are likely to affect FHOD1-N2G interactions.

The multivalent feature of the model seems at odds with previous results showing that mN2G, which lacks the FHOD1 interacting site but contains CH domains, rescues TAN line formation and nuclear movement in N2G depleted cells [3]. However, since mN2G was overexpressed in these rescue studies, the high levels of CH domains available for interacting with actin cables likely compensate for the multivalent attachment through a single N2G.

A detailed structure of N2G and FHOD1 in association with actin filaments awaits higher resolution studies. Nonetheless, the extended structure of SR proteins and the conserved 5 nm length of SR repeats makes a prediction about the geometry of N2G relative to the actin filament when it is bound via its CH domains and FHOD1's N-terminal ABS. The CH domains and the FHOD1 interacting region (SRs 11-12) in N2G would be expected to be separated by as much as 50 nm. Given that the N2G-interacting site and the ABS in the N-terminus of FHOD1 likely span less than 10 nm [173], this predicts that N2G bound to actin via its CH domains and FHOD1 will lie nearly parallel to the long axis of the actin filament (as depicted in Fig. 2.5f)

rather than perpendicular as has been predicted in earlier models of N2G interaction with actin filaments [11, 181].

The involvement of FHOD1 in moving nuclei is a novel function for a formin. Most formins stimulate actin filament elongation by processively binding the barbed end of the actin filament through their FH2 domain. Although the FH2 domain of FHOD1 is highly conserved compared to other DRFs, and it behaves as if it binds to actin barbed ends, it does not seem to stimulate actin polymerization either in vitro or in cells [168]. Instead, the main biochemical activity of FHOD1 is in bundling actin filaments and binding along their length. Previous studies have shown that these activities require the unique N-terminal ABS [168, 178]. FHOD1's FH2 domain contributes to bundling activity by establishing the dimeric nature of FHOD1. Our results suggest that FHOD1's FH2 domain may not contribute directly to its activity in TAN line formation. Yet, the lack of complete rescue of nuclear movement with FHOD1 constructs bearing FH2 domain mutations or deletions does suggest that the FH2 domain plays some role, perhaps by promoting dimer formation which would additionally stabilize the TAN line structure by cross-linking adjacent nesprins.

The function we have described for FHOD1 in nuclear movement resembles that recently described for the formin INF2 in binding ER membranes and contributing to their scission by deforming them in an actin-dependent fashion [182]. There are 15 formin family members in mammals and it will be interesting to test whether other members of this family also function as proteins that mediate force transmission between the actin cytoskeleton and membranes.

Materials and Methods

Reagents. LPA was from Avanti Polar Lipids. Alexa647-phalloidin was from Invitrogen. 4',6-diamidino-2-phenylindole,dihydrochloridewas from LifeTechnologies. Unless noted, all other chemicals were from Sigma-Aldrich. Lifeact-mCherry [183] was from ibidi. HA-FHOD1 expression plasmids (WT, ΔC, 1-339, 1-569) were described earlier [169, 184]. GFP-FHOD1 constructs were made by amplifying the corresponding sequences from HA-FHOD1 and insertion into pEGFP-C2 (Clontech) using EcoRI. GFP-FHOD1I705A was made by PCR based mutagenesis. mRFP-FHOD1 WT and ΔC were made by excising the corresponding FHOD1 sequences with EcoRI from pEGFP-C2 plasmids and inserting into the EcoRI site of EF-pLINK2-FLAG-mRFP (gift from R. Grosse, Marburg). N2G1340-1678 was amplified from HeLa cell cDNA and cloned into pGEX-2TK (GE Healthcare) via SmaI restriction site. GFP-mN2G was described earlier [3]. mCherry-mN2G was prepared by inserting the mN2G sequence from GFP-mN2G into the SalI and XbaI sites of pmCherry-C1 (Clontech). The GFP-N2G H and HI fragments were prepared by PCR amplifying the corresponding regions from NIH3T3 fibroblast cDNA and inserting into the NotI site of pEGFP-C4. GFP-α-actinin CH (residues 1-269) was made by PCR amplifying it from HeLa cell cDNA and inserting the product into BamHI and NotI sites of pEGFP-C4 vector. GFP-NCH was made by fusing α-actinin CH domains to the C-terminus of FHOD1 1-339 without a linker and then inserting the chimera into BamHI and NotI sites of pEGFP-C4. All constructs were verified by sequencing.

Cell culture. NIH3T3 fibroblasts were cultured in DMEM (Corning Cellgro) plus 10 % calf serum (Hyclone or Thermo Fisher Scientific) and serum-starved for 36-48 h as previously described[185]. For centrosome orientation, wounded monolayers of starved NIH3T3 fibroblasts

were treated with 10 µM LPA in serum-free DMEM as previously described [177]. For some experiments, cDNAs (25-75 ng μl^{-1}) were microinjected into nuclei of cells at the edge of wounds and allowed to express for 1-2 h before LPA stimulation. HEK293T cells were grown in DMEM (Gibco) with 10 % FBS (Hyclone or BiochromAG).

Yeast-two hybrid screening. The initial Y2H screen that identified N2G 1340-1678 as a binding partner of FHOD1 1-339 was performed by Hybrigenics Services. FHOD1 1-339 was cloned into the Y2H bait vectors pB29 (N-bait-LexA-C fusion) and pB43 (N-bait-GAL4-C fusion) and screened against a human leucocyte/activated mononuclear cell RP1 cDNA library. In total, more than 166 million interactions were analysed and yielded 85 putative interacting clones. Among these, 20 in frame cDNA clones were isolated, of which only N2G was identified using both bait vectors.

The directed interaction screen was done using the membrane yeast two-hybrid system [186] using FHOD1 1-339 as prey and fragments along the length of N2G as bait. Mouse N2G for the baits was PCR amplified from NIH3T3 fibroblast cDNA (see Supplementary Table for sequence differences between NIH3T3 N2G sequence and that reported for mouse N2G on NCBI). Each N2G fragment was directly fused with the N-terminus of a N2G construct containing the C-terminal transmembrane domain (termed TM Base, encoding residues 6551-6892 of mouse N2G) without a linker. These N2G fragments were inserted into yeast expression vectors pBT3-N or pTLB-1 with the following restriction sites (N2G fragment/plasmid/restriction sites): TM base/pBT3-N/NcoI-SacII, A1/pBT3-N/NcoI-SacII, A2/pBT3-N/NcoI-SacII, B/pTLB-1/SacII, C/pTLB-1/SacII, D/pBT3-N/NcoI-SacII, E/pBT3-N/NcoI-SacII, F/pBT3-N/NcoI-SacII, G/pBT3-N/NcoI-SacII, H/pTLB-1/SacII, I/pTLB-1/SacII, and J/pBT3-N/NcoI-SacII. The FHOD1 prey

constructs were inserted into BamHI and EcoRI restriction sites of pPR3-N vector. Interactions were screened by growth using pOST-NubIand pOST-NubGas positive and negative and controls, respectively.

Co-immunoprecipitation and pulldown. HEK293T cells were transfected with plasmids encoding tagged proteins using polyethylenimine (Sigma-Aldrich) according to manufacturer's instructions. After 20 h, cells were lysed in 1 % Triton X-100, 25 mM Tris-HCl, pH 8.0, 2 mM EDTA, 150 mM NaCl, and protease inhibitor mix (Roche). A small aliquot of the lysate was kept as input sample. The lysate was incubated with rabbit anti-nesprin-2G or mouse anti-HA for 5 h at 4°C. Antibody complexes were recovered on protein A-Sepharose (GE Healthcare), preblocked with cell lysate from untransfected cells, and then eluted with SDS-PAGE sample buffer with boiling. Immunoprecipitates were run on NuPAGE gradient gel (Invitrogen) (for detection of endogenous N2G) or 10 % Tris-Glycine SDS-PAGE gels for co-IP with GFP-N2G HI and western blots were developed with the following antibodies: rabbit anti-N2G (1:10,000) [3], mouse anti-HA (1:500, SC-7392, Santa Cruz Biotechnology), rabbit anti-His (1:500, SC-804, Santa Cruz Biotechnology), and mouse anti-GFP (1:2000, G6539, Sigma-Aldrich).

GST-N2G1340-1678, various GST-N2G spectrin repeats, or GST proteins for pulldowns were expressed in E. coli BL21 (DE3) by induction with 1 mM IPTG. Bacteria were spun down and the pellet was resuspended in ice cold TBS, 10 mM $MgCl_2$, 1 mM DTT and protease inhibitor mix (Roche). After sonication the bacterial lysate was supplemented with 1 % Triton X-100 and incubated on a shaker for 30 minutes at 4°C. After centrifugation, the cleared supernatant was incubated with glutathione-Sepharose (GE Healthcare) for 3 h to bind GST or GST-tagged N2G proteins. Following washing, 10 % glycerol was added and the Sepharose suspension was

aliquoted, quick frozen in liquid nitrogen and stored at -80°C. For pulldowns, HEK293T cells were transfected with HA-tagged FHOD1 WT, FHOD11-339 or FHOD1ΔC using Lipofectamine 2000 (Life Technologies). Cells were lysed in 1 % Triton X-100, 25 mM Tris-HCl, pH 8.0, 2 mM EDTA, supplemented with 50 mM NaCl (for HA-FHOD1-1-339) or 100 mM NaCl (for FHOD1 WT and ΔC). After clearing, lysates were incubated for 4 h at 4°C with GST- or GST-N2G 1340-1678 Sepharose that had been preblocked with cell lysate from untransfected cells. After washing with lysis buffer supplemented with 50, 100 or 150 mM NaCl for HA-FHOD1-1-339, FHOD1 WT and HA-FHOD1 ΔC, respectively, bound proteins were eluted with SDS sample buffer, boiled, and analysed by western blotting with mouse anti-GST (1:1000, SC-138, Santa Cruz Biotechnology) and mouse anti-HA (1:500, SC-7392, Santa Cruz Biotechnology). For pulldown of HA-tagged FHOD1 1-339 with various GST-N2G spectrin repeats constructs, HEK293T cells were transfected with HA-tagged FHOD1 1-339 by calcium phosphate. Two days after transfection, cells were lysed in 1 % Triton X-100, 25 mM Tris-HCl, pH 7.4, 150 mM NaCl, 5 mM EDTA, 1 mM Na_3VO_4, 1 mM NaF, 10% glycerol, and protease inhibitor mix (Roche). After clearing, lysates were incubated for 2 h at 4 °C with GST or GST fused with various N2G spectrin repeats immobilized on Sepharose. After washing with the lysis buffer, bound proteins were eluted with SDS sample buffer, boiled, and analysed by coomassie brilliant blue staining or western blotting with rabbit anti-HA (1:1000, H6908, Sigma-Aldrich). Western blot membranes of GST- and immunoprecipitates were developed with ECL signal enhancer (Thermo Scientific) to enhance the sensitivity of signal detection.

siRNA Knockdown. Duplex siRNAs (21-mers) were purchased from Shanghai GenePharma. The sequences used for FHOD1 were: FHOD1-1, 5’ GAGCGGUCCUAGAGCCUUATT 3’; FHOD1-

2, 5' GGGCGGAAGCCCACGUUAATT 3'; FHOD1-3, 5’ CCAGUAUUGUGAACAGUAUTT 3’; FHOD1-4, 5’ UACCAGAGCUACAUCCUUAUU 3’ and that for GAPDH was 5′ AAAGUUGUCAUGGAUGACCTT 3′ as predicted by BIOPREDsi. Noncoding siRNA was used as a control in some experiments. Transfection with Lipofectamine RNAiMAX (Invitrogen) was carried out according to the manufacturer’s instructions. Efficiency of protein depletion was determined by western blot analysis of total cell lysates using rabbit anti-FHOD1 antibody at 1:500[187].

Immunostaining. Cells on coverslips were fixed with either 4 % paraformaldehyde in PBS for 10 min followed by permeabilization with 0.1 % Triton X-100 in PBS for 3 min or -20 ° C methanol for 5 min. Fixed cells were stained with the following antibodies: rabbit N2G 1:100 [3], rabbit anti-pericentrin (1:400, PRB-432C, Covance), rat anti-Tyr tubulin (1:40, YL1/2 European Collection of Animal Cell Cultures), chicken anti-GFP (1:100, AB16901, EMD Millipore). Rhodamine-phalloidin (1:200, A12379, Invitrogen) was used to stain F-actin. Stained cells were mounted in Vectorshield (Invitrogen) or Fluoromount-G (Southern Biotech). Images were acquired with either 40X Planapo (NA1.0) or 60X Planapo (NA1.4) objectives and a CoolSNAP HQ CCD camera on a Nikon TE300 inverted microscope controlled by Metamorph (Molecular Devices) and processed with ImageJ (NIH) or with 60X or 100X Planapo objectives and a Olympus U-CMAP3 camera on an Olympus IX81 microscope controlled by CellM Olympus software.

Centrosome reorientation and nuclear movement assays and data analysis. Centrosome orientation to a position between the nucleus and the leading edge was analysed as previously described using cells immunofluorescently stained for pericentrin, Tyr tubulin and nuclei[26,27].

Nuclear and centrosomal positions were determined from images of cells immunofluorescently stained for the centrosome (pericentrin), cell boundaries (actin or microtubules) and nuclei (DAPI). Images were uploaded into custom software (available on request) that identifies the positions of the nuclear and cell centroids, the centrosome, cell boundaries and the wound direction[28]. Software determinations of cell boundaries were inspected and corrected manually where necessary using the software to adjust computer drawn boundaries. The x/y positions (x, parallel to wound edge; y, perpendicular) of both the nucleus centroid and centrosome were calculated and normalized to the average cell radius calculated by the software. Only the y positions are depicted in the graphs as little movement of the nucleus or centrosomes along the x-axis occurred in the experiments reported.

Quantification of dorsal actin cables and F-actin. LPA- and serum-stimulated wound-edge NIH3T3 fibroblasts that had been stained for F-actin and nuclei were used to assess the effect of siRNA-mediated FHOD1 knockdown on dorsal actin cables above the nucleus and total F-actin in the cytoplasm and associated with the nucleus. Dorsal actin cables above the nucleus were manually counted from single plane images taken of F-actin and nuclei counting only those actin cables that passed over the nucleus. Total F-actin in the cytoplasm and associated with the nucleus were determined by measurement of rhodamine phalloidin fluorescence in the region of interest using ImageJ.

Time lapse microscopy and analysis. *Retrograde Actin Cable Flow*. NIH3T3 fibroblasts stably expressing Lifeact-GFP were grown to confluency on glass coverslip dishes, serum-starved for 48 hr and then wounded and transferred to recording media (MEM amino acids, HBSS, 1 % penicillin/streptomycin, 25 mM glucose, 4 mM glutamine, 2 μM sodium pyruvate, 20 mM Hepes,

pH 7.4; GIBCO). Cells were stimulated with LPA and then maintained in a TokaiHit chamber at 35 ° C on a Nikon Ti microscope. Images at multiple planes were acquired every 5 min using a 60X Planapo objective (NA 1.49) and an Andor iXon X3 EMCCD camera controlled by Nikon's NIS software. Kymographs were prepared with NIS software and exported to ImageJ to calculate the rate of movement of dorsal actin cables in the leading lamella.

Cell migration. Phase contrast live cell movies were prepared of multiple fields of wounded monolayers of NIH3T3 fibroblasts and analysed to determine the migration velocity as previously described .

Image processing and statistical analysis. Images of western blots, yeast two hybrid, immunofluorescence, and phase contrast are representative of results from three or more separate experiments, except for Fig. 2.1d, and S1d, which were repeated twice. Images were processed for contrast and brightness and assembled into figures using Adobe Illustrator/Photoshop. For quantitative results, statistical analysis was performed on parametric data using unpaired two-tailed t-test and non-parametric data using Fisher's exact test by GraphPad Prism 5 or Excel.

Sequence comparison. Sequence alignments were created by CLC Sequence Viewer software (CLC bio, Qiagen Inc.) using ClustalW algorithm. The conservation score for each position (range; 1-9, lowest to highest) was obtained from the ClustalW2 program (EMBL-EBI). To calculate an overall conversation score for N2G SRs in the FHOD1 interaction region, positions with a conservation score $\geq$ 8 was counted as positive and percent conservation calculated as the percentage of positive residues to total residues.

Acknowledgements

We thank Drs. Dennis Discher and Matthias Geyer for helpful discussion. This work was in part funded by the Deutsche Forschungsgemeinschaft (GRK1188 to S.K., grant FA 378/6-2 to O.T.F) and NIH (grant GM099481 to G.G.G.). O.T.F. is a member of the CellNetworks Cluster of Excellence EXC81.

Author Contributions

G.G.G. and O.T.F. conceived the study, designed experiments and wrote the manuscript. S.K., R.Z., S.A., G.W.L. and I.S. designed and conducted experiments and discussed and interpreted the data together with O.T.F. and G.G.G.

Competing Financial Interests

The authors declare no competing financial interests.

Figures

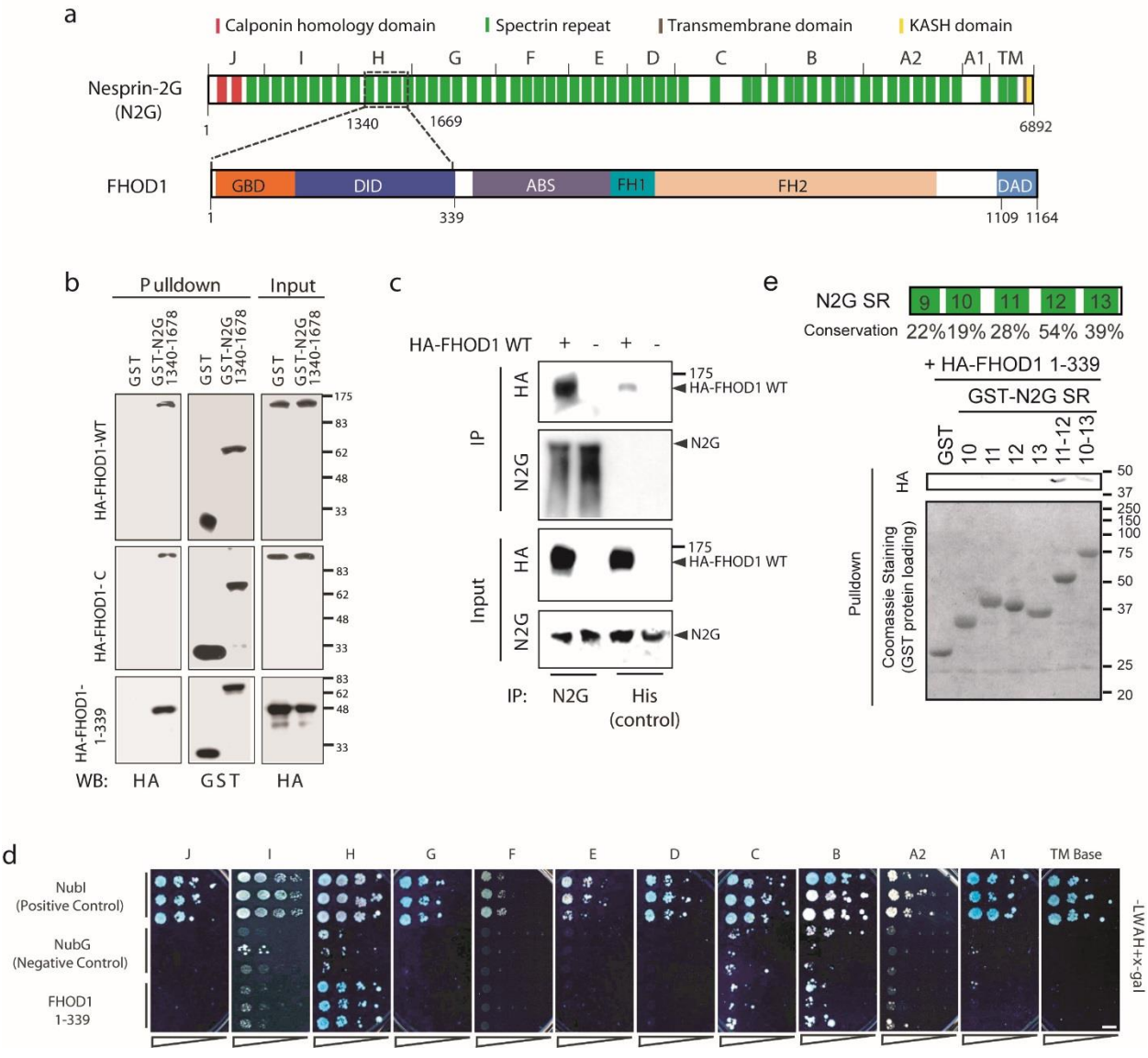
a
Calponin homology domain
Spectrin repeat
Transmembrane domain
KASH domain
J I H G F E D C B A2 A1 TM
Nesprin-2G (N2G)
1
1340
1669
6892
FHOD1
GBD
DID
ABS
FH1
FH2
DAD
1
339
1109 1164
b
Pulldown
Input
GST
GST-N2G 1340-1678
HA-FHOD1-WT
HA-FHOD1- C
HA-FHOD1- 1-339
175
83
62
48
33
WB: HA GST HA
c
HA-FHOD1 WT + - + -
IP
HA
N2G
175
HA-FHOD1 WT
N2G
Input
HA
N2G
175
HA-FHOD1 WT
N2G
IP: N2G His (control)
e
N2G SR
9 10 11 12 13
Conservation 22% 19% 28% 54% 39%
+ HA-FHOD1 1-339
GST-N2G SR
GST 10 11 12 13 11-12 10-13
HA
Pulldown
Coomassie Staining (GST protein loading)
50
37
250
150
100
75
50
37
25
20
d
J I H G F E D C B A2 A1 TM Base
NubI (Positive Control)
NubG (Negative Control)
FHOD1 1-339
-LWAH+x-gal

Figure 2.1 FHOD1 interacts with N2G.

(**a**) Schematic representation of the interaction site between human FHOD1 and N2G identified by yeast two hybrid is shown mapped onto mouse N2G and is indicated by the dotted box. The letters above N2G refer to fragments used for the directed yeast two hybrid in d. Domains in FHOD1 are: GBD, GTPase binding domain; DID, Diaphanous inhibitory domain; ABS, actin binding site; FH1, formin homology 1 domain; FH2, formin homology 2 domain; DAD, Diaphanous autoregulatory domain. (**b**) Pull down of HA-FHOD1 constructs with GST-N2G 1340-1678. HEK293T cell lysates containing the indicated HA-FHOD1 constructs were pulled down with GST-N2G 1340-1678 or GST and analysed by western blotting (WB) with HA or GST antibody. (**c**) Co-immunoprecipitation of HA-FHOD1 WT with antibody to endogenous N2G (or unrelated His antibody as a control) from lysates of transfected 293T cells. Immunoprecipitates were analysed by western blotting with antibodies to HA and N2G. (**d**) Directed membrane yeast two hybrid with the N2G fragments as baits and FHOD1 1-339 as prey and positive and negative controls. Triplicates at increasing dilution are shown. Only fragment H interacted above background level with FHOD1 1-339. (**e**) Pull down of HA-FHOD1 1-339 with indicated SRs from the interacting region of N2G. The evolutionary conservation of the residues in each of the SRs is indicated (see Methods and Supplementary Fig. 2.1). Lysates from 293T cells expressing HA-FHOD1 1-339 were pulled down with the indicated GST-tagged N2G SR constructs or GST alone and analysed by Western blotting with an antibody to HA. Coomassie staining is shown for GST loads. Bars: 50 μm.

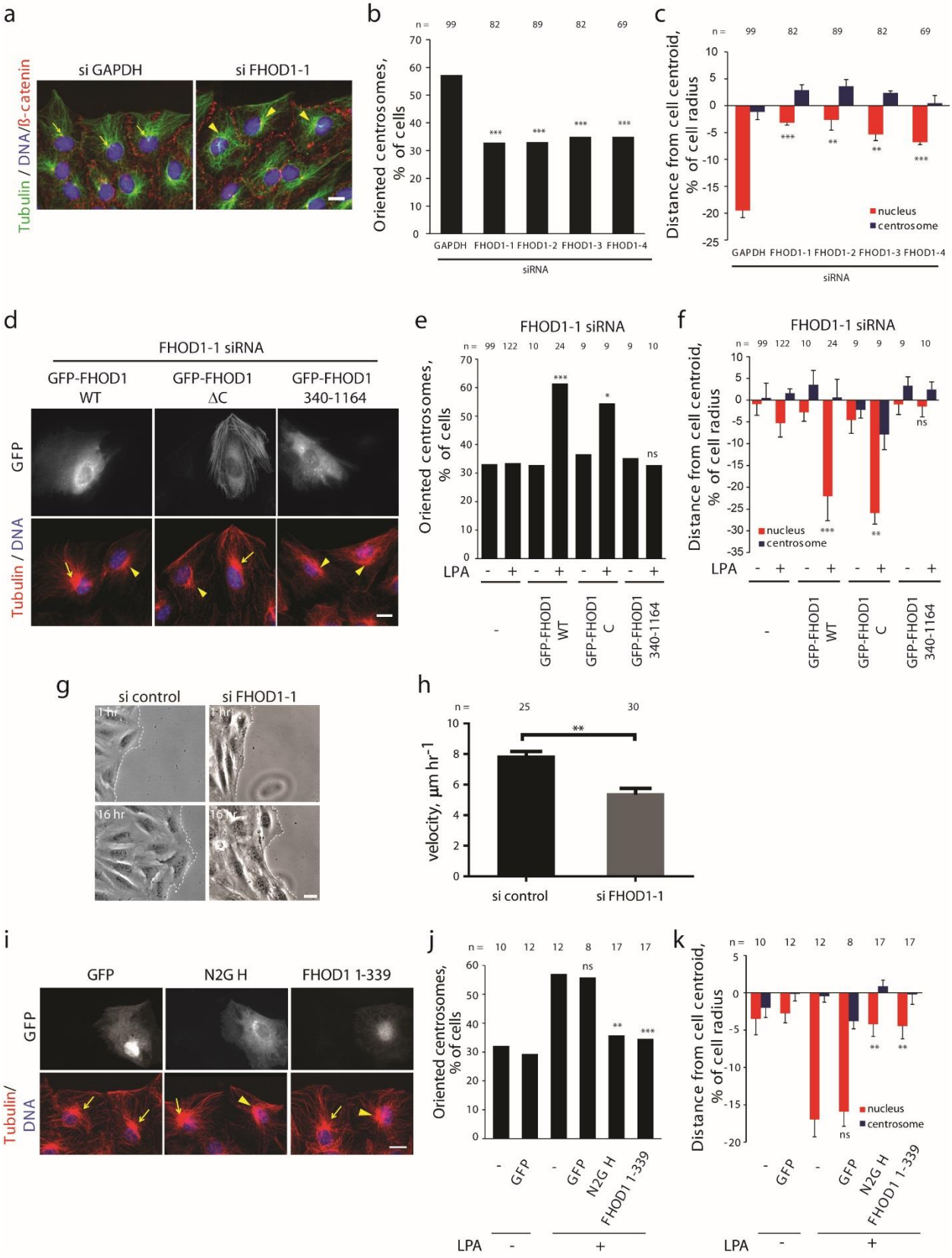
a
si GAPDH
si FHOD1-1
Tubulin / DNA/β-catenin
b
n = 99 82 89 82 69
Oriented centrosomes, % of cells
GAPDH FHOD1-1 FHOD1-2 FHOD1-3 FHOD1-4
siRNA
c
n = 99 82 89 82 69
Distance from cell centroid, % of cell radius
nucleus
centrosome
GAPDH FHOD1-1 FHOD1-2 FHOD1-3 FHOD1-4
siRNA
d
FHOD1-1 siRNA
GFP-FHOD1 WT
GFP-FHOD1 ΔC
GFP-FHOD1 340-1164
GFP
Tubulin / DNA
e
FHOD1-1 siRNA
n = 99 122 10 24 9 9 9 10
Oriented centrosomes, % of cells
LPA
GFP-FHOD1 WT
GFP-FHOD1 C
GFP-FHOD1 340-1164
f
FHOD1-1 siRNA
n = 99 122 10 24 9 9 9 10
Distance from cell centroid, % of cell radius
nucleus
centrosome
LPA
GFP-FHOD1 WT
GFP-FHOD1 C
GFP-FHOD1 340-1164
g
si control
si FHOD1-1
1 hr
16 hr
h
n = 25 30
velocity, μm hr-1
si control
si FHOD1-1
i
GFP
N2G H
FHOD1 1-339
GFP
Tubulin/ DNA
j
n = 10 12 12 8 17 17
Oriented centrosomes, % of cells
LPA
GFP
N2G H
FHOD1 1-339
k
n = 10 12 12 8 17 17
Distance from cell centroid, % of cell radius
nucleus
centrosome
LPA
GFP
N2G H
FHOD1 1-339

Figure 2.2 FHOD1 is required for nuclear movement.

(**a**) Immunofluorescence images of LPA- stimulated, wounded monolayers of NIH3T3 fibroblasts depleted of either GAPDH or FHOD1 and stained for tubulin, β-catenin and DNA (DAPI). The wound is towards the top in this and all subsequent figures. Arrows indicate oriented centrosomes in cells at the wound edge; arrowheads indicate non-oriented centrosomes. (**b**) Quantification of LPA-stimulated centrosome orientation in NIH3T3 fibroblasts depleted of either GAPDH or FHOD1 (numbers refer to different siRNA used for FHOD1). Centrosome orientation between the leading edge and nucleus was scored as described previously; random orientation is 33% by this measure (see ref 13). (**c**) Quantification of centrosome and nucleus position along the front-back axis in LPA-stimulated NIH3T3 fibroblasts depleted of either GAPDH or FHOD1. The cell centroid is defined as "0"; positive values, toward the leading edge; negative, away. Data in b,c are from 3 experiments in which $\geq$89 cells were analysed. (**d**) Immunofluorescence images of LPA-stimulated, wounded monolayers of FHOD1-1 siRNA treated NIH3T3 fibroblasts re-expressing the indicated FHOD1 constructs and stained for GFP, tubulin and DNA (DAPI). Arrows indicate oriented centrosomes; arrowheads, non-oriented centrosomes. (**e**) Quantification of centrosome orientation in the experiment shown in d. (**f**) Analysis of centrosome and nucleus position in the experiment shown in d. Data in e,f are from 3 experiments in which $\geq$ 24 cells (FHOD1 WT), $\geq$ 9 cells (FHOD1 ΔC), > 10 cells (FHOD1 340-1164) were analysed. **(g)** Images from a phase contrast movie of NIH3T3 fibroblast migrating into wounds after treatment with FHOD1-1 siRNA or scrambled siRNA control. The dashed line shows the wound edge. **(h)** Velocity of wound closure in NIH3T3 fibroblasts treated with FHOD1-1 siRNA or scrambled siRNA control. Data are from 3 individual experiments in which $\geq$25 cells from multiple wounds

were measured.. (**i**) Immunofluorescence images of LPA-stimulated, wounded monolayers of NIH3T3 fibroblasts expressing interacting regions of N2G or FHOD1 and immunostained for GFP, tubulin, and DNA (DAPI). Arrows indicate oriented centrosomes; arrowheads, non-oriented centrosomes. (**j**) Quantification of centrosome orientation in the experiment shown in i. (**k**) Analysis of centrosome and nucleus position in the experiment shown in i. Data in j-k are from 4 experiments in which $\geq$ 8 cells were analysed for each condition. Bars, a, d, g, i: 10 μm. Error bars for c,f,h,k: SEM. ***, $P<0.001$; **, $P<0.01$; *, $P<0.05$; ns, not significantly difference by Fisher's exact test (b,e,j) and two-tailed t-test (c,f,h,k). n represents cell number in each experiment and N represents independent experiments number.

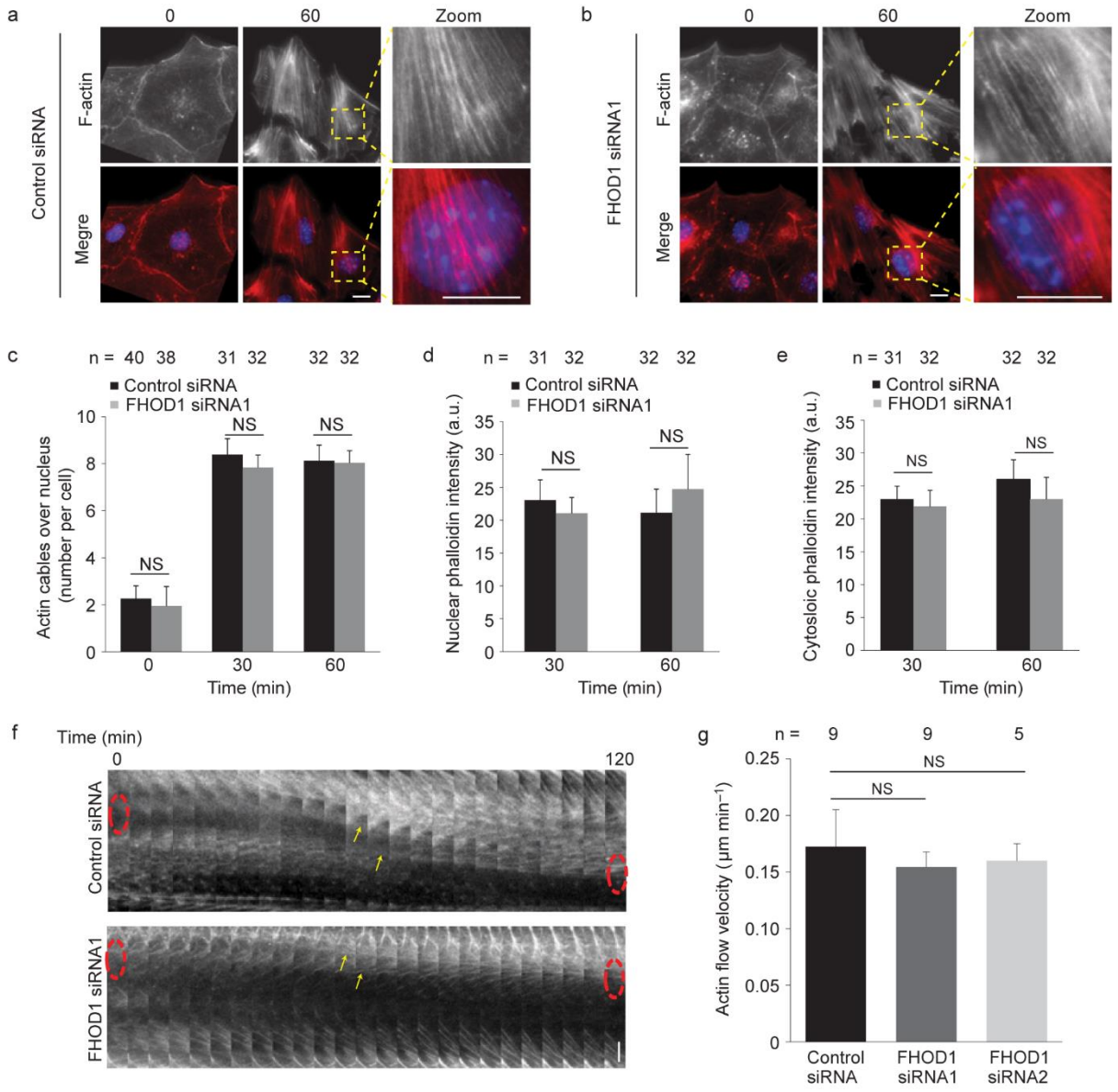
a
0
60
Zoom
Control siRNA
F-actin
Megre
b
0
60
Zoom
FHOD1 siRNA1
F-actin
Merge
c
n = 40 38 31 32 32 32
Control siRNA
FHOD1 siRNA1
Actin cables over nucleus (number per cell)
NS
NS
NS
Time (min)
d
n = 31 32 32 32
Control siRNA
FHOD1 siRNA1
Nuclear phalloidin intensity (a.u.)
NS
NS
Time (min)
e
n = 31 32 32 32
Control siRNA
FHOD1 siRNA1
Cytosloic phalloidin intensity (a.u.)
NS
NS
Time (min)
f
Time (min)
0
120
Control siRNA
FHOD1 siRNA1
g
n = 9 9 5
NS
NS
Actin flow velocity (μm min−1)
Control siRNA
FHOD1 siRNA1
FHOD1 siRNA2

Figure 2.3 FHOD1 is dispensable for formation of dorsal actin cables and retrograde actin flow.

(**a, b**) Fluorescence images of F-actin (phalloidin) and DNA (DAPI) in LPA-stimulated NIH3T3 fibroblasts treated with (a) control or (b) FHOD1 siRNAs. Time in min after LPA stimulation is shown at top. Zoomed images of the outlined regions in the 60 min time point show dorsal actin cables over the nucleus. (**c-e**) Quantification of (c) the number of dorsal actin cables above nuclei, (d) nuclear phalloidin intensity, and (e) cytosolic phalloidin intensity in NIH3T3 fibroblasts treated with control or FHOD1 siRNAs and stimulated with LPA for the indicated time. Data in c-e are from 5 experiments in which $\geq$ 30 cells were analysed. (**f**) Kymographs from movies of Lifeact-GFP stably expressed in NIH3T3 fibroblasts treated with control or FHOD1-specific siRNA. Time (min) is shown above the kymograph; each panel is 5 min. Arrows, retrogradely moving dorsal actin cables; dashed circles, position of nucleus. (**g**) Velocity of actin cable retrograde flow in NIH3T3 fibroblasts treated with control or FHOD1 siRNAs determined from kymographs as in (f). Data are from 3 experiments in which $\geq$ 9 (FHOD1-1) or 5 (FHOD1-2) cells were analysed. Bars, a,b: 10 μm; f, 5 μm. Error bars (c-e, g), SEM. ns, not significantly different by two-tailed t-test (c-e).

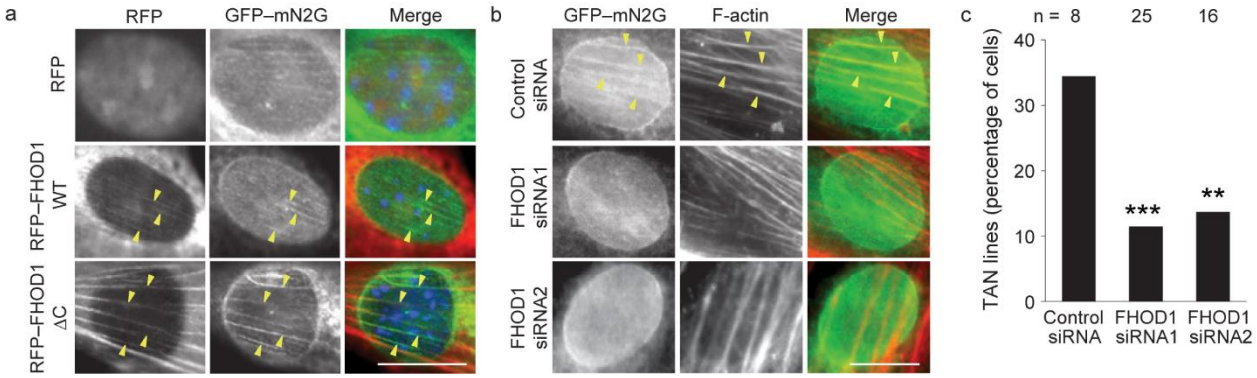
a
RFP
GFP–mN2G
Merge
RFP
RFP–FHOD1 WT
RFP–FHOD1 ΔC
b
GFP–mN2G
F-actin
Merge
Control siRNA
FHOD1 siRNA1
FHOD1 siRNA2
c
n = 8
25
16
TAN lines (percentage of cells)
40
30
20
10
0
***
**
Control siRNA
FHOD1 siRNA1
FHOD1 siRNA2

Figure 2.4 FHOD1 is essential for TAN line formation.

(**a**) Fluorescence images of the indicated RFP-FHOD1 constructs or RFP as a control and GFP-mN2G (a TAN line marker) on the dorsal surface of wound edge NIH3T3 fibroblasts. Arrowheads, FHOD1 colocalizing with mN2G in TAN lines. (**b**) Fluorescence images of GFP-mN2G and F-actin (phalloidin) on the dorsal surface of wound edge NIH3T3 fibroblasts treated with control or FHOD1 siRNA. Arrowheads, TAN lines with colocalized GFP-mN2G and F-actin. (**c**) Quantification of the frequency of wound-edge NIH3T3 fibroblasts with TAN lines following treatment with the indicated siRNAs. Data are from 3 experiments in which $\geq$ 10 (control), 25 (FHOD1-1) and 16 (FHOD1-2) cells were analysed. Bars, a,b: 10 μm. (c) ***, $P<0.001$; **, $P<0.01$ by Fisher's exact test.

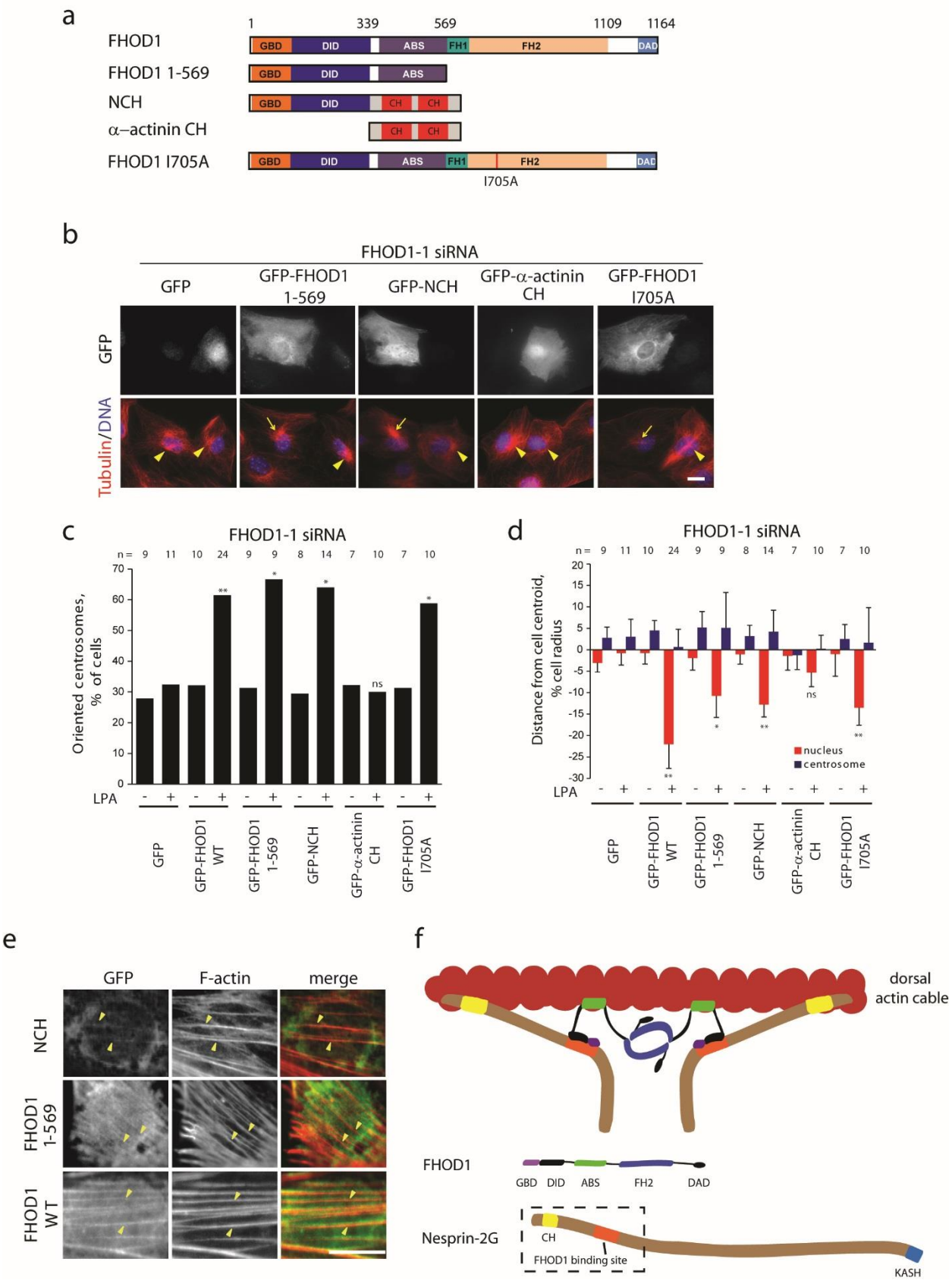
a
1
339
569
1109
1164
FHOD1
GBD
DID
ABS
FH1
FH2
DAD
FHOD1 1-569
NCH
CH
α–actinin CH
FHOD1 I705A
I705A
b
FHOD1-1 siRNA
GFP
GFP-FHOD1 1-569
GFP-NCH
GFP-α-actinin CH
GFP-FHOD1 I705A
Tubulin/DNA
c
FHOD1-1 siRNA
n = 9 11 10 24 9 9 8 14 7 10 7 10
Oriented centrosomes, % of cells
LPA
GFP
GFP-FHOD1 WT
GFP-FHOD1 1-569
GFP-NCH
GFP-α-actinin CH
GFP-FHOD1 I705A
ns
d
FHOD1-1 siRNA
Distance from cell centroid, % cell radius
nucleus
centrosome
e
GFP
F-actin
merge
NCH
FHOD1 1-569
FHOD1 WT
f
dorsal actin cable
FHOD1
GBD DID ABS FH2 DAD
Nesprin-2G
CH
FHOD1 binding site
KASH

Figure 2.5 The N-terminal actin binding site of FHOD1 provides N2G with an additional contact to actin filaments required for TAN line formation.

(**a**) Schematic of constructs used. (**b**) Immunofluorescence images of LPA-stimulated, wounded monolayers of FHOD1-1 siRNA treated NIH3T3 fibroblasts expressing the indicated constructs and stained for GFP, Tyr tubulin, and DNA (DAPI). Arrows indicate oriented centrosomes; arrowheads, non-oriented centrosomes. (**c**) Quantification of centrosome orientation in the experiment shown in (b). (**d**) Analysis of centrosome and nucleus position in the experiment shown in (b). Data in c,d are from 3 experiments in which $\geq$ 9 cells were analysed for each condition. (**e**) Immunofluorescence images of the indicated GFP constructs and F-actin (phalloidin) over nuclei of wound-edge NIH3T3 fibroblasts depleted of FHOD1. Arrowheads, examples of expressed GFP protein colocalizing with dorsal actin cables over the nucleus. (**f**) Model of multivalent connection of N2G to actin filaments established by FHOD1-N2G interaction. N2G's paired CH domains provide one connection to the actin filament; FHOD1 associated with N2G provides a second actin filament binding site through FHOD1's N-terminal ABS. FHOD1 is enlarged relative to N2G to allow depiction of its domains. Bars, b,e: 10 μm. Error bars d: SEM. **, $P < 0.01$; *, $P < 0.05$; ns, not significantly different by Fisher's exact test (c) and two-tailed t-test (d).

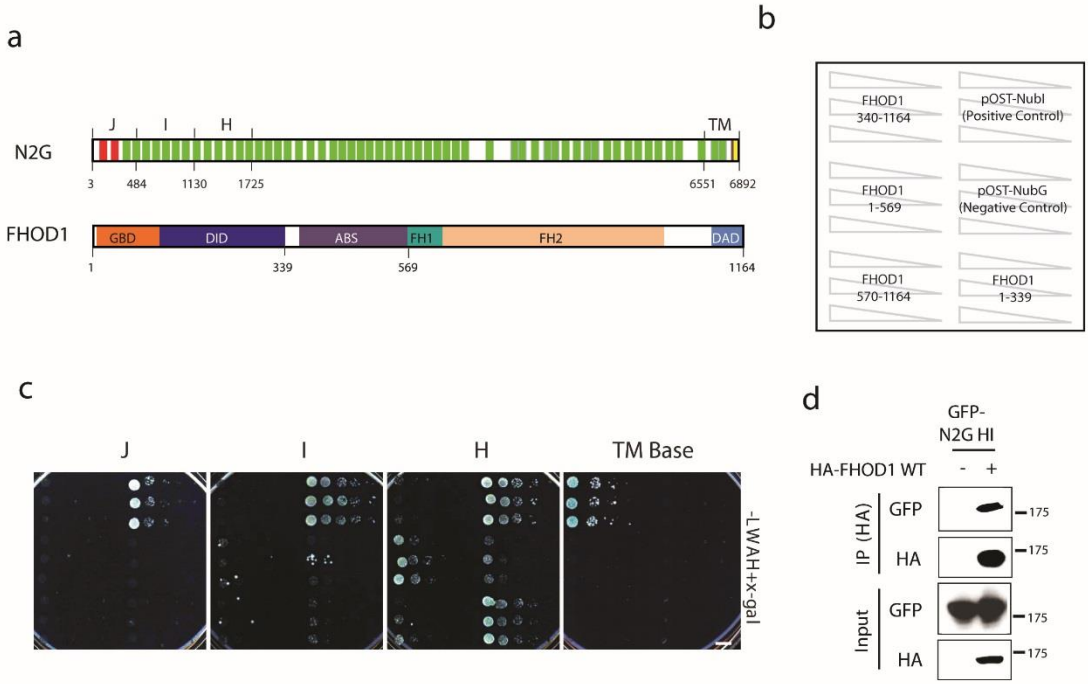

e

SR9

```
                    20        40        60        80        100
                    |         |         |         |         |
Human  NIQDSIAKQTEICNRLEEPGNFVL--KELHPFDLHAMQNIILKYKTQFEGMNHRVQRSEDTLKA
Mouse  DIRDSIAKQTRVCTSLEEPSNSVP--RELHTLDQCAIQDIVLKCRLQLETMNQKVEMREDALDA
Chicken ELQRSILNQTEVCKQLEHLDSSAR--DEFNPIDLQAASKIMFYYQNQLEEMSHKMQIRETVLKD
Frog   DVQSSVEDETRKCEDLQT-SAELC--ESLSPVDFQEFHSTLYDFKANLKETNKDVKEREAVLKV
Fish   CVDESIKKELFLLNERESLVGDGTDLSHIELQTHLPLQQTLHNRTKCLEQQRHCVQKSESALVA
Consensus ....SI...I..C..LE.....--.....D.............LE.....V...E..L..
```

SR10

```
Human  LEDFLASLRTAKLSAEPVTDLSASDTQVAQENTLTVKNKEGEIHLMKDKAKHLKCLKMLD--MSFKDAERGDDTSCENLLDAFSIKLSETH--GYGVQ
Mouse  LEGFLASLRAAKLSAELPADRPAPKAPEVLS---------EDILLMKEKAGPLGERIRTLG--INIKDAEGGENTTCERLVGALSVNLVAMD--GQSKE
Chicken LEAFMASLRKIKSSVEHLTDPLGQPEIQGKTWR----EAAQELSHMAKEAQCLGERLKTVD--ICLEDAEFGRNTSCEKLVQTLSEELNVSG--DHSSE
Frog   LKKFLFSLKTAKLNIEEQSVVLERDRPALEDKQTNLTILEKEVFRLEQEAQLLGGSLEMAG--VYLEDPVSGGKTSCQDLIGGFSERVGSAK--ENILQ
Fish   LEKLLSHLQQLNDELNAHRTSDQSYSSVSFQKS---------LEQVREDSLQLQTMLDDAGLRITLDDKAGSCVEMVSALEEGFQVRLVEGQRVSDGGR
Consensus LE.FL.SL...K...E.....A..LD..L....--....D...G..T.C..L....S..L....--.....
```

SR11

```
Human  EEF-TEENKLLEACIFKNNELLKNIQDVQSQISKTGLKDFTVPAVKHEKKSLIRLDKVLDEYEEEKRHLQEMANSLPHFKDGREKTVNQQCQNTVVLVEENTKALVT
Mouse  EGP-PEDKLLEACSSKNLEEFKNIQDLQNQISKTGLKDFTAPAVKHEKKSLLRLDKDLDGLEEEKVRIQKIAGSLPRFKDGSEKNVIQQCEDTAALVESTKASVT
Chicken QML-TEGNDLYKIFSTRNEELLKNIQDLHDRINKTGLKDFTAPAIQQEVKSLMELEKELDCSAVEMKSMREITNKLLQMKEEKAEESNEQCRVTERSVEDTKLLLA
Frog   ELRNLQWREDLEKLAVRQKEICKCVDDIYDKVDDIGLSDFTISMSVQQELKHLDELEKELDSHVNEKMDISKGLTDLLQIAQGKDFIGDE---DTETLVEDARQHII
Fish   KGREKQEKKEERAFGRKRMGELVTLREVLAALERHVLKEFTLPALQHELRFLTDMESKLHALRSEIDDLRDANTSDTNLS--------------ELQTQVETAHRSVT
Consensus .....EL.K..QD.....IGLKDPT.PA...R.K.L..L.K.LD....E.........L.............QC..T...WE.....
```

SR12

```
Human  ECLEQCGRVLELLKQYDNFKSITTLIQKEESVISLCASYMGKENLKKRIAEIEIVKEEFNEHLEVVDKINQVCKNLCFYLNKMKTFEEPPFEKEANIIVDRWLCINEKTED
Mouse  ESLEQCGSALELLRQYDNIKNNLTALIQKEEGIISQCASYMGKDNLKKKIAEIETVKEEFSDHLEVVDKINQICKNLCQYHLNKMKTFEDPPFEKEANAIVDRWLEINEKTEE
Chicken ECQEQCARALELLKQYDSCKSSLTSIIQKQEIVLSQQNSYMGKDNLNRLITKIEEAKEEFNDHAEDVDKINQICKNLCFQLNKMRSFEEPPFENEANIIVDRWLEINEKTEN
Frog   YCKEQLEKVMELLRKFQKCKATLSSSLIHKGEITVSQQSSYMGKENVHKKLTEVDAVKQEFNEHSENIQELSSICKKLCFHLSRMKSCGNPPFQDEAHMIVDKWLCANEKLDS
Fish   ESRKQLASLTELLKKFDSCRNNLGGTLQRAEQTIGDLASYMGKDNLQLLISKVISIKSDISGLGDGVEEFRSVCRQLLSLVRRVLDCTDAPEESADTLMDRWLEVTEKTDC
Consensus E..EQC....ELL...Q..K..L...IQK.E...S.Q.SYMGK.NL...I.....K.EF..H.E.VD.....CK.LQ..L..M.....PPFE.EA..IVDRWLD.NEKT..
```

SR13

```
Human  YYENLGRALAIWDKLFNLKNVIDEWTEKALQKMELH--QLTEEGRERLKEEIQVHEQKTSEFSRRVAETGFLLQSSEIPLELQVMESSILNLKMEHVQKCLTGES
Mouse  YGENLGRALALWDKLFIIKNNIDEWTEQILGKAESH--ELTEEGRGRLKEEIKVLEEQSAEFSRRVADTQSLLQSNEKPLELQVMESSVLSLKMKDVKTHVAGGS
Chicken YCDNLGRAQALWDKLLGLSGTIDAWANAELKNAEGR--CLTNEGLTQLKACLCVQEQKLQKFDNTVAELEELLNSNEPPLELQVIRSSIVQKMELIKDLLTTKR
Frog   YSDNIKSASCLWNKLLQLSEDIDQWAECKIKYCKGS--VLTEHDVLSLKAELQLHVEKIEDVSAKSFQIQKIIELSDPPLELQVIKTSLLKKMDQIHEY-----
Fish   YLDNLQAGFSLWEKLLLLAEEVEGWSAQKLMTLAQSNPFDTEVDVSALQNELKKVQEENIHEHRRSSEIQELLQSQEFPLELQVIESQLRKKVAEVKEL-----
Consensus Y..NL..A..LW.KL..L...ID.W....L.....--.LTE.D...LK.EL.V.E.....F.....IQ.LL.S.E.PLELQV..SS...KM..........
```

Supplementary Figure 2.1 Additional evidence that the interaction between FHOD1's N-terminus and nesprin-2G (N2G) is specific and phylogenetic comparison of the FHOD1 interacting region of N2G.

(**a**) Schematic of N2G and FHOD1 with boundaries for constructs used in membrane yeast-two hybrid. (**b**) Legend for yeast two-hybrid indicating the FHOD1 fragments used as a bait for the experiment shown in panel c. (**c**) Yeast two-hybrid results for the interaction between N2G J,H and I fragments and FHOD1 fragments indicated in panel b. Bar, 5 mm. (**d**) N2G HI fragment interacts with HA FHOD WT in cell lysates. GFP-N2G HI was expressed alone or co-expressed with HA-FHOD1 WT in 293T cells and lysates were immunoprecipitated with HA antibody. Western blots were probed with antibodies for HA and GFP. Input shows level of expression of transfected proteins. (**e**) Phylogenetic comparison between spectrin repeats (SRs) 9-13 of N2G. Red indicates residues conserved between at least four of the five species; pink indicates residues that are conserved in at least three of the species. Consensus residues are shown below for highly conserved positions. Sequences were obtained from the following sources. Human (H. sapiens, NP_878918.2, NCBI), Mouse (M. musculus, NIH3T3 fibroblast cDNA), Chicken (G. gallus, XP_003641488, NCBI), Frog (X. tropicanis, XP_002933763, NCBI), Fish (D. rerio, F1QVC9, Uniport).

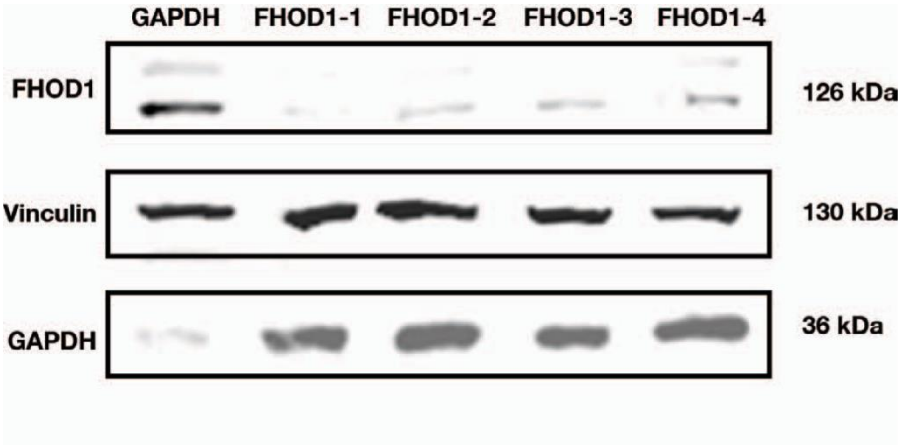
GAPDH
FHOD1-1
FHOD1-2
FHOD1-3
FHOD1-4
FHOD1
126 kDa
Vinculin
130 kDa
GAPDH
36 kDa

Supplementary Figure 2.2 FHOD1 knock down by siRNAs.

Western blot of FHOD1 levels in NIH3T3 fibroblasts after knockdown with four different siRNAs targeting FHOD1. Control siRNA knockdown of GAPDH is shown for comparison. Vinculin is a loading control.

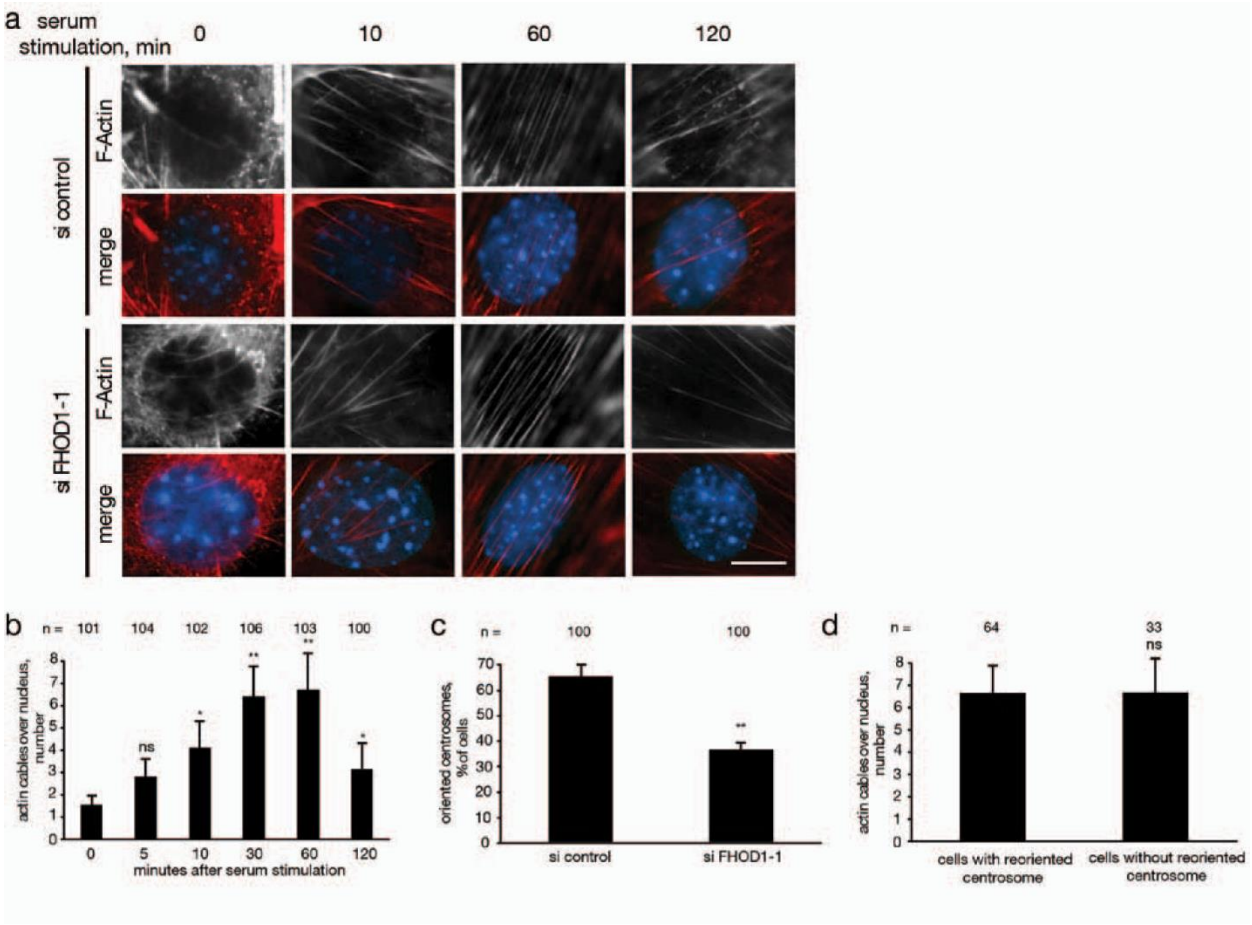
a
serum stimulation, min
0
10
60
120
si control
si FHOD1-1
F-Actin
merge
b
n = 101 104 102 106 103 100
actin cables over nucleus, number
ns
minutes after serum stimulation
c
n = 100 100
oriented centrosomes, % of cells
si control
si FHOD1-1
d
n = 64 33
ns
actin cables over nucleus, number
cells with reoriented centrosome
cells without reoriented centrosome

Supplementary Figure 2.3 FHOD1 knockdown does not affect actin structures induced by serum.

Starved NIH3T3 fibroblasts were stimulated with 20 % FCS, fixed at indicated time points and stained with rhodamine phalloidin for F-actin (red) and DAPI for DNA (blue). (**a**) Fluorescence images of dorsal actin cables over the nucleus. Bar, 10 µm. (**b**) Quantification of the number of actin cables over the nucleus per cell in control siRNA cells at various time points after serum stimulation. (**c**) Quantification of centrosome orientation in serum-stimulated wound edge NIH3T3 fibroblasts. (**d**) Comparison of dorsal actin cables over nuclei in siFHOD1 treated cells with oriented and non-oriented centrosomes. Data in b-d are from 3 experiments; n = number of cells analysed per experiment is shown in (b, c, d). Error bars: SD. **, $P < 0.01$; *, $P < 0.05$; ns, not significantly different by two-tailed t-test.

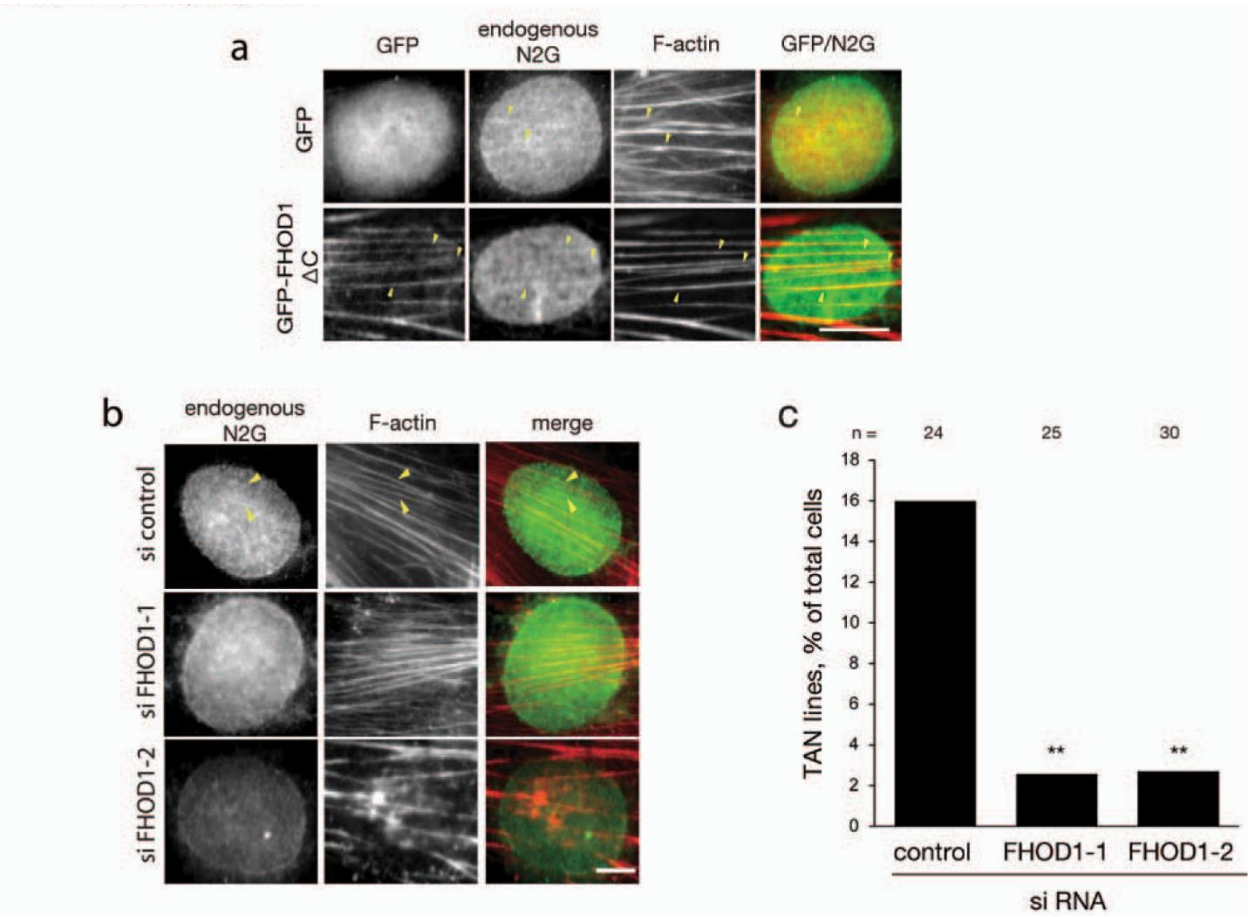
a
GFP
endogenous N2G
F-actin
GFP/N2G
GFP
GFP-FHOD1 ΔC
b
endogenous N2G
F-actin
merge
si control
si FHOD1-1
si FHOD1-2
c
n =
24
25
30
TAN lines, % of total cells
18
16
14
12
10
8
6
4
2
0
**
**
control
FHOD1-1
FHOD1-2
si RNA

Supplementary Figure 2.4 Localization of FHOD1 ΔC with endogenous TAN lines and effect of FHOD1 knockdown on endogenous TAN lines.

(**a**) Immunofluorescence images of GFP-FHOD1 DC and endogenous N2G on the dorsal surface of nuclei in LPA-stimulated NIH3T3 fibroblasts. Arrowheads, TAN lines containing N2G and dorsal actin cables and GFP-FHOD1 ΔC (bottom panels). Leading edge of the cell is toward the top. . Bar, 10 µm. (**b**) Immunofluorescence images of endogenous N2G (N2G antibody-stained) and F-actin (rhodamine phalloidin) in NIH3T3 fibroblasts treated with the indicated siRNAs. Arrowheads, TAN lines containing N2G co-localized with dorsal actin cables in control siRNA-treated cells. TAN lines are not observed in FHOD1 siRNA-treated cells. Bar, 5 µm. (**c**) Quantification of endogenous TAN lines in control siRNA- and FHOD1 siRNA-treated cells. Data are from 3 experiments; n = number of cells analysed per experiment shown in (c). **, $P<0.01$ by Fisher's exact test.

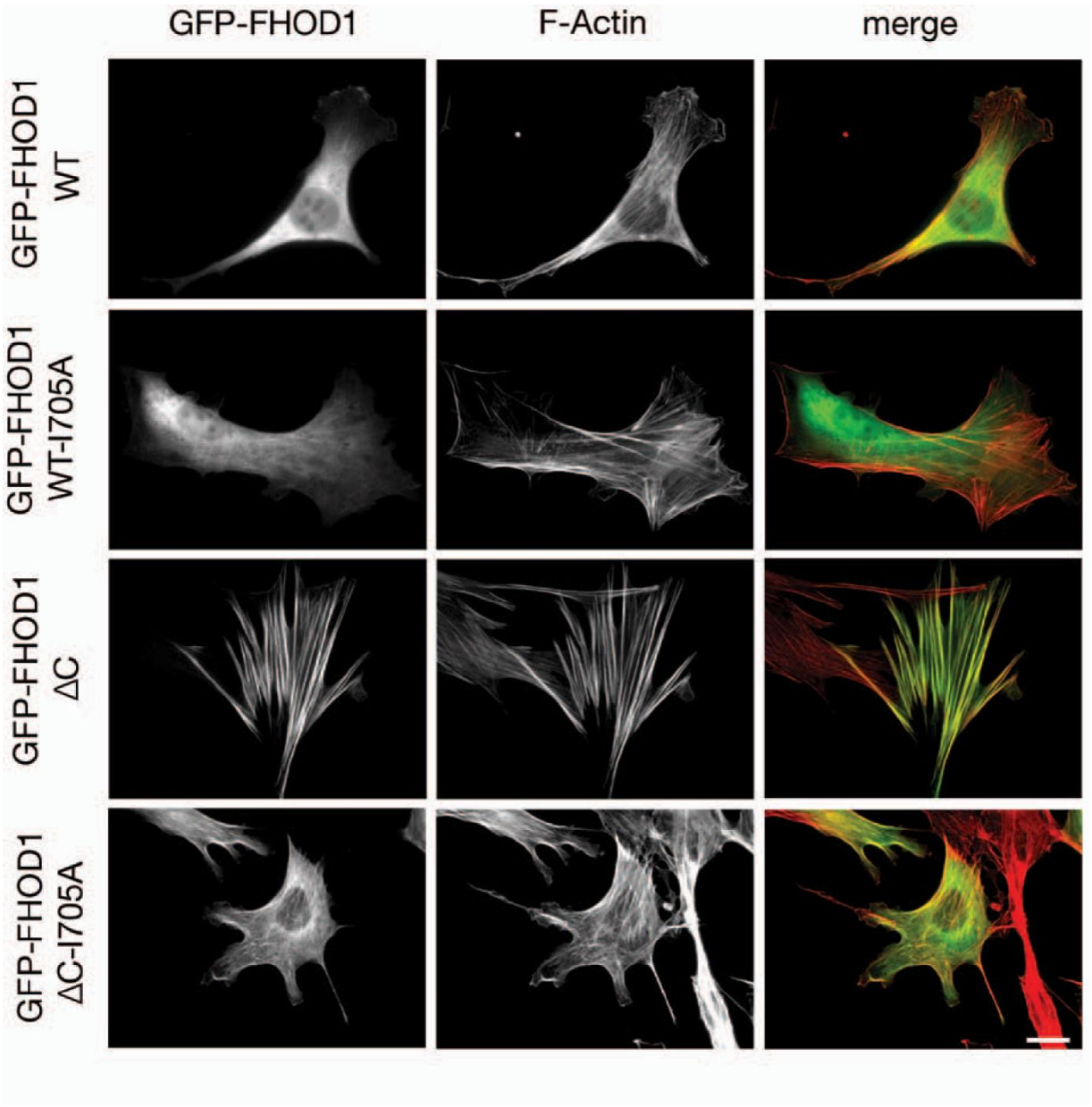
GFP-FHOD1
F-Actin
merge
GFP-FHOD1 WT
GFP-FHOD1 WT-I705A
GFP-FHOD1 ΔC
GFP-FHOD1 ΔC-I705A

Supplementary Figure 2.5 The I705A mutation in active FHOD1 ΔC disrupts its induction of and localization with thick actin filament bundles.

NIH3T3 cells expressing the indicated GFP-FHOD1 variants were stained for F-actin with rhodamine phalloidin. Note that active FHOD1 ΔC induces the formation of thick F-actin bundles associates with them. Actin bundle formation and actin filament association of FHOD1 is potently disrupted by the I705A mutation. Bar, 20 μm.

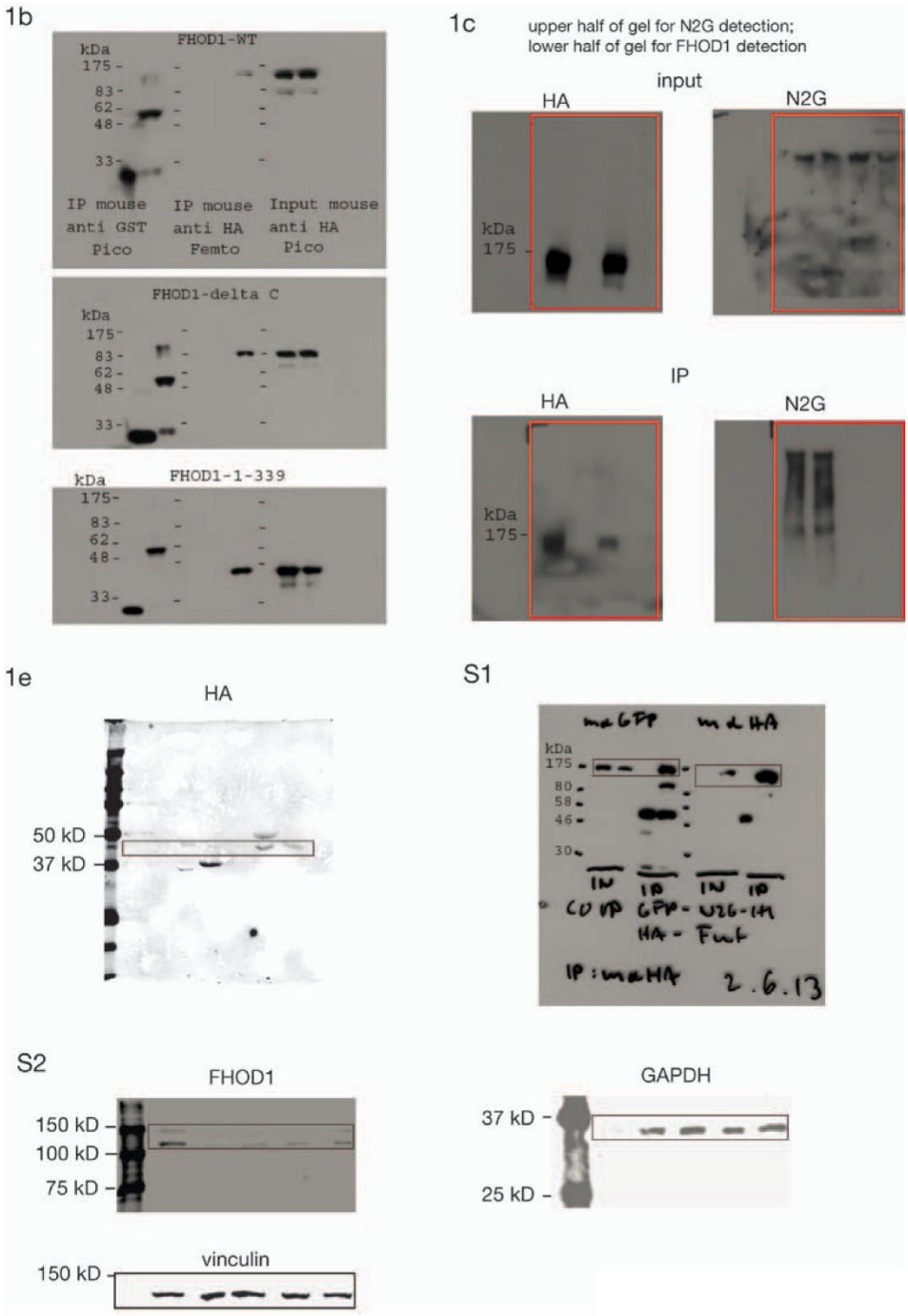

Supplementary Figure 2.6 Uncropped Western Blot figures

Table

Supplementary Table 2.1 NIH3T3 sequence compared to mouse SYNE2 (NM_001005510)

Sequence Position*	NIH3T3 sequence compared to mouse SYNE2 (NM_001005510)
2007-2008	insertion GAG
13244-13246	deletion GCA
14400	G → A
14443	C → A
14453	A → G
14505	C → G
14622	T → A
14676	A → G
15138	G → A
15294	A → G
15702	A → G
15757	C → A
15774	G → A
15777	A → G
15781	G → A
15783	A → G
15815	T → C
16504	A → G
19300-19301	Insertion ATGTAGAAATCCCTGAAAATCCTGAGGCTTATCTTAAAATGACCACA AAATCTTTGCAAGCATCTTCTG
20341-20365	Substitution AGTCCAAGGCCCCGCTGGACCTTCT for TTTGGAG

* Start codon is first base pair for numbering

Chapter Three: Centrifugal Displacement of Nuclei Reveals Multiple LINC Complex Mechanisms for Homeostatic Nuclear Positioning

This chapter is from a manuscript: **Ruijun Zhu**, Susumu Antoku and Gregg G. Gundersen. Centrifugal Displacement of Nuclei Reveals Multiple LINC Complex Mechanisms for Homeostatic Nuclear Positioning. *In Press, Current Biology* (2017).

Abstract

Nuclear movement is critical for developmental events, cell polarity and migration and is usually mediated by LINC complexes connecting the nucleus to cytoskeletal elements. Compared to active nuclear movement, relatively little is known about homeostatic positioning of nuclei including whether it is an active process. To explore homeostatic nuclear positioning, we developed a method to displace nuclei in adherent cells using centrifugal force. Nuclei displaced by centrifugation rapidly recentered by mechanisms that depended on cell context. In cell monolayers with wounds oriented orthogonal to the force, nuclei were displaced toward the front and back of the cells on the two sides of the wound. Nuclei recentered from both positions, but at different rates and with cytoskeletal linkage mechanisms. Rearward recentering was actomyosin-, nesprin-2G- and SUN2-dependent, whereas forward recentering was microtubule-, dynein-, nesprin-2G- and SUN1-dependent. Nesprin-2G engaged actin through its N-terminus and microtubules through a novel dynein interacting site near its C-terminus. Both activities were necessary to maintain nuclear position in uncentrifuged cells. Thus, even when not moving, nuclei are actively maintained in position by engaging the cytoskeleton through the LINC complex.

Introduction

The nucleus is positioned specifically in single cell organisms such as yeast to complex multi-cellular plants and animals [10, 11]. This positioning influences diverse processes including cell division, polarity, migration and differentiation. Disruption of normal nuclear positioning is associated with diseases such as muscular dystrophy, cardiomyopathy and lissencephaly [11, 12].

Mechanisms of nuclear positioning have been characterized for actively moving nuclei. From these studies, the linker of nucleoskeleton and cytoskeleton (LINC) complex [15], which spans the inner and outer nuclear membrane, has emerged as a widely employed connection between moving nuclei and the cytoskeleton [12, 13]. The LINC complex is composed of outer nuclear membrane KASH proteins (nesprins in vertebrates) and inner nuclear membrane SUN proteins [13, 15, 181]. These proteins interact in the luminal space via the short KASH peptide and the SUN domain. The LINC complex is anchored by interaction of SUN proteins with lamin A/C, but other proteins may be involved [13, 15, 35].

Depending on the specific KASH protein, LINC complexes can engage actin filaments or microtubules (MTs) for nuclear positioning. For example, in *C. elegans* ANC-1 interacts with actin filaments through paired calponin homology (CH) domains [82], whereas UNC-83 engages MTs through kinesin-1 and cytoplasmic dynein motor proteins [101]. In mammalian cells, nesprin-1G and nesprin-2G ("G" refers to the giant isoform) have paired CH domains that interact with actin filaments [3, 110, 136], but also engage MTs through MT motors [114-116, 188]. Nesprin-2G's interaction with actin filaments is reinforced by its interaction with two other actin binding proteins, FHOD1 and fascin [16, 189]. Nesprin-3 engages intermediate filaments and has been implicated

in the nuclear piston mechanism for 3D cell migration [190, 191]. Nesprin-4 interacts with MTs through kinesin-1 [87].

In most cases of nuclear movement, a single KASH protein-cytoskeletal pair mediates the movement. For example, in the well-characterized hyp7 hypodermal precursor cell system in *C. elegans*, the SUN protein UNC-84 interacts with the KASH protein UNC-83, which in turn interacts with MT motors to move nuclei from one side of the cell to the other [100, 101, 192]. Consistent with the predominant movement of the nucleus toward MT plus ends, kinesin-1 plays a major role, yet both kinesin-1 and dynein are required. In mammalian fibroblasts and myoblasts, a SUN2-nesprin-2G LINC complex associates with actin cables to move nuclei rearward and polarize the cell for migration after LPA stimulation [3, 180]. During mouse brain development, nesprin-2 contributes to nuclear movement necessary for neuronal migration, probably by interacting with MTs through kinesin and/or dynein motors [115]. Similarly, nesprin-2 contributes to nuclear spacing in multi-nucleated myotubes by interacting with MTs via kinesin-1 [114]. Nesprin-4 interacts with kinesin-1 to move the nucleus away from the centrosome in epithelial cells and disruption of nesprin-4 leads nuclear positioning defects in hair cells and deafness [41, 87].

We know far less about the factors that control the position of the nucleus when it is not moving. A seminal study showed that the KASH protein ANC-1 and its interaction with actin filaments maintained nuclear spacing in syncytial hypodermal cells of *C. elegans* to resist dispersion by the contraction of the underlying muscle [82]. A*nc-1* mutants also showed an intermediate nuclear positioning defect in bi-nucleated intestinal cells [193]. In mature mouse skeletal muscle, nesprin-1α2, which lacks actin-binding domains, functions in maintaining nuclear

spacing likely through interacting with kinesin-1 [194]. It is unclear whether similar sorts of mechanism are widespread in cells and tissues that experience lower mechanical forces and/or do not have syncytial nuclei. Indeed, in most cases, it is not even clear whether static nuclei are actively positioned, for example, by a balance-of-forces mechanism analogous to that which positions the centrosome [195]. Nonetheless, nuclei occupy specific positions characteristic of cell and tissue type suggesting active positioning mechanisms [11]. For example, nuclei in epithelia are positioned basally, centrally or apically depending on epithelial type. Nuclei in most cultured cells localize near the cell centroid, but move rearward upon initiation of migration [1, 3, 136, 196].

To understand nuclear positioning, it would be useful to have a means to physically displace nuclei in addition to molecular approaches that disrupt nuclear membrane proteins. Nuclei can be moved with microneedle techniques [159, 197], but these produce only local movements and are limited to single cell analysis. Centrifugation has been used to displace nuclei in yeast and has helped elucidate mechanisms by which the nucleus determines the cell division plane [198]. Here, we develop a technique to displace nuclei in cultured adherent cells using centrifugal force. With this system, we identify novel nuclear linkage mechanisms to the actin and MT cytoskeletons that contribute to homeostatic nuclear positioning.

Results

Centrifugal force displaces selectively displaces nuclei in adherent cells

We modified protocols to enucleate cells using centrifugation [157] to instead displace nuclei within adherent cells. By omitting cytoskeletal drugs needed for enucleation and reducing actin filament density by serum starvation, we found that centrifugation at a modest force (5,000 *g* for 30 min) displaced nuclei within cells. In NIH3T3 fibroblasts, centrifugation displaced nuclei to similar extents in cells at the edge of a wounded monolayer and cells within monolayers (Figure 1B and 1C). Interestingly, in monolayers with wounds oriented orthogonal to the centrifugal force (as depicted in Figure 3.1A), nuclei were displaced equivalently toward the cell front on one side of the wound and toward the cell rear on the other (Figure 3.1B and 3.1C). Nuclei were also displaced in sparse cells grown in serum, although longer centrifugation was required (Figure 3.1C and S3.1A). Thus, in both unpolarized cells (within the monolayer and sparsely plated) and polarized cells (at the wound edge) centrifugation was effective in displacing nuclei.

To more broadly explore the relationship between force and nuclear displacement, we varied centrifugal force from 1,000 - 20,000 *g* and examined nuclear displace in wound edge, serum-starved NIH3T3 fibroblasts. Nuclear displacement increased with centrifugal force and occurred to the same extent on both sides of the monolayer (Figure 3.1D). Centrosomes were also displaced in the direction of centrifugal force, but less so (Figure 3.1D). Both nuclear and centrosomal displacement was linearly correlated with centrifugal force (Figure S3.1B). Interestingly, centrifugation at 5,000 *g* for 30 min generated nuclear displacement similar to that following stimulation with the serum factor lysophosphatidic acid (LPA) (Figure 3.1D) [1].

Given the similarity to a physiological displacement of the nucleus, we further characterized the effect of 5,000 *g* on NIH3T3 fibroblasts. Cell shape indicated by circularity and aspect ratio, together with cellular area, were unaltered by 5,000 *g* (Figure S3.1C). Cell-cell contacts, MTs, and actin distribution also did not appear to be grossly affected by centrifugation (Figure 3.1B and S3.1D). There was some increase in actin filament staining after centrifugation (Figure S3.1D), consistent with the response of fibroblasts to mechanical force [199, 200], although there was no difference between the two sides of the wound. Whereas the nucleus was displaced ~25% of the cell radius by 5,000 *g*, the centrosome was moved less than 10%, and the ER, mitochondria and Golgi, as measured by their summed centroid position, were displaced less than 5% (Figure S3.1E and S3.1F). The relatively larger displacement of the nucleus is consistent with organelles responding to centrifugal force according to their relative size and density. The displacement of many of the smaller organelles may be additionally restricted by their tethering to MTs.

Displaced nuclei actively recenter

If nuclei are actively positioned near the centroid of the cell, then their displacement by centrifugation should reflect a meta-stable position. Indeed, when centrifuged monolayers were incubated at 37 °C and examined after different intervals, nuclei repositioned toward the cell centroid from both sides of the wound over about one hour (Figure 3.2A and 3.2B). This recentration of nuclei after centrifugation was reversibly blocked if cells were allowed to recover at 4 °C and then shifted to 37 °C (Figure 3.2A and 3.2B). Similar recentration of centrifugally

displaced nuclei was observed in cells within the monolayer and in sparse cells (Figure 3.2C). Centrosomes also recentered, although the total distance moved was much less.

To test whether other adherent cells actively positioned their nuclei, we centrifuged mouse C2C12 myoblasts and human HeLa adenocarcinoma and HT1080 fibrosarcoma cells. Increased centrifugal time (compared to NIH3T3 fibroblasts) was needed to displace nuclei in some of these cell types, yet in each case, nuclei recentered within an hour after centrifugation (Figure S3.2A-D).

The above results indicate that cells faithfully restore their nuclear position after centrifugation. To test this further, we used centrifugation to displace nuclei in serum starved NIH3T3 fibroblasts and then stimulated them with LPA, which causes nuclei at both sides of the wound to move rearward [1, 3]. Nuclei in centrifuged cells stimulated with LPA repositioned rearward of the cell center on both sides of the wound, similar to the position of nuclei in uncentrifuged cells stimulated with LPA (Figure S3.2E). These results show that centrifugation does not alter the underlying mechanisms that position nuclei either centrally or eccentrically.

Distinct cytoskeletal mechanisms mediate forward and rearward nuclear recentration

We noted that 30 min after centrifugation, nuclei displaced forward were already recentered, while those displaced rearward were not (Figure 3.2A). Measurements of nuclear position at fixed time points following centrifugation confirmed this impression and showed that nuclei moving rearward from the front of the cell completed recentration sooner that those moving forward from the rear (Figure 3.2D). Time lapse phase contrast movies showed directly

that nuclei moved faster during rearward than forward recentration (Figure 3.2E and 3.2F). These movies also revealed that the leading edge did not protrude or retract during nuclear recentration and once nuclei recentered, they ceased movement and remained in place for at least 30 min (Figure 3.2E).

Displaced nuclei in cells at the edge of wounded monolayers provided a unique opportunity to explore the mechanisms for nuclear recentration. Displaced nuclei in these cells recentered in different directions (relative to the front-back axis of the cells) and moved at different rates, suggesting the possibility that distinct mechanism were involved. Accordingly, we treated wounded monolayers after centrifugation with cytoskeletal drugs and measured the extent of recentration. Drugs that disrupted actin filaments or inhibited myosin II ATPase inhibited rearward nuclear recentration, but not forward recentration (Figure 3.3A and 3.3B). Conversely, drugs that disrupted MTs or inhibited dynein ATPase [201] inhibited forward, but not rearward, nuclear recentration. Knockdown of dynein heavy chain (DHC) or the dynactin subunit $p150^{Glued}$ also specifically prevented forward re-centering (Figure 3.3C, S3.3A and S3.3B). Thus, different cytoskeletal systems mediate nuclear recentration in the two directions in wound edge cells. In contrast, nuclear recentration in serum starved cells within the monolayer was inhibited by MT, but not actin drugs (Figure 3.3D and S3.3C). Interestingly, nuclear recentration in non-serum starved cells within the monolayer was sensitive to both MT and actin drugs (Figure 3.3E). Together, these results show that mechanisms for nuclear recentering are context dependent.

To visualize actin filaments and MTs during recentration, we prepared stable NIH3T3 cell lines expressing GFP-Lifeact or GFP-tubulin. In wound edge cells with rearward recentering

nuclei, retrograde flow of actin cables was detected in 60% (N= 29) of the cells and occurred at the same rate as that of rearward nuclear recentration (Figure 3.3F and 3.3G). Movies of forward recentering nuclei in GFP-tubulin expressing cells revealed that in 61% of the cases (N=18), the nucleus re-centered by moving towards and then passing the centrosome (Figure 3.3H). In most of the other cases, the nucleus appeared to pivot around the centrosome as it moved forward (Figure S3.3D). Thus, for most cells, forward recentration occurred toward the minus ends of MTs, consistent with the involvement of dynein.

Forward and rearward nuclear recentration require distinct LINC complex components

Many nuclear movements depend on the LINC complex [11]. We first tested whether either rearward or forward nuclear recentration in wound edge cells was LINC complex-dependent by overexpressing a dominant negative GFP-KASH construct, which disrupts all LINC complexes [3, 15, 82]. GFP-KASH expression drove endogenous nesprin-2G out of the nuclear envelope (Figure S4A) and strongly inhibited both forward and rearward nuclear recentration (Figure 3.4A). GFP-KASH expression also increased the displacement of nuclei subjected to lower centrifugal forces (Figure 3.4B or Figure S3.4B). These results show that LINC complexes participate both in the active recentering of the nucleus and it is static positioning at the cell center.

We next tested the role of nesprin-2G during recentering because of its known role in attaching retrogradely moving actin cables to the nucleus during LPA-stimulated rearward nuclear movement in fibroblasts and myoblasts [3, 16, 136]. Interestingly, knocking down

nesprin-2G inhibited both rearward and forward recentration, (Figure 3.4B and S3.4B). These defects were rescued by reexpressing appropriate nesprin-2G constructs (see Figure 3.5A)

We next knocked down the only SUN proteins expressed in NIH3T3 fibroblasts: SUN1 and SUN2 [3, 202, 203]. SUN1 knockdown inhibited forward nuclear recentration without affecting rearward recentration (Figure 3.4C and S3.4C). Conversely, SUN2 knockdown inhibited rearward nuclear recentration, without affecting forward recentration. Knockdown of both SUNs inhibited both forward and rearward recentration. The nuclear recentration defects in the knockdown cells were rescued by reexpressing the appropriate RNAi resistant human SUNs, but not the inappropriate SUN (i.e., SUN2 did not rescue SUN1 knockdown and vice versa) (Figure 3.4D and 3.4E).

Interestingly, while re-expression of the knocked down SUN protein rescued the original nuclear recentration defect, it inhibited recentration in the opposite direction (Figure 3.4D and 3.4E), suggesting that the SUNs exerted trans-dominant negative effects on each other. Such an effect was confirmed by overexpressing myc-tagged SUNs in wildtype cells. SUN1 overexpression specifically inhibited rearward recentration, whereas SUN2 overexpression specifically inhibited forward recentration (Figure 3.4F). As knockdown of one SUN protein did not affect the level of the other, and both MT-dependent forward and actin-dependent rearward nuclear recentration required nesprin-2G, these results suggest that SUN proteins compete for a limited amount of nesprin-2G.

To determine whether the trans-dominant effect of SUN protein over-expression depended on engagement of nesprin-2G with the cytoskeleton, we inhibited MTs or actin in SUN overexpressing cells after centrifugation. Interestingly, disrupting MTs restored actin-dependent

rearward movement in SUN1 overexpressing cells (Figure 3.4G), whereas disrupting actin filaments restored MT-dependent forward movement in SUN2 overexpressing cells (Figure 3.4H). These results imply that proper engagement of nesprin-2G by the cytoskeleton stabilizes the nesprin-2G-SUN interaction and are consistent with the idea that different nesprin-2G-SUN complexes preferentially interact with MTs or actin (see Discussion).

Mechanism of MT-dependent, forward nuclear recentering

Because actomyosin, nesprin-2G and SUN2 are required for LPA-stimulated rearward nuclear movement, we tested another factor involved in this movement, the formin FHOD1 [16, 17]. Knockdown of FHOD1 by shRNAs inhibited rearward, but not forward, nuclear recentration (Figure S3.4D and S3.4E). Additionally, adhesive TAN (transmembrane actin-dependent nuclear) lines, which mediate LPA-stimulated nuclear movement [3, 136, 180], also formed during rearward nuclear recentration (Figure S3.4F). These results strongly suggest that rearward nuclear recentration occurs by a similar mechanism as LPA-stimulated rearward nuclear movement in NIH3T3 fibroblasts and C2C12 myoblasts [3, 136].

It was less clear how MT-dependent forward recentering occurred. A kinesin-1– nesprin-2 interaction contributes to nuclear spacing in syncytial myotubes [114], but forward nuclear recentering primarily occurred toward MT minus ends and depended on dynein (Figure 3.3). Dynein and nesprin-2 contribute to centrosomal-directed nuclear movement in migrating neurons, and dynein has been reported to associate with nesprin-2 [115, 144]. To explore how nesprin-2 contributed to MT- and dynein-dependent forward nuclear recentration, we first sought

to identify the region of nesprin-2 responsible. As expected, re-expression of nesprin-2 constructs harboring the N-terminal actin-binding calponin homology (CH) domains rescued rearward, but not forward, nuclear recentration in nesprin-2G depleted cells (Figure 3.5A and S3.5A). Nesprin-2 constructs containing the C-terminal spectrin repeats (SR) 52-56 of nesprin-2G rescued forward, but not rearward, nuclear recentration. Constructs containing both the CH domains and SR52-56 rescued recentration in both directions (Figure 3.5A and S3.5A). Thus, forward and rearward nuclear recentering activities of nesprin-2G can be separated, but individual constructs of nesprin-2G combining its independent activities rescued nuclear recentration in both directions.

The nesprin-2 SR52-56 KASH construct that rescued forward nuclear recentration contains a kinesin-1 binding LEWD motif [114]. Reexpression of nesprin-2 SR52-56 KASH LEAA, in which the LEWD domain is mutated to make it deficient in kinesin-1 binding (ref 17 and Figure S3.5B), restored most of the forward recentering in nesprin-2G depleted cells (Figure 3.5A and S3.5A). Additionally, knock down of the most abundant kinesin heavy and light chains expressed in NIH3T3 fibroblasts (Kif5b and KLC1) with multiple siRNAs did not consistently inhibit forward recentration despite substantially reducing Kif5b and KLC1 levels (Figure S3.5C and S3.5D). These results suggest that kinesin-1 does not play a major role in forward nuclear recentration.

We next probed immunoprecipitates of GFP-nesprin-2 SR52-56 KASH to test whether it interacted with dynein or dynactin. Both DHC and the $p150^{Glued}$ subunit of dynactin co-immunoprecipitated with nesprin-2 SR52-56 KASH (Figure 3.5B). Additionally, GST-tagged fragments spanning nesprin-2 SR52-56 showed that SR52-AD and SR52-54, but not SR52 or

SR52-53, pulled down DHC and p150^{Glued} from cell lysates (Figure 3.5C). Lastly, both WT and the LEAA mutant forms of nesprin-2 SR52-56 KASH interacted with dynactin even though the mutant form failed to interact with kinesin-1 (Figure S3.5B). These data are consistent with dynein and dynactin mediating MT-dependent forward nuclear recentration by interacting with a region near the C-terminus of nesprin-2 that includes SR52-53 and the "adaptive domain" [204].

To test the role of dynein and dynactin further, we compared their localization in NIH3T3 fibroblasts overexpressing the nesprin-2 rescue constructs. Dynein intermediate chain (DIC) and p150^{Glued} localization on the nuclear envelope were enhanced in cells overexpressing SR52-56 KASH and SR52-56 KASH LEAA compared to SR54-56 KASH, which does not contain the dynein interacting site (Figure 3.5D and 3.5E). These results strengthen the conclusion that the C-terminus of nesprin-2 recruits dynein and dynactin to the nuclear envelope for forward nuclear recentration.

The actin and MT activities of nesprin-2 are required for homeostatic nuclear positioning

To determine whether the nuclear recentering mechanisms we identified in centrifuged cells were important to position nuclei in uncentrifuged cells, we examined the effect of knocking down nesprin-2 expression on nuclear position in otherwise unperturbed NIH3T3 fibroblasts. Whereas nuclei were localized near the cell centroid in control knock down cells, they were much more scattered in nesprin-2 depleted cells (Figure 3.6A and 3.6B). Treating this scattering as a diffusive process revealed a significant difference in the mean squared displacement of the nucleus in nesprin-2 depleted cells (Figure 3.6B). We re-expressed nesprin-2

constructs in the depleted cells to determine whether the actin or MT motor binding activities of nesprin-2 were critical for maintaining nuclei near the cell centroid. Reexpression of nesprin-2 constructs that bind actin (miniN2G) or MT motors (SR51-56 KASH) alone failed to rescued the centroid position of nuclei; in fact, their expression seemed to cause further scattering (Figure 3.6A and 3.6B). In contrast, a nesprin construct that binds both actin and MT motors (CH-SR51-56 KASH) fully rescued the centroid positioning of the nucleus.

Discussion

Our studies reveal active mechanisms of homeostatic nuclear positioning in adherent cells. We prefer the term homeostatic nuclear positioning to describe our results rather than the previously used “nuclear anchorage” [82, 205], because it encompasses the concept that nuclei actively return to a preset position. It has been hypothesized that nuclei localize to the cell center due to their linkage to the centrosome, whose central position is known to be maintained by microtubules [195]. Yet, in acentrosomal mouse oocytes actin centers the nucleus by an active diffusion process [206] and actin is important for anchoring nuclei in worm hypodermal cells [82]. Here, we find that both actin- and MT-dependent LINC complexes contribute to homeostatic positioning of the nucleus. Interestingly, the requirement for these cytoskeletal elements for positioning the nucleus depended on cellular context and polarization. Thus, polarized cells at the wound edge recentered displaced nuclei by actin or MTs depending on the initial nuclear location (Figure 3.6C), whereas nuclei in cells within the monolayer required only MTs unless they were first stimulated with serum, which activated an additional requirement for actin. These different mechanisms for homeostatic nuclear positioning likely reflect different activity states of the actin cytoskeleton, such as the retrograde flow of actin that is activated in wound edge cells.

The existence of active homeostatic mechanisms for nuclear positioning has important implications for nuclear movement and function. It has been assumed that nuclear movement during developmental or cell polarization is initiated by the activation of the motility machinery that propels the nucleus. Our results suggest that homeostatic mechanisms may be modulated to allow for nuclear movement. For example, in monolayer cells in serum where both actin and

MTs maintain the nucleus in the cell center, it would be possible to initiate movement of the nucleus by decreasing nuclear connections to one of the two cytoskeletal elements. According to this idea, the homeostatic mechanism we have described would keep the nucleus in a state of readiness for movement.

The existence of active mechanisms for homeostatic nuclear positioning also implies that the nucleus is under constant force by the cytoskeleton. This conclusion is consistent with the findings of other recent studies. For example, a nesprin-2-based actin tension sensor revealed that static nuclei of mouse and human fibroblasts are under constant actomyosin force [162] and local displacement of nuclei by microneedles showed cytoskeletal dependent restoring forces [159, 197]. Also, in both the differentiation of mouse embryonic stem cells and early Drosophila development, nuclei are reported to be prestressed as their shape is altered by disrupting cytoskeletal elements [207]. Given these findings, and our results that active homeostatic positioning occurs in varied cellular contexts, we suggest that a constantly stressed nucleus may be a general feature of eukaryotic cells. The stressed state of the nucleus may impact functions beyond nuclear positioning, for example by activating mechanotransduction pathways inside the nucleus [163] or by altering gene expression [208].

Our study also reveals previously unexpected aspects of LINC complex function, particularly for nesprin-2G's interaction with the cytoskeleton and SUN proteins. Nesprin-2G is one of two giant nesprin isoforms in vertebrates (nesprin-1G is the other) and both were initially thought to specifically mediate connections to the actin cytoskeleton through their paired CH domains in their N-terminus. These proteins do indeed use their CH domains to link the nucleus to the actin [3, 110, 112] and at least for nesprin-2G additionally connect to actin cables through

the formin FHOD1 and the actin bundling protein fascin [16, 189]. However, both nesprin-1 and nesprin-2 contain LEWD motifs in their C-terminus and nesprin-2 has been shown to bind kinesin-1 through this motif to space nuclei in myotubes [114]. We now identify a site in the C-terminus of nesprin-2 that interacts with dynactin and dynein and is important for homeostatic positioning of nuclei in several cellular contexts. The fact that nesprin-2G can interact with both actin and MTs through kinesin and dynein motors to exert force on the nucleus, suggests it should be considered a general nuclear scaffold for the cytoskeletal. Indeed, our data show that a single nesprin-2G construct can rescue both actin- and MT-dependent recentering activities. Perhaps this explains in part the large size of nesprin-2G. Although we cannot be certain in our case that a single nesprin-2G is engaged simultaneously by both cytoskeletal elements, it will be interesting to understand how these cytoskeletal activities are regulated. The cytoskeletal scaffolding function of nesprin-2G, its large size and SRs comprising the bulk of its secondary structure, bears striking resemblance to another class of proteins, the spectraplakins, which also act as cytoskeletal linkers in the cytoplasm [209].

Our results also show a striking specificity of cytoskeletal function for the two SUN proteins. SUN1 was required for MT-based recentering of the nucleus, whereas SUN2 was required for actin-based recentering. This conclusion is supported by the results from the individual knockdowns of the SUN proteins and from their trans-dominant effects when overexpressed, which show that SUN1 and SUN2 are in competition for nesprin-2G. Although initial knockout studies in mice suggested SUN1 and SUN2 act redundantly during development [115, 116, 210], recent studies in mice support separate functions for SUN proteins [41, 81, 211].

That SUNs seem to differentially engage the cytoskeleton raises the interesting question of how the SUNs "know" which cytoskeletal element nesprin-2G is engaged with. It is unlikely that the nesprin-2G KASH domain interacts differentially with the SUN1 and SUN2 domains, as studies show that the affinities are the same [76]. Perhaps the forces exerted though nesprin-2G by actin and MTs somehow select for one SUN protein over the other. Indeed, our results showing that the trans-dominant effect of overexpressed SUN proteins is lost upon disruption of cytoskeletal elements supports this view. Other factors that may contribute to this are the different oligomeric structures for the SUN proteins, known to be a trimer for SUN2 [43, 44] and suspected to be di- or tetramer for SUN1 [49]. SUN1 and SUN2 are also differentially anchored to the lamina with some evidence that SUN1 is more tightly associated [15, 76].

The method of centrifugal displacement of the nucleus we have developed should be broadly useful to address additional questions about the forces and connections of the cytoskeleton to the nucleus. For example, it should now be possible to address whether homeostatic nuclear positioning mechanism are altered during developmental or physiological events, such as when stem cells are differentiated into mature cells or when cells receive a physiological stimulus such as a chemotactic factor. It may be possible to adapt the method to relate how much centrifugal force is necessary to displace the nucleus to address questions about the strength of the underlying nuclear-cytoskeletal connections. For example, we found that in KASH expressing cells centrifugal displacement of nuclei is increased. This suggests it will be useful to use centrifugation to examine whether homeostatic nuclear positioning is altered by disease causing variants of the LINC complex or nuclear lamins.

Experimental Procedures

KEY RESOURCES TABLE

	SOURCE	IDENTIFIER
Antibodies		
Rabbit polyclonal anti-SUN2	Abcam	CAT # ab87036
Mouse monoclonal anti-p150[Glued]	BD Biosciences	CAT # 610473
Mouse monoclonal anti-GM130	BD Biosciences	CAT # 610822
Mouse monoclonal anti-pericentrin	BD biosciences	CAT # 611814
Rabbit polyclonal anti-pericentrin	Covance	CAT # PRB-432C
Rat monoclonal anti-Tyr tubulin	European Collection of Animal Cell Cultures	YL1/2
Rabbit polyclonal anti-SUN1	Gift of Dr. S. Shackleton, U. of Leicester	NA
Mouse monoclonal anti-DIC	Gift of Dr. R. B. Vallee, Columbia U	NA
Mouse monoclonal anti-KLC 63-90	Gift of Dr. S. T. Brady, U. of Illinois at Chicago	NA
Donkey anti-chicken Alexa 488	Jackson ImmunoResearch Laboratories	CAT # 703-545-155

Donkey anti-mouse Alexa 488	Jackson ImmunoResearch Laboratories	CAT # 715-545-151
Donkey anti-mouse Cy3	Jackson ImmunoResearch Laboratories	CAT # 715-165-151
Donkey anti-rabbit Cy2	Jackson ImmunoResearch Laboratories	CAT # 711-225-152
Donkey anti-rabbit Cy3	Jackson ImmunoResearch Laboratories	CAT # 711-165-152
Donkey anti-rat Alexa 647	Jackson ImmunoResearch Laboratories	CAT # 712-605-153
Donkey anti-mouse IRDye® 680	LI-COR Biosciences	P/N # 925-68072
Donkey anti-rabbit IRDye® 680	LI-COR Biosciences	P/N # 925-68073
Donkey anti-mouse IRDye® 800CW	LI-COR Biosciences	P/N # 925-32212
Donkey+A20 anti-rabbit IRDye® 800CW	LI-COR Biosciences	P/N # 925-32213
Rabbit polyclonal anti-nepsin 2G	[3]	S2-CH
Mouse monoclonal anti-KHC	Millipore	MAB1614. Clone H2. CAT # MAB1614
Chicken polyclonal anti-GFP	Millipore	CAT # AB16901

Mouse monoclonal anti-MYC	Roche	Clone 9e10 CAT # 11667149001
Mouse monoclonal anti-FHOD1	Santa Cruz	D-6. CAT # sc-365437
Rabbit polyclonal anti-DHC	Santa Cruz	R-325. CAT # sc-9115
Goat anti-rabbit IgG-HRP	Santa Cruz	CAT # sc-2004
Goat anti-mouse IgG-HRP	Santa Cruz	CAT # sc-2005
Mouse monoclonal anti-PDI	Stressgen	Clone 1D3. CAT # SPA-891
Rabbit polyclonal anti-GFP	Thermo Fisher Scientific	CAT # A11122
Mouse monoclonal anti-beta catenin	Thermo Fisher Scientific	Clone CAT-5H10, CAT # 13-8400
Mouse monoclonal anti-GAPDH	Thermo Fisher Scientific	CAT # AM4300
Rabbit polyclonal anti-GAPDH	Santa Cruz	CAT # sc-25778
Chemicals, Peptides, and Recombinant Proteins		
LPA	Avanti Polar Lipids	CAT # 857130P
Cytochalasin D	Sigma-Aldrich	CAT # C8273
Latrunculin A	Sigma-Aldrich	CAT # L5163

Blebbistatin	Sigma-Aldrich	CAT # B0560
Nocodazole	Sigma-Aldrich	CAT # M1404
Taxol	Sigma-Aldrich	CAT # T7402
HPI-4	Sigma-Aldrich	CAT # H4541
Fluoromount-G	Southern Biotech	CAT # 0100-01
Rhodamine Phalloidin	Thermo Fisher Scientific	CAT # R415
MitoTracker Red CMXRos	Thermo Fisher Scientific	CAT # M7512
Halt protease and phosphatase inhibitor cocktail (78440, Thermo Fisher Scientific,	Thermo Fisher Scientific	CAT # 78440
4’ , 6-diamidino-2-phenylindole (DAPI)	Sigma-Aldrich	CAT # D9542
Critical Commercial Assays		
QuikChange Lightning Site-Directed Mutagenesis Kit	Agilent	CAT # 210518
Dynabeads Protein G for Immunoprecipitation	Thermo Fisher Scientific	CAT # 10003D
Lipofectamine RNAiMAX Transfection Reagent	Thermo Fisher Scientific	CAT # 13778150
Experimental Models: Cell Lines		

NIH3T3	ATCC	ATCC CRL-1658
C2C12	Gift of Dr. H. J. Worman	ATCC CRL-1772
HeLa	Gift of Dr. Y. Mao	ATCC CCL-2
HT1080	ATCC	ATCC CCL-121
293T	ATCC	ATCC CRL-3216
Oligonucleotides: siRNA		
siRNA against DHC, oligo 1 (DHC-1): GGGAGGAGGUUAUGUUUAATT and UUAAACAUAACCUCCUCCCTT	This paper	NA
siRNA against DHC, oligo 2 (DHC-2): GGGUAAAGCUAGAGAGAAUTT and AUUCUCUCUAGCUUUACCCTT	This paper	NA
siRNA against p150[glued], oligo 1 (p150[glued]-1): GGAGAUUCUCAAGGCUGAATT	This paper	NA
siRNA against KLC1, oligo 1 (KLC1-1): ACGAGGAGGUGGAGUAUUATT	This paper	NA
siRNA against KLC1, oligo 3 (KLC1-3): GAGUAUGGCGGCUGGUAUATT	This paper	NA
siRNA against KLC1, oligo 4 (KLC1-4): GAGAGUGGCUGAAGUGCUATT	This paper	NA

siRNA against nesprin-2G: CCAUCAUCCUGCACUUUCATT	[3]	NA
siRNA against SUN2: GGGUCAUUCUGCAGCCAGATT	[3]	NA
siRNA against Kif5b, oligo 1 (Kif5b-1): GAGCUAAACCGUUGGCGUATT	[212]	NA
siRNA against Kif5b, oligo 2 (Kif5b-2): GCAAGAAGUAGACCGGAUATT	[212]	NA
siRNA against Kif5b, oligo 3 (Kif5b-3): CAACAGACAUGUCGCAGUUTT	[212]	NA
siRNA against Kif5b, oligo 4 (Kif5b-4): CAGGACAGAUGAAGUAUAATT	[212]	NA
Oligonucleotides: primers		
See Table S1-S2		
Recombinant DNA		
pMSCV-puro myc-hSUN1	This paper	NA
pMSCV-puro myc-hSUN2	This paper	NA
pSUPER.retro.puro SUN1	This paper	NA
pSUPER.retro.puro nesprin-2	[213]	NA
pMSCV-puro GFP-mini-N2G	[136]	NA

pMSCV-puro GFP-Lifeact	This paper	NA
pMSCV-puro GFP-tubulin	This paper	NA
pMSCV-puro GFP-KASH	This paper	NA
pSUPER.retro.puro FHOD1-1	[214]	NA
pSUPER.retro.puro FHOD1-2	[214]	NA
Nesprin-2G constructs:		
pMSCV-puro GFP-miniN2G SR2-13	This paper	NA
pMSCV-puro GFP-miniN2G SR49-56	This paper	NA
pMSCV-puro GFP-miniN2G SR51-56	This paper	NA
pMSCV-puro GFP-SR49-56 KASH	This paper	NA
pMSCV-puro GFP-SR51-56 KASH	This paper	NA
pMSCV-puro GFP-SR52-56 KASH	This paper	NA
pMSCV-puro GFP-SR52-56 KASH LEAA	This paper	NA
pMSCV-puro GFP-SR53-56 KASH	This paper	NA
pMSCV-puro GFP-AD-56 KASH	This paper	NA
pMSCV-puro GFP-SR54-56 KASH	This paper	NA

pMSCV-puro GFP-AD-56 KASH	This paper	NA
pMSCV-puro GFP-SR49-53 KASH	This paper	NA
pMSCV-puro GFP-SR51-53 KASH	This paper	NA
pMSCV-puro GFP-SR52-56 KASH ΔAD	This paper	NA
pMSCV-puro GFP-SR53-56 KASH ΔAD	This paper	NA
pGEX 6P-4 SR52-54	This paper	NA
pGEX 6P-4 SR52-53	This paper	NA
pGEX 6P-4 SR52-AD	This paper	NA
pGEX 6P-4 SR52	This paper	NA
Software and Algorithms		
Metamorph	MDS Analytical Technologies	NA
NIS-Element	NIKON	NA
Fiji	ImageJ	NA
Graphpad	Prism	NA
Excel	Microsoft	NA
Cell Plot	[215]	NA

Other		
Attofluor Cell Chamber	Thermo Fisher Scientific	CAT # A7816
Chamber for replaceable 22x22mm square coverslips	Bioscience Tools	CAT # CSC-22x22
Ultraclear centrifuge tubes	Beckman Coulter	Part # 344058
Polyallomer centrifuge tubes	Beckman Coulter	Part # 326819

Cell culture

Low passage NIH3T3 fibroblasts (originally from ATCC) were grown in DMEM (Corning Cellgro) plus 10 % calf serum (Hyclone). For wounded monolayers, NIH3T3 fibroblasts were plated on 1.5 mm acid-washed coverslips, grown to confluency, wounded and treated either with 10 μM LPA to trigger rearward nuclear movement and centrosome orientation as previously described [185, 216] or used in centrifugation experiments. 293T cells (ATCC) were grown in DMEM plus 10% calf serum (Hyclone). Mouse C2C12 myoblasts (gift from Howard Woman, Columbia U), HeLa cells [217] (ATCC, CCL-2; gift from Yinghui Mao, Columbia U) and human fibrosarcoma HT1080 cells (ATCC) were grown in DMEM plus 10% fetal bovine serum and 10 mM HEPES, pH 7.4. All cell lines were cultured in 5% CO_2 at 37 °C.

Plasmids and Chemicals

All labeled GFP-tagged constructs used in this paper are EGFP-tagged proteins. Constructs of pSUPER.retro.puro nesprin-2 and pMSCV-puro GFP-mini-N2G were described previously [136, 213]. Constructs of myc-hSUN1 and myc-hSUN2 from previous study are cloned into pMSCV-puro plasmid to make pMSCV-puro myc-hSUN1 and pMSCV-puro myc-hSUN2. pMSCV-puro GFP-C4 Lifeact was prepared by introducing the Lifeact sequence (MGVADLIKKFESISKEE) to the C-terminus of GFP with BglII and BamHI restriction sites. The mouse miniN2G sequence was PCR amplified from GFP-mini-N2G described previously[3] and sub-cloned into the pMSCV vector (Clontech Laboratories, Mountain View, CA) at the NotI site. For the chimeric GFP-tagged nesprin-2 constructs used in the rescue experiments, portions of the N-terminus and C-terminus of mouse nesprin-2G were amplified by PCR (for primers, see Table S1), ligated and then the joined fragment was amplified by PCR. The joined fragment was digested by NotI and inserted into pMSCV-puro EGFP-C4 vector. For constructs containing the region between SR53 and 54, we used the sequence obtained from nesprin-2G in NIH3T3 fibroblasts and embryonic mouse forebrain, which is different from that in NCBI (2014), as previously reported [16]. For the GST-tagged N2G constructs, NIH3T3 cDNA or existing N2G constructs were used as templates. Primers for all the C-terminal GFP-nesprin-2 rescue constructs together with the GST-nesprin-2 pull down constructs are listed in Table S2. The LEWD motif in mouse nesprin-2G SR52-56 was mutated to LEAA by site-directed mutagenesis using QuikChange Lightning (Agilent Technologies, Santa Clara, CA) as previously described [217]. Constructs containing shFHOD1-1 (5'-aggagccgaagatcactagaag-3') and shFHOD1-2 (5'-gctgtgccaaggtggactttga-3') were prepared using previously validated shRNA sequences [218] and cloning into the pSUPER.retro.puro vector

(Oligoengine, Seattle, WA). Construct containing shSUN1 (5'- aggctattgattcgcacatta-3') was cloned into pSUPER.retro.puro. All constructs were verified by sequencing. LPA was from Avanti Polar Lipids (Alabaster, AL). Other chemicals were purchased from Sigma-Aldrich (St Louis, MO) unless otherwise noted.

Adaptor and Centrifugation

Initial centrifugation experiments were conducted with custom centrifuge adaptors (10 mm diameter) that were the generous gifts of Vladimir Rodionov (U Connecticut). Based on their design, custom polysulfone adaptors (22 mm in diameter) were prepared allowing coverslips up to 22 mm^2 to be used. Adaptors containing coverslips were assembled into ultraclear centrifuge tubes (Beckman No. 344058) for 22mm adaptor or polyallomer centrifuge tubes (Beckman No. 326819) for 10 mm adaptor, filled with conditioned serum free media and centrifuged in a swinging bucket rotor (Beckman Type 55 or 28) in a pre-heated 36 °C centrifuge. Samples were fixed for immunofluorescence or mounted into cell chambers (Attofluor® No. A7816, Thermo Fisher Scientific) or an imaging adaptor (Bioscience Tools, No. CSC-22x22) for live cell recording.

Protein knockdown and Western blot analysis

Viruses containing shRNA targeting FHOD1 and SUN1 were prepared by expressing the aforementioned pSUPER constructs in 293T cells. NIH3T3 fibroblasts were infected with shRNA encoding viruses to achieve protein knockdown as described previously [47]. shLuciferase was

used as a control in these experiments. siRNAs sequences to SUN2, nesprin-2G and Kif5b were previously described [3, 212] . Other siRNA sequences (see Table S3) were predicted by either Dharmacon or Invitrogen siRNA designer. All siRNAs (21-mers) were from obtained Shanghai GenePharma. Noncoding siRNA was used as a control in the experiments. Transfection was with Lipofectamine RNAiMAX (Thermo Fisher Scientific, Waltham, MA) according to the manufacturer's instructions. Efficiency of protein depletion was determined by western blot analysis of total cell lysates as previously described previously [213], using: rabbit anti-SUN2 (1:1000; No.87036, Abcam), rabbit anti-Nesprin 2G (1:1000) [3], rabbit anti-SUN1 (1:1000; gift from Sue Shackleton, University of Leicester), mouse anti-FHOD1 (1:1000; Clone: D-6, Santa Cruz Biotechnology, Dallas, TX), rabbit anti-dynein heavy chain (1:500; 9115 Santa Cruz Biotechnology, Dallas), mouse anti-kinesin heavy chain (1:500; MAB1614, clone H2, EMD Millipore, Billerica, MA), mouse anti-kinesin light chain 63-90 (1:1000; gift from Scott Brady, U Illinois-Chicago), mouse anti-p150^{glued} (1:500; 610473, RUO, BD Biosciences, Franklin Lakes, NJ), and mouse anti-dynein intermediate chain (1:1000; gift from Richard Vallee, Columbia U). Western blots were developed with IRDye® 680 and IRDye® 800CW secondary antibodies raised in donkey (LI-COR Biosciences, Lincoln, NE) and imaged with Odyssey.

Immunofluorescence

Cells were fixed with 4 % paraformaldehyde in PBS for 10 min at room temperature and then permeabilized with 0.5% Triton™ X-100. For staining MTs and dynein/dynactin, cells were fixed in -20 °C methanol for 5 min; for dynein/dynactin staining, starved cells were additionally pretreated for 1 hr with 10 µM nocodazole before fixation [148]. Cells were blocked with blocking

buffer (1X PBS; 5% BSA; 0.3% Triton™ X-100) in room temperature for 1 hr and then incubated with primary antibodies diluted in the antibody buffer (1X PBS; 1% BSA; 0.3% Triton™ X-100) for 1 hr at room temperature or overnight at 4 °C. The following antibodies were used: rabbit anti-nesprin 2G [3] (1:100), rabbit anti-pericentrin (1:400; PRB-432C, Covance), mouse anti-pericentrin (1:100; No. 611814 BD biosciences), mouse anti- -catenin (1:400; CAT-5H10, Thermo Fisher Scientific) rat anti-Tyr tubulin (1:40; YL1/2 European Collection of Animal Cell Cultures), mouse anti-myc (1:400; 9E10, Roche), chicken anti-GFP (1:100; AB16901, EMD Millipore). Rhodamine-phalloidin (1:200; A12379, Thermo Fisher Scientific) was used to stain F-actin. After washing with PBS, cells were incubated with fluorescent secondary antibodies absorbed to minimize species cross-reactivity (Jackson ImmunoResearch, West Grove, PA) for 1 hr at room temperature and mounted in Fluoromount-G (Southern Biotech, Birmingham, AL).

Microscopy

Images of stained cells were acquired with either 40× Plan Apo (NA1.0) or 60× Plan Apo (NA1.4) objectives and a CoolSNAP HQ CCD camera on a Nikon TE300 inverted microscope controlled by Metamorph (Molecular Devices) or with 60× Apo TIRF (NA 1.49) objective and a camera (Andor iXon3 888, back-illuminated EMCCD) on an inverted microscope (Nikon Eclipse Ti) controlled by NIS elements software. Phase contrast live cell imaging was performed on a Nikon TE300 microscope equipped with 20× Plan Fluor (NA 0.45) objective, a motorized xyz stage and a temperature controller. Fluorescence live cell imaging of cells expressing GFP-tubulin or GFP-Lifeact was performed in recording medium [219] on the Nikon Eclipse Ti microscope with equipped a 60× Apo TIRF (NA 1.49) objective, a motorized xyz stage, a Perfect Focus System

and a temperature controller. Quantification of nuclear and centrosome position relative to the cell centroid was as described previously [16].

Immunoprecipitation and pulldown assays

Co-immunoprecipitation was performed from lysates of 293T cells overexpressing GFP-nesprin-2G constructs. Cells were lysed in KLB buffer (25 mM Tris pH 7.4; 10 % glycerol; 150 mM NaCl;1% Triton X-100; 1 mM NaF; 1 mM Na_3VO_4) with Halt™ protease and phosphatase inhibitor cocktail (78440, Thermo Fisher Scientific, Waltham, MA) and GFP-tagged proteins were immunoprecipitated with rabbit anti-GFP (A11122, Thermo Fisher Scientific) and Dynabeads®-protein G (Thermo Fisher Scientific, Waltham, MA) following a published method [220] with a minor change (incubation at 4 °C for 1 hr). Beads were washed with RIPA buffer (50 mM Tris HCl pH 8.0; 150 mM NaCl; 1.0% NP-40; 0.5% sodium deoxycholate; 0.1% SDS) and then bound proteins eluted with SDS sample buffer and analyzed by western blotting. Pull down assays were with GST-tagged proteins purified from bacteria lysed with 50 mM EDTA, 1% Triton X-100, 10% glycerol, 1% aprotinin, 1mM PMSF, 1 mM DTT (Gold Biotechnology, St Louis, MO) in PBS. NIH3T3 cells were lysed with KLB buffer with Halt™ inhibitor cocktail on ice for 30min and clarified lysates (20,000 g for 30 min) were then incubated with glutathione-agarose beads containing GST-tagged proteins for 3 hrs. After washing in 50 mM Tris, pH 7.5, 150 mM NaCl, 10mM EDTA and protease inhibitors, bound proteins were eluted with SDS sample buffer and analyzed by western blotting. The dynein and kinesin-1 interaction assays used GST-tagged proteins expressed in NIH3T3 fibroblasts by viral infection. Cells were lysed with KLB buffer on ice for 30 min and lysates clarified by centrifugation (20,000 *g* for 30 min at 4 °C). Clarified lysates

were incubated with glutathione-Sepharose™ 4B beads (GE Healthcare) for 3 hr at 4 °C and after washing with PBS plus 0.1% Triton X-100 and RIPA buffer, bound proteins were eluted with SDS sample buffer and analyzed by western blot.

Image processing and statistical analysis

Images of western blots, immunofluorescence and phase contrast are representative of results from three or more separate experiments, except for those in Figure 5c and Supplemental Figure S5b, which were repeated twice. All data for statistical analysis were numerical. When sample size was bigger than 30, normal distribution was assumed, based on central limit theorem, and two-tail t-test was used for statistical analysis. Images were processed for contrast and brightness and assembled into figures using Adobe Illustrator. For quantitative results, statistical analysis was performed on parametric data using unpaired two-tailed t-test by GraphPad Prism 5 or Excel.

Acknowledgments

We thank members of the Gundersen laboratory for helpful discussions and Chenshu Liu (Columbia University) for drawing the model. We thank Vladimir Rodionov (U Connecticut) for the kind gift of centrifugation adaptor prototype and Gary Johnson from Columbia Instrument Shop for preparing custom centrifuge adaptors. This work was funded by an NIH grant (GM099481 to G.G.G.) and an AHA predoctoral fellowship (15PRE25400002 to R.Z.).

Author Contributions

R.Z. designed and conducted all of the experiments. R.Z. and G.G.G. conceived the study, analyzed and interpreted the data and wrote the manuscript. S.A. generated constructs and helped with the design of experiments.

Figures

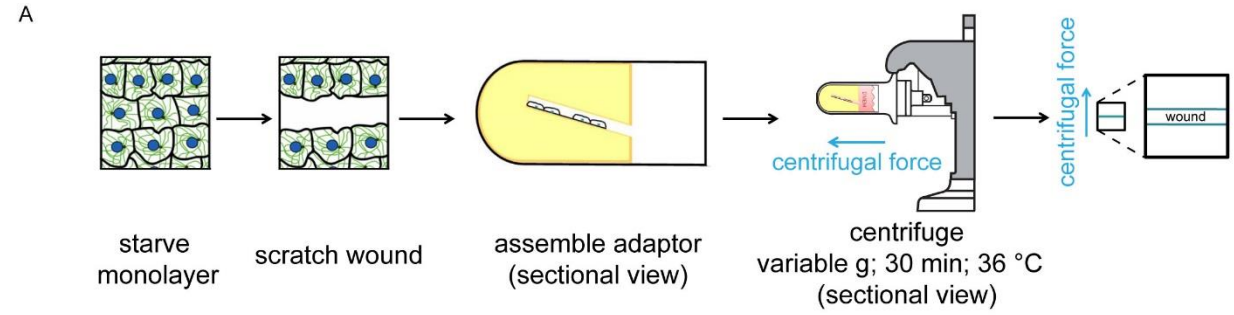
A
starve monolayer
scratch wound
assemble adaptor (sectional view)
centrifuge variable g; 30 min; 36 °C (sectional view)
centrifugal force
centrifugal force
wound

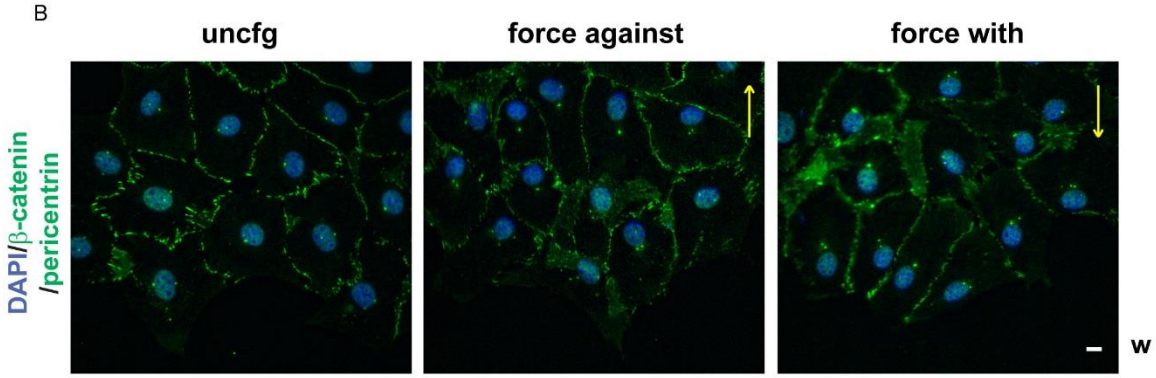
B
uncfg
force against
force with
DAPI/β-catenin /pericentrin
w

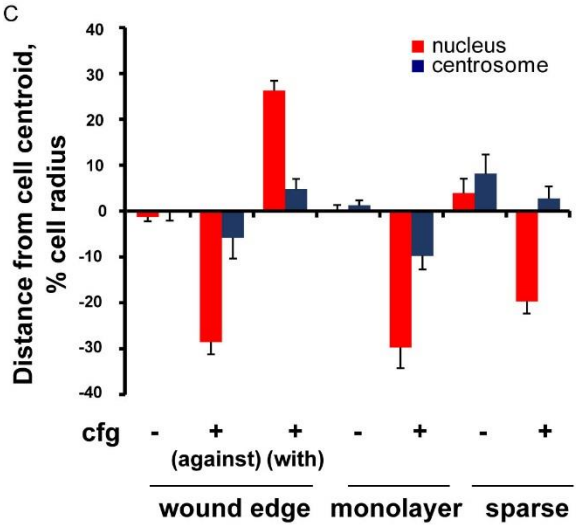
C
Distance from cell centroid, % cell radius
nucleus
centrosome
cfg
(against) (with)
wound edge
monolayer
sparse

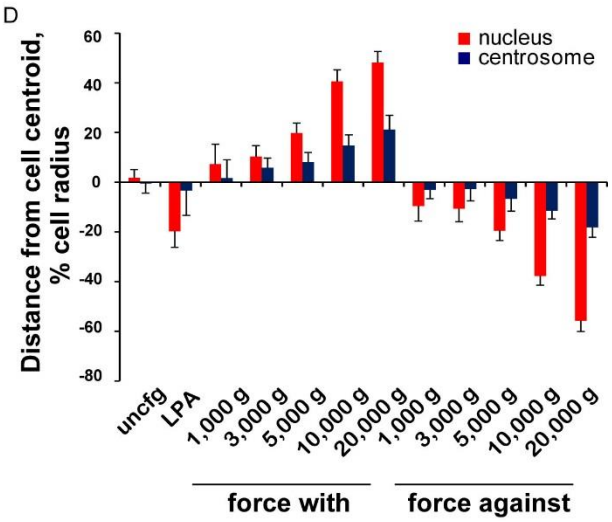
D
Distance from cell centroid, % cell radius
nucleus
centrosome
uncfg
LPA
1,000 g
3,000 g
5,000 g
10,000 g
20,000 g
force with
force against

Figure 3.1 Centrifugation displaces nuclei in the direction of force.

A. Schematic of the centrifugation method to displace nuclei. Coverslips containing adherent cells are placed in a custom adaptor; shown is a wounded monolayer oriented so that centrifugal force would be orthogonal to the wound. The rotor diagram was adapted from Beckman booklet PN L5-TB-069PE. B. Images of centrifuged wounded monolayers stained to reveal nuclei (DAPI), cell junctions (β-catenin) and centrosomes (pericentrin). Different fields are depicted in each panel. Wound edge ("w") is at the bottom. Yellow arrows indicate the direction of centrifugal force. Bar: 10 μm. C. Quantification of nuclear and centrosomal position relative to the cell centroid in serum-starved cells at the wound edge and within the monolayer after centrifugation (cfg) at 5,000 g for 30 min or in proliferating sparse cells after centrifugation at 5,000 g for 45 min. For wound edge cells, positive values are toward the leading edge, negative values are toward the cell rear. Nuclear and centrosome positions were measured along an axis parallel to the centrifugal force. "Against" and "with" refer to the direction of force relative to the direction of cell migration. Error bars: SD from three experiments for monolayer and wound edge cells; four experiments for sparse cells (n>30 cells for each measurement). D. Quantification of nuclear and centrosomal displacement relative to the cell centroid in serum starved wound edge cells subjected to different centrifugal forces. Positive values are toward the leading edge; negative values toward the cell rear. Uncentrifuged wound edge cells treated without (uncfg) or with LPA for 2 hr are shown for comparison. Error bars: SEM from 3 experiments (n > 30 cells for each condition).

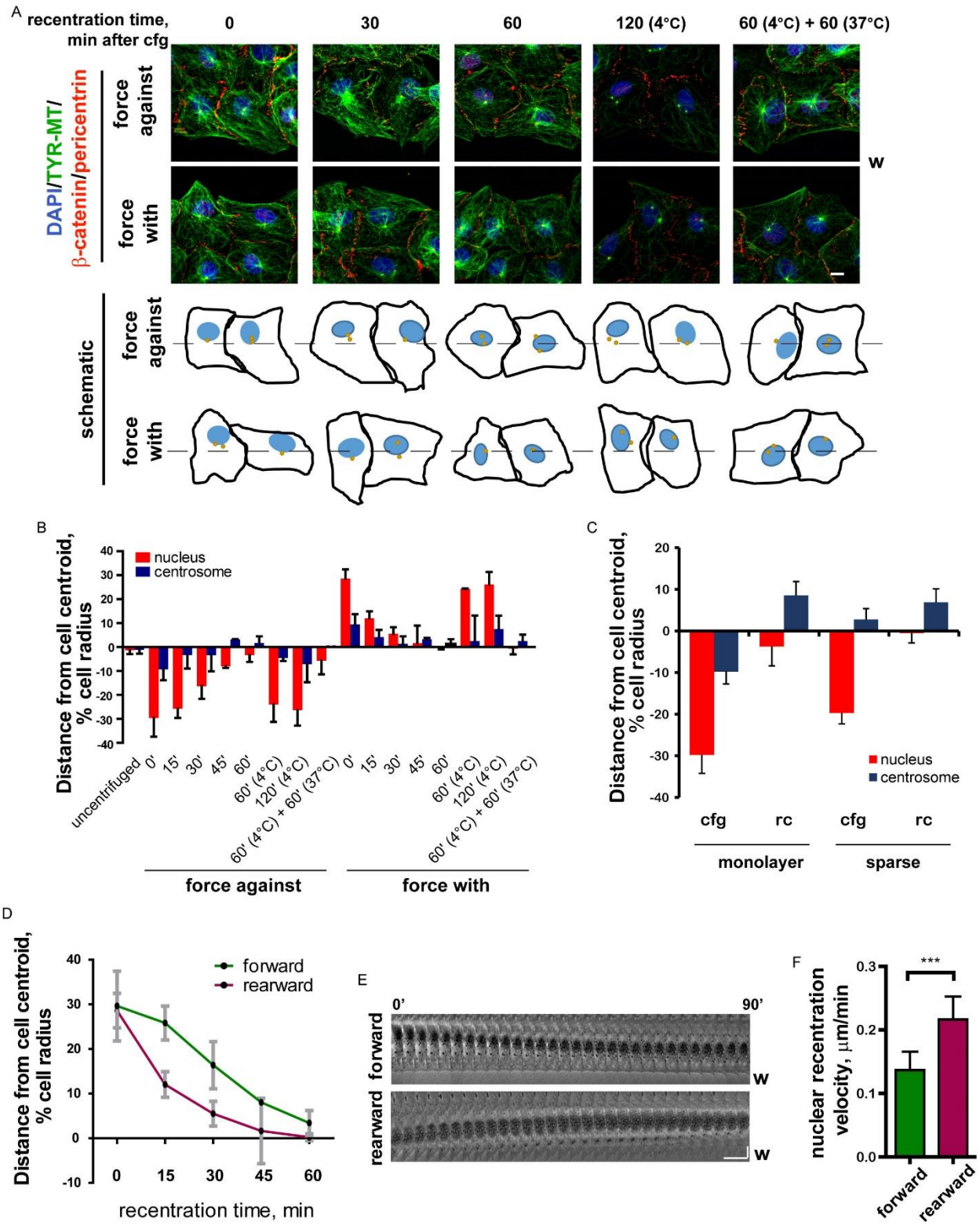
A
recentration time, min after cfg
0
30
60
120 (4°C)
60 (4°C) + 60 (37°C)
DAPI/TYR-MT/ β-catenin/pericentrin
force against
force with
w
schematic
force against
force with
B
Distance from cell centroid, % cell radius
nucleus
centrosome
uncentrifuged
0'
15'
30'
45'
60'
60' (4°C)
120' (4°C)
60' (4°C) + 60' (37°C)
force against
force with
C
Distance from cell centroid, % cell radius
nucleus
centrosome
cfg
rc
cfg
rc
monolayer
sparse
D
Distance from cell centroid, % cell radius
forward
rearward
recentration time, min
E
0'
90'
forward
rearward
w
w
F
nuclear recentration velocity, μm/min
***
forward
rearward

Figure 3.2 Nuclei actively re-center after centrifugal displacement.

A. Top, images of wounded monolayers at the indicated intervals after centrifugation (5,000 g for 30 min). Cells were stained for MTs (Tyr-MTs), cell-cell junctions (β-catenin), centrosomes (pericentrin) and nuclei (DAPI). Bottom, schematic traces of cells from above depicting nuclei (blue) and centrosomes (orange) relative to the cell centroid (dashed line). Centroids of the cells were aligned to allow comparisons of nuclear and centrosome positions. Bar: 10 μm. "w" is the indication of wound. B. Quantification of nuclear and centrosomal position relative to the cell centroid in wound edge cells at different intervals after centrifugation (5,000 g for 30 min). Incubation after centrifugation was at 37 ˚C except as indicated. Error bars, SEM from three experiments (n > 30 cells for each condition). C. Quantification of nuclear and centrosomal position in monolayer and sparse cells after centrifugation (cfg) (5,000 g for 30 min and 45 min respectively) and recentering (rc) for 60 min. (Cfg data is same as that used in Figure 1C). Error bars, SD from three experiments for monolayer cells; four experiments for sparse cells (n > 30 cells for each measurement). D. Comparison of mean distance between the nucleus and cell centroid at different intervals after centrifugation (5,000 g for 30 min) in cells from two sides of a wound. Data are replotted from B. "Forward" indicates nuclear recentration from cell rear to center, whereas "rearward" indicates nuclear recentration from cell front to center. E. Kymographs from phase contrast movies of nuclear recentration in cells from two sides of the wound (w) after centrifugal displacement. Note the lack of leading edge movement during nuclear recentration. Bars: x, 6 min; y, 10 μm. F. Quantification of the velocity of nuclear re-centration determined from movies. Error bars, SEM from 10 and 12 movies for forward and rearward recentration respectively; ***, $p < 0.001$ by two-tailed t-test.

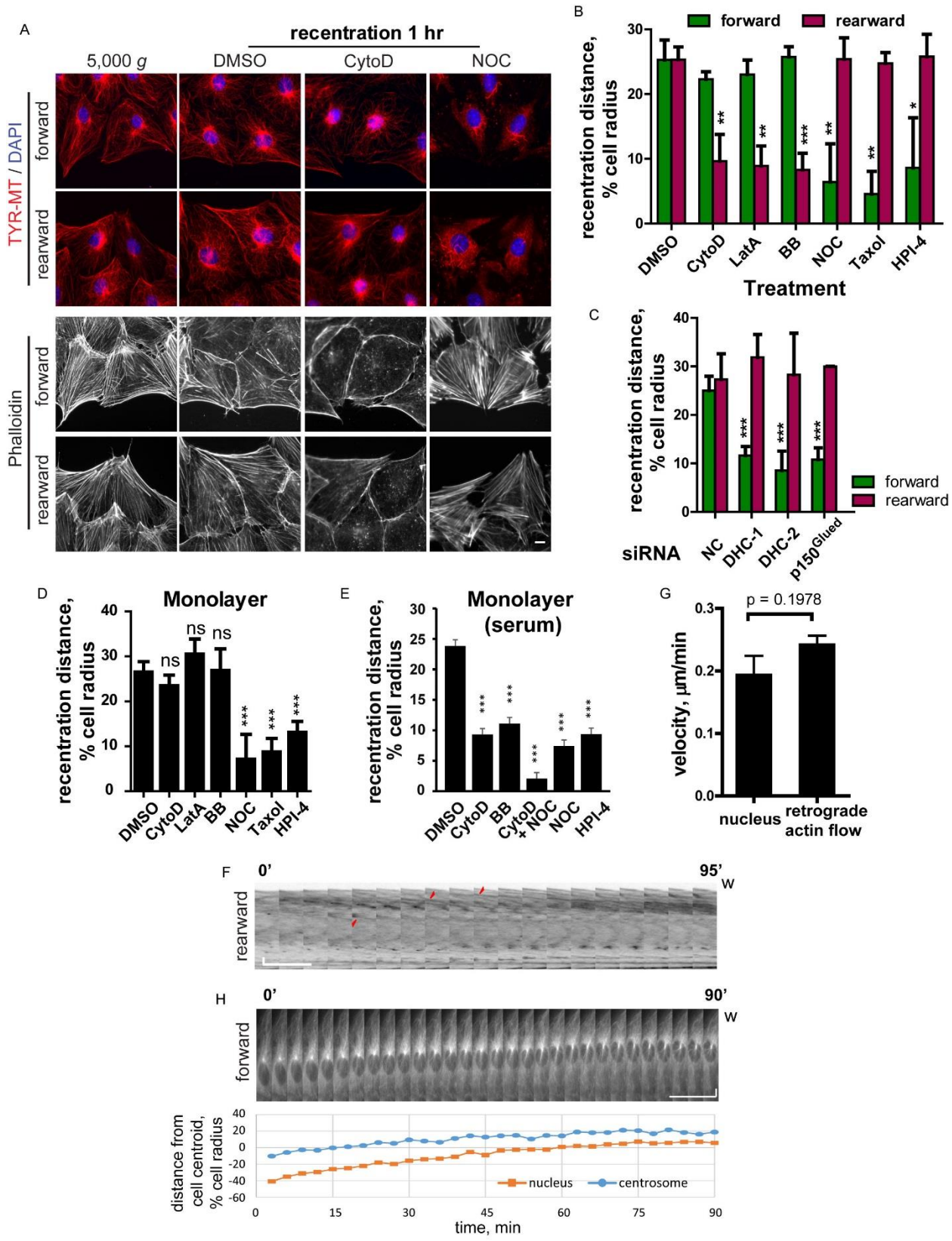
A
recentration 1 hr
5,000 g
DMSO
CytoD
NOC
TYR-MT / DAPI
forward
rearward
Phalloidin
forward
rearward
B
forward
rearward
recentration distance, % cell radius
DMSO
CytoD
LatA
BB
NOC
Taxol
HPI-4
Treatment
C
recentration distance, % cell radius
forward
rearward
siRNA
NC
DHC-1
DHC-2
p150Glued
D
Monolayer
recentration distance, % cell radius
ns
ns
ns
DMSO
CytoD
LatA
BB
NOC
Taxol
HPI-4
E
Monolayer (serum)
recentration distance, % cell radius
DMSO
CytoD
BB
CytoD + NOC
NOC
HPI-4
G
p = 0.1978
velocity, µm/min
nucleus
retrograde actin flow
F
0'
95'
W
rearward
H
0'
90'
W
forward
distance from cell centroid, % cell radius
nucleus
centrosome
time, min

Figure 3.3 Different cytoskeletal systems are required for forward and rearward nuclear recentration.

A. Representative images of centrifuged wounded monolayers treated with 250 nM cytochalasin D (CytoD) or 10 μM nocodazole (NOC) during recentration. Cells were stained for Tyr-MTs and nuclei (DAPI) (top panels) and F-actin (phalloidin) (bottom panels). Bar: 10 μm. B. Quantification of nuclear recentration in wound edge cells treated with the following drugs: 250 nM CytoD, 50 nM latrunculin A (LatA); 10 μM blebbstatin (BB); 10 μM NOC; 10 μM Taxol, or 28 μM HPI-4. In b and c, error bars: SD from 3 experiments (n > 30 cells for each condition); *, $p < 0.05$; **, $p < 0.01$; ***, $p < 0.001$ based on two-tail t-test between the treatment and DMSO control in the same direction. C. Quantification of nuclear recentration in cells treated with the indicated siRNAs. NC, noncoding siRNA control. D-E. Quantification of nuclear recentration in (D) starved cells and (E) serum grown cells within the monolayer after 5000 g centrifugation for 30min and treatment with drugs as in B. Error bars: SD from 3 experiments (n > 30 cells for each condition); ***, $p < 0.001$; ns, not significant based on two-tail t-test between the treatment and DMSO control. F. Representative kymograph of GFP-Lifeact labeled actin cables (red arrowheads) moving retrogradely in a wound edge cell after centrifugation. The wound is denoted by a "w". Bars: x, 10 min; y, 10 μm. G. Quantification of the rate of retrograde actin cable flow and nuclear recentration measured from movies as in F. Error bars: SEM, from 17 movies; p value from two-tailed t-test. H. Top, representative kymograph of GFP-tubulin showing nuclear and centrosome movement in a wound edge cell after centrifugation. The wound is denoted by a "w". Bars: x, 9 min; y, 10 μm. Below, a trace of the nucleus and centrosome movement relative to the cell centroid from the kymograph.

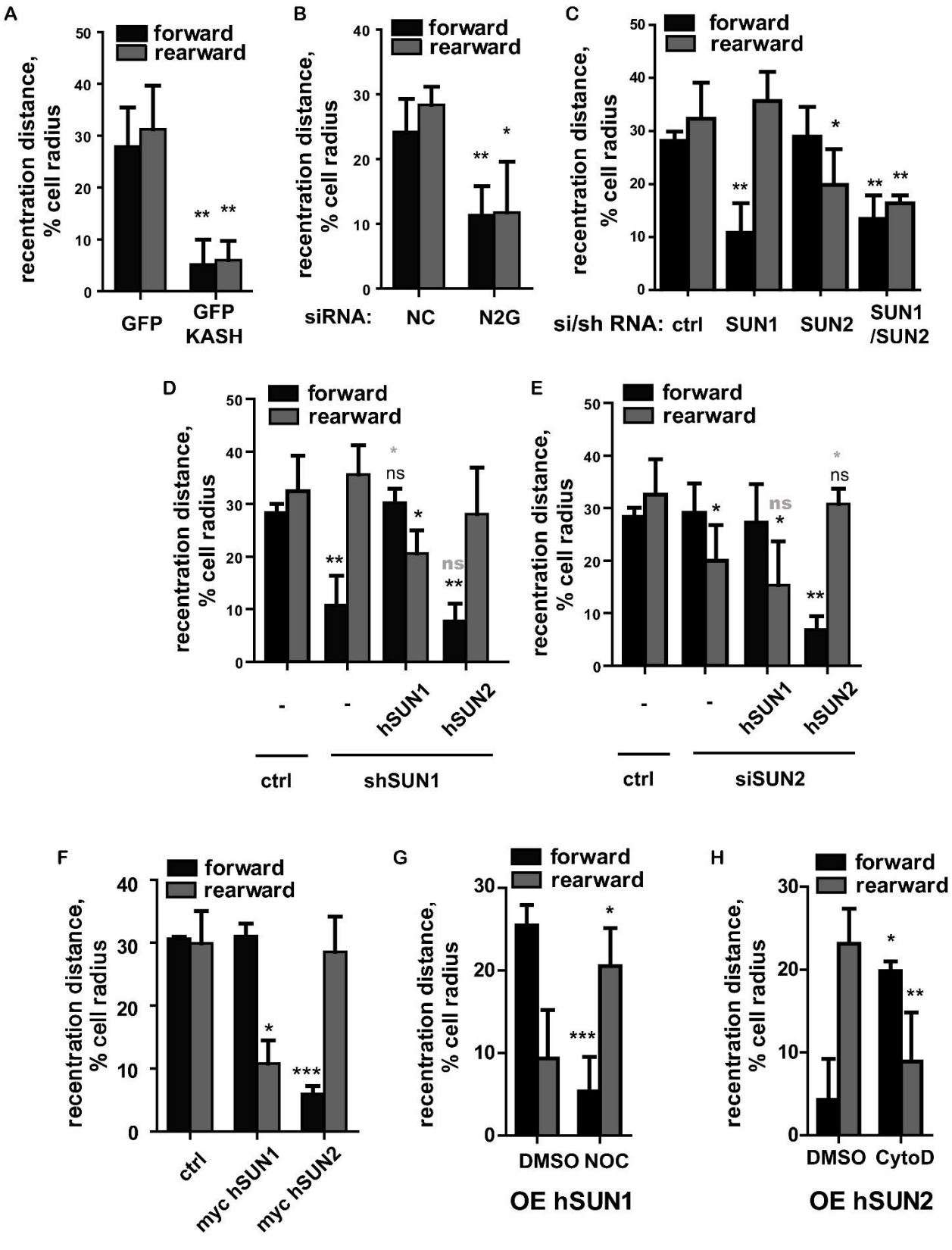
A
recentration distance, % cell radius
forward
rearward
GFP
GFP KASH
B
siRNA:
NC
N2G
C
si/sh RNA:
ctrl
SUN1
SUN2
SUN1 /SUN2
D
hSUN1
hSUN2
ctrl
shSUN1
E
siSUN2
F
ctrl
myc hSUN1
myc hSUN2
G
DMSO NOC
OE hSUN1
H
DMSO CytoD
OE hSUN2

Figure 3.4 Distinct LINC complexes are required for forward and rearward nuclear recentration.

Distinct LINC complexes are required for forward and rearward nuclear recentration. A-F. Quantification of nuclear recentration in: (A) GFP or GFP-KASH expressing cells; (B) cells treated with non-coding (NC) or nesprin-2G (N2G) siRNAs; (C) cells treated with control RNAs (shLuciferase and siNC), SUN1 shRNA, SUN2 siRNA or both; (D) Cells treated with SUN1 shRNA re-expressing myc-hSUN1 or myc-hSUN2 (ctrl is cells treated with siNC and shLuciferase); (E) Cells treated with SUN2 siRNAs re-expressing myc-hSUN1 or myc-hSUN2; and (F) myc-hSUN1 and myc-hSUN2 overexpressing cells. (G) Cells overexpressing myc-hSUN1 treated with 10 μM NOC or vehicle (DMSO) during recentration. (H) Cells overexpressing with myc-hSUN2 treated with 250 nM CytoD or vehicle (DMSO) during recentration. For A-H, error bars: SD from 3 experiments ($n > 30$ cells for each condition) except for control and siSUN2 in C-E and G-H, SD from 4 experiments; *, $p < 0.05$; **, $p < 0.01$; ***, $p < 0.001$ by two-tailed t-test. Black notation is the statistics between the group of interest to control; grey notation in D and E, are the statistics between group of interest to SUN knockdown alone.

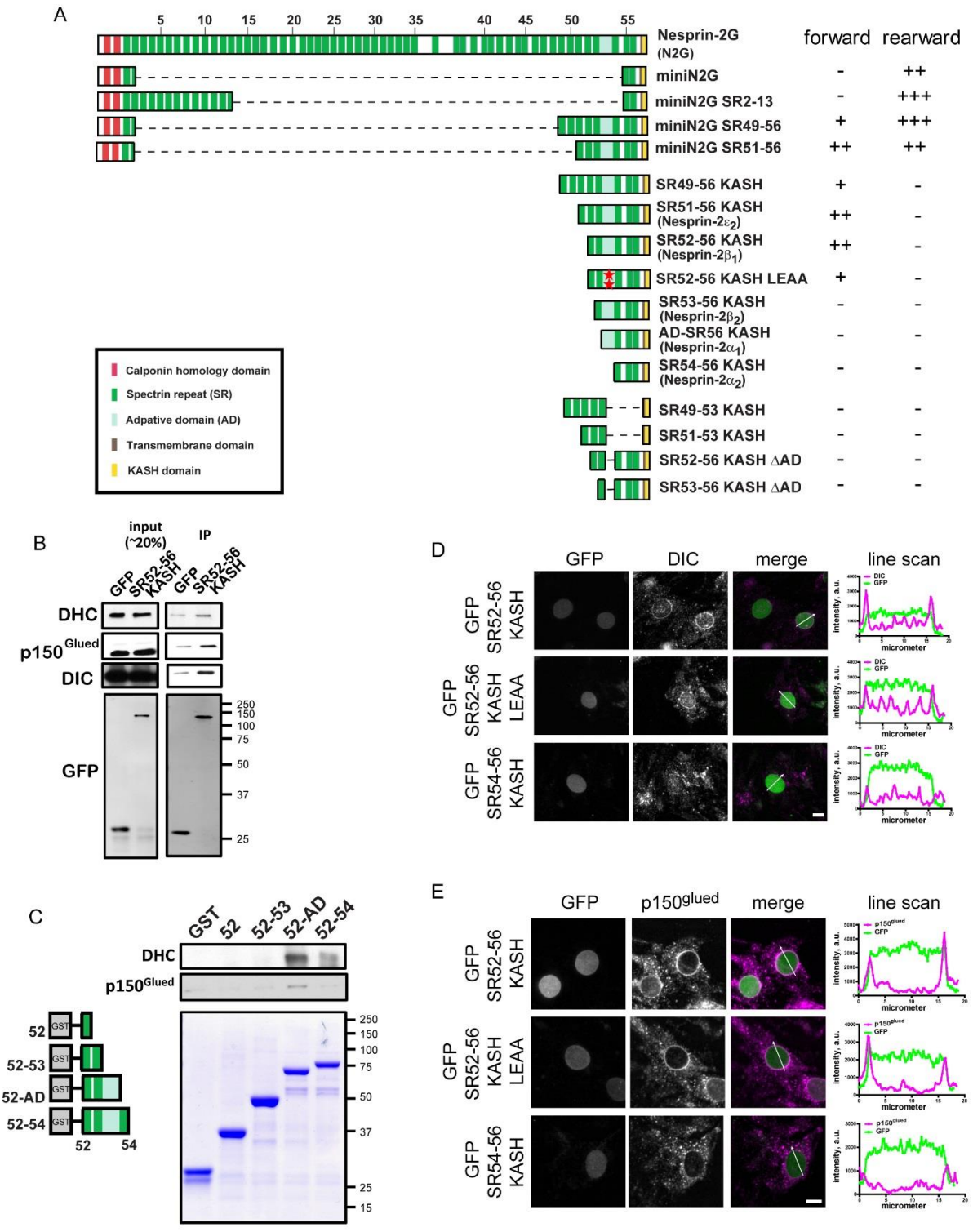
A
5 10 15 20 25 30 35 40 45 50 55
Nesprin-2G (N2G)
forward rearward
miniN2G - ++
miniN2G SR2-13 - +++
miniN2G SR49-56 + +++
miniN2G SR51-56 ++ ++
SR49-56 KASH + -
SR51-56 KASH (Nesprin-2ε2) ++ -
SR52-56 KASH (Nesprin-2β1) ++ -
SR52-56 KASH LEAA + -
SR53-56 KASH (Nesprin-2β2) - -
AD-SR56 KASH (Nesprin-2α1) - -
SR54-56 KASH (Nesprin-2α2) - -
SR49-53 KASH - -
SR51-53 KASH - -
SR52-56 KASH ΔAD - -
SR53-56 KASH ΔAD - -
Calponin homology domain
Spectrin repeat (SR)
Adpative domain (AD)
Transmembrane domain
KASH domain
B
input (~20%)
IP
GFP
SR52-56 KASH
DHC
p150 Glued
DIC
GFP
250
150
100
75
50
37
25
C
GST
52
52-53
52-AD
52-54
DHC
p150Glued
250
150
100
75
50
37
25
15
D
GFP
DIC
merge
line scan
GFP SR52-56 KASH
GFP SR52-56 KASH LEAA
GFP SR54-56 KASH
intensity, a.u.
micrometer
E
GFP
p150glued
merge
line scan
GFP SR52-56 KASH
GFP SR52-56 KASH LEAA
GFP SR54-56 KASH
intensity, a.u.
micrometer

Figure 3.5 Dynein interacts with nesprin-2 for MT-dependent nuclear recentration.

A. Schematic of GFP-nesprin-2 constructs (GFP is not depicted) expressed in N2G-depleted cells and summary of their effects on recentration expressed as level of significance by two-tail t-test: +, $p < 0.05$; ++, $p < 0.01$; +++, $p < 0.001$; and -, $p > 0.05$. See Figure S5B for raw data. B. Co-immunoprecipitation of GFP-nesprin-2 SR52-56 KASH expressed in 293T cells with endogenous dynein heavy chain (DHC), dynein intermediate chain (DIC) and dynactin (p150Glued). C. GST pulldowns of dynein heavy chain (DHC) and dynactin (p150Glued) in NIH3T3 cell lysates with the indicated nesprin-2 constructs. D-E. Localization and line scan analysis of (D) DIC and (E) p150Glued in NOC-treated, starved fibroblasts overexpressing the indicated GFP-nesprin-2 constructs. Bars, 10 μM.

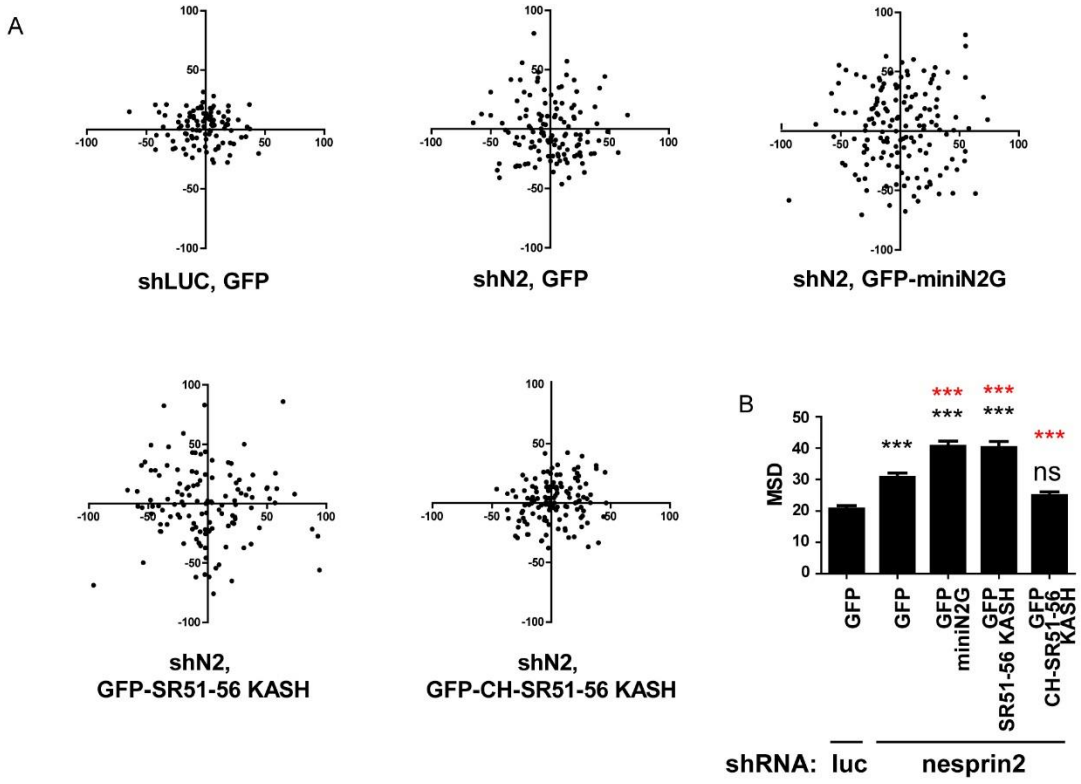
A
shLUC, GFP
shN2, GFP
shN2, GFP-miniN2G
shN2,
GFP-SR51-56 KASH
shN2,
GFP-CH-SR51-56 KASH
B
MSD
GFP
GFP
GFP miniN2G
GFP SR51-56 KASH
GFP CH-SR51-56 KASH
***
ns
shRNA: luc
nesprin2

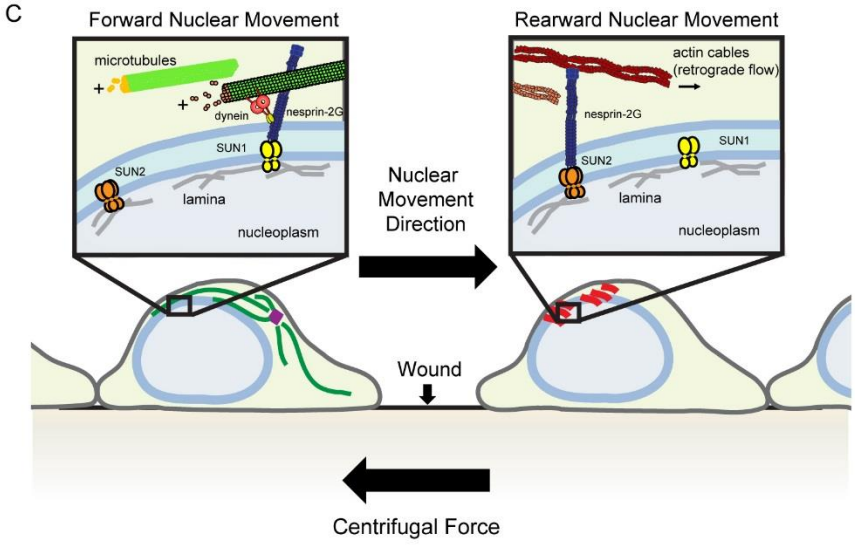
C
Forward Nuclear Movement
Rearward Nuclear Movement
microtubules
dynein
nesprin-2G
SUN1
SUN2
lamina
nucleoplasm
actin cables
(retrograde flow)
Nuclear
Movement
Direction
Wound
Centrifugal Force

Figure 3.6 The interaction of nesprin-2 with both actin and MTs is necessary for homeostatic nuclear positioning.

A. Scatter plots of nuclear position in sparse NIH3T3 fibroblasts following nesprin-2 knockdown by shRNA (shN2) and re-expression of GFP or the indicated GFP-nesprin-2 constructs. The axes represent the percentage of cell radius relative to the cell centroid (0,0). Data are from 3 experiments. B. Quantification of mean square displacement (MSD) of the nucleus following nesprin-2 knockdown and re-expression of GFP or the indicated GFP-nesprin-2 constructs. Error bars: SEM from 3 experiments ($n>30$ cells for each condition); ***, $p < 0.001$; ns, not significant by t-test. Red asterisks, results compared to shN2; black asterisks, results compared to shLUC. C. Model of forward and rearward nuclear re-centration after centrifugation induced nuclear displacement.

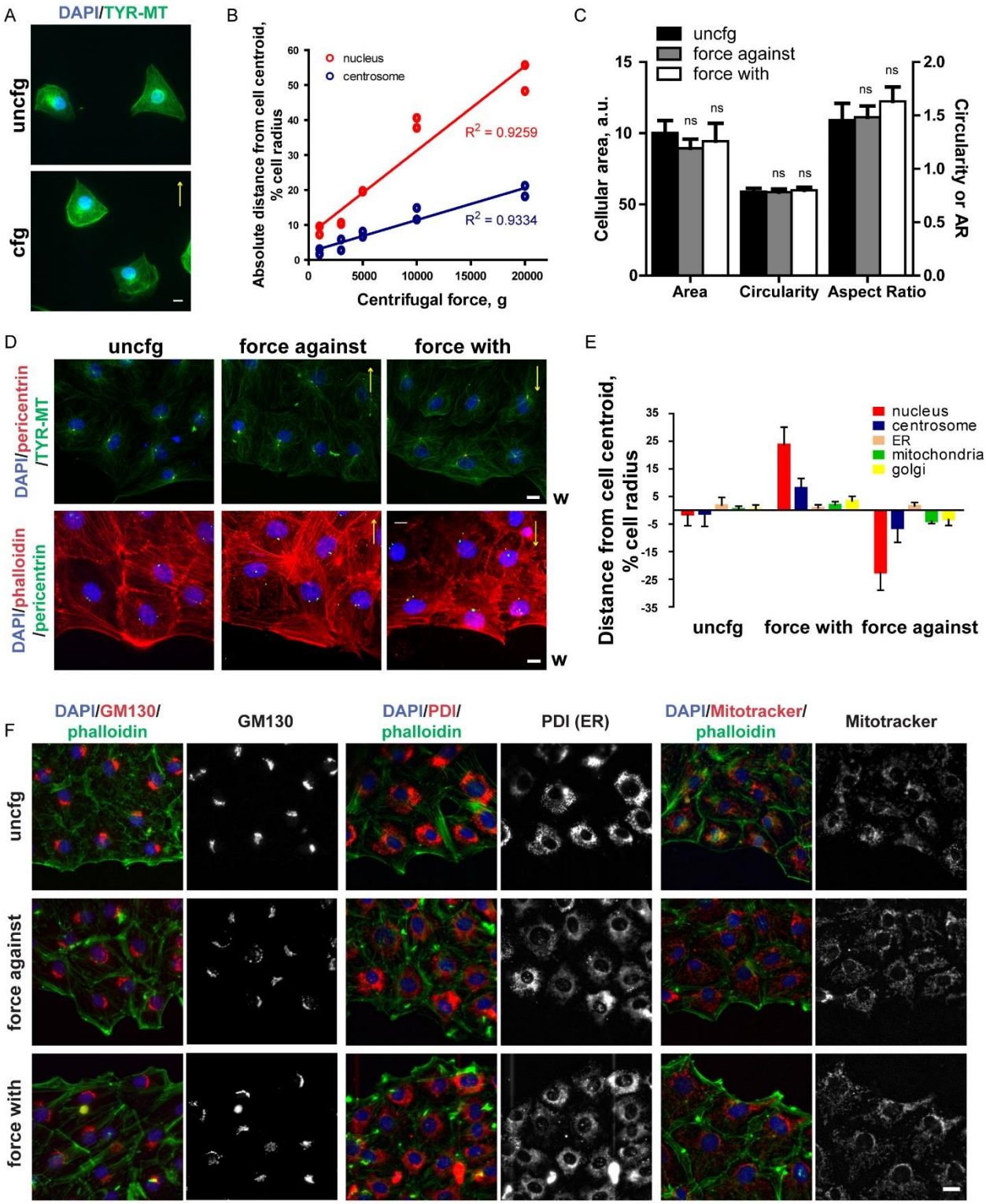
A
DAPI/TYR-MT
uncfg
cfg
B
nucleus
centrosome
R^2 = 0.9259
R^2 = 0.9334
Absolute distance from cell centroid, % cell radius
Centrifugal force, g
C
uncfg
force against
force with
Cellular area, a.u.
Circularity or AR
ns
Area
Circularity
Aspect Ratio
D
uncfg
force against
force with
DAPI/pericentrin /TYR-MT
DAPI/phalloidin /pericentrin
w
E
Distance from cell centroid, % cell radius
nucleus
centrosome
ER
mitochondria
golgi
uncfg
force with
force against
F
DAPI/GM130/ phalloidin
GM130
DAPI/PDI/ phalloidin
PDI (ER)
DAPI/Mitotracker/ phalloidin
Mitotracker
uncfg
force against
force with

Supplementary Figure 3.1 Effect of centrifugation on cell parameters and other organelles. Related to Figure 3.1. A. Images of uncentrifuged and centrifuged sparse NIH3T3 fibroblasts stained to reveal nuclei (DAPI) and Tyr-MTs. Yellow arrow indicates the direction of centrifugal force. Scale bar: 10 µm. In b-f, serum-starved, wound edge NIH3T3 fibroblasts were used. B. Relationship between centrifugal force and nuclear and centrosomal displacement from the cell centroid using values from Figure 1D. R2 values indicate the fit to a linear relationship. C. Quantification of cellular area, cell shape (circularity) and aspect ratio (AR) in centrifuged cells. Error bars, SEM from 3 experiments (n > 30 cells per measurement); ns, not significant by two-tail t-test. D. Images of uncentrifuged and centrifuged wounded monolayers stained to reveal nuclei (DAPI), centrosomes (pericentrin) and either MTs (TYR-MT) or F-actin (phalloidin). Different fields are depicted in each panel. Wound edge ("w") is at the bottom. Yellow arrows indicate the direction of centrifugal force. Bars: 10 µm. E. Quantification of displacement of the indicated organelles relative to the cell centroid after centrifugation (5,000 g for 30 min). Error bars, SEM from 3 experiments (n > 30 cells per condition). F. Representative images of organelle localization after centrifugation (5,000 g for 30 min). Cells were stained for Golgi (GM130), ER (PDI) or mitochondria (Mitotracker) together with actin (phalloidin) and nuclei (DAPI). Scale bar: 10 µm.

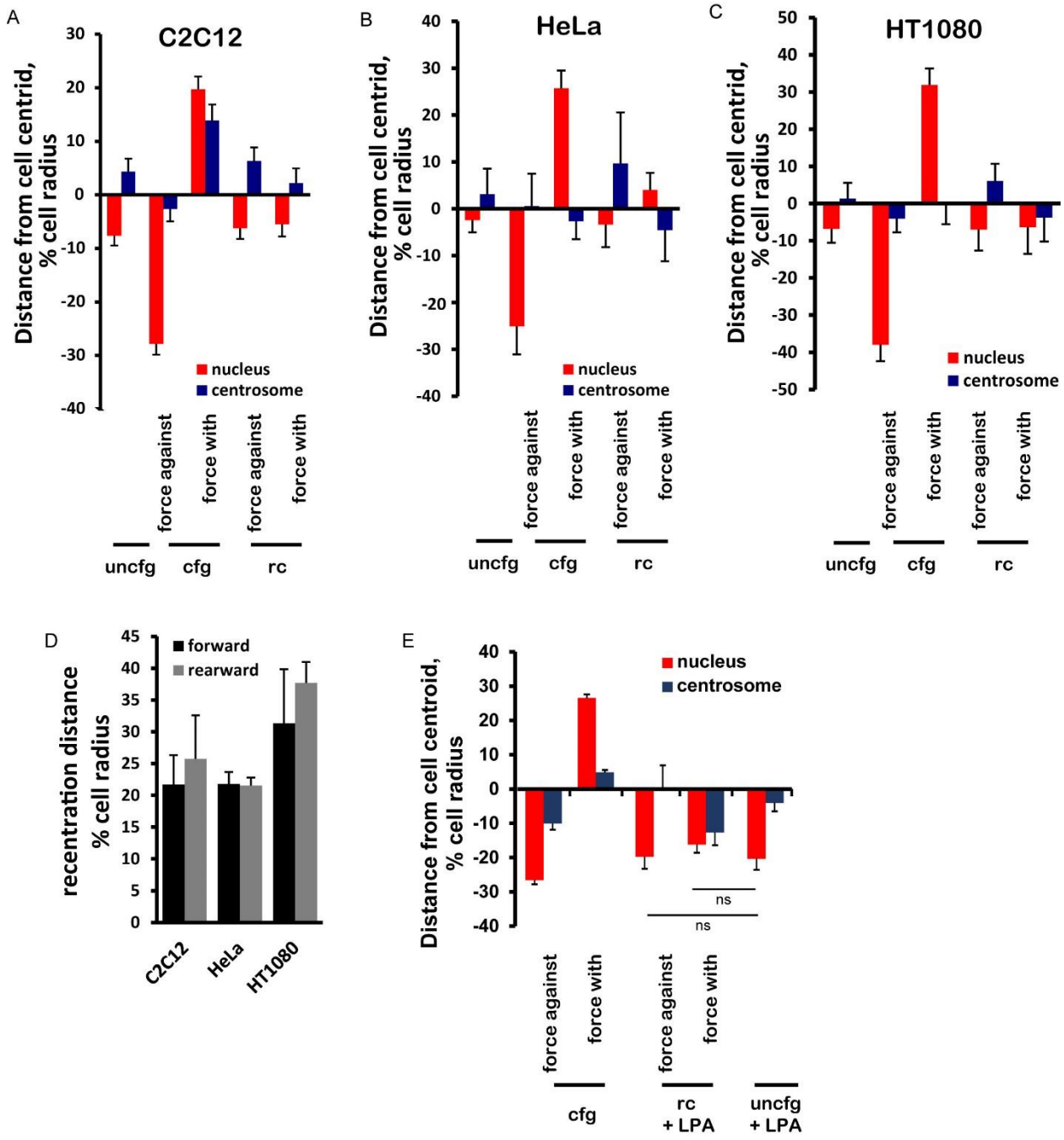
A
C2C12
Distance from cell centrid, % cell radius
nucleus
centrosome
force against
force with
force against
force with
uncfg
cfg
rc
B
HeLa
C
HT1080
D
forward
rearward
recentration distance % cell radius
C2C12
HeLa
HT1080
E
Distance from cell centroid, % cell radius
ns
ns
cfg
rc + LPA
uncfg + LPA

Supplementary Figure 3.2 Nuclear recentration different cell lines.

Related to Figure 3.2. A-C. Quantification of nuclear and centrosomal position before centrifucation (uncfg), after centrifugation (cfg) and after recentration (rc) in serum-starved mouse myoblast C2C12, HeLa and HT1080 cells. A, C2C12 cells (5,000g, 30 min); B, HeLa cells (5,000g, 45 min); C, HT1080 cells (5,000g, 45 min). Recentration was 60 min in each case. Error bars, SD from (A) 5 and (B-C) 3 experiments (n > 30 cells per condition). D. Quantification of recentration distance in C2C12, HeLa and HT1080 cells. Forward and rearward nuclear displacement is the difference between the mean nuclear position after centrifugation and recentration. Error bars, SD from 3 experiments (n > 30 cells per condition). E. Quantification of nuclear and centrosomal position in serum-starved, wound edge NIH3T3 fibroblasts after cfg and then rc in the presence of LPA. Nuclear and centrosome positions in uncentrifuged (uncfg) LPA stimulated cells is shown for comparison. Error bars, SD from 3 experiments (n > 30 cells per condition); ns, not significant by two-tail t-test of nuclear position rc and uncfg + LPA.

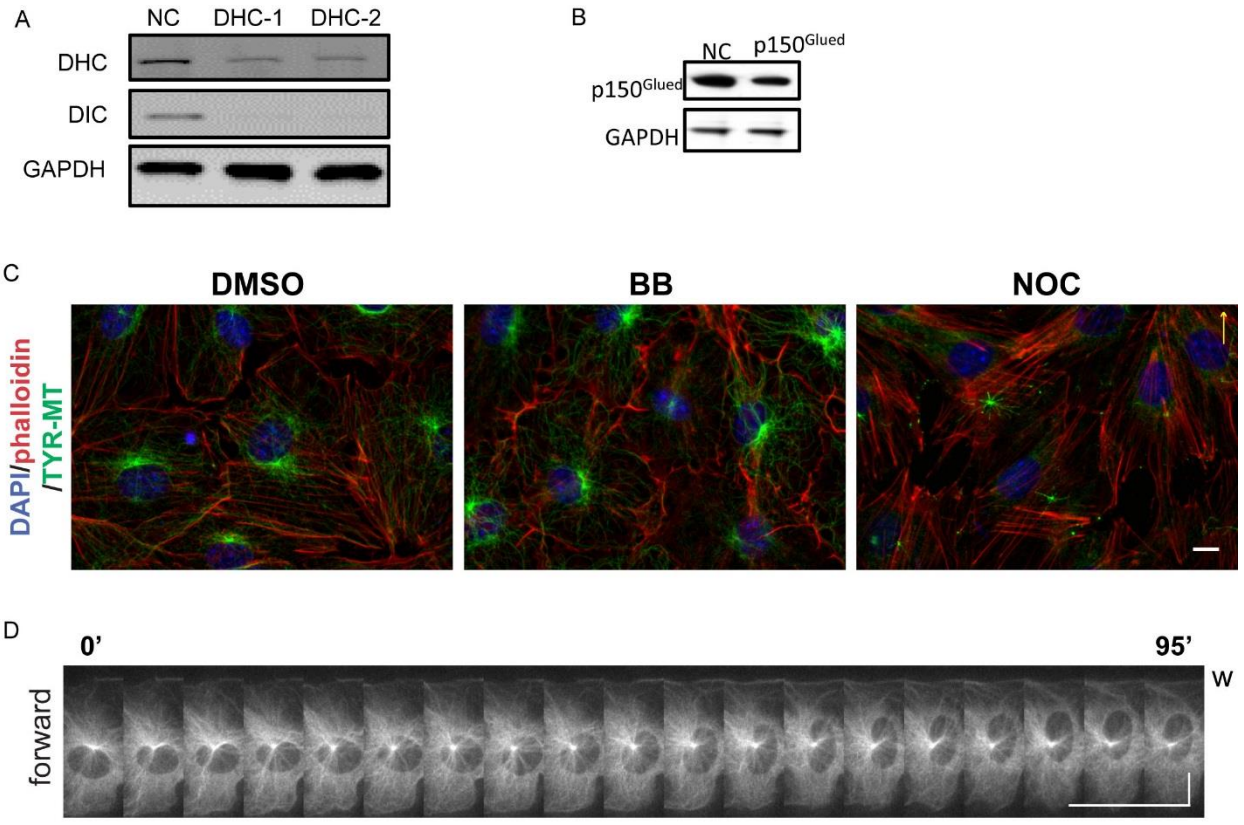
A
NC
DHC-1
DHC-2
DHC
DIC
GAPDH
B
NC
p150Glued
p150Glued
GAPDH
C
DMSO
BB
NOC
DAPI/phalloidin
/TYR-MT
D
0'
95'
forward
W

Supplementary Figure 3.3 Analysis of dynein and dynactin knockdowns, nuclear recentration within monolayer cells and nuclear rotation during forward recentration. Related to Figure 3.3. A. Western blots of dynein heavy chain (DHC) and intermediate chain (DIC) after treatment with noncoding (NC) or two different DHC siRNAs. GAPDH is a loading control. B. Western blot of dynactin p150Glued subunit after treatment with noncoding (NC) and p150Glued siRNA. GAPDH is a loading control. C. Representative images of serum-starved NIH3T3 fibroblasts within the monolayer stained to reveal nuclei (DAPI, blue), MTs (green) and F-actin, (phalloidin, red) after centrifugation (5,000 g, 30 min) followed by recentration (60 min) in the presence of the indicated drugs. Yellow arrow indicated direction of centrifugation. Scale bar: 10 μm. D. Representative kymograph from a movie of GFP-tubulin in a wound edge NIH3T3 fibroblast during forward recentration after centrifugation. Note nuclear rotation around the centrosome. The wound is denoted by a "w". Bars: x, 10 min; y, 10 μm.

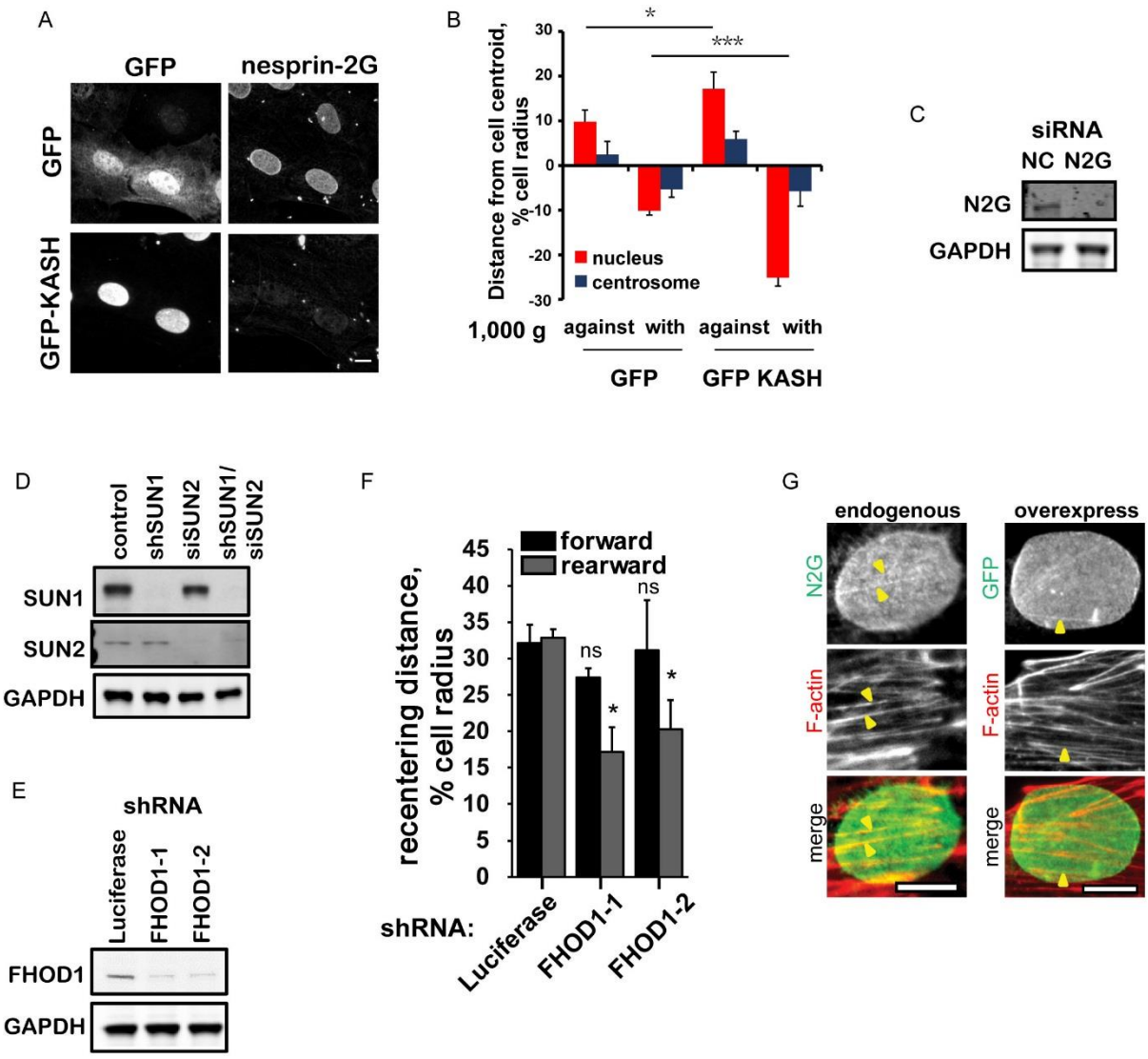
A
GFP
nesprin-2G
GFP
GFP-KASH
B
*
***
Distance from cell centroid, % cell radius
30
20
10
0
-10
-20
-30
nucleus
centrosome
1,000 g against with against with
GFP
GFP KASH
C
siRNA
NC N2G
N2G
GAPDH
D
control
shSUN1
siSUN2
shSUN1/ siSUN2
SUN1
SUN2
GAPDH
E
shRNA
Luciferase
FHOD1-1
FHOD1-2
FHOD1
GAPDH
F
forward
rearward
recentering distance, % cell radius
45
40
35
30
25
20
15
10
5
0
ns
*
ns
*
shRNA:
Luciferase
FHOD1-1
FHOD1-2
G
endogenous
overexpress
N2G
GFP
F-actin
F-actin
merge
merge

Supplementary Figure 3.4 Effects of disrupting LINC complex components and FHOD1 on nuclear recentering.

Related to Figure 3.4. A. Immunofluorescence images of GFP and endogenous nesprin-2G in GFP and GFP-KASH overexpressing NIH3T3 fibroblasts. Bar, 10 μm. B. Quantification of nuclear and centrosomal displacement relatuive to the cell center ("0") in GFP-KASH overexpressing cells centrifuged at 1,000 g (30 min). Error bars: SD from 4 experiments ($n > 30$ cells in each condition). ***, $p < 0.001$; *, $p < 0.05$ by two-tailed t-test. CB. Western blot of NIH3T3 fibroblasts treated with noncoding (NC) and nesprin-2G siRNAs. GAPDH is a loading control in CB-ED. DC. Western blot of NIH3T3 fibroblasts treated with control, SUN1 shRNA, SUN2 siRNA or both SUN1 shRNA and SUN2 siRNA. ED. Western blot of NIH3T3 fibroblasts treated with control (luciferase) or two separate FHOD1 shRNAs. FE. Quantification of nuclear recentration in serum-starved, wound edge NIH3T3 fibroblasts treated with control (luciferase) or FHOD1 shRNAs. Error bars, SD from 2 experiments ($n > 30$ measurements per condition); *, $p < 0.05$, ns, not significant by t-test compared to luciferase control. GF. Representative images of TAN lines on nuclei in NIH3T3 fibroblasts during nuclear recentering by rearward movement. Left column shows endogenous nesprin-2G (N2G), right shows a cell overexpressing GFP-miniN2G. Cells were stained for nesprin-2G (N2G) or GFP and F-actin (phalloidin). Yellow arrowheads indicate TAN lines. Bars, 10 μm.

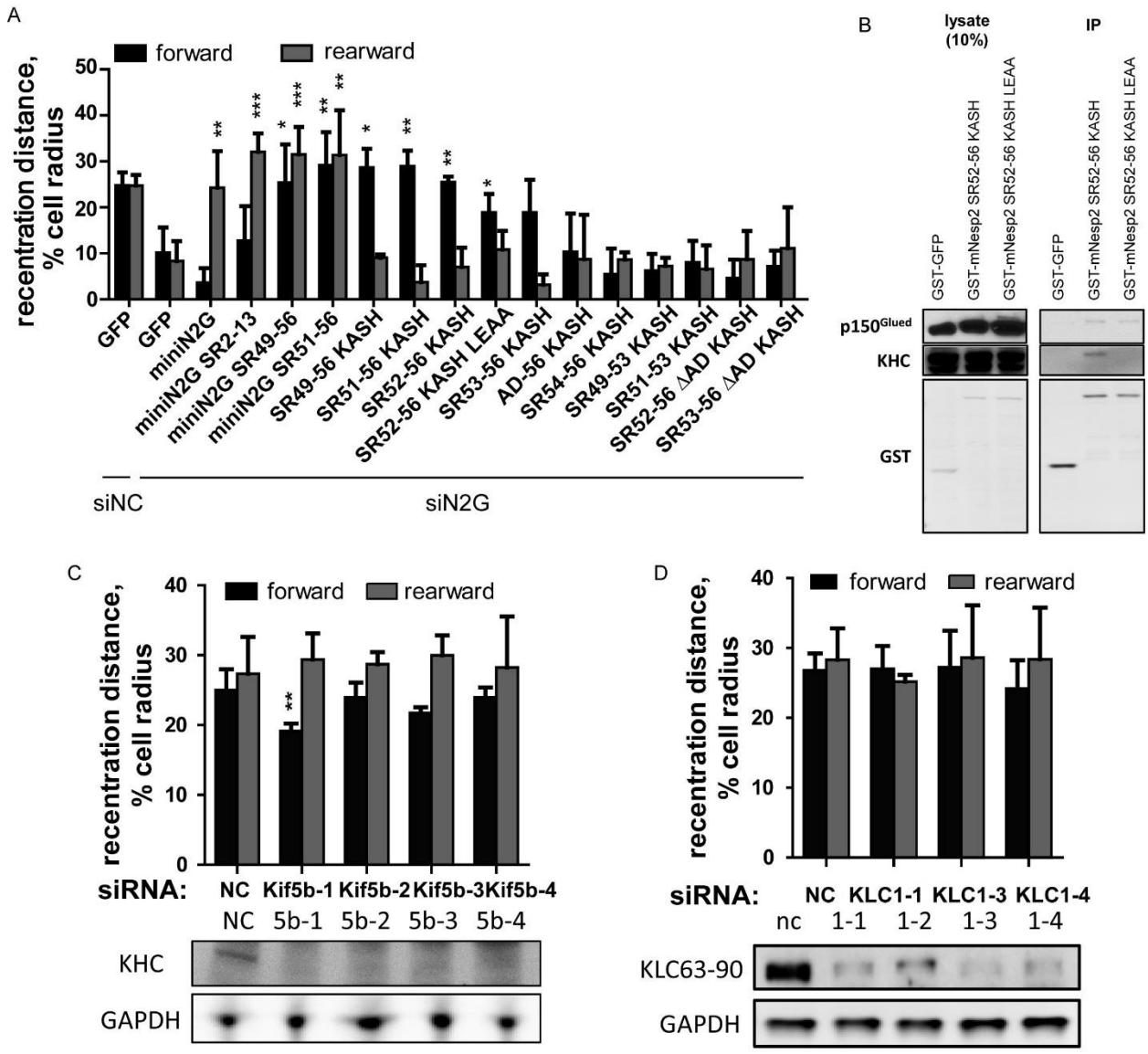
A
forward
rearward
recentration distance, % cell radius
GFP
GFP
miniN2G
miniN2G SR2-13
miniN2G SR49-56
miniN2G SR51-56
SR49-56 KASH
SR51-56 KASH
SR52-56 KASH
SR52-56 KASH LEAA
SR53-56 KASH
AD-56 KASH
SR54-56 KASH
SR49-53 KASH
SR51-53 KASH
SR52-56 ΔAD KASH
SR53-56 ΔAD KASH
siNC
siN2G
B
lysate (10%)
IP
GST-GFP
GST-mNesp2 SR52-56 KASH
GST-mNesp2 SR52-56 KASH LEAA
p150Glued
KHC
GST
C
forward
rearward
recentration distance, % cell radius
siRNA:
NC
Kif5b-1
Kif5b-2
Kif5b-3
Kif5b-4
NC
5b-1
5b-2
5b-3
5b-4
KHC
GAPDH
D
forward
rearward
recentration distance, % cell radius
siRNA:
NC
KLC1-1
KLC1-3
KLC1-4
nc
1-1
1-2
1-3
1-4
KLC63-90
GAPDH

Supplementary Figure 3.5 Rescue of nuclear recentration by re-expression of nesprin-2 constructs in cells depleted of nesprin-2G, analysis of nesprin-2 interaction with kinesin-1 and dynein and effect of kinesin-1 knockdown on nuclear recentration.

Related to Figure 5. A. Quantification of nuclear recentration in serum-starved, wound edge NIH3T3 fibroblasts treated with nesprin-2G (siN2G) or noncoding (siNC) siRNAs and reexpressing the indicated nesprin-2 constructs or GFP as a control. Error bars, SD from at least 3 experiments (except for SR49-56 KASH where N=2) (n > 30 cells analyzed for each experiment); *, $p < 0.05$; **, $p < 0.01$; ***, $p < 0.001$ by two-tailed t-test compared to GFP expression in siN2G treated cells. B. Western blots of lysates and GST-immunoprecipitated proteins from cells expressing GST-tagged GFP, nesprin-2 SR52-56 KASH or nesprin-2 SR52-56 KASH LEAA. Western blots were probed for p150Glued subunit of dynactin, kinesin heavy chain (KHC) or GST. C. Quantification of nuclear recentration and western blots of kinesin heavy chain (KHC) in serum-starved, wound edge NIH3T3 fibroblasts treated with four Kif5b or non-coding (NC) siRNAs. GAPDH is a loading control in the western blot. D. Quantification of nuclear recentration and western blots of kinesin light chain (KLC) in serum-starved, wound edge NIH3T3 fibroblasts treated with four KLC1 or non-coding (NC) siRNAs. GAPDH is a loading control. In C and D, error bars, SD from at least 3 experiments (except siKif5b-4 where N=2) (n = 30 cells analyzed per condition); **, $p < 0.01$ compared to NC control by two tailed t-test; all other comparisons are not significant.

Tables

Supplementary Table 3.1 Primers for NC-terminal N2G constructs PCR

Construct	N and C portions	Source	forward /reverse	Sequence
miniN2G SR2-13	CH-SR2-13	NIH3T3	F	GTTAGCGGCCGCGCTAGCCCTGTGCTGCC
			R	ATGTGTTTTCACATCTTTCATCTTGC
	CORE	pEGFP-C1 miniN2G (NIH3T3)	F	CTTCACAGCAAGCTCAGGCTC
			R	GTTAGCGGCCGCCTAGGTGGGAGGTGGCCC
miniN2G SR49-56	CH	pEGFP-C1 miniN2G (NIH3T3)	F	GTTAGCGGCCGCGCTAGCCCTGTGCTGCC
			R	CTCCAGGAGTGGGATGAAG
	SR49-CORE	Mouse Forebrain E14.5	F	CTCAGGCTTCCCCTCAGTG
			R	GTTAGCGGCCGCGCTAGCCCTGTGCTGCC
miniN2G SR51-56	CH	pEGFP-C1 miniN2G (NIH3T3)	F	GTTAGCGGCCGCGCTAGCCCTGTGCTGCC
			R	CTCCAGGAGTGGGATGAAG
	SR51-CORE	NIH3T3	F	TTTGCTTTCATTCAGCAGTTAGAC
			R	GTTAGCGGCCGCGCTAGCCCTGTGCTGCC

Supplementary Table 3.2 Primers for C-terminal N2G constructs and GST-tagged SR52-45

N2G constructs PCR

primer	**sequences**	**restriction site**
3'KASH	GATAGCGGCCGCTCAggaggtcaggcggcgg	NotI
5' SR49	GTACGCGGCCGCACCATGctcaggcttcccctcagtg	NotI
5' SR51	GTACGCGGCCGCACCATGtttgctttcattcagcag	NotI
5' SR52	GTACGCGGCCGCACCATGtggcggctttggcagaaatttttag	NotI
5' AD	GCGCGCGGCCGCACCATGgatgagaaggaggcgtctg	NotI
5' SR53	GTACGCGGCCGCACCATGaccaaccagagggaagagtttg	NotI
5' SR54	GTACGCGGCCGCACCATGtggcatgttcctgacagccc	NotI
5' 49-53	GTACAGATCTACCATGactgcagagacctgggac	BglII
5' SR52-GST	GATGAGATCTACCATGcggctttggcagaaatttttag	BglII
3' SR52 GST	GATAGCGGCCGCTCAgaagtacctgagtctccg	NotI
3' SR53 GST	GATAGCGGCCGCTCActcatcatctaagcccgg	NotI
3' AD GST	GATAGCGGCCGCTCActcagtcctgtcaccttc	NotI
3' SR54 GST	GATAGCGGCCGCTCActgtttgagcctgagcttg	NotI
5' ΔAD overhang	gggcttagatccttcccattccaagcatcac	
3' ΔAD overhang	gaatgggaaggatctaagcccggggtgtg	
5' LEAA	ctggag**GCGGC**tcacacaggtgacg	
3' LEAA	gtga**GCCGC**ctccagagggatagagtcc	

Chapter Four: Interaction of Nesprin-2 with Both Actin and Microtubule Is Required for Efficient Collective, but Not Single Cell Migration

Abstract

Nesprin-2 giant (N2G) is an enormous (>800 kDa) protein that resides in the outer nuclear membrane. It interacts with actin filaments through its N-terminal calponin homology domains and microtubule (MT) motors through C-terminal domains. N2G's actin interaction is important for nuclear movement during fibroblast polarization of for migration whereas its MT interaction has been implicated for nuclear migration during neuronal and muscle development, suggesting that N2G engages cytoskeletal elements separately to perform its cellular function. Additionally, interaction with both actin filaments and MTs is critical for homoeostatic nuclear positioning in fibroblasts and probably other cells. Here we show that N2G's interaction with both actin and MT motors is specifically required for efficient collective whereas only its interaction with MTs is critical for single cell migration. Previously, in nuclear recentration after displacement by centrifugation, we found that actin-dependent rearward re-centering required the actin binding N-terminus of N2G, whereas MT/dynein-dependent forward re-centering required the dynein-binding C-terminal domain. To address which N2G interactions were critical for cell migration, we re-expressed N2G N-terminal, C-terminal and chimeric N- and C-terminal constructs in nesprin-2 depleted cells and assessed cell migration parameters in both wounded monolayers and sparse cells. Cell migration velocity during wound healing was reduced in the knockdown cells and only rescued by the chimeric N- and C-construct capable of interacting with both actin and MT. Conversely, in sparse cell migration the persistence, but not the velocity was reduced in the nesprin-2 depleted cells and this could be rescued by re-expressing constructs containing the MT interacting domain, but not the actin interacting domain. These results reveal that distinct N2G cytoskeletal interactions are required for single vs. collective cell migration and identify

collective cell migration as the first type of cell migration that requires N2G's ability to interact with both actin and MT.

Introduction

Cell migration is important for development, immune response, wound healing and cancer metastasis. In many cases, cells migrate as individual cells, such as neutrophils "chasing" microorganisms during the innate immune response and neurons migrating to their position in the cerebral cortex during development. In most cases, single cell migration occurs as a cycle of four repeated steps: protrusion, adhesion, de-adhesion and contraction [221]. Variations on this basic cycle can occur in complex 3D environments, including cases in which specific adhesion and deadhesion steps are not evident [222].

A distinct form of migration is collective cell migration. Collective cell migration refers to the concerted movement of groups of cells in sheets, strands, tubes or clusters [223, 224]. Collective cell migration occurs in a number of developmental settings including invading epithelial strands, vascular sprouts and movements of neural crest cell clusters [225, 226]. Some tumor cells migrate as clusters of cells during invasive migration away from the tumor [227, 228]. The movement of *Drosophila* border cells in the developing ovary is a classical system that has been used to genetically dissect the requirements for collective cell migration [229, 230]. Collective cell migration is also seen experimentally in 2D in vitro wound assays and in 3D extracellular matrix cultures and these systems have provided important information about collective cell migration [224].

A defining characteristic of collective cell migration is that cells retain their cell-cell junctions and this is critical for coordinating the collective movement of groups of cells [231-233]. Junctional molecules involved in maintaining collectively migrating cells include: cadherins, immunoglobulin superfamily members such as NCAM and gap junction connexins.

Cell junction molecules physically maintain the cell-cell interactions necessary for collective cell migration and may also send mechanical and biochemical signals that integrate behaviors of groups of cells.

By interacting with the cytoskeleton through LINC complexes, the nucleus may also provide a means to integrate behaviors of groups of cells. For example, disrupting the LINC complex in wounded monolayers of NIH3T3 fibroblasts and C2C12 myoblasts results in reduced cell migration velocity into the wound [3, 136]. Disrupting LINC complexes with a dominant negative KASH construct in breast epithelial sheets, results in rounding of the nucleus in the cell expressing the KASH construct, but also in adjacent neighboring cells [234]. These results raise the important question of whether the LINC complex is differentially engaged in single cells compared to clusters of cells. We set out to address this question by examining the need of the nesprin-2G LINC complexes for single and collective cell migration and whether nesprin-2G's ability to interact with actin and MT was required in both cases.

Results

To test the requirement for nesprin-2G interaction with MTs and/or actin filaments in migrating cells, we further characterized nesprin-2G constructs that were used to explore homeostatic nuclear positioning mechanisms in Chapter 3. These included an N-terminal chimera encoding the actin interacting calponin homology (CH) domains joined to spectrin repeats (SRs) 55-56 adjacent to the KASH domain (renamed N2-N for this study), a C-terminal construct encoding the dynein (SR52-54) and kinesin-1 (LEWD motif) interacting sites attached to SR55-56 KASH (renamed N2-C) and a chimera containing both actin and dynein/kinesin-1 interacting sites attached to SR55-56 KASH (renamed N2-NC) (Figure 4.1a). Expression of these constructs in NIH3T3 fibroblasts revealed that all three constructs localized to the nuclear envelope as expected (Supplementary Figure 4.1a). Interestingly, N2-C and N2-NC were concentrated at one pole of the nucleus rather than uniformly distributed, as was N2-N. The polar accumulations of N2-C and N2-NC were always on the side of the nucleus distal to the centrosome. As these constructs contain both dynein and kinesin-1 interacting sites, this suggests that the kinesin-1 interaction may play a bigger role in localizing nesprin-2 than the dynein interaction.

We next expressed these constructs in cells depleted of all nesprin-2 isoforms by an shRNA against the 3'UTR of nesprin-2 described previously [213] (Supplementary Figure 4.1b). Western blot of the N2 shRNA treated cells with a nesprin-2G antibody recognizing the N-terminal CH domains of nesprin-2G [3] revealed three species (~800kD, ~380kD, ~220kD) that were decreased suggesting that the shRNA reliably knocked down nesprin-2 isoforms. The GFP-tagged rescue constructs (N2-N, N2-C and N2-NC) were expressed well with the correct

molecular weight, although the largest construct (N2-NC) was expressed at lower levels that the other two constructs. (Supplementary Figure 4.1b).

We then tested the ability of NIH3T3 fibroblasts depleted of nesprin-2 and expressing these nesprin-2 rescue constructs to migrate in single cell assays. Cells were starved overnight to synchronize the cells in G_o before plating onto fibronectin coated glass bottom dishes and stimulating with serum for 2 hr before preparing movies. The cell shape measured by circularity and aspect ratio (AR) and cell spread area was similar in all cell types (Supplementary Figure 4.2b), indicating that cell spreading was not affected. Cell were recorded for 15 hr at 10 min intervals and then analyzed by automatically tracking the cell contour by MATLAB (Supplementary Figure 4.2a) to produce single cell traces of the migration paths (Figure 4.1a). Cells depleted of nesprin-2 wandered more and migrated less directionally than the control, with greater than 30% reduction in persistence (Figure 4.1c). In nesprin-2 depleted cells expressing N2-N, migration became even less directed than the knockdown cells, although the persistence was not significantly different (Figure 4.1c). Interestingly, both N2-C and N2-NC rescued the directionality deficit observed in the knockdown cells without affecting the velocity (Figure 4.1c,d). This suggests that the MT-interactive domain, but not the actin-interactive domain, of nesprin-2 is important for the directed migration of single cells. When we quantified the nuclear position relative to the direction of migration, we found that the nucleus was in the rear of the cell in more than 60% of the cases in the control condition. However, there was no periodic nuclear positioning observed in the control cells (Supplementary Figure 4.2c-e). And when we plotted the instant migration velocity and nuclear positioning during the 15 hr migration, there was no obvious linear correlation between the velocity and nuclear positioning (Supplementary

Figure 4.2f). The analysis of nuclear position in the knockdown cells re-expressing the N2 constructs is ongoing.

We then used the same nesprin-2 knockdown and reexpressing cells in wound healing assays. Wounded monolayers that were starved overnight were treated with serum. During the first 10 hours of wound healing in NIH3T3 fibroblast monolayer, cells migrate as cell sheet and such behavior can be characterized as collective cell migration [224]. Indeed, in wounded monolayers of NIH3T3 fibroblasts, both β-catenin and N-cadherin decorate cell-cell junctions [2, 235]. We found that nesprin-2 knockdown inhibited cell migration velocity when measuring the displacement of cells at the wound edge within 10 hrs (Figure 4.2a, 4.2c). This inhibition is similar to that of fibroblasts depleted with nesprin-2G by siRNA [3]. This defect was not rescued by re-expressing either N2-N or N2-C but was rescued by re-expressing N2-NC (Figure 4.2a, 4.2c).This shows that during collective cell migration, both the actin- and MT- interactive domains of nesprin-2 are important for migration velocity.

When we measured the persistence during migration into the wounded monolayers, we found that nesprin-2 knockdown reduced the mean persistence from 0.936 ± 0.068 (control: mean ± Standard Deviation) to 0.892 ± 0.121 (knockdown: mean ± Standard Deviation), a small but statistically significance difference, whereas the persistence in cells re-expressing the N2 constructs was not significantly different from the knockdown (Figure 4.2b). Given that the persistence was not rescued, this suggests that this was a non-specific effect or required a particular level of N2 expression. Persistence of migration in wounded monolayers may not be biologically relevant because during the first 10 hr, the cells migrated in a sheet-like fashion in which neighboring cells around them would restrict directional migration toward the wound.

Moreover, when we quantified the position of the nucleus during migration, we found that the nucleus was in the rear in all conditions and there was a trend of less rear nuclear positioning in the nesprin-2 depletion cells (Figure 4.2d). This apparent defect in rearward nuclear positioning was rescued by N2-N and N2-NC but not by N2-C (Figure 4.2d), suggesting that during cell collective migration, the actin-interactive domain of nesprin-2 plays a role in maintaining the nucleus rearward. These results indicate that the MT-interaction domain of nesprin-2 is important for persistence during single cell migration, whereas both actin- and MT- interaction domains of nesprin-2 are important for velocity during collective cell migration (Figure 4.3).

To extend this analysis to 3-D cell migration, we overexpressed the aforementioned nesprin-2 constructs in MDA-MB-231 breast cancer cells and performed invasion assay using Matrigel plugs. The constructs were expressed at the appropriate size in MDA-MB-231 cells (Supplementary Figure 4.3a) and did not affect transmigration through 8 μm pore (Supplementary Figure 4.3c) used to support the Matrigel (see Supplementary Figure 4.3b: 0 μm panel). After 96 hrs, few cells penetrated the Matrigel between 45-60 μm visualized by two-photon microscope, which is consistent with previous studies [189, 236, 237]. Thus we quantified the total cell number at least 45 μm from the membrane and found that cells expressing N2-C and N2-NC inhibited cell invasion, whereas N2-N did not (Supplementary Figure 4.3d). Because overexpressing these KASH-domain constructs could in principle saturated endogenous SUN binding pocket and function as dominant negative, this suggests that interaction between nesprin-2 and MT inhibits cell invasion while the actin-dependent interaction of nesprin-2 may promote cell invasion.

Discussion

We found that mechanisms of how nesprin-2's interactions with MTs and actin filaments contributed to cell migration were context-dependent. Nesprin-2's interaction with MTs and dynein was required to rescue the directionality deficit in nesprin-2-depleted cells during sparse cell migration while nesptrin-2's interaction with both actin filaments and MTs/dynein was required to rescue the velocity deficit in nesprin-2-depleted cells during wound healing migration. Preliminary result from overexpressing these constructs during 3D invasion suggested that nesprin-2's interaction with actin filaments promoted invasion whereas its interaction with MTs may inhibit invasion. These results suggest that different cytoskeletal modules on nesprin-2 may be specifically activated or inactivated depending on the modes of migration.

It is unclear why different nucleo-cytoskeletal interactions may be important for one form of migration compared to another. The force exerted by the actin and MT cytoskeletons on the nucleus through nesprin-2 may be different, which can be tested by a recent nesprin-2 based actin-dependent FRET sensor [162]. Regulation of the interaction of the nucleus with the cytoskeleton in different types of migration was implied by a previous study where nesprin-3 is identified as nuclear piston during 3D lobopodial-based cell migration that does not function in either 2D or 3D lamellipodial-based migration [126, 238]. That nesprin-2 actin-dependent domain is not required for single cell migration but for collective cell migration may reflect the requirement for cell-cell adhesion and the role of actin filaments in applying force to the adhesions. Whether cell-cell adhesion and other force bearing elements such as focal adhesions are altered in these conditions will be tested in the future to tease apart the potential actin- and MT- involvement of one nuclear envelope protein during cell-cell or cell-matrix crosstalk.

The preliminary 3D migration results suggest that nesprin-2's interaction with actin filaments is required. However, the number of cells accumulated above 45 μm may result from not only cell migration, but also cell division. It will be important to measure the mitotic index in those aforementioned conditions to check whether nesprin-2 depletion also affects cell proliferation. Live cell recordings of 3D migration, despite technical hurdle, may provide information of how the nuclear connection to actin filaments contributes to invasive migration.

We noticed that the collective migration velocity we observed was the quantitative multiplication of the single cell velocity and persistence. This leads us to hypothesize that during collective cell migration there might be constraints on a cell from neighboring cells that result in directional persistence and slower overall velocity. This can be tested by putting directionality compromised single cells in a 1D micro-patterned coverslip and recording the migration velocity of the cell. On the other hand, the requirement of actin-dependent nesprin-2 suggests to us that extrinsic or non-autonomous cues for collective migration could also be important for collective cell migration.

By tracking the nucleus in movies during single or collective cell migration, we showed that the nucleus primarily resided in the cell rear during single and collective migration [11]. However, we did not observe any neuronal migration - like 2-stroke movement of the nucleus nor find any direct linear correlation between the nuclear positioning and cell migration speed during sparse cell migration, which could be a consequence of limited frequency of sampling during migration. Other factors such as protrusion and retraction could be further tested in nesprin-2 depleted cells. Also, people have hypothesized that the centrosome-nucleus axis is important for migration directionality [239], which can be further examined by visualizing

fluorescently labeled centrosome in nesprin-2 depleted cells re-expressing nesprin-2 constructs that differently engage actin filaments and MTs during single cell migration. We also started to analyze the nuclear positioning during collective cell migration and find there is trend of nuclear mis-positioning in nesprin-2 depleted cells. More samples should be included to confirm this result.

Materials and Methods

Chemicals and cell cultures All chemicals have been purchased from Sigma unless described. NIH3T3 (ATCC) were cultured in DMEM and 10% calf serum (Hyclone) as previously described [16]. MDA-MB-231 (ATCC) were cultured in DMEM and 15% fetal bovine serum (Hyclone). For serum starvation, cells plated on acid-washed coverslips were transferred to serum-free medium (DMEM, 10 mM HEPES pH7.4) overnight. Plasmids used in this study were described in Chapter 3. Virus infection was used for overexpressing constructs in cells. pLP-VSVG (Addgene) and pCMV MMLV gag-pol (Addgene) were used as packaging system to make retrovirus capable of infecting MDA cells. Virus infection was described in Chapter 3. After overexpressing nesprin-2, shRNA against nesprin-2's untranslated region was performed in those cells. The procedures were described in earlier study [213].

Sparse cell migration Four-chamber CELLview^{TM} 35mm glass bottom dishes (Greiner Bio-One) were coated with 5 µg/ml fibronectin for 3-4 hr in room temperature. Cells starved overnight were plated onto the fibronectin-coated coverslip. Seeded cells were incubate in 37 °C incubator with 2% BCS DMEM for 2hrs before mounting onto an automated stage for live recording by phase microscopy described in Chapter 3.

Wound healing migration Cells were plated onto 8-well Lab-Tek II Chambered slides (Thermo Fisher Scientific), grown to confluency and then starved overnight. The monolayer was wounded by scratching. Cells were stimulated with 2% BCS DMEM after being mounted onto the automated stage with incubator on microscope with DIC light. The protocols for the phase, DIC and epi-fluorescent microscopy are described in Chapter 3.

Matrigel invasion in inverted transwell Matrigel plugs were made in Transwell (8.0 μm pore, 6.5 mm diameter, 24 wells) with 150 μl of matrix in each well (500 μl of 10 mg/ml Matrigel Growth Factor reduced; 25 μl of 1 mg/ml Fibronectin; 475ul of PBS). The plug was left in a 37 °C incubator to dry. Meanwhile MDA-MB-231 cells were trypsinized and concentrated to 1.0 x 10^6 cells/ml and 100 μl of cells were plated on top of the inverted transwell for 3 hr. 750 μl of serum free Ham F-12/DMEM medium was then added to each well. Three hours after plating, the bottom surface of transwell was washed by dipping into dish containing serum free DMEM/F12 medium and put back to the well. 250 μl of 10% CS and 20 μg/ml EGF Ham F-12/DMEM medium was used onto the top of the matrix. Cells were allowed to migrate for 96 hrs, and then fixed with 4% PFA (1ml on the bottom of transwell and 0.5 ml on the top of transwell) for 1 hr. Cells for quantifying transmigration were fixed after 24 hr with 4% PFA. Cells were stained with DAPI in room temperature for 1hr before imaging.

Two-photon microscopy Nikon A1RMP Confocal system with W Apo LWD 25x water objective was used for imaging cells in Matrigel invasion assays. The red laser line was used to focus on the membrane holes and the top of the membrane was then set as 0 μm. (See Supplementary Figure 4.3). Images were then acquired with illumination from the blue laser line at 3 μm steps for 115 μm above the membrane.

Quantification and software Data was quantified by Excel, GraphPad and Origin. All data for statistical analysis were numerical. If sample size was bigger than 30, normal distribution was assumed based on central limit theorem, and two-tail t-test was used for statistical analysis. Automated tracing for cell contour was achieved by MATLAB (version 2015b).

Figures

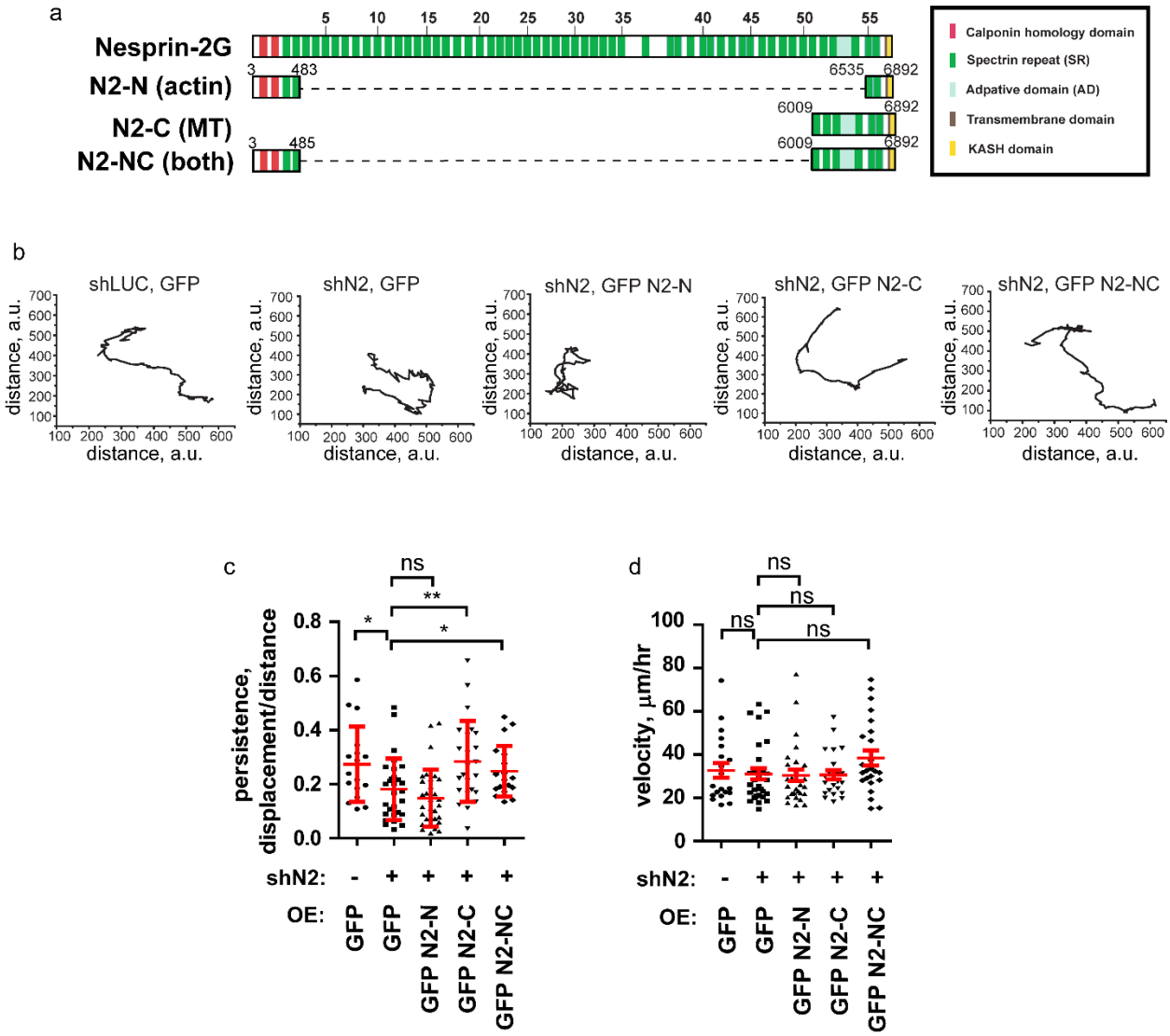
a
Nesprin-2G
N2-N (actin)
N2-C (MT)
N2-NC (both)
Calponin homology domain
Spectrin repeat (SR)
Adpative domain (AD)
Transmembrane domain
KASH domain
b
shLUC, GFP
shN2, GFP
shN2, GFP N2-N
shN2, GFP N2-C
shN2, GFP N2-NC
distance, a.u.
c
persistence, displacement/distance
d
velocity, µm/hr
ns
shN2:
OE:
GFP
GFP N2-N
GFP N2-C
GFP N2-NC

Figure 4.1 Only the C-terminal MT-interacting domain of nesprin-2 is required for single cell migration.

a) Schematic diagram of nesprin-2 constructs. Mini-N2G described in a previous paper [3] is renamed here as N2-N; SR 51-56 KASH and mini-N2G SR51-56 KASH (Chapter 3) are renamed NC-C and NC-NC, respectively. b) Representative traces of sparse NIH3T3 fibroblast migration over a 15-hr period. NIH3T3 fibroblasts expressing GFP or the indicated GFP-tagged N2 constructs were treated with shRNA against nesprin-2 (shN2) or luciferase (shLUC) as a control. c-d) Quantification of persistence (c) and velocity (d) of NIH3T3 fibroblasts expressing GFP or GFP-tagged N2 constructs and treated with shN2 (+) or shLUC (-) in sparse cell migration. Data were from 4 experiments (N = 21, 29, 30, 24, 28 movies in each condition); error bars are SD. Two-tailed t-test was used. *: $p < 0.05$; **: $p < 0.01$; ns: not significant.

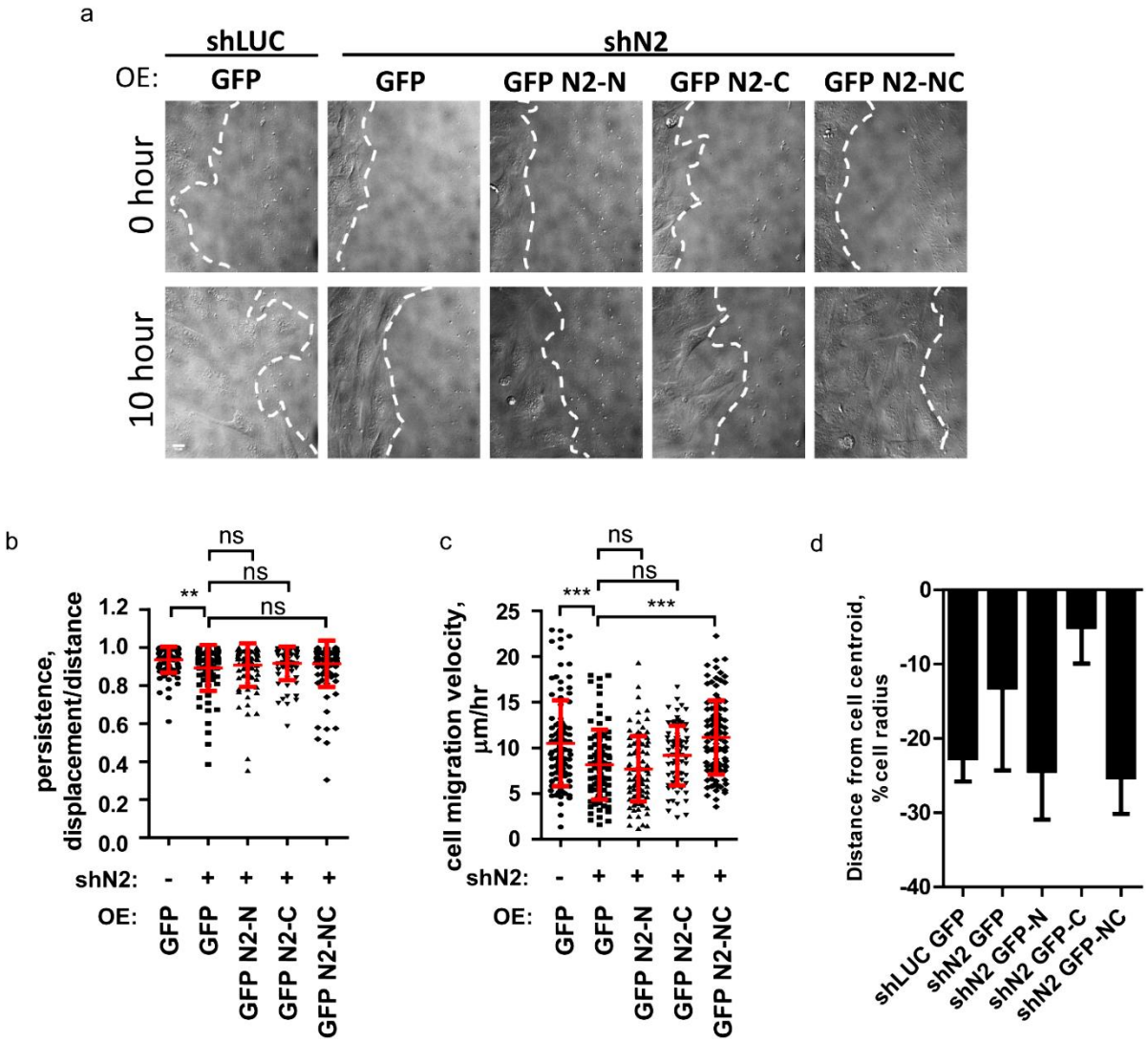
a
shLUC
shN2
OE:
GFP
GFP
GFP N2-N
GFP N2-C
GFP N2-NC
0 hour
10 hour
b
persistence, displacement/distance
ns
ns
ns
**
shN2:
OE:
GFP
GFP
GFP N2-N
GFP N2-C
GFP N2-NC
c
cell migration velocity, µm/hr
ns
ns
***
***
shN2:
OE:
GFP
GFP
GFP N2-N
GFP N2-C
GFP N2-NC
d
Distance from cell centroid, % cell radius
shLUC GFP
shN2 GFP
shN2 GFP-N
shN2 GFP-C
shN2 GFP-NC

Figure 4.2 Both N-terminal actin- and C-terminal MT- interacting domains of nesprin-2 are required for collective cell migration.

a) Representative DIC images of wound healing migration of NIH3T3 fibroblasts expressing GFP or the indicated GFP-tagged N2 constructs and treated with shLUC (control) or shN2. Scale bar: 10 μm. b-c) Quantification of persistence (b) and velocity (c) of NIH3T3 fibroblasts expressing GFP or GFP-tagged N2 constructs and treated with shN2 (+) or shLUC (-) in wound healing cell migration. d) Quantification of nuclear position during cell migration. Data were from 3 experiments (N = 102, 89, 97, 75, 112 cells from N = 42, 38, 46, 33, 46 movies in each condition); error bars are SD. Two-tailed t-test was used. *: $p < 0.05$; **: $p < 0.01$; ***: $p < 0.001$; ns: not significant.

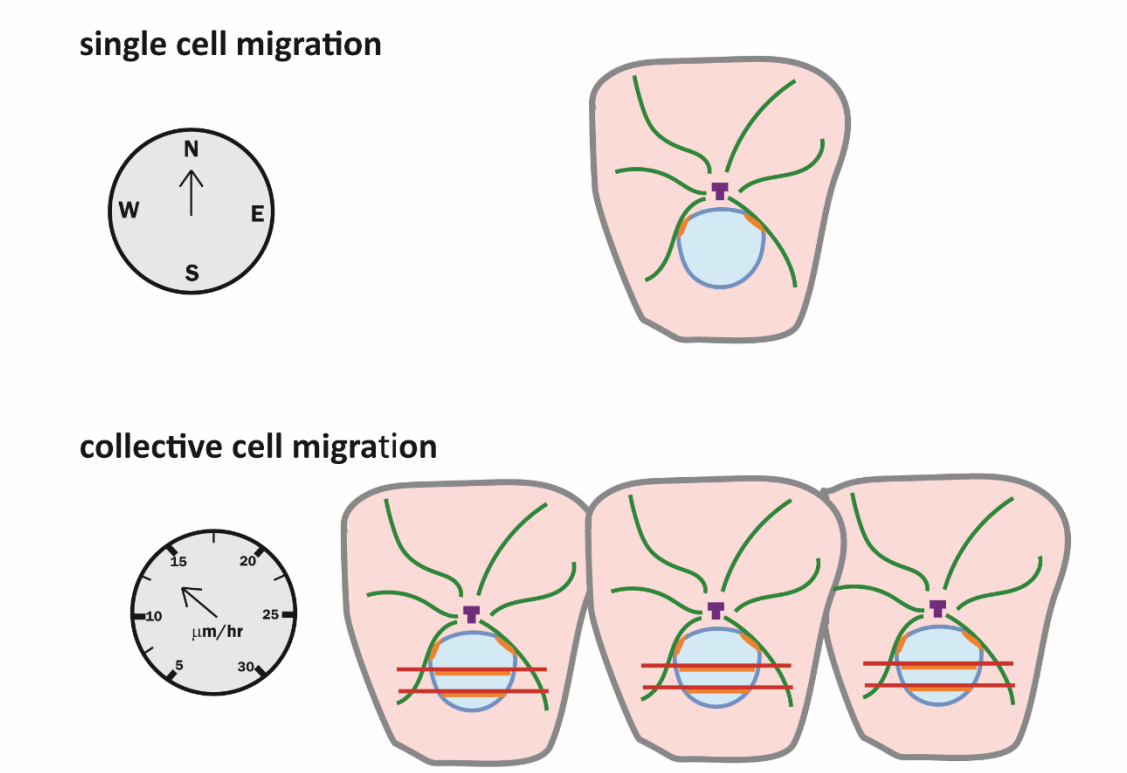

Figure 4.3 Model of nesprin-2 involvement during single vs. collective cell migration.

Red: actin filaments; green: MTs; purple: centrosome; orange: interaction sites between nesprin-2 and cytoskeletal elements.

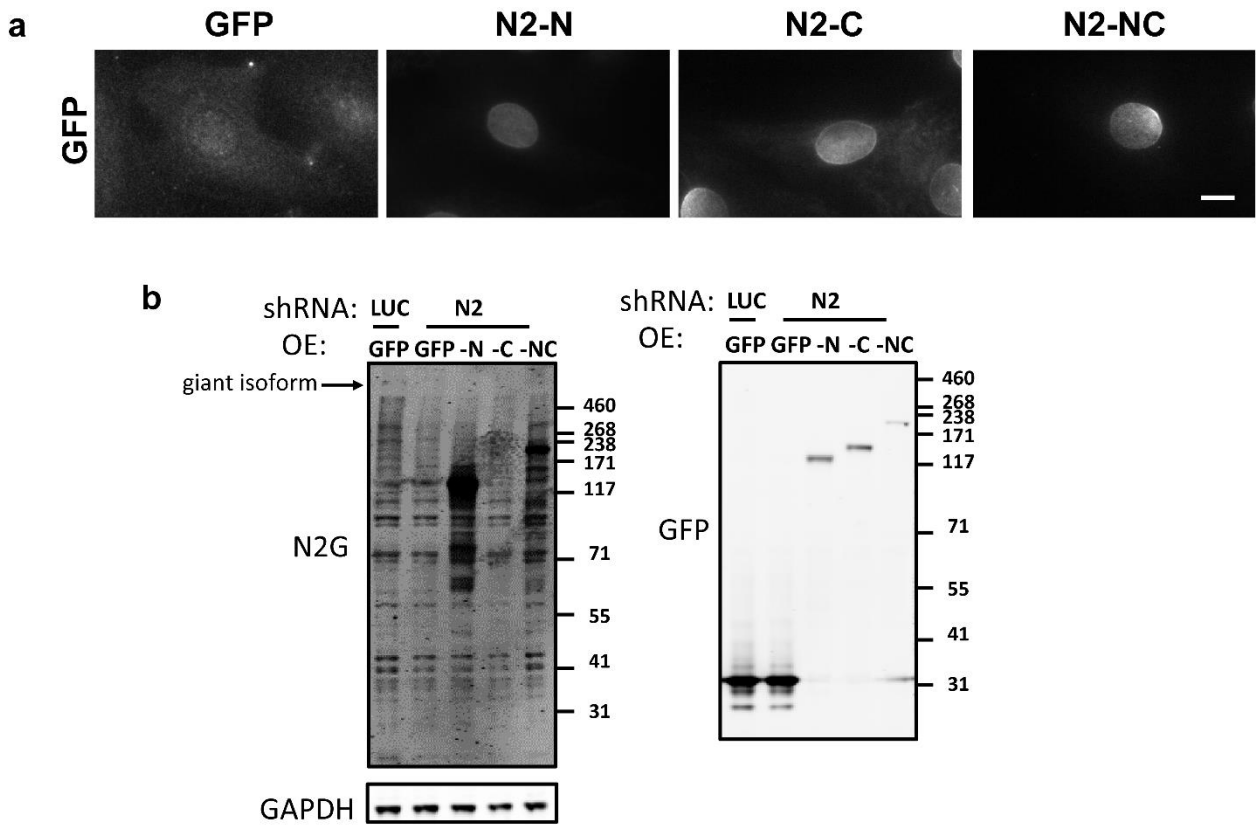

Supplementary Figure 4.1 Characterization of the re-expression of nesprin-2 construct in nesprin-2 depleted fibroblasts.

a) Representative fluorescent images of nesprin-2 constructs in NIH3T3 fibroblasts. Cells were stained with GFP antibody. Note polarized distribution of N2-C and N2-NC. Scale bar: 10 µm.

b) Western blots of re-expressed nesprin-2 constructs in NIH3T3 fibroblasts infected with shN2 or shLUC as a control. Blots were stained with nesprin-2G, GAPDH and GFP antibodies. The nesprin-2G antibody detects N2-N and N2-NC constructs.

a


Binary gradient mask (canny) → bothat mask → fill the hole → find the biggest shape→ draw outline

b

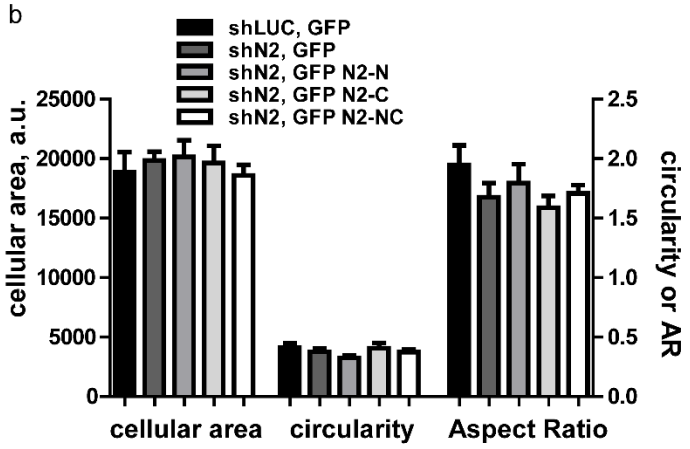
shLUC, GFP
shN2, GFP
shN2, GFP N2-N
shN2, GFP N2-C
shN2, GFP N2-NC
cellular area, a.u.
circularity or AR
25000
20000
15000
10000
5000
0
2.5
2.0
1.5
1.0
0.5
0.0
cellular area
circularity
Aspect Ratio

c

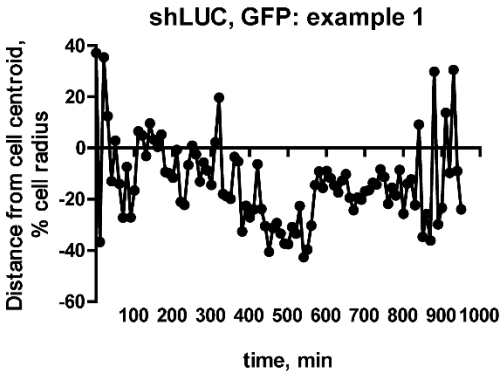
shLUC, GFP: example 1
Distance from cell centroid, % cell radius
40
20
0
-20
-40
-60
100 200 300 400 500 600 700 800 900 1000
time, min

f

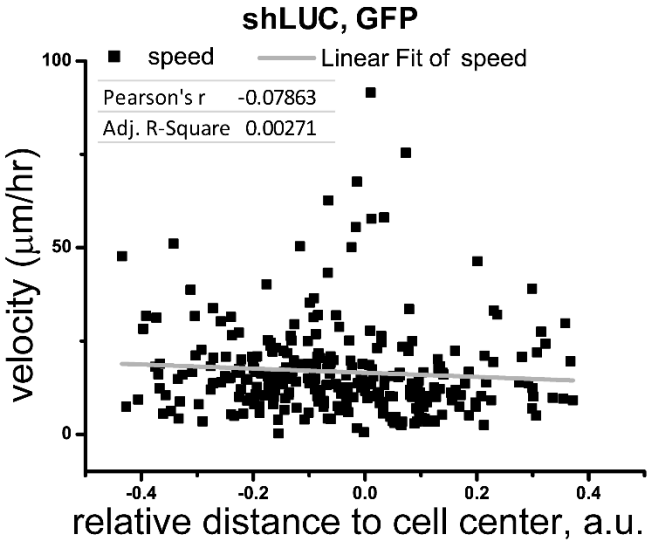
shLUC, GFP
speed
Linear Fit of speed
Pearson's r -0.07863
Adj. R-Square 0.00271
velocity (μm/hr)
100
50
0
-0.4
-0.2
0.0
0.2
0.4
relative distance to cell center, a.u.

d

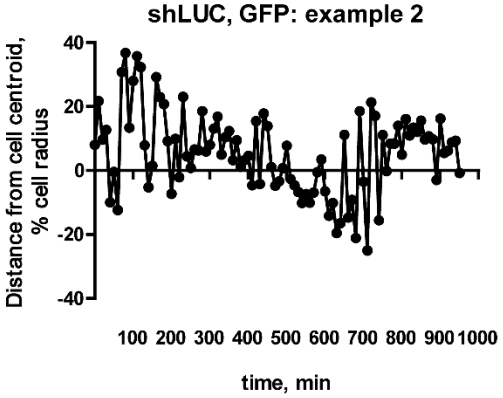
shLUC, GFP: example 2
Distance from cell centroid, % cell radius
40
20
0
-20
-40
100 200 300 400 500 600 700 800 900 1000
time, min

e

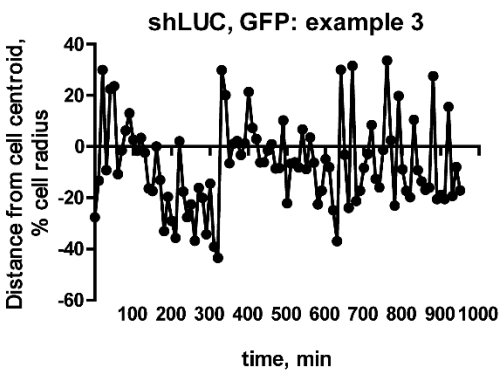
shLUC, GFP: example 3
Distance from cell centroid, % cell radius
40
20
0
-20
-40
-60
100 200 300 400 500 600 700 800 900 1000
time, min

Supplementary Figure 4.2 Procedures of processing sparse cell migration movies and nuclear positioning quantification in control condition of sparse cell migration.

a) Representative images of processing steps in MATLAB to automate detecting of the position of a migrating cell from live cell recordings of migrating cells. b) Quantification of cellular area, circularity and AR of NIH3T3 fibroblasts treated with the indicated shRNAs and expressing the indicated constructs 2 hr after spreading when the movies of migration were started. c-e) Plots of nuclear position over time in migrating control NIH3T3 fibroblasts (treated with shLUC and expressing GFP). Nuclear position relative to the cell centroid was determined every 10 min. f) Linear fitting and parameters of control NIH3T3 fibroblast (shLUC and expressing GFP) migration velocity and nuclear positioning relative to cell centroid in the control condition. Data were from 4 experiments with N = 288 time points in total.

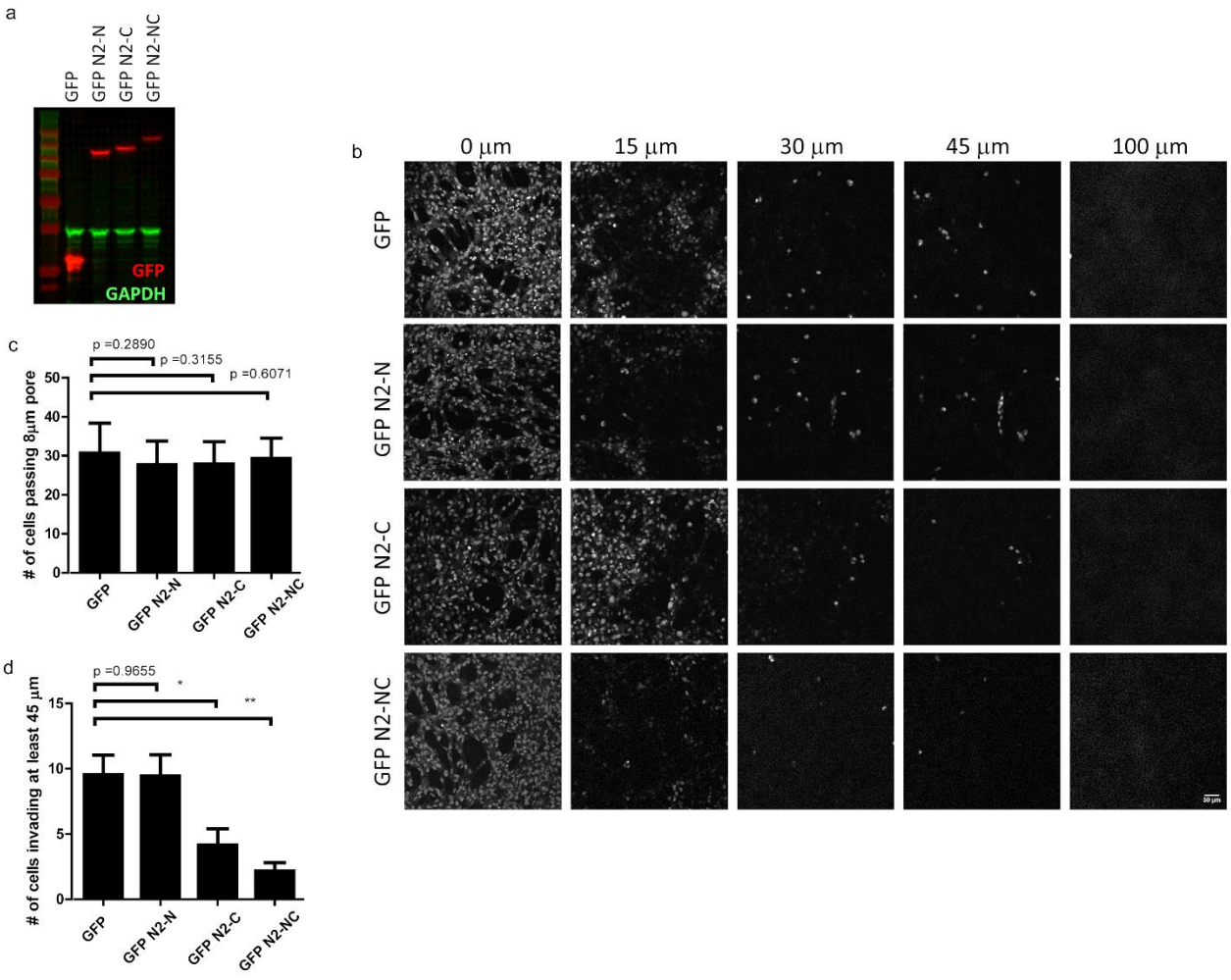
a
GFP
GFP N2-N
GFP N2-C
GFP N2-NC
GFP
GAPDH
b
0 µm
15 µm
30 µm
45 µm
100 µm
GFP
GFP N2-N
GFP N2-C
GFP N2-NC
c
p =0.2890
p =0.3155
p =0.6071
# of cells passing 8µm pore
50
40
30
20
10
0
GFP
GFP N2-N
GFP N2-C
GFP N2-NC
d
p =0.9655
*
**
# of cells invading at least 45 µm
15
10
5
0
GFP
GFP N2-N
GFP N2-C
GFP N2-NC

Supplementary Figure 4.3 Matrigel 3D invasion assay of MDA-MB-231 cells overexpressing with nesprin-2 constructs.

a) Western blot of GFP or GFP-N2 construct expression in MDA-MB-231 cells. b) Representative two-photon fluorescent images of nuclei in invading MDA-MB-231 cells expressing the indicated N2 constructs at different distances above the membrane. Scale bar: 50 μm. c) Quantification of cells migrating through 8 μm pores. Two independent experiments with 24, 18, 12, 12 fields in each condition were quantified. d) Quantification of cells invading at least 45 μm above membrane in different conditions. Two independent experiments with 20, 10, 10, 10 fields in each condition were quantified. Error bars: SD. Two-tailed t-test was performed with p value shown for not significant. *: $p < 0.05$; **: $p < 0.01$.

Chapter Five: Conclusion and Future Direction

For this thesis, I identified the formin FHOD1 as the first cytoplasmic component of TAN lines and showed that FHOD1 reinforces TAN line structure by binding N2G (Chapter 2). Also, by establishing a novel method to artificially displace nuclei, I revealed the mechanisms of nucleo-cytoskeletal systems contributing to homeostatic positioning of the nucleus in adherent cells (Chapter 3). Additionally, I applied what I have learned in a physiological context to examine the actin- and MTs- dependent roles of nesprin-2 during both single and collective cell migration (Chapter 4).

The centrifugation method for displacing nuclei that I have developed should be broadly useful for examining questions of nuclear positioning. It is easy to manipulate. We can adjust the nuclear displacement by changing the centrifugal force amount and presumably the time as well. Centrifugal force can systematically displace all the nuclei on the overslip and the force exerted on each cell is almost the same. Cells on one end of the coverslip are farther away from the rotor center than cells on the other end, thus on two sides of the wound, the exact centrifugal force exerted on the cells are slightly different. However, when we quantified nuclear displacement in cells on the wound edge, we did not find any statistical difference (Figure 3.1, Supplementary Figure 3.1). Besides, the system error caused by this deviation in centrifugal radius when centrifuging a 22 mm coverslip in SW28 Beckman centrifuge would only be around 1%, which is at the similar scale as observation error. Thus, we hypothesize that this difference can be ignored.

The centrifugation method can be used as a preparative tool to study nuclear recentration in other adherent cells as I discussed in Chapter 3, however additional comparisons with non-centrifuged physiological system are needed in order to rule out artifacts from this non-

physiological method (see Figure 3.6 and Chapter 4). The method also might be used as an analytical tool to test how engaged the nucleus is under different physiological states. For example, in preliminary studies, I showed that nuclei in lamin A/C depleted cells moved further during centrifugation than those in wild type cells (Figure 5.2). As lamin A/C enhances LINC complex anchoring, centrifugation provides a direct test of this hypothesis. Additionally, the process of centrifugal displacement of nuclei can potentially be visulized and studied in real-time with the centrifugal microscopy invented by S. Inoue [240].

The Role of Nuclear Positioning

Although multiple mechanisms of nuclear positioning have been reported, the million-dollar question of why the nucleus is moved and positioned remains unanswered. Interestingly, alterations in genes encoding LINC complex components as well as other nuclear envelope proteins like lamin A/C are observed in muscular dystrophy and other diseases [12, 117, 118]. Moreover, defects in mouse models depleted with certain SUN and KASH domain proteins include neuromuscular junction, muscle, and hearing system. SUN1/SUN2 double knockout mice are reported to die from a breathing defect with unexpanded alveoli sacs [115]. One hypothesis from these correlations of NE proteins and mechanosensitive systems could be that the more “mechanosensitive” the tissue, the more importance of “strength” of a nuclear linkage formed by LINC complexes. However, this mechanosensitive explanation for the importance of the LINC complex does not explain its role in neuronal migration during brain development as the brain is generally considered a soft tissue with limited mechanical inputs.

The potential importance of nuclear positioning can be postulated as follows:

1) Spatial factor: During cell migration when the nucleus is toward the rear of the cell, it is closer to the rear while further away from the leading edge. Effectors (if any) around the nucleus may be regulated to be closer (thus more concentrated) or farther away from certain cellular region and may affect protrusion or retraction. This hypothesis can be tested by closely monitoring the protrusion and retraction in centrifuged wounded monolayer. However, since the nucleus will re-center, cells depleted of nesprin-2, where a slower migration velocity and reduced recentration are observed, can be used. If nesprin-2 depletion affects any protrusion/retraction processes in monolayer, then does centrifugation induced nuclear displacement at least partially rescue the deficit? It could be even more interesting to monitor these centrifuged nesprin-2-depleted cells to see whether the cell migration defect can be restored. Another reason for controlling the nuclear position in cells may be related to local translation. When the nucleus occupies a certain area, the transcripts translated near the nucleus will be subsequently accumulated in the same area. Without moving transcripts to different regions in the cell by motors, changing nuclear position may achieve a similar yet more efficient result, with transcripts at the same time affected. An interesting observation during muscle regeneration is that the nucleus moves back to the fiber center after muscle damage; is it possible that by positioning the nucleus in the center, the transcription/translation for repair will be more efficient?

2) “Mechano-factor”: It is worth mentioning that mechanical force transmission is much faster than biochemical diffusion and molecular transportation [241]. Similar to any protein modification, force applied on any molecule could potentially change its confirmation. Thus, any mechanic activity on the nucleus may trigger downstream pathways faster. Force induces

deformation, displacement or defection. The shape, rotation and positioning of the nucleus have all been studied. The change of nuclear shape may affect chromosome organization, transcription and translation [208]. A change in nuclear position may affect local force transmission, for example by moving the nucleus from a low to a high force environment.

3) Polarity/trafficking: It is possible that the nucleus is also participating in the vesicular event in cells because it is composed of lipid and linked to other membrane structures like ER. Moreover, the position of the nucleus along with the centrosome creates an axis in the cell [239]. As the Golgi is localized near the centrosome, one consequence of this may be to direct membrane trafficking toward a particular site. Thus, the change of nuclear positioning might affect the efficiency of the vesicular trafficking in cells. Recent studies show a form of nuclear membrane blebbing, analogous to that seen during herpesvirus egress from the nucleus, may be involved in transport of very large RNA particles that are too large to pass through the nucleus pores [242].

TAN Lines Formation and Structure

FHOD1's actin binding and N2G binding are both required for rescuing the nuclear movement defect in fibroblasts depleted of FHOD1. Based on the evidence, we conclude that FHOD1 provides additional binding sites between actin filaments and nesprin-2 (Figure 5.1). It can be inferred that the binding "affinity" between actin filaments and the nucleus will be strengthened, which could be corroborated by both structural and biochemical study between FHOD1, nesprin-2 and actin filaments. A previous study in *Drosophila* oocyte suggested that the force to push the nucleus at 4 μm/hour forward in the oocyte yielded a drag force of 10 pN by

Stoke's Law [146]. Because the average fibroblast nuclear radius is at least twice as large as the oocyte and the velocity of nuclear movement is at least 3-fold faster [3], the drag force on migrating nucleus in fibroblast is about 60 pN assuming the cytoplasmic viscosity is similar in these two cells. If the technical hurdles could be overcomed, it would be interesting to measure the force generated by actin filaments and test whether the linkage between actin and N2G under certain amount of force (pN level from the calulation) is stable with or without FHOD1 *in vitro*. Other actin-binding protein inplicated in TAN lines formation like fascin [189] could also be tested in this context.

However, how FHOD1 facilitates TAN lines formation remains unknown. FHOD1 could be necessary to resist the force on the actin cable during nuclear movement. In order to test this hypothesis, another actin bundling protein could be expressed in the absence of FHOD1 to see whether the bundled actin cable is sufficient to resuce the nuclear movement defect. Because the chimera FHOD1 construct (Figure 2.5) partially rescues the nuclear movement in FHOD1 depleted fibroblasts, it would be interesting to look at the TAN lines in these cells. Also prior to TAN lines formation, FHOD1 may decorate actin filaments before they reach the nucleus, or it be attached to N2G; in either case, this may help N2G to attach to the dorsal actin cable. Answers to these questions have been hampered by the lack of a good FHOD1 antibody with the detection of the endogenous localization of FHOD1. Current data of tagged FHOD1 expression in fixed cells showed that the active form of FHOD1 (FHOD1-ΔC) as well as wildtype FHOD1 decorated dorsal actin cable (Figure 2.4 and Supplementary Fig. 2.5) and that not all dorsal actin cables on the nucleus are co-localized with N2G in a fixed snapshot (Figure 2.4a). To further study the role of FHOD1 during initiation of TAN lines formation, live imaging of fluorescent

labeled FHOD1 together with fluorescent labeled N2G and fluorescent labeled Liveact during LPA stimulation could be informative, although protein overexpression may cause artifact.

Mechanisms of Nuclear Recentration after Centrifugation and Homeostatic Nuclear Positioning

The results in Chapter 3 identify homoeostatic nuclear positioning mechanisms and suggest that different mechanisms are employed dependening on cellular contexts. As summarized in Figure 5.2a, in starved cells at the wound edge, actin-dependent machinery is responsible for nuclear recentration when the nucleus is displaced to the cell front whereas MT-dependent machinery is reponsible for nuclear recentration for nuclei displaced to the cell rear. In cells within starved monolayers, only MT-dependent machinery is responsible for homeostatic nuclear positioning. In monolayers stimulated with serum, both actin- and MT- dependent machineries are responsible for the nuclear positioning (Figure 5.2a). These results can be further tested by imaging the nuclear position in live cells treated with either actin or MT inhibitors and by imaging actin and MTs during nuclear recentration.

Interestingly, in centrifuged cells at the wound edge treated with cytoskeletal drugs to disrupt actin filaments or MTs, we did not observe recentering nuclei to move past a position near the cell centroid, suggesting either that the active force generated by actin filaments or MTs or that there is a non-actin-, non-MT- dependent anchorage near the cell center.

One way to visualize the cytoskeletal engagement of nesprin-2 is to use nesprin-2 FRET tension sensors. A FRET-based nesprin-2 actin tension sensor has been developed and shows

that nuclei in adherent cells are under constant actomyosin tension [162]. It would be useful to generate a nesprin-2 based MT FRET sensor to measure kinesin and dynein forces on the nucleus (Figure 5.3). Each functional sensor can be expressed in different cellular contexts (Figure 5.2a) and FRET index can be measured at different times during nuclear recentration and in unperturbed cells. In doing so, we may be able to map the regions where nesprin-2 is engaged by actin, MT and MT/dynein.MT-

In Chapter 3, measurement of recentration distance was used to quantify the ability of nuclear re-centering because the centrifuged displacement was similar, at least in cells treated with siRNA or shRNA against N2G, SUN1 and SUN2 (Figure 5.2d). This indicates that at least N2G, SUN1 and SUN2 do not affect the ability of the nuclei to be displaced by centrifugal force. This also validates the measurements of nuclear recentration as an accurate reflection of the role of N2G, SUN1 and SUN2 in the recentering process.

However, centrifuged displacement was larger in cells depleted of lamin A/C and the nuclei returned to a location ~20% away from the cell center in both rearward and forward directions. This result could be due to the misshaped nuclear phenotype caused by a reduced lamina and/or a more pliant nucleus. When I quantified the recentration distance in lamin A/C depleted cells, I found that the extent of rearward recentration, but not forward recentration was not sigfinicantly different from the control (Figure 5.2b,c). This suggests that: 1) even when the nuclei were displaced more than control, the recentration system was still somewhat active to move the nuclei back because the centrifugation displacement was significantly different from the recentration displacement; 2) lamin A/C was required for both recentrations because the extent of recentration was significantly different from starved cells; and/or 3) recentration

distance should be interpreted carefully in the experiment group when the nuclear displacement after centrifugation was significantly different from the control. A previous study has shown that lamin A/C variants affect nuclear positioning and centrosome reorientaion. EDMD and dilated cardiomyopathy (DCM) lamin A/C variants prevent anchoring of TAN lines during LPA-stimulated nuclear movement [35] (Table 5.1). Therefore, I predict these would be defective in rearward actin-depedent recentering. It would be interesting to test lamin A/C variants that cause Dunnigan-type familial partial lipodystrophy (FPLD), since these variants do not affect LPA-stimulated actin movement but do have an effect on the centrosome reorientation by disrupting centrosome positioning [35]. It might be possible that these variants affect MT-dependent forward nuclear recentration or the ability of the cells to find the cell center during recentration.

A further considering in cases in which nuclear recentration is inhibited, is whether this reflects a complete or kinetic block. In all my experiments, I assessed nuclear recentration at 60 min. It is possible some of the partial effects I observed (e.g., SUN2, FHOD1), represent slower movement rather than blocked nuclear recentation.

Participation of Other KASH Proteins during Homeostatic Nuclear Positioning

My data with nesprin-2-depleted cell re-expressing N2 constructs (Figure 3.6) indicate that nesprin-2 is required for homeostatic nuclear positioning. However it does not exclude the role of other KASH proteins nor other isoforms of nesprin-2 during the process. Given that the efficiency of siRNA against N2G is sufficient to silence its function, the fact that overexpression of dominant negative KASH in recentration generated more inhibition is consistent with the possibility of participation of other KASH proteins during recentration (Figure 3.4). This

hypothesis can easily be tested by knocking down other KASH proteins in cells subjected to recentration assay. Nesprin-1, which associates with dynein in rat brain lysates [115] would be a good place to start to test other KASH proteins.

It is quite interesting that a single N2G construct containing both N-terminal CH domains and C-terminal dynein interaction domain rescued the defect of nesprin-2 knockdown in the nuclear recentration and scattering assays, arguing that both actin- and MT- depedent interaction are important for these processes. However, it is still unclear whether individual nesprin-2 molecules interact with actin and MTs simultaneously. Also, because the shRNA used to knockdown nesprin-2 was directed against nesprin-2's 3'UTR, we cannot rule out the possibility that other nesprin-2 isoforms may be required to maintain the homeostatic nuclear position in steady state cells. This is hard to test because there isn't an efficient way to detect each isoform at the protein level in cells.

Prelimary Molecular Exploration of SUN1 and SUN2

We found that SUN1 is required for MT-dependent forward nuclear movement while SUN2 is required for actin-dependent rearward nuclear movement (Figure 3.4), suggesting these two proteins may compete for nesprin-2. The transdominant effect of overexpressing SUN proteins on nuclear recentration suggests that the stoichiometry between SUN1 and SUN2 is important as well. Why is SUN1 important for nesprin-2-dependent nuclear movement by MT whereas SUN2 is important for nesprin-2-dependent nuclear movement by actin? There are at least five non-exclusive possibilities: 1) the cytoskeleton itself may be important for this discrimination; 2) nesprin-2 selection from different forces generated by actin and MT; 3)

different conformations of nesprin-2 when binding to different cytoskeletons; 4) different binding affinities between full-length SUN1/2 and nesprin-2 *in vivo*; 5) different anchorages in the nuclear lamina. Nevertheless, the seperation of function is very likely the result of differences in the primary structure of SUN1 and SUN2. As I discussed in the introduction, mouse SUN1 has more conserved cysteines, more predicted coiled-coil domains and a longer nucleoplasmic domain compared to SUN2 (Figure 1.2 and 1.3), all of which could contribute to the functional separation between the two proteins. Additionally, SUN2 is trimeric whereas SUN1 is reported to be a dimer or tetramer [49].

In Chapter 3, I further tested the first hypothesis by determining whether the trans-dominant effects of SUN protein overexpression were dependent on the cytoskeleton. Strikingly, inhibiting MTs restored the disrupted actin-dependent nuclear movement in SUN1 overexpressing cells and actin disruption restored the disrupted MT-dependent nuclear movement in SUN2 overexpressing cells (Figure 3.4G-H). This is consistent with the possibility that the interaction of nesprin-2G with actin generated different force on nesprin-2G than the interaction with MTs, which may favor interaction of one SUN protein over the other, especially given that they are likely to exhibit different oligomeric states.

Since the most conserved cysteine of nesprin1/2 has been shown to form a disulfide bond with SUN2 in the crystal structure by Sosa et al [43], I decided to mutate the conserved cysteine in both SUN1 and SUN2 to see whether there was a disulfide bridge between SUN proteins and nesprin-2 in fibroblasts. Also, I have mutated the conserved cysteine in the KASH domain of mini-N2G [3]. When I overexpressed these mutants in cells and lysed the sample in either reducing (with DTT) or non-reducing (without DTT) condition, I found that KASH cysteine is

required for disulfide bond formation between nesprin-2 KASH and both SUN1 and SUN2 (Figure 5.4a-b). So are the cysteines in SUN domains of both SUN1 and SUN2. Interestingly, while full-length SUN2 is mainly in a non-disulfide form; overexpressed SUN1, regardless of WT or mutant, is more likely to be in a oligemeric form in non-reducing conditions, suggesting that there are other cysteines capable of forming a disulfide bond in SUN1 besides C759. These results reinforce the idea that there are molecular distinctions between SUN1 and SUN2. However more controls of nesprin-2, SUN1 and SUN2 knockdowns in these protein expression experiments should be carried out. Besides, it would also be interesting to use immunoprecipitation to enrich and purify the expressed proteins to verify the specificity of the bands of similar size that is labeled in Figure 5.4a and 5.4b. Also, we can test the role of these disulfide bond variants in actin- and MT- dependent nuclear recentration by re-expressing these constructs in cells depleted of SUN1 or SUN2. For example, if SUN2 disulfide bond variant failed to rescue the actin-dependent rearward nuclear recentration, it would suggest that SUN2 C577 is important for actin-dependent nuclear movement, which could also be tested in a LPA-stimulated nuclear movement assay.

Application of Centrifugation in Muscle to Study Muscle Differentiation and Disease Mechanisms

Nuclear positioning reaches a pinnacle in muscle cells. Specific nuclear positioning events occur in each stage of muscle differentiation. Nuclei are positioned rearward in migrating myoblasts, nuclei move into the center and spread along the length of myotubes after fusion of myoblasts into myotubes, and nuclei move from the center of the myotubes to the periphery

during myofiber formation [243, 244]. Finally, nuclei are anchored at equi-distance sites along the mature myofiber and at small cluster of nuclei under the neuromuscular junction. The LINC complex is known to participate in some of these events, yet the specific mechanisms involved, particularly those coupling nuclei to specific cytoskeletal structures have not been defined. As noted in the Introduction, nuclear positioning is disrupted in muscle diseases, including EDMD which seems to specifically involve LINC complex proteins and proteins anchoring the LINC complex.

Because I have shown feasibility of centrifuging myoblast C2C12 cells (Supplementary Figure 3.2), it would be very interesting to use centrifugation to identify specific nuclear positioning pathways in muscle cells, focusing on those in myoblasts, myotubes and if time permits, early myofibers.

There are unresolved issues concerning the role of LINC complex proteins in muscle differentiation. Most studies have made use of a dominant negative KASH construct derived from nesprins to test the role of the LINC complex in nuclear positioning and they come to different conclusions. While KASH dominant negative disrupts nuclear alignment and rotation in C2C12 mouse myotubes [114, 245], it has also been reported to have no effect and affect only the number of peripheral nuclei and myofiber thickness in later stage myofibers prepared from primary muscle myoblasts [246]. In myotubes in developing Drosophila larva, KASH dominant negative does not affect nuclear alignment, which is instead dependent on a microtubule MAPs and motor proteins [246]. Additionally, these studies have not addressed the role of LINC complexes engaging actin in positioning nuclei during muscle differentiation despite the fact that there is accumulating evidence for a role of actin in nuclear positioning in muscle cells: actin-

driven nuclear movement is found in myoblasts and TAN lines are observed during this movement [136]; the actin nucleator N-WASP and actin dynamics regulator amphiphysin-1 are required for peripheral nuclear positioning in myofibers [247, 248]. These results suggest that multiple cytoskeletal and LINC complex systems position nuclei in differentiating muscle cells and suggest that there may be a switch from one LINC complex system to another during muscle development. Thus, it is important to interrogate these events in a more controlled fashion in the same species to test the role of both actin and MT on nuclear positioning during muscle development.

Figures

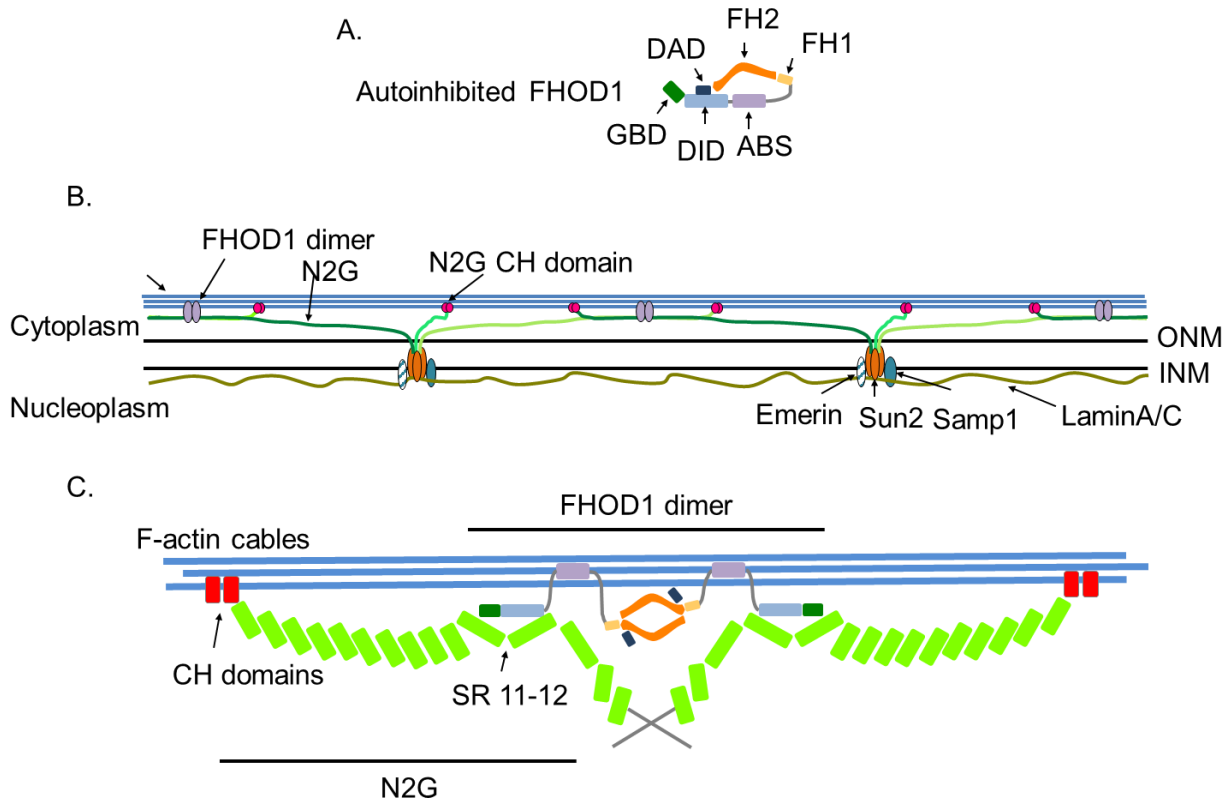

Figure 5.1 * Multi-site attachment model for TAN lines.

* This figure is reproduced from Antoku, Zhu, Kutscheidt, Fackler and Gundersen. Reinforcing the LINC complex connection to actin filaments: the role of FHOD1 in TAN line formation and nuclear movement. 2015. *Cell Cycle*

(**A**) Schematic of the autoinhibited form of FHOD1 (shown as a monomer to emphasize domains). Individual domains are described in the text. (**B**) Model for the multi-site attachment of nesprin-2G (N2G) and FHOD1 to actin cables in TAN lines. The interaction of nesprin-2G with FHOD1 forms a branched connection between nesprin-2G and the actin cable with one connection provided by nesprin-2G's CH domains and the other by FHOD1s unique ABS. This branched connection is proposed to strengthen the association between the nesprin and the actin cable. In the perinuclear space between the inner (INM) and outer nuclear membrane (ONM), KASH domains of nesprin-2G interact with the SUN2 trimer. In the nucleoplasm, SUN2 is anchored by interaction with lamin A/C of the lamina and with the INM proteins Samp1 and

emerin. (**C**) A detailed view showing FHOD1 interacting with SRs 11–12 of nesprin-2G through its N-terminal GBD and DID and to the actin cable through its ABS. The dimeric nature of FHOD1 may bring multiple nesprin-2Gs together.

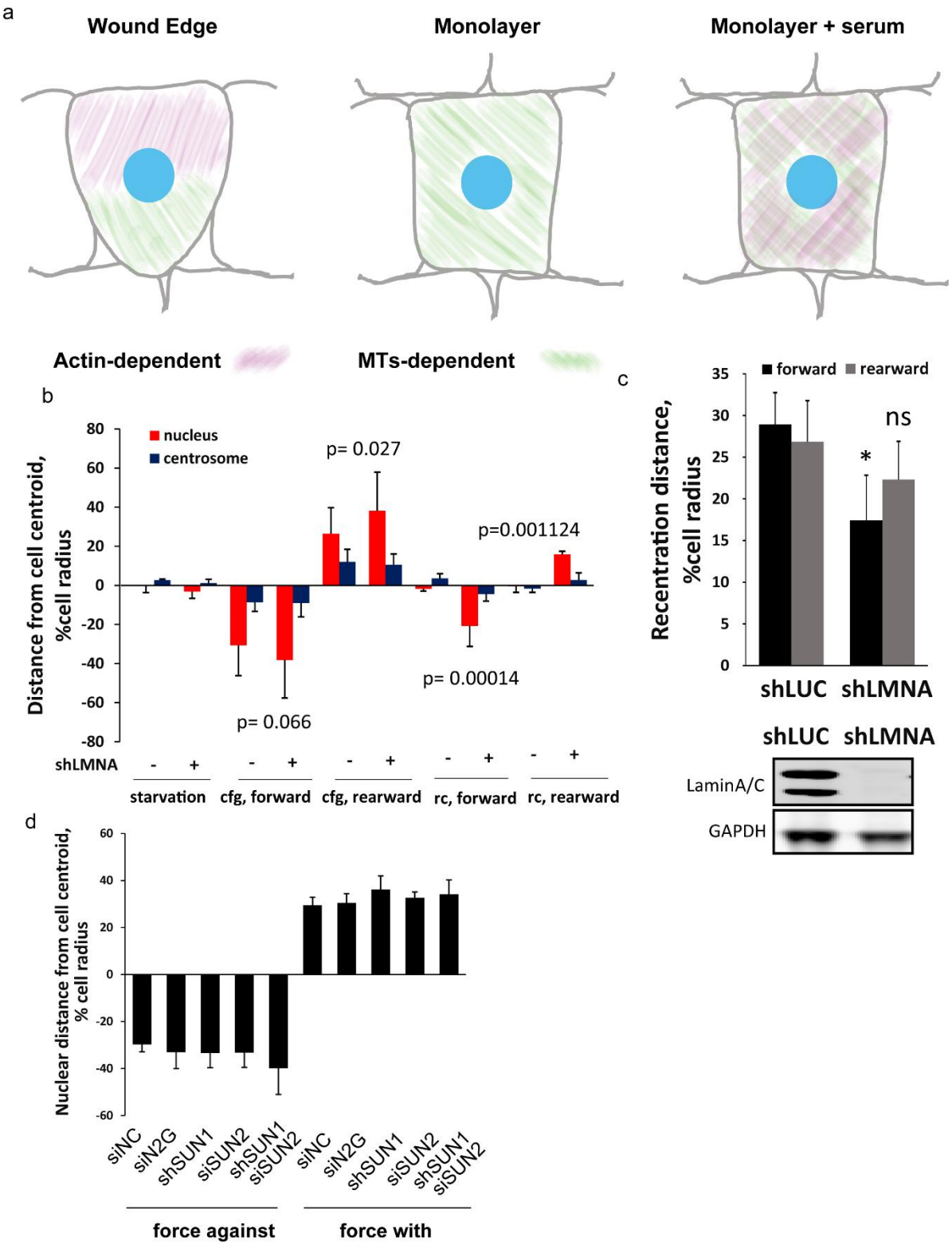
a
Wound Edge
Monolayer
Monolayer + serum
Actin-dependent
MTs-dependent
b
Distance from cell centroid, %cell radius
nucleus
centrosome
p= 0.027
p=0.001124
p= 0.00014
p= 0.066
shLMNA
starvation
cfg, forward
cfg, rearward
rc, forward
rc, rearward
c
Recentration distance, %cell radius
forward
rearward
ns
*
shLUC
shLMNA
LaminA/C
GAPDH
d
Nuclear distance from cell centroid, % cell radius
siNC
siN2G
shSUN1
siSUN2
shSUN1
siSUN2
force against
force with

Figure 5.2 Model of regional cctivity of homeostatic nuclear position mechanisms and nuclear recentration in both LINC and LMNA KD cells

a) Distribution of actin-dependent (magenta) and MT-dependent (green) homeostatic mechanisms in wound edge, monolayer and serum stimulated monolayer. b) Quantification of nuclear and centrosomal displacement after 5,000 g for 30 min centrifugation (cfg) and 1 hr recentration (rc) in NIH3T3 fibroblasts depleted of lamin A/C with shLMNA. c) Quantification of nuclear recentration distance in LMNA knockdown cells and western blotting of lamin A/C in shLUC (control) and shLMNA treated cNIH3T3 fibroblasts. In b-c, error bars are SD from 3 independent experiments; two-tailed t-test is performed between control (shLuciferace, or shLUC) and shLMNA. d) Quantification of nuclear displacement after 5,000 g for 30 min in siRNA/shRNA against N2G, SUN1, SUN2. Error bars are SD from 3 independent experiments.

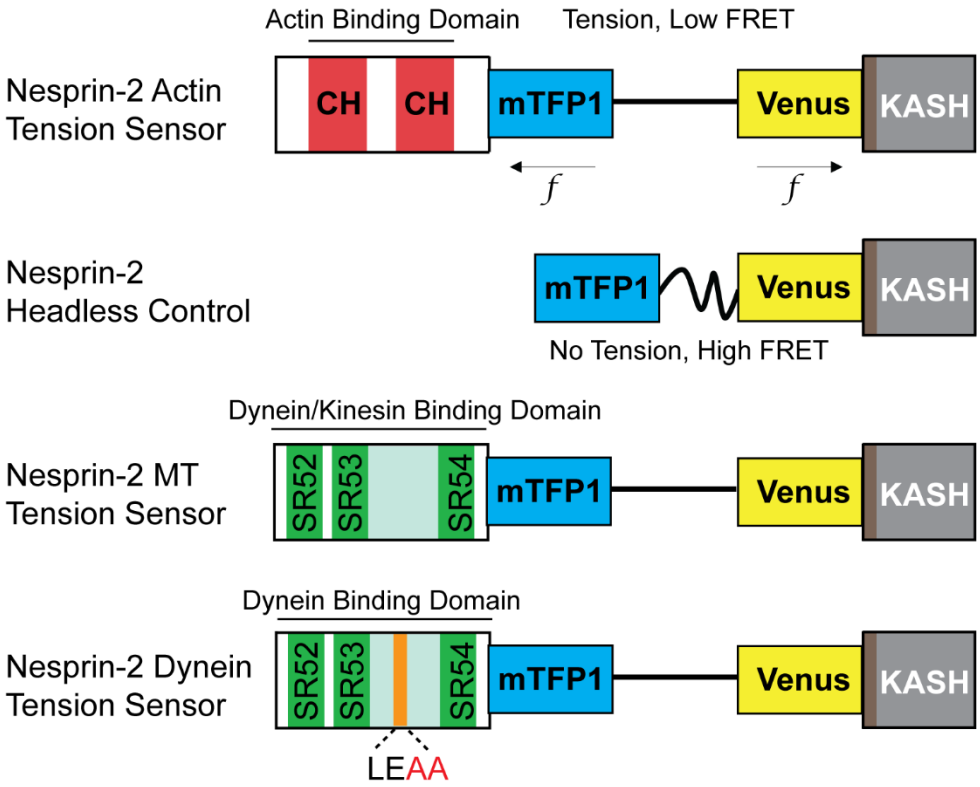

Figure 5.3 Nesprin-2 based FRET sensor scheme.

Schematic diagram of actin-, MT- and dynein- tension sensors based on nesprin-2. Each domain is marked in the figure, except for Adpative Domain (AD) (light green) flanked by spectrin repeats (SRs) (green) and transmembrane domain (brown).

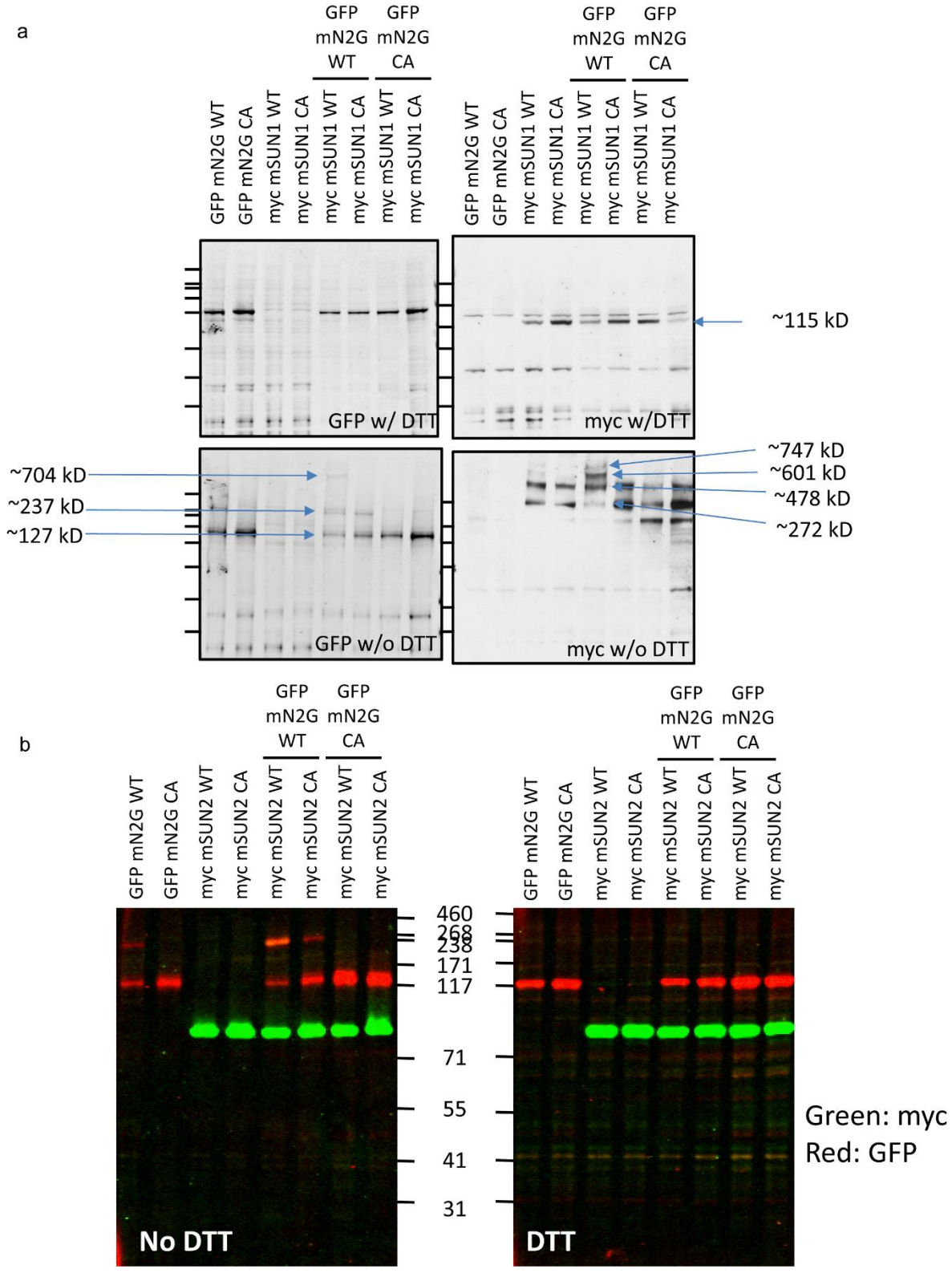
a
GFP mN2G WT
GFP mN2G CA
myc mSUN1 WT
myc mSUN1 CA
GFP w/ DTT
myc w/DTT
~115 kD
~704 kD
~237 kD
~127 kD
~747 kD
~601 kD
~478 kD
~272 kD
GFP w/o DTT
myc w/o DTT
b
GFP mN2G WT
GFP mN2G CA
myc mSUN2 WT
myc mSUN2 CA
460
268
238
171
117
71
55
41
31
No DTT
DTT
Green: myc
Red: GFP

Figure 5.4 Presence of a disulfide bridge between SUN proteins and nesprin-2 KASH domain in NIH3T3 fibroblasts.

a) NIH3T3 fibroblasts stably expressing GFP-tagged mini-N2G wildtype and CA mutant (C6869A in full length mouse N2G sequence) as well as myc-tagged mouse SUN1 wildtype and CA mutant (C759A) were lysed with under reducing (with DTT) or non-reducing (without DTT) conditions. Blots were probed for GFP or myc tags. Molecular weight was estimated after linear fitting of log(Mass) and migrating distance. b) NIH3T3 fibroblasts stably expressed with GFP-tagged mini-N2G wildtype and CA mutant (C6869A in full length mouse N2G sequence) as well as myc-tagged mouse SUN2 wildtype and CA mutant (C577A) were lysed with under reducing (with DTT) or non-reducing (without DTT) conditions. Blots were probed for myc and GFP tags. Green: myc; Red: GFP.

Table

Table 5.1 LMNA disease related mutants to be tested in centrifugation induced recentration assay

Disease	Variant	Nuclear Movement	Centrosome Reorientation
EDMD (Emery–Dreifuss muscular dystrophy)	**E358K**	+	+
	M371K	+	+
	R386K	+	+
	R453W	+	+
	W520S	+	+
	R527P	+	+
	T528K	-	-
	L53P	+	+
DCM (dilated cardiomyopathy)	R60G	+	+
	L85R	+	+
	N195K	+	+
	E203G	+	+
FPLD (Dunnigan-type familial partial lipodystrophy)	R482Q	-	-
	R482W	-	+
	K486N	-	+
	R584H	-	+

The table is summarized from Folker et al[35]. Variant in bold are the ones prepared in virus plasmid and ready to be tested. Plus sign means the defect is observed while minus sign means the phenotype in the variant is not significantly different from the LMNA WT control.

Bibliography

1. Gomes, E.R., S. Jani, and G.G. Gundersen, *Nuclear movement regulated by Cdc42, MRCK, myosin, and actin flow establishes MTOC polarization in migrating cells.* Cell, 2005. **121**(3): p. 451-63.

2. Schmoranzer, J., J.P. Fawcett, M. Segura, S. Tan, R.B. Vallee, T. Pawson, and G.G. Gundersen, *Par3 and dynein associate to regulate local microtubule dynamics and centrosome orientation during migration.* Curr Biol, 2009. **19**(13): p. 1065-74.

3. Luxton, G.W., E.R. Gomes, E.S. Folker, E. Vintinner, and G.G. Gundersen, *Linear arrays of nuclear envelope proteins harness retrograde actin flow for nuclear movement.* Science, 2010. **329**(5994): p. 956-9.

4. Abercrombie, M. and J.E. Heaysman, *Observations on the social behaviour of cells in tissue culture. I. Speed of movement of chick heart fibroblasts in relation to their mutual contacts.* Exp Cell Res, 1953. **5**(1): p. 111-31.

5. Woodland, H.R. and J.B. Gurdon, *RNA synthesis in an amphibian nuclear-transplant hybrid.* Developmental Biology, 1969. **20**(2): p. 89-104.

6. Poste, G. and P. Reeve, *Enucleation of mammalian cells by cytochalasin B. II. Formation of hybrid cells and heterokaryons by fusion of anucleate and nucleated cells.* Exp Cell Res, 1972. **73**(2): p. 287-94.

7. Veomett, G., D.M.Prescott, J. Shay, and K.R.Porter, *Reconstruction of Mammalian Cells from Nuclear and Cytoplasmic Components Separated by Treatment with Cytochalasin B.* Proc Natl Acad Sci U S A, 1974. **71**(5): p. 1999-2002.

8. Abercrombie, M., J.E. Heaysman, and S.M. Pegrum, *The locomotion of fibroblasts in culture. I. Movements of the leading edge.* Exp Cell Res, 1970. **59**(3): p. 393-8.

9. Guilluy, C., L.D. Osborne, L. Van Landeghem, L. Sharek, R. Superfine, R. Garcia-Mata, and K. Burridge, *Isolated nuclei adapt to force and reveal a mechanotransduction pathway in the nucleus.* Nat Cell Biol, 2014. **16**(4): p. 376-381.

10. Bone, C.R. and D.A. Starr, *Nuclear migration events throughout development.* Journal of Cell Science, 2016. **129**(10): p. 1951-1961.

11. Gundersen, G.G. and H.J. Worman, *Nuclear positioning.* Cell, 2013. **152**(6): p. 1376-89.

12. Horn, H.F., *Chapter Six - LINC Complex Proteins in Development and Disease*, in *Current Topics in Developmental Biology*, L.S. Colin, Editor. 2014, Academic Press. p. 287-321.

13. Chang, W., H.J. Worman, and G.G. Gundersen, *Accessorizing and anchoring the LINC complex for multifunctionality.* The Journal of Cell Biology, 2015. **208**(1): p. 11-22.

14. Haque, F., D.J. Lloyd, D.T. Smallwood, C.L. Dent, C.M. Shanahan, A.M. Fry, R.C. Trembath, and S. Shackleton, *SUN1 Interacts with Nuclear Lamin A and Cytoplasmic Nesprins To Provide a Physical Connection between the Nuclear Lamina and the Cytoskeleton.* Molecular and Cellular Biology, 2006. **26**(10): p. 3738-3751.

15. Crisp, M., Q. Liu, K. Roux, J.B. Rattner, C. Shanahan, B. Burke, P.D. Stahl, and D. Hodzic, *Coupling of the nucleus and cytoplasm: Role of the LINC complex.* The Journal of Cell Biology, 2006. **172**(1): p. 41-53.

16. Kutscheidt, S., R. Zhu, S. Antoku, G.W.G. Luxton, I. Stagljar, O.T. Fackler, and G.G. Gundersen, *FHOD1 interaction with nesprin-2G mediates TAN line formation and nuclear movement.* Nat Cell Biol, 2014. **16**(7): p. 708-715.

17. Antoku, S., R. Zhu, S. Kutscheidt, O.T. Fackler, and G.G. Gundersen, *Reinforcing the LINC complex connection to actin filaments: the role of FHOD1 in TAN line formation and nuclear movement.* Cell Cycle, 2015. **14**(14): p. 2200-2205.

18. Hatten, M.E., *Central nervous system neuronal migration.* Annu Rev Neurosci, 1999. **22**: p. 511-39.

19. Sorokin, L., *The impact of the extracellular matrix on inflammation.* Nat Rev Immunol, 2010. **10**(10): p. 712-723.

20. Martin, P., *Wound healing--aiming for perfect skin regeneration.* Science, 1997. **276**(5309): p. 75-81.

21. Chen, W.T., *Mechanism of retraction of the trailing edge during fibroblast movement.* J Cell Biol, 1981. **90**(1): p. 187-200.

22. Luxton, G.W.G. and G.G. Gundersen, *Orientation and function of the nuclear–centrosomal axis during cell migration.* Current Opinion in Cell Biology, 2011. **23**(5): p. 579-588.

23. Callan-Jones, A.C. and R. Voituriez, *Actin flows in cell migration: from locomotion and polarity to trajectories.* Curr Opin Cell Biol, 2016. **38**: p. 12-7.

24. Dantas, T.J., A. Carabalona, D.J. Hu, and R.B. Vallee, *Emerging roles for motor proteins in progenitor cell behavior and neuronal migration during brain development.* Cytoskeleton (Hoboken), 2016. **73**(10): p. 566-576.

25. Hodge, R.G. and A.J. Ridley, *Regulating Rho GTPases and their regulators.* Nat Rev Mol Cell Biol, 2016. **17**(8): p. 496-510.

26. Ridley, A.J., M.A. Schwartz, K. Burridge, R.A. Firtel, M.H. Ginsberg, G. Borisy, J.T. Parsons, and A.R. Horwitz, *Cell migration: integrating signals from front to back.* Science, 2003. **302**(5651): p. 1704-9.

27. Friedl, P. and R. Mayor, *Tuning Collective Cell Migration by Cell-Cell Junction Regulation.* Cold Spring Harb Perspect Biol, 2017. **9**(4).

28. Boettcher, B., T.T. Marquez-Lago, M. Bayer, E.L. Weiss, and Y. Barral, *Nuclear envelope morphology constrains diffusion and promotes asymmetric protein segregation in closed mitosis.* The Journal of Cell Biology, 2012. **197**(7): p. 921-937.

29. Gonzalez, Y., K. Meerbrey, J. Chong, Y. Torii, N.N. Padte, and S. Sazer, *Nuclear shape, growth and integrity in the closed mitosis of fission yeast depend on the Ran-GTPase system, the spindle pole body and the endoplasmic reticulum.* Journal of Cell Science, 2009. **122**(14): p. 2464-2472.

30. Hildebrandt, E.R. and M.A. Hoyt, *Mitotic motors in Saccharomyces cerevisiae.* Biochimica et Biophysica Acta (BBA) - Molecular Cell Research, 2000. **1496**(1): p. 99-116.

31. Daga, R.R. and F. Chang, *Dynamic positioning of the fission yeast cell division plane.* Proc Natl Acad Sci U S A, 2005. **102**(23): p. 8228-32.

32. Wilson, E.B., *Experimental analysis in cytology. II. Some phenomena of fertilization and cell-division in etherised eggs. III. The effect on clevage of artificial obliteration of the first cleavage-furrow.* Archiv Fur Entwicklungsmechanik Der Organismen, 1901. **13**(3): p. 353-395.

33. Oegema, K. and A.A. Hyman, *Cell division.* WormBook, 2006: p. 1-40.

34. Dupin, I., Y. Sakamoto, and S. Etienne-Manneville, *Cytoplasmic intermediate filaments mediate actin-driven positioning of the nucleus.* J Cell Sci, 2011. **124**(Pt 6): p. 865-72.

35. Folker, E.S., C. Ostlund, G.W. Luxton, H.J. Worman, and G.G. Gundersen, *Lamin A variants that cause striated muscle disease are defective in anchoring transmembrane actin-associated nuclear lines for nuclear movement.* Proceedings of the National Academy of Sciences, 2011. **108**(1): p. 131-6.

36. Tsai, J.-W., W.-N. Lian, S. Kemal, A.R. Kriegstein, and R.B. Vallee, *Kinesin 3 and cytoplasmic dynein mediate interkinetic nuclear migration in neural stem cells.* Nat Neurosci, 2010. **13**(12): p. 1463-1471.

37. Cooper, J.A., *Mechanisms of cell migration in the nervous system.* The Journal of Cell Biology, 2013. **202**(5): p. 725-734.

38. Reiner, O., R. Carrozzo, Y. Shen, M. Wehnert, F. Faustinella, W.B. Dobyns, C.T. Caskey, and D.H. Ledbetter, *Isolation of a Miller-Dieker lissencephaly gene containing G protein beta-subunit-like repeats.* Nature, 1993. **364**(6439): p. 717-21.

39. Tsai, J.-W., Y. Chen, A.R. Kriegstein, and R.B. Vallee, *LIS1 RNA interference blocks neural stem cell division, morphogenesis, and motility at multiple stages.* The Journal of Cell Biology, 2005. **170**(6): p. 935-945.

40. Maguire, K.K., L. Lim, S. Speedy, and T.A. Rando, *Assessment of disease activity in muscular dystrophies by noninvasive imaging.* J Clin Invest, 2013. **123**(5): p. 2298-305.

41. Horn, H.F., Z. Brownstein, D.R. Lenz, S. Shivatzki, A.A. Dror, O. Dagan-Rosenfeld, L.M. Friedman, K.J. Roux, S. Kozlov, K.T. Jeang, M. Frydman, B. Burke, C.L. Stewart, and K.B. Avraham, *The LINC complex is essential for hearing.* J Clin Invest, 2013. **123**(2): p. 740-50.

42. Malone, C.J., W.D. Fixsen, H.R. Horvitz, and M. Han, *UNC-84 localizes to the nuclear envelope and is required for nuclear migration and anchoring during C. elegans development.* Development, 1999. **126**(14): p. 3171-81.

43. Sosa, B.A., A. Rothballer, U. Kutay, and T.U. Schwartz, *LINC Complexes Form by Binding of Three KASH Peptides to Domain Interfaces of Trimeric SUN Proteins.* Cell, 2012. **149**(5): p. 1035-47.

44. Zhou, Z., X. Du, Z. Cai, X. Song, H. Zhang, T. Mizuno, E. Suzuki, M.R. Yee, A. Berezov, R. Murali, S.L. Wu, B.L. Karger, M.I. Greene, and Q. Wang, *Structure of Sad1-UNC84 homology (SUN) domain defines features of molecular bridge in nuclear envelope.* J Biol Chem, 2012. **287**(8): p. 5317-26.

45. Wang, W., Z. Shi, S. Jiao, C. Chen, H. Wang, G. Liu, Q. Wang, Y. Zhao, M.I. Greene, and Z. Zhou, *Structural insights into SUN-KASH complexes across the nuclear envelope.* Cell Research, 2012. **22**(10): p. 1440-1452.

46. Rothballer, A. and U. Kutay, *The diverse functional LINCs of the nuclear envelope to the cytoskeleton and chromatin.* Chromosoma, 2013. **122**(5): p. 415-29.

47. Meinke, P., E. Mattioli, F. Haque, S. Antoku, M. Columbaro, K.R. Straatman, H.J. Worman, G.G. Gundersen, G. Lattanzi, M. Wehnert, and S. Shackleton, *Muscular dystrophy-associated SUN1 and SUN2 variants disrupt nuclear-cytoskeletal connections and myonuclear organization.* PLoS Genet, 2014. **10**(9): p. e1004605.

48. Jahed, Z., H. Shams, and M.R. Mofrad, *A Disulfide Bond Is Required for the Transmission of Forces through SUN-KASH Complexes.* Biophys J, 2015. **109**(3): p. 501-9.

49. Lu, W., J. Gotzmann, L. Sironi, V.M. Jaeger, M. Schneider, Y. Luke, M. Uhlen, C.A. Szigyarto, A. Brachner, J. Ellenberg, R. Foisner, A.A. Noegel, and I. Karakesisoglou, *Sun1 forms immobile macromolecular assemblies at the nuclear envelope.* Biochim Biophys Acta, 2008. **1783**(12): p. 2415-26.

50. Powell, L. and B. Burke, *Internuclear exchange of an inner nuclear membrane protein (p55) in heterokaryons: in vivo evidence for the interaction of p55 with the nuclear lamina.* J Cell Biol, 1990. **111**(6 Pt 1): p. 2225-34.

51. Soullam, B. and H.J. Worman, *Signals and structural features involved in integral membrane protein targeting to the inner nuclear membrane.* J Cell Biol, 1995. **130**(1): p. 15-27.

52. Turgay, Y., R. Ungricht, A. Rothballer, A. Kiss, G. Csucs, P. Horvath, and U. Kutay, *A classical NLS and the SUN domain contribute to the targeting of SUN2 to the inner nuclear membrane.* EMBO J, 2010. **29**(14): p. 2262-75.

53. Tapley, E.C., N. Ly, and D.A. Starr, *Multiple mechanisms actively target the SUN protein UNC-84 to the inner nuclear membrane.* Mol Biol Cell, 2011. **22**(10): p. 1739-52.

54. Gardner, J.M., C.J. Smoyer, E.S. Stensrud, R. Alexander, M. Gogol, W. Wiegraebe, and S.L. Jaspersen, *Targeting of the SUN protein Mps3 to the inner nuclear membrane by the histone variant H2A.Z.* J Cell Biol, 2011. **193**(3): p. 489-507.

55. Murphy, S.P., C.R. Simmons, and H.W. Bass, *Structure and expression of the maize (Zea mays L.) SUN-domain protein gene family: evidence for the existence of two divergent classes of SUN proteins in plants.* BMC Plant Biol, 2010. **10**: p. 269.

56. Moriguchi, K., T. Suzuki, Y. Ito, Y. Yamazaki, Y. Niwa, and N. Kurata, *Functional isolation of novel nuclear proteins showing a variety of subnuclear localizations.* Plant Cell, 2005. **17**(2): p. 389-403.

57. Oda, Y. and H. Fukuda, *Dynamics of Arabidopsis SUN proteins during mitosis and their involvement in nuclear shaping.* Plant J, 2011. **66**(4): p. 629-41.

58. Zhou, X., K. Graumann, D.E. Evans, and I. Meier, *Novel plant SUN-KASH bridges are involved in RanGAP anchoring and nuclear shape determination.* J Cell Biol, 2012. **196**(2): p. 203-11.

59. Hagan, I. and M. Yanagida, *The product of the spindle formation gene sad1+ associates with the fission yeast spindle pole body and is essential for viability.* J Cell Biol, 1995. **129**(4): p. 1033-47.

60. Wanat, J.J., K.P. Kim, R. Koszul, S. Zanders, B. Weiner, N. Kleckner, and E. Alani, *Csm4, in collaboration with Ndj1, mediates telomere-led chromosome dynamics and recombination during yeast meiosis.* PLoS Genet, 2008. **4**(9): p. e1000188.

61. Conrad, M.N., C.Y. Lee, J.L. Wilkerson, and M.E. Dresser, *MPS3 mediates meiotic bouquet formation in Saccharomyces cerevisiae.* Proc Natl Acad Sci U S A, 2007. **104**(21): p. 8863-8.

62. Bupp, J.M., A.E. Martin, E.S. Stensrud, and S.L. Jaspersen, *Telomere anchoring at the nuclear periphery requires the budding yeast Sad1-UNC-84 domain protein Mps3.* J Cell Biol, 2007. **179**(5): p. 845-54.

63. Friederichs, J.M., S. Ghosh, C.J. Smoyer, S. McCroskey, B.D. Miller, K.J. Weaver, K.M. Delventhal, J. Unruh, B.D. Slaughter, and S.L. Jaspersen, *The SUN protein Mps3 is required for spindle pole body insertion into the nuclear membrane and nuclear envelope homeostasis.* PLoS Genet, 2011. **7**(11): p. e1002365.

64. Sulston, J.E. and H.R. Horvitz, *Abnormal cell lineages in mutants of the nematode Caenorhabditis elegans.* Dev Biol, 1981. **82**(1): p. 41-55.

65. Horvitz, H.R. and J.E. Sulston, *Isolation and genetic characterization of cell-lineage mutants of the nematode Caenorhabditis elegans.* Genetics, 1980. **96**(2): p. 435-54.

66. Fridkin, A., E. Mills, A. Margalit, E. Neufeld, K.K. Lee, N. Feinstein, M. Cohen, K.L. Wilson, and Y. Gruenbaum, *Matefin, a Caenorhabditis elegans germ line-specific SUN-domain nuclear membrane protein, is essential for early embryonic and germ cell development.* Proc Natl Acad Sci U S A, 2004. **101**(18): p. 6987-92.

67. Sato, A., B. Isaac, C.M. Phillips, R. Rillo, P.M. Carlton, D.J. Wynne, R.A. Kasad, and A.F. Dernburg, *Cytoskeletal forces span the nuclear envelope to coordinate meiotic chromosome pairing and synapsis.* Cell, 2009. **139**(5): p. 907-19.

68. Penkner, A., L. Tang, M. Novatchkova, M. Ladurner, A. Fridkin, Y. Gruenbaum, D. Schweizer, J. Loidl, and V. Jantsch, *The nuclear envelope protein Matefin/SUN-1 is required for homologous pairing in C. elegans meiosis.* Dev Cell, 2007. **12**(6): p. 873-85.

69. Kracklauer, M.P., S.M. Banks, X. Xie, Y. Wu, and J.A. Fischer, *Drosophila klaroid encodes a SUN domain protein required for Klarsicht localization to the nuclear envelope and nuclear migration in the eye.* Fly (Austin), 2007. **1**(2): p. 75-85.

70. Kracklauer, M.P., H.M. Wiora, W.J. Deery, X. Chen, B. Bolival, D. Romanowicz, R.A. Simonette, M.T. Fuller, J.A. Fischer, and K.M. Beckingham, *The Drosophila SUN protein Spag4 cooperates with the coiled-coil protein Yuri Gagarin to maintain association of the basal body and spermatid nucleus.* Journal of Cell Science, 2010. **123**(16): p. 2763-2772.

71. Gob, E., J. Schmitt, R. Benavente, and M. Alsheimer, *Mammalian sperm head formation involves different polarization of two novel LINC complexes.* PLoS One, 2010. **5**(8): p. e12072.

72. Kennedy, C., K. Sebire, D.M. de Kretser, and M.K. O'Bryan, *Human sperm associated antigen 4 (SPAG4) is a potential cancer marker.* Cell Tissue Res, 2004. **315**(2): p. 279-83.

73. Xing, X.W., L.Y. Li, G. Liu, J.J. Fu, X.J. Tan, and G.X. Lu, *Identification of a novel gene SRG4 expressed at specific stages of mouse spermatogenesis.* Acta Biochim Biophys Sin (Shanghai), 2004. **36**(5): p. 351-9.

74. Frohnert, C., S. Schweizer, and S. Hoyer-Fender, *SPAG4L/SPAG4L-2 are testis-specific SUN domain proteins restricted to the apical nuclear envelope of round spermatids facing the acrosome.* Mol Hum Reprod, 2011. **17**(4): p. 207-18.

75. Tapley, E.C. and D.A. Starr, *Connecting the nucleus to the cytoskeleton by SUN–KASH bridges across the nuclear envelope.* Current Opinion in Cell Biology, 2013. **25**(1): p. 57-62.

76. Östlund, C., E.S. Folker, J.C. Choi, E.R. Gomes, G.G. Gundersen, and H.J. Worman, *Dynamics and molecular interactions of linker of nucleoskeleton and cytoskeleton (LINC) complex proteins.* Journal of Cell Science, 2009. **122**(22): p. 4099-4108.

77. Chi, Y.H., L.I. Cheng, T. Myers, J.M. Ward, E. Williams, Q. Su, L. Faucette, J.Y. Wang, and K.T. Jeang, *Requirement for Sun1 in the expression of meiotic reproductive genes and piRNA.* Development, 2009. **136**(6): p. 965-73.

78. Horn, H.F., D.I. Kim, G.D. Wright, E.S. Wong, C.L. Stewart, B. Burke, and K.J. Roux, *A mammalian KASH domain protein coupling meiotic chromosomes to the cytoskeleton.* J Cell Biol, 2013. **202**(7): p. 1023-39.

79. Chi, Y.-H., L.I. Cheng, T. Myers, J.M. Ward, E. Williams, Q. Su, L. Faucette, J.-Y. Wang, and K.-T. Jeang, *Requirement for Sun1 in the expression of meiotic reproductive genes and piRNA.* Development (Cambridge, England), 2009. **136**(6): p. 965-973.

80. Lei, K., X. Zhang, X. Ding, X. Guo, M. Chen, B. Zhu, T. Xu, Y. Zhuang, R. Xu, and M. Han, *SUN1 and SUN2 play critical but partially redundant roles in anchoring nuclei in skeletal muscle cells in mice.* Proc Natl Acad Sci U S A, 2009. **106**(25): p. 10207-12.

81. Stewart, R.M., A.E. Zubek, K.A. Rosowski, S.M. Schreiner, V. Horsley, and M.C. King, *Nuclear–cytoskeletal linkages facilitate cross talk between the nucleus and intercellular adhesions.* The Journal of Cell Biology, 2015. **209**(3): p. 403-418.

82. Starr, D.A. and M. Han, *Role of ANC-1 in Tethering Nuclei to the Actin Cytoskeleton.* Science, 2002. **298**(5592): p. 406-409.

83. Borgese, N., S. Brambillasca, and S. Colombo, *How tails guide tail-anchored proteins to their destinations.* Curr Opin Cell Biol, 2007. **19**(4): p. 368-75.

84. Shao, S. and R.S. Hegde, *Membrane protein insertion at the endoplasmic reticulum.* Annu Rev Cell Dev Biol, 2011. **27**: p. 25-56.

85. McGee, M.D., R. Rillo, A.S. Anderson, and D.A. Starr, *UNC-83 Is a KASH Protein Required for Nuclear Migration and Is Recruited to the Outer Nuclear Membrane by a*

Physical Interaction with the SUN Protein UNC-84. Molecular Biology of the Cell, 2006. **17**(4): p. 1790-1801.

86. Ketema, M., M. Kreft, P. Secades, H. Janssen, and A. Sonnenberg, *Nesprin-3 connects plectin and vimentin to the nuclear envelope of Sertoli cells but is not required for Sertoli cell function in spermatogenesis.* Mol Biol Cell, 2013. **24**(15): p. 2454-66.

87. Roux, K.J., M.L. Crisp, Q. Liu, D. Kim, S. Kozlov, C.L. Stewart, and B. Burke, *Nesprin 4 is an outer nuclear membrane protein that can induce kinesin-mediated cell polarization.* Proceedings of the National Academy of Sciences, 2009. **106**(7): p. 2194-9.

88. Stewart-Hutchinson, P.J., C.M. Hale, D. Wirtz, and D. Hodzic, *Structural requirements for the assembly of LINC complexes and their function in cellular mechanical stiffness.* Exp Cell Res, 2008. **314**(8): p. 1892-905.

89. Lu, W., M. Schneider, S. Neumann, V.M. Jaeger, S. Taranum, M. Munck, S. Cartwright, C. Richardson, J. Carthew, K. Noh, M. Goldberg, A.A. Noegel, and I. Karakesisoglou, *Nesprin interchain associations control nuclear size.* Cell Mol Life Sci, 2012. **69**(20): p. 3493-509.

90. Wang, Q., X. Du, Z. Cai, and M.I. Greene, *Characterization of the structures involved in localization of the SUN proteins to the nuclear envelope and the centrosome.* DNA Cell Biol, 2006. **25**(10): p. 554-62.

91. Shimi, T., M. Kittisopikul, J. Tran, A.E. Goldman, S.A. Adam, Y. Zheng, K. Jaqaman, and R.D. Goldman, *Structural organization of nuclear lamins A, C, B1, and B2 revealed by superresolution microscopy.* Mol Biol Cell, 2015. **26**(22): p. 4075-86.

92. Xu, X.M., T. Meulia, and I. Meier, *Anchorage of plant RanGAP to the nuclear envelope involves novel nuclear-pore-associated proteins.* Curr Biol, 2007. **17**(13): p. 1157-63.

93. Lee, C.Y., M.N. Conrad, and M.E. Dresser, *Meiotic chromosome pairing is promoted by telomere-led chromosome movements independent of bouquet formation.* PLoS Genet, 2012. **8**(5): p. e1002730.

94. Kosaka, H., M. Shinohara, and A. Shinohara, *Csm4-dependent telomere movement on nuclear envelope promotes meiotic recombination.* PLoS Genet, 2008. **4**(9): p. e1000196.

95. Conrad, M.N., C.Y. Lee, G. Chao, M. Shinohara, H. Kosaka, A. Shinohara, J.A. Conchello, and M.E. Dresser, *Rapid telomere movement in meiotic prophase is promoted by NDJ1, MPS3, and CSM4 and is modulated by recombination.* Cell, 2008. **133**(7): p. 1175-87.

96. Miki, F., A. Kurabayashi, Y. Tange, K. Okazaki, M. Shimanuki, and O. Niwa, *Two-hybrid search for proteins that interact with Sad1 and Kms1, two membrane-bound components of the spindle pole body in fission yeast.* Mol Genet Genomics, 2004. **270**(6): p. 449-61.

97. King, M.C., T.G. Drivas, and G. Blobel, *A network of nuclear envelope membrane proteins linking centromeres to microtubules.* Cell, 2008. **134**(3): p. 427-38.

98. Walde, S. and M.C. King, *The KASH protein Kms2 coordinates mitotic remodeling of the spindle pole body.* J Cell Sci, 2014. **127**(Pt 16): p. 3625-40.

99. Malone, C.J., L. Misner, N. Le Bot, M.C. Tsai, J.M. Campbell, J. Ahringer, and J.G. White, *The C. elegans hook protein, ZYG-12, mediates the essential attachment between the centrosome and nucleus.* Cell, 2003. **115**(7): p. 825-36.

100. Fridolfsson, H.N. and D.A. Starr, *Kinesin-1 and dynein at the nuclear envelope mediate the bidirectional migrations of nuclei.* The Journal of Cell Biology, 2010. **191**(1): p. 115-28.

101. Fridolfsson, H.N., N. Ly, M. Meyerzon, and D.A. Starr, *UNC-83 coordinates kinesin-1 and dynein activities at the nuclear envelope during nuclear migration.* Dev Biol, 2010. **338**(2): p. 237-50.

102. Yu, J., D.A. Starr, X. Wu, S.M. Parkhurst, Y. Zhuang, T. Xu, R. Xu, and M. Han, *The KASH domain protein MSP-300 plays an essential role in nuclear anchoring during Drosophila oogenesis.* Dev Biol, 2006. **289**(2): p. 336-45.

103. Wang, S., A. Reuveny, and T. Volk, *Nesprin provides elastic properties to muscle nuclei by cooperating with spectraplakin and EB1.* J Cell Biol, 2015. **209**(4): p. 529-38.

104. Volk, T., *A new member of the spectrin superfamily may participate in the formation of embryonic muscle attachments in Drosophila.* Development, 1992. **116**(3): p. 721-30.

105. Rosenberg-Hasson, Y., M. Renert-Pasca, and T. Volk, *A Drosophila dystrophin-related protein, MSP-300, is required for embryonic muscle morphogenesis.* Mech Dev, 1996. **60**(1): p. 83-94.

106. Elhanany-Tamir, H., Y.V. Yu, M. Shnayder, A. Jain, M. Welte, and T. Volk, *Organelle positioning in muscles requires cooperation between two KASH proteins and microtubules.* J Cell Biol, 2012. **198**(5): p. 833-46.

107. Patterson, K., A.B. Molofsky, C. Robinson, S. Acosta, C. Cater, and J.A. Fischer, *The functions of Klarsicht and nuclear lamin in developmentally regulated nuclear migrations of photoreceptor cells in the Drosophila eye.* Mol Biol Cell, 2004. **15**(2): p. 600-10.

108. Fischer, J.A., S. Acosta, A. Kenny, C. Cater, C. Robinson, and J. Hook, *Drosophila klarsicht has distinct subcellular localization domains for nuclear envelope and microtubule localization in the eye.* Genetics, 2004. **168**(3): p. 1385-93.

109. Apel, E.D., R.M. Lewis, R.M. Grady, and J.R. Sanes, *Syne-1, a dystrophin- and Klarsicht-related protein associated with synaptic nuclei at the neuromuscular junction.* J Biol Chem, 2000. **275**(41): p. 31986-95.

110. Zhang, Q., J.N. Skepper, F. Yang, J.D. Davies, L. Hegyi, R.G. Roberts, P.L. Weissberg, J.A. Ellis, and C.M. Shanahan, *Nesprins: a novel family of spectrin-repeat-containing proteins that localize to the nuclear membrane in multiple tissues.* Journal of Cell Science, 2001. **114**(24): p. 4485-4498.

111. Rajgor, D., J.A. Mellad, F. Autore, Q. Zhang, and C.M. Shanahan, *Multiple novel nesprin-1 and nesprin-2 variants act as versatile tissue-specific intracellular scaffolds.* PLoS One, 2012. **7**(7): p. e40098.

112. Zhen, Y.Y., T. Libotte, M. Munck, A.A. Noegel, and E. Korenbaum, *NUANCE, a giant protein connecting the nucleus and actin cytoskeleton.* Journal of Cell Science, 2002. **115**(Pt 15): p. 3207-22.

113. Padmakumar, V.C., S. Abraham, S. Braune, A.A. Noegel, B. Tunggal, I. Karakesisoglou, and E. Korenbaum, *Enaptin, a giant actin-binding protein, is an element of the nuclear membrane and the actin cytoskeleton.* Exp Cell Res, 2004. **295**(2): p. 330-9.

114. Wilson, M.H. and E.L.F. Holzbaur, *Nesprins anchor kinesin-1 motors to the nucleus to drive nuclear distribution in muscle cells.* Development, 2015. **142**(1): p. 218-228.

115. Zhang, X., K. Lei, X. Yuan, X. Wu, Y. Zhuang, T. Xu, R. Xu, and M. Han, *SUN1/2 and Syne/Nesprin-1/2 complexes connect centrosome to the nucleus during neurogenesis and neuronal migration in mice.* Neuron, 2009. **64**(2): p. 173-87.

116. Yu, J., K. Lei, M. Zhou, C.M. Craft, G. Xu, T. Xu, Y. Zhuang, R. Xu, and M. Han, *KASH protein Syne-2/Nesprin-2 and SUN proteins SUN1/2 mediate nuclear migration during mammalian retinal development.* Hum Mol Genet, 2011. **20**(6): p. 1061-73.

117. Zhang, Q., C. Bethmann, N.F. Worth, J.D. Davies, C. Wasner, A. Feuer, C.D. Ragnauth, Q. Yi, J.A. Mellad, D.T. Warren, M.A. Wheeler, J.A. Ellis, J.N. Skepper, M. Vorgerd, B. Schlotter-Weigel, P.L. Weissberg, R.G. Roberts, M. Wehnert, and C.M. Shanahan, *Nesprin-1 and -2 are involved in the pathogenesis of Emery Dreifuss muscular dystrophy and are critical for nuclear envelope integrity.* Hum Mol Genet, 2007. **16**(23): p. 2816-33.

118. Gros-Louis, F., N. Dupre, P. Dion, M.A. Fox, S. Laurent, S. Verreault, J.R. Sanes, J.P. Bouchard, and G.A. Rouleau, *Mutations in SYNE1 lead to a newly discovered form of autosomal recessive cerebellar ataxia.* Nat Genet, 2007. **39**(1): p. 80-5.

119. Synofzik, M., K. Smets, M. Mallaret, D. Di Bella, C. Gallenmuller, J. Baets, M. Schulze, S. Magri, E. Sarto, M. Mustafa, T. Deconinck, T. Haack, S. Zuchner, M. Gonzalez, D. Timmann, C. Stendel, T. Klopstock, A. Durr, C. Tranchant, M. Sturm, W. Hamza, L. Nanetti, C. Mariotti, M. Koenig, L. Schols, R. Schule, P. de Jonghe, M. Anheim, F.

Taroni, and P. Bauer, *SYNE1 ataxia is a common recessive ataxia with major non-cerebellar features: a large multi-centre study.* Brain, 2016. **139**(Pt 5): p. 1378-93.

120. Puckelwartz, M.J., E. Kessler, Y. Zhang, D. Hodzic, K.N. Randles, G. Morris, J.U. Earley, M. Hadhazy, J.M. Holaska, S.K. Mewborn, P. Pytel, and E.M. McNally, *Disruption of nesprin-1 produces an Emery Dreifuss muscular dystrophy-like phenotype in mice.* Hum Mol Genet, 2009. **18**(4): p. 607-20.

121. Zhang, J., A. Felder, Y. Liu, L.T. Guo, S. Lange, N.D. Dalton, Y. Gu, K.L. Peterson, A.P. Mizisin, G.D. Shelton, R.L. Lieber, and J. Chen, *Nesprin 1 is critical for nuclear positioning and anchorage.* Hum Mol Genet, 2010. **19**(2): p. 329-41.

122. Banerjee, I., J. Zhang, T. Moore-Morris, E. Pfeiffer, K.S. Buchholz, A. Liu, K. Ouyang, M.J. Stroud, L. Gerace, S.M. Evans, A. McCulloch, and J. Chen, *Targeted ablation of nesprin 1 and nesprin 2 from murine myocardium results in cardiomyopathy, altered nuclear morphology and inhibition of the biomechanical gene response.* PLoS Genet, 2014. **10**(2): p. e1004114.

123. Wilhelmsen, K., S.H. Litjens, I. Kuikman, N. Tshimbalanga, H. Janssen, I. van den Bout, K. Raymond, and A. Sonnenberg, *Nesprin-3, a novel outer nuclear membrane protein, associates with the cytoskeletal linker protein plectin.* J Cell Biol, 2005. **171**(5): p. 799-810.

124. Postel, R., M. Ketema, I. Kuikman, J.M. de Pereda, and A. Sonnenberg, *Nesprin-3 augments peripheral nuclear localization of intermediate filaments in zebrafish.* J Cell Sci, 2011. **124**(Pt 5): p. 755-64.

125. Morgan, J.T., E.R. Pfeiffer, T.L. Thirkill, P. Kumar, G. Peng, H.N. Fridolfsson, G.C. Douglas, D.A. Starr, and A.I. Barakat, *Nesprin-3 regulates endothelial cell morphology, perinuclear cytoskeletal architecture, and flow-induced polarization.* Molecular Biology of the Cell, 2011. **22**(22): p. 4324-4334.

126. Petrie, R.J., H. Koo, and K.M. Yamada, *Generation of compartmentalized pressure by a nuclear piston governs cell motility in a 3D matrix.* Science, 2014. **345**(6200): p. 1062-5.

127. Behrens, T.W., J. Jagadeesh, P. Scherle, G. Kearns, J. Yewdell, and L.M. Staudt, *Jaw1, A lymphoid-restricted membrane protein localized to the endoplasmic reticulum.* J Immunol, 1994. **153**(2): p. 682-90.

128. Lindeman, R.E. and F. Pelegri, *Localized products of futile cycle/lrmp promote centrosome-nucleus attachment in the zebrafish zygote.* Curr Biol, 2012. **22**(10): p. 843-51.

129. Morimoto, A., H. Shibuya, X. Zhu, J. Kim, K. Ishiguro, M. Han, and Y. Watanabe, *A conserved KASH domain protein associates with telomeres, SUN1, and dynactin during mammalian meiosis.* J Cell Biol, 2012. **198**(2): p. 165-72.

130. Lee, K.K., D. Starr, M. Cohen, J. Liu, M. Han, K.L. Wilson, and Y. Gruenbaum, *Lamin-dependent localization of UNC-84, a protein required for nuclear migration in Caenorhabditis elegans.* Mol Biol Cell, 2002. **13**(3): p. 892-901.

131. Padmakumar, V.C., T. Libotte, W. Lu, H. Zaim, S. Abraham, A.A. Noegel, J. Gotzmann, R. Foisner, and I. Karakesisoglou, *The inner nuclear membrane protein Sun1 mediates the anchorage of Nesprin-2 to the nuclear envelope.* J Cell Sci, 2005. **118**(Pt 15): p. 3419-30.

132. Shibuya, H. and Y. Watanabe, *The meiosis-specific modification of mammalian telomeres.* Cell Cycle, 2014. **13**(13): p. 2024-8.

133. Daniel, K., D. Trankner, L. Wojtasz, H. Shibuya, Y. Watanabe, M. Alsheimer, and A. Toth, *Mouse CCDC79 (TERB1) is a meiosis-specific telomere associated protein.* BMC Cell Biol, 2014. **15**: p. 17.

134. Schmitt, J., R. Benavente, D. Hodzic, C. Hoog, C.L. Stewart, and M. Alsheimer, *Transmembrane protein Sun2 is involved in tethering mammalian meiotic telomeres to the nuclear envelope.* Proc Natl Acad Sci U S A, 2007. **104**(18): p. 7426-31.

135. Hedgecock, E.M. and J. Nichol Thomson, *A gene required for nuclear and mitochondrial attachment in the nematode caenorhabditis elegans.* Cell, 1982. **30**(1): p. 321-330.

136. Chang, W., S. Antoku, C. Östlund, H.J. Worman, and G.G. Gundersen, *Linker of nucleoskeleton and cytoskeleton (LINC) complex-mediated actin-dependent nuclear positioning orients centrosomes in migrating myoblasts.* Nucleus, 2015. **6**(1): p. 77-88.

137. Alam, S.G., D. Lovett, D.I. Kim, K.J. Roux, R.B. Dickinson, and T.P. Lele, *The nucleus is an intracellular propagator of tensile forces in NIH 3T3 fibroblasts.* Journal of Cell Science, 2015. **128**(10): p. 1901-1911.

138. Wu, J., I.A. Kent, N. Shekhar, T.J. Chancellor, A. Mendonca, R.B. Dickinson, and T.P. Lele, *Actomyosin pulls to advance the nucleus in a migrating tissue cell.* Biophys J, 2014. **106**(1): p. 7-15.

139. Levy, J.R. and E.L.F. Holzbaur, *Dynein drives nuclear rotation during forward progression of motile fibroblasts.* Journal of Cell Science, 2008. **121**(Pt 19): p. 3187.

140. Ayala, R., T. Shu, and L.H. Tsai, *Trekking across the brain: the journey of neuronal migration.* Cell, 2007. **128**(1): p. 29-43.

141. Vallee, R.B., G.E. Seale, and J.W. Tsai, *Emerging roles for myosin II and cytoplasmic dynein in migrating neurons and growth cones.* Trends Cell Biol, 2009. **19**(7): p. 347-55.

142. Tsai, J.W., K.H. Bremner, and R.B. Vallee, *Dual subcellular roles for LIS1 and dynein in radial neuronal migration in live brain tissue.* Nat Neurosci, 2007. **10**(8): p. 970-9.

143. Solecki, D.J., N. Trivedi, E.E. Govek, R.A. Kerekes, S.S. Gleason, and M.E. Hatten, *Myosin II motors and F-actin dynamics drive the coordinated movement of the centrosome and soma during CNS glial-guided neuronal migration.* Neuron, 2009. **63**(1): p. 63-80.

144. Tsai, J.-W., K.H. Bremner, and R.B. Vallee, *Dual subcellular roles for LIS1 and dynein in radial neuronal migration in live brain tissue.* Nat Neurosci, 2007. **10**(8): p. 970-979.

145. Tran, P.T., L. Marsh, V. Doye, S. Inoué, and F. Chang, *A Mechanism for Nuclear Positioning in Fission Yeast Based on Microtubule Pushing.* J Cell Biol, 2001. **153**(2): p. 397-411.

146. Zhao, T., O.S. Graham, A. Raposo, and D. St Johnston, *Growing Microtubules Push the Oocyte Nucleus to Polarize the Drosophila Dorsal-Ventral Axis.* Science, 2012. **336**(6084): p. 999-1003.

147. Adames, N.R. and J.A. Cooper, *Microtubule Interactions with the Cell Cortex Causing Nuclear Movements in Saccharomyces cerevisiae.* J Cell Biol, 2000. **149**(4): p. 863-874.

148. Hu, D.J., A.D. Baffet, T. Nayak, A. Akhmanova, V. Doye, and R.B. Vallee, *Dynein recruitment to nuclear pores activates apical nuclear migration and mitotic entry in brain progenitor cells.* Cell, 2013. **154**(6): p. 1300-13.

149. Splinter, D., D.S. Razafsky, M.A. Schlager, A. Serra-Marques, I. Grigoriev, J. Demmers, N. Keijzer, K. Jiang, I. Poser, A.A. Hyman, C.C. Hoogenraad, S.J. King, and A. Akhmanova, *BICD2, dynactin, and LIS1 cooperate in regulating dynein recruitment to cellular structures.* Mol Biol Cell, 2012. **23**(21): p. 4226-41.

150. Bolhy, S., I. Bouhlel, E. Dultz, T. Nayak, M. Zuccolo, X. Gatti, R. Vallee, J. Ellenberg, and V. Doye, *A Nup133-dependent NPC-anchored network tethers centrosomes to the nuclear envelope in prophase.* J Cell Biol, 2011. **192**(5): p. 855-71.

151. Penkner, A.M., A. Fridkin, J. Gloggnitzer, A. Baudrimont, T. Machacek, A. Woglar, E. Csaszar, P. Pasierbek, G. Ammerer, Y. Gruenbaum, and V. Jantsch, *Meiotic chromosome homology search involves modifications of the nuclear envelope protein Matefin/SUN-1.* Cell, 2009. **139**(5): p. 920-33.

152. Wynne, D.J., O. Rog, P.M. Carlton, and A.F. Dernburg, *Dynein-dependent processive chromosome motions promote homologous pairing in C. elegans meiosis.* J Cell Biol, 2012. **196**(1): p. 47-64.

153. Link, J., D. Jahn, J. Schmitt, E. Gob, J. Baar, S. Ortega, R. Benavente, and M. Alsheimer, *The meiotic nuclear lamina regulates chromosome dynamics and promotes efficient homologous recombination in the mouse.* PLoS Genet, 2013. **9**(1): p. e1003261.

154. Jahn, D., S. Schramm, R. Benavente, and M. Alsheimer, *Dynamic properties of meiosis-specific lamin C2 and its impact on nuclear envelope integrity.* Nucleus, 2010. **1**(3): p. 273-83.

155. Lottersberger, F., R.A. Karssemeijer, N. Dimitrova, and T. de Lange, *53BP1 and the LINC complex promote microtubule-dependent DSB mobility and DNA repair.* Cell, 2015. **163**(4): p. 880-893.

156. Li, P. and A.A. Noegel, *Inner nuclear envelope protein SUN1 plays a prominent role in mammalian mRNA export.* Nucleic Acids Research, 2015. **43**(20): p. 9874-9888.

157. Rodionov, V., E. Nadezhdina, J. Peloquin, and G. Borisy, *Digital Fluorescence Microscopy of Cell Cytoplasts with and without the Centrosome.* Methods in Cell Biology, 2001. **67**: p. 43-51.

158. Inoue, S., G. M, and K.R. A., *Centrifuge polarizing microscope. II. Sample biological applications.* Journal of Microscopy, 2001. **201**: p. 357-367.

159. Neelam, S., T.J. Chancellor, Y. Li, J.A. Nickerson, K.J. Roux, R.B. Dickinson, and T.P. Lele, *Direct force probe reveals the mechanics of nuclear homeostasis in the mammalian cell.* Proceedings of the National Academy of Sciences, 2015. **112**(18): p. 5720-5725.

160. Tkachenko, E., E. Gutierrez, S.K. Saikin, P. Fogelstrand, C. Kim, A. Groisman, and M.H. Ginsberg, *The nucleus of endothelial cell as a sensor of blood flow direction.* Biology Open, 2013. **2**(10): p. 1007-1012.

161. Grashoff, C., B.D. Hoffman, M.D. Brenner, R. Zhou, M. Parsons, M.T. Yang, M.A. McLean, S.G. Sligar, C.S. Chen, T. Ha, and M.A. Schwartz, *Measuring mechanical tension across vinculin reveals regulation of focal adhesion dynamics.* Nature, 2010. **466**(7303): p. 263-6.

162. Arsenovic, Paul T., I. Ramachandran, K. Bathula, R. Zhu, Jiten D. Narang, Natalie A. Noll, Christopher A. Lemmon, Gregg G. Gundersen, and Daniel E. Conway, *Nesprin-2G, a Component of the Nuclear LINC Complex, Is Subject to Myosin-Dependent Tension.* Biophysical Journal, 2016. **110**(1): p. 34-43.

163. Guilluy, C., L.D. Osborne, L. Van Landeghem, L. Sharek, R. Superfine, R. Garcia-Mata, and K. Burridge, *Isolated nuclei adapt to force and reveal a mechanotransduction pathway in the nucleus.* Nat Cell Biol, 2014. **16**(4): p. 376-81.

164. Palazzo, A.F., H.L. Joseph, Y.-J. Chen, D.L. Dujardin, A.S. Alberts, K.K. Pfister, R.B. Vallee, and G.G. Gundersen, *Cdc42, dynein, and dynactin regulate MTOC reorientation independent of Rho-regulated microtubule stabilization.* Current Biology, 2001. **11**(19): p. 1536-1541.

165. McDonnell, A.V., T. Jiang, A.E. Keating, and B. Berger, *Paircoil2: improved prediction of coiled coils from sequence.* Bioinformatics, 2006. **22**(3): p. 356-8.

166. Chesarone, M.A., A.G. DuPage, and B.L. Goode, *Unleashing formins to remodel the actin and microtubule cytoskeletons.* Nat Rev Mol Cell Biol, 2010. **11**(1): p. 62-74.

167. Bartolini, F. and G.G. Gundersen, *Formins and microtubules.* Biochim Biophys Acta, 2010. **1803**(2): p. 164-73.

168. Schonichen, A., H.G. Mannherz, E. Behrmann, A.J. Mazur, S. Kuhn, U. Silvan, C.A. Schoenenberger, O.T. Fackler, S. Raunser, L. Dehmelt, and M. Geyer, *FHOD1 is a combined actin filament capping and bundling factor that selectively associates with actin arcs and stress fibers.* J Cell Sci, 2013. **126**(Pt 8): p. 1891-901.

169. Gasteier, J.E., R. Madrid, E. Krautkramer, S. Schroder, W. Muranyi, S. Benichou, and O.T. Fackler, *Activation of the Rac-binding partner FHOD1 induces actin stress fibers via a ROCK-dependent mechanism.* J Biol Chem, 2003. **278**(40): p. 38902-12.

170. Alvarez, D.E. and H. Agaisse, *The formin FHOD1 and the small GTPase Rac1 promote vaccinia virus actin-based motility.* J Cell Biol, 2013. **202**(7): p. 1075-1090.

171. Truong, D., D. Brabant, M. Bashkurov, L.C. Wan, V. Braun, W.D. Heo, T. Meyer, L. Pelletier, J. Copeland, and J.H. Brumell, *Formin-mediated actin polymerization promotes Salmonella invasion.* Cell Microbiol, 2013.

172. Iskratsch, T., C.H. Yu, A. Mathur, S. Liu, V. Stévenin, J. Dwyer, J. Hone, E. Ehler, and M.P. Sheetz, *FHOD1 Is Needed for Directed Forces and Adhesion Maturation during Cell Spreading and Migration* Developmental Cell, 2013. **27**: p. 545-559.

173. Schulte, A., B. Stolp, A. Schonichen, O. Pylypenko, A. Rak, O.T. Fackler, and M. Geyer, *The human formin FHOD1 contains a bipartite structure of FH3 and GTPase-binding domains required for activation.* Structure, 2008. **16**(9): p. 1313-23.

174. Koka, S., C.L. Neudauer, X. Li, R.E. Lewis, J.B. McCarthy, and J.J. Westendorf, *The formin-homology-domain-containing protein FHOD1 enhances cell migration.* J Cell Sci, 2003. **116**(Pt 9): p. 1745-55.

175. Simpson, J.G. and R.G. Roberts, *Patterns of evolutionary conservation in the nesprin genes highlight probable functionally important protein domains and isoforms.* Biochem Soc Trans, 2008. **36**(Pt 6): p. 1359-67.

176. Autore, F., M. Pfuhl, X. Quan, A. Williams, R.G. Roberts, C.M. Shanahan, and F. Fraternali, *Large-scale modelling of the divergent spectrin repeats in nesprins: giant modular proteins.* PLoS One, 2013. **8**(5): p. e63633.

177. Palazzo, A.F., T.A. Cook, A.S. Alberts, and G.G. Gundersen, *mDia mediates Rho-regulated formation and orientation of stable microtubules.* Nat Cell Biol, 2001. **3**(8): p. 723-9.

178. Takeya, R. and H. Sumimoto, *Fhos, a mammalian formin, directly binds to F-actin via a region N-terminal to the FH1 domain and forms a homotypic complex via the FH2 domain to promote actin fiber formation.* J Cell Sci, 2003. **116**(Pt 22): p. 4567-75.

179. Bartolini, F., J.B. Moseley, J. Schmoranzer, L. Cassimeris, B.L. Goode, and G.G. Gundersen, *The formin mDia2 stabilizes microtubules independently of its actin nucleation activity.* J Cell Biol, 2008. **181**(3): p. 523-36.

180. Luxton, G.W.G., E.R. Gomes, E.S. Folker, H.J. Worman, and G.G. Gundersen, *TAN lines: A novel nuclear envelope structure involved in nuclear positioning.* Nucleus, 2011. **2**(3): p. 173-181.

181. Starr, D.A. and H.N. Fridolfsson, *Interactions between nuclei and the cytoskeleton are mediated by SUN-KASH nuclear-envelope bridges.* Annu Rev Cell Dev Biol, 2010. **26**: p. 421-44.

182. Korobova, F., V. Ramabhadran, and H.N. Higgs, *An actin-dependent step in mitochondrial fission mediated by the ER-associated formin INF2.* Science, 2013. **339**(6118): p. 464-7.

183. Riedl, J., A.H. Crevenna, K. Kessenbrock, J.H. Yu, D. Neukirchen, M. Bista, F. Bradke, D. Jenne, T.A. Holak, Z. Werb, M. Sixt, and R. Wedlich-Soldner, *Lifeact: a versatile marker to visualize F-actin.* Nat Methods, 2008. **5**(7): p. 605-7.

184. Madrid, R., J.E. Gasteier, J. Bouchet, S. Schroder, M. Geyer, S. Benichou, and O.T. Fackler, *Oligomerization of the diaphanous-related formin FHOD1 requires a coiled-coil motif critical for its cytoskeletal and transcriptional activities.* FEBS Lett, 2005. **579**(2): p. 441-8.

185. Cook, T.A., T. Nagasaki, and G.G. Gundersen, *Rho guanosine triphosphatase mediates the selective stabilization of microtubules induced by lysophosphatidic acid.* The Journal of Cell Biology, 1998. **141**(1): p. 175-85.

186. Iyer, K., L. Burkle, D. Auerbach, S. Thaminy, M. Dinkel, K. Engels, and I. Stagljar, *Utilizing the split-ubiquitin membrane yeast two-hybrid system to identify protein-protein interactions of integral membrane proteins.* Sci STKE, 2005. **2005**(275): p. pl3.

187. Gasteier, J.E., S. Schroeder, W. Muranyi, R. Madrid, S. Benichou, and O.T. Fackler, *FHOD1 coordinates actin filament and microtubule alignment to mediate cell elongation.* Exp Cell Res, 2005. **306**(1): p. 192-202.

188. Schneider, M., W. Lu, S. Neumann, A. Brachner, J. Gotzmann, A.A. Noegel, and I. Karakesisoglou, *Molecular mechanisms of centrosome and cytoskeleton anchorage at the nuclear envelope.* Cellular and Molecular Life Sciences, 2011. **68**(9): p. 1593-1610.

189. Jayo, A., M. Malboubi, S. Antoku, W. Chang, E. Ortiz-Zapater, C. Groen, K. Pfisterer, T. Tootle, G. Charras, Gregg G. Gundersen, and M. Parsons, *Fascin Regulates Nuclear*

Movement and Deformation in Migrating Cells. Developmental Cell, 2016. **38**(4): p. 371-383.

190. Wilhelmsen, K., S.H.M. Litjens, I. Kuikman, N. Tshimbalanga, H. Janssen, I. van den Bout, K. Raymond, and A. Sonnenberg, *Nesprin-3, a novel outer nuclear membrane protein, associates with the cytoskeletal linker protein plectin.* The Journal of Cell Biology, 2005. **171**(5): p. 799-810.

191. Petrie, R.J., H. Koo, and K.M. Yamada, *Generation of compartmentalized pressure by a nuclear piston governs cell motility in a 3D matrix.* Science, 2014. **345**(6200): p. 1062-1065.

192. Meyerzon, M., H.N. Fridolfsson, N. Ly, F.J. McNally, and D.A. Starr, *UNC-83 is a nuclear-specific cargo adaptor for kinesin-1-mediated nuclear migration.* Development, 2009. **136**(16): p. 2725-33.

193. Hedgecock, E.M. and J. Nichol Thomson, *A gene required for nuclear and mitochondrial attachment in the nematode caenorhabditis elegans.* Cell. **30**(1): p. 321-330.

194. Stroud, M.J., W. Feng, J. Zhang, J. Veevers, X. Fang, L. Gerace, and J. Chen, *Nesprin 1α2 is essential for mouse postnatal viability and nuclear positioning in skeletal muscle.* The Journal of Cell Biology, 2017.

195. Burakov, A., E. Nadezhdina, B. Slepchenko, and V. Rodionov, *Centrosome positioning in interphase cells.* The Journal of Cell Biology, 2003. **162**(6): p. 963-9.

196. Desai, R.A., L. Gao, S. Raghavan, W.F. Liu, and C.S. Chen, *Cell polarity triggered by cell-cell adhesion via E-cadherin.* Journal of Cell Science, 2009. **122**(7): p. 905-911.

197. Maniotis, A.J., C.S. Chen, and D.E. Ingber, *Demonstration of mechanical connections between integrins, cytoskeletal filaments, and nucleoplasm that stabilize nuclear structure.* Proceedings of the National Academy of Sciences, 1997. **94**(3): p. 849-854.

198. Daga, R.R. and F. Chang, *Dynamic positioning of the fission yeast cell division plane.* Proceedings of the National Academy of Sciences, 2005. **102**(23): p. 8228-32.

199. Hoffman, L.M., C.C. Jensen, A. Chaturvedi, M. Yoshigi, and M.C. Beckerle, *Stretch-induced actin remodeling requires targeting of zyxin to stress fibers and recruitment of actin regulators.* Molecular Biology of the Cell, 2012. **23**(10): p. 1846-1859.

200. Burridge, K. and E.S. Wittchen, *The tension mounts: stress fibers as force-generating mechanotransducers.* The Journal of Cell Biology, 2013. **200**(1): p. 9-19.

201. Firestone, A.J., J.S. Weinger, M. Maldonado, K. Barlan, L.D. Langston, M. O'Donnell, V.I. Gelfand, T.M. Kapoor, and J.K. Chen, *Small-molecule inhibitors of the AAA+ ATPase motor cytoplasmic dynein.* Nature, 2012. **484**(7392): p. 125-129.

202. Razafsky, D. and D. Hodzic, *Bringing KASH under the SUN: the many faces of nucleo-cytoskeletal connections.* The Journal of Cell Biology, 2009. **186**(4): p. 461-472.

203. Schwanhausser, B., D. Busse, N. Li, G. Dittmar, J. Schuchhardt, J. Wolf, W. Chen, and M. Selbach, *Global quantification of mammalian gene expression control.* Nature, 2011. **473**(7347): p. 337-342.

204. Zhong, Z., S.A. Chang, A. Kalinowski, K.L. Wilson, and K.N. Dahl, *Stabilization of the spectrin-like domains of nesprin-1α by the evolutionarily conserved "adaptive" domain.* Cellular and Molecular Bioengineering, 2010. **3**(2): p. 139-150.

205. Starr, D.A., *ANChors away: an actin based mechanism of nuclear positioning.* J Cell Sci, 2003. **116**(2): p. 211-216.

206. Almonacid, M., W.W. Ahmed, M. Bussonnier, P. Mailly, T. Betz, R. Voituriez, N.S. Gov, and M.-H. Verlhac, *Active diffusion positions the nucleus in mouse oocytes.* Nat Cell Biol, 2015. **17**(4): p. 470-479.

207. Mazumder, A. and G.V. Shivashankar, *Emergence of a prestressed eukaryotic nucleus during cellular differentiation and development.* Journal of the Royal Society Interface, 2010. **7**(Suppl 3): p. S321-S330.

208. Alam, S.G., Q. Zhang, N. Prasad, Y. Li, S. Chamala, R. Kuchibhotla, B. Kc, V. Aggarwal, S. Shrestha, A.L. Jones, S.E. Levy, K.J. Roux, J.A. Nickerson, and T.P. Lele, *The mammalian LINC complex regulates genome transcriptional responses to substrate rigidity.* Sci Rep, 2016. **6**: p. 38063.

209. Liem, R.K., *Cytoskeletal Integrators: The Spectrin Superfamily.* Cold Spring Harb Perspect Biol, 2016. **8**(10).

210. Lei, K., X. Zhang, X. Ding, X. Guo, M. Chen, B. Zhu, T. Xu, Y. Zhuang, R. Xu, and M. Han, *SUN1 and SUN2 play critical but partially redundant roles in anchoring nuclei in skeletal muscle cells in mice.* Proceedings of the National Academy of Sciences, 2009. **106**(25): p. 10207-12.

211. Razafsky, D.S., C.L. Ward, T. Kolb, and D. Hodzic, *Developmental regulation of linkers of the nucleoskeleton to the cytoskeleton during mouse postnatal retinogenesis.* Nucleus, 2013. **4**(5): p. 399-409.

212. Kidane, D., D. Sakkas, T. Nottoli, J. McGrath, and J.B. Sweasy, *Kinesin 5B (KIF5B) Is Required for Progression through Female Meiosis and Proper Chromosomal Segregation in Mitotic Cells.* PLoS ONE, 2013. **8**(4): p. e58585.

213. Li, Y., D. Lovett, Q. Zhang, S. Neelam, Ram A. Kuchibhotla, R. Zhu, Gregg G. Gundersen, Tanmay P. Lele, and Richard B. Dickinson, *Moving Cell Boundaries Drive Nuclear Shaping during Cell Spreading.* Biophysical Journal, 2015. **109**(4): p. 670-686.

214. Iskratsch, T., C.H. Yu, A. Mathur, S. Liu, V. Stevenin, J. Dwyer, J. Hone, E. Ehler, and M. Sheetz, *FHOD1 is needed for directed forces and adhesion maturation during cell spreading and migration.* Dev Cell, 2013. **27**(5): p. 545-59.

215. Chang, W., E.S. Folker, H.J. Worman, and G.G. Gundersen, *Emerin organizes actin flow for nuclear movement and centrosome orientation in migrating fibroblasts.* Mol Biol Cell, 2013. **24**(24): p. 3869-80.

216. Ezratty, E.J., M.A. Partridge, and G.G. Gundersen, *Microtubule-induced focal adhesion disassembly is mediated by dynamin and focal adhesion kinase.* Nat Cell Biol, 2005. **7**(6): p. 581-90.

217. Liu, C. and Y. Mao, *Diaphanous formin mDia2 regulates CENP-A levels at centromeres.* The Journal of Cell Biology, 2016. **213**(4): p. 415-424.

218. Iskratsch, T., C.H. Yu, A. Mathur, S. Liu, V. Stevenin, J. Dwyer, J. Hone, E. Ehler, and M. Sheetz, *FHOD1 is needed for directed forces and adhesion maturation during cell spreading and migration.* Developmental Cell, 2013. **27**(5): p. 545-59.

219. Gomes, E.R. and G.G. Gundersen, *Real-Time Centrosome Reorientation During Fibroblast Migration*, in *Methods in Enzymology*. 2006, Academic Press. p. 579-592.

220. Liu, C., J.-Z. Chuang, C.-H. Sung, and Y. Mao, *A dynein independent role of Tctex-1 at the kinetochore.* Cell Cycle, 2015. **14**(9): p. 1379-1388.

221. T. J. Mitchison and L.P. Cramer, *Actin-Based Cell Motility and Cell Locomotion.* Cell, 1996.

222. Petrie, R.J. and K.M. Yamada, *Multiple mechanisms of 3D migration: the origins of plasticity.* Curr Opin Cell Biol, 2016. **42**: p. 7-12.

223. Haeger, A., K. Wolf, M.M. Zegers, and P. Friedl, *Collective cell migration: guidance principles and hierarchies.* Trends Cell Biol, 2015. **25**(9): p. 556-66.

224. Friedl, P., *Prespecification and plasticity: shifting mechanisms of cell migration.* Curr Opin Cell Biol, 2004. **16**(1): p. 14-23.

225. Theveneau, E., B. Steventon, E. Scarpa, S. Garcia, X. Trepat, A. Streit, and R. Mayor, *Chase-and-run between adjacent cell populations promotes directional collective migration.* Nat Cell Biol, 2013. **15**(7): p. 763-72.

226. Scarpa, E. and R. Mayor, *Collective cell migration in development.* J Cell Biol, 2016. **212**(2): p. 143-55.

227. Canel, M., A. Serrels, D. Miller, P. Timpson, B. Serrels, M.C. Frame, and V.G. Brunton, *Quantitative in vivo imaging of the effects of inhibiting integrin signaling via Src and*

FAK on cancer cell movement: effects on E-cadherin dynamics. Cancer Res, 2010. **70**(22): p. 9413-22.

228. Cui, Y. and S. Yamada, *N-cadherin dependent collective cell invasion of prostate cancer cells is regulated by the N-terminus of alpha-catenin.* PLoS One, 2013. **8**(1): p. e55069.

229. Pocha, S.M. and D.J. Montell, *Cellular and molecular mechanisms of single and collective cell migrations in Drosophila: themes and variations.* Annu Rev Genet, 2014. **48**: p. 295-318.

230. Montell, D.J., W.H. Yoon, and M. Starz-Gaiano, *Group choreography: mechanisms orchestrating the collective movement of border cells.* Nat Rev Mol Cell Biol, 2012. **13**(10): p. 631-45.

231. Shih, W. and S. Yamada, *N-cadherin as a key regulator of collective cell migration in a 3D environment.* Cell Adh Migr, 2012. **6**(6): p. 513-7.

232. Kotini, M. and R. Mayor, *Connexins in migration during development and cancer.* Dev Biol, 2015. **401**(1): p. 143-51.

233. Theveneau, E. and R. Mayor, *Cadherins in collective cell migration of mesenchymal cells.* Curr Opin Cell Biol, 2012. **24**(5): p. 677-84.

234. Neelam, S., P.R. Hayes, Q. Zhang, R.B. Dickinson, and T.P. Lele, *Vertical uniformity of cells and nuclei in epithelial monolayers.* Sci Rep, 2016. **6**: p. 19689.

235. Wei, C.J., R. Francis, X. Xu, and C.W. Lo, *Connexin43 associated with an N-cadherin-containing multiprotein complex is required for gap junction formation in NIH3T3 cells.* J Biol Chem, 2005. **280**(20): p. 19925-36.

236. Caswell, P.T., H.J. Spence, M. Parsons, D.P. White, K. Clark, K.W. Cheng, G.B. Mills, M.J. Humphries, A.J. Messent, K.I. Anderson, M.W. McCaffrey, B.W. Ozanne, and J.C. Norman, *Rab25 associates with alpha5beta1 integrin to promote invasive migration in 3D microenvironments.* Dev Cell, 2007. **13**(4): p. 496-510.

237. Caswell, P.T., M. Chan, A.J. Lindsay, M.W. McCaffrey, D. Boettiger, and J.C. Norman, *Rab-coupling protein coordinates recycling of alpha5beta1 integrin and EGFR1 to promote cell migration in 3D microenvironments.* J Cell Biol, 2008. **183**(1): p. 143-55.

238. Doyle, A.D., F.W. Wang, K. Matsumoto, and K.M. Yamada, *One-dimensional topography underlies three-dimensional fibrillar cell migration.* J Cell Biol, 2009. **184**(4): p. 481-90.

239. Luxton, G.W. and G.G. Gundersen, *Orientation and function of the nuclear-centrosomal axis during cell migration.* Curr Opin Cell Biol, 2011. **23**(5): p. 579-88.

240. Inoue, S., R.A. Knudson, M. Goda, K. Suzuki, C. Nagano, N. Okada, H. Takahashi, K. Ichie, M. Iida, and K. Yamanaka, *Centrifuge polarizing microscope. I. Rationale, design and instrument performance.* J Microsc, 2001. **201**(Pt 3): p. 341-56.

241. Wang, N., J.D. Tytell, and D.E. Ingber, *Mechanotransduction at a distance: mechanically coupling the extracellular matrix with the nucleus.* Nat Rev Mol Cell Biol, 2009. **10**: p. 75-82.

242. Speese, Sean D., J. Ashley, V. Jokhi, J. Nunnari, R. Barria, Y. Li, B. Ataman, A. Koon, Y.-T. Chang, Q. Li, Melissa J. Moore, and V. Budnik, *Nuclear Envelope Budding Enables Large Ribonucleoprotein Particle Export during Synaptic Wnt Signaling.* Cell, 2012. **149**(4): p. 832-846.

243. Folker, E.S. and M.K. Baylies, *Nuclear positioning in muscle development and disease.* Frontiers in Physiology, 2013. **4**: p. 363.

244. Cadot, B., V. Gache, and E.R. Gomes, *Moving and positioning the nucleus in skeletal muscle – one step at a time.* Nucleus, 2015. **6**(5): p. 373-381.

245. Wilson, M.H. and E.L.F. Holzbaur, *Opposing microtubule motors drive robust nuclear dynamics in developing muscle cells.* Journal of Cell Science, 2012. **125**(17): p. 4158-4169.

246. Metzger, T., V. Gache, M. Xu, B. Cadot, E.S. Folker, B.E. Richardson, E.R. Gomes, and M.K. Baylies, *MAP and kinesin-dependent nuclear positioning is required for skeletal muscle function.* Nature, 2012. **484**(7392): p. 120-4.

247. Falcone, S., W. Roman, K. Hnia, V. Gache, N. Didier, J. Laine, F. Aurade, I. Marty, I. Nishino, N. Charlet-Berguerand, N.B. Romero, G. Marazzi, D. Sassoon, J. Laporte, and E.R. Gomes, *N-WASP is required for Amphiphysin-2/BIN1-dependent nuclear positioning and triad organization in skeletal muscle and is involved in the pathophysiology of centronuclear myopathy.* EMBO Mol Med, 2014. **6**(11): p. 1455-75.

248. D'Alessandro, M., K. Hnia, V. Gache, C. Koch, C. Gavriilidis, D. Rodriguez, A.S. Nicot, N.B. Romero, Y. Schwab, E. Gomes, M. Labouesse, and J. Laporte, *Amphiphysin 2 Orchestrates Nucleus Positioning and Shape by Linking the Nuclear Envelope to the Actin and Microtubule Cytoskeleton.* Dev Cell, 2015. **35**(2): p. 186-98.